Interfacial Phenomena in Pharmaceutical Process Development

by

Eftychios Hadjittofis

A dissertation submitted to Imperial College London for the degree of Doctor of Philosophy

Department of Chemical Engineering
Imperial College London South
Kensington Campus SW7 2AZ London
United Kingdom

October 2018

Την τιμή κανένας δεν μπορεί να σου την αφαιρέσει. Την τιμή μπορείς μονάχα να την χάσεις.

Νίκος Ζαχαριάδης
28 Ιούλη 1973

Abstract

Interfacial phenomena are of crucial importance in both pharmaceutical process development and drug product development. Inverse Gas Chromatography (IGC), is an adsorption-based technique providing a versatile framework for the investigation of interfacial phenomena. In the light of fundamental concepts of thermodynamics, new IGC protocols have been developed enabling the accurate determination of the surface energy and the surface energy heterogeneity of crystalline materials and of the Hansen Solubility Parameter (HSP) of amorphous materials.

Experimental and *in silico* studies are deployed to reveal the importance of sample preparation in the accuracy of IGC measurements. In this context, Monte Carlo simulations were developed to support the experimental findings. The importance of spreading pressure in IGC measurements is investigated as well. A separate chapter discusses the importance of temperature and carrier gas flow rate in the measurement of HSP, of amorphous materials. Results obtained from the three chapters, are used, alongside with the results from complimentary techniques, to investigate the facet specific interactions of copovidone solutions, with macroscopic single crystals of p-monoclinic carbamazepine. Very intriguing findings are reported, highlighting among other things, the correlation between the aggregation behaviour of the polymer and wettability. In the next chapter IGC measurements are deployed, among other techniques, to investigate the mechanism of dehydration induced concomitant polymorphism of carbamazepine dihydrate. As part of this chapter a novel bioinspired crystal growth technique has been developed, enabling the growth of macroscopic hydrates of poorly water-soluble molecules.

Overall this thesis, constitutes a unique piece of work combining a plethora of characterisation techniques, with novel *in silico* tools to investigate interfacial phenomena, of

high importance in pharmaceutical industry. It highlights the importance of fundamental notions of surface thermodynamics in the development of an in-depth understanding of interfacial phenomena and it reveals the prospects of IGC as a potential game changer in pharmaceutical process development and drug product development.

Contents

Abstract 3
Acknowledgements 11
Originality Declaration and Copyright 12
Peer Reviewed Journal Papers and Book Chapters 13
Presentations in refereed conferences 14
Figures and Tables 15
List of figures 15
List of tables 20
Nomenclature 21
1. Introduction 26
1.1 Background 26
1.2 Objectives 29
2. Fundamentals of interfacial phenomena 31
2.1 Introduction 31
2.2 Fundamentals of intermolecular forces 33
2.2.1 Van der Waals forces 34
2.2.2 Thermodynamics of van der Waals forces 35
2.2.2.1 Hamaker's approach 35
2.2.2.2 Lifshitz's approach 37
2.3 Thermodynamics of particles in solutions 38
2.3.1 DLVO theory 38
2.3.2 Tracking the behaviour of particles in solution, using Dynamic Light Scattering 43
2.4 Surface Tension and Surface Energy 48
2.4.1 Fundamentals 48
2.4.2 The deconvolution of surface energy 50
2.4.2.1 Acid-base interactions 53
2.5 Thermodynamics of solid-liquid interfaces 55
2.5.1 Fundamentals 55
2.5.2 Experimental techniques 56
2.5.2.1 Sessile drop contact angle 56
2.5.2.2 Surface roughness and wettability 59
2.5.2.3 Solutions containing surface active molecules – Langmuir-Blodgett trough 60
2.6 Solid-vapour interface 63
2.6.1 Introduction 63
2.6.2 Heterogeneous adsorption 67

2.6.2.1 Mapping of energetic surface heterogeneity 69
2.6.3 Inverse gas chromatography (IGC) 71
2.6.3.1 Thermodynamics of IGC 72
2.7 Solid-solid interface 79
2.7.1 Fundamental thermodynamics 79
2.7.2 Experimental techniques 80
2.7.2.1 Scanning Electron Microscope (SEM) 81
2.7.2.2 X-Ray Photoelectron Spectroscopy (XPS) 81
2.8 Liquid – liquid interface 82
2.8.1 The Flory-Huggins theory 84
2.8.2 Using IGC to measure the χ interaction parameter and beyond 91
2.8.3 Hansen Solubility Parameters 94
3. Implications of interfacial phenomena in drug product development and pharmaceutical process development. 97
3.1 Introduction 97
3.2 Implications of Solid-Liquid Interfaces 98
3.2.1 Crystal nucleation and growth 99
3.2.1.1 Crystal nucleation in solution 99
3.2.1.2 Introduction to crystal growth in solution 101
3.2.1.3 The influence of solution conditions in crystal growth 106
3.2.1.4 The influence of additives in crystal growth 109
3.2.1.5 Interfacial phenomena in the crystallisation of amorphous materials 112
3.2.3 Crystal dissolution 113
3.2.3.1 Funamentals 113
3.2.3.2 Anisotropy wettability of crystalline materials 115
3.2.3.3 The importance of defects in dissolution 116
3.2.3.4 Crystal engineering approaches for enhanced dissolution 117
3.2.3.5 The effects of surface active additives in crystal growth and dissolution 119
3.3 Implications of Solid-Vapour Interfaces 120
3.3.1 Moisture content in pharmaceutical materials 121
3.3.2 Drying 122
3.4 Implications of Solid-Solid Interfaces 124
3.4.1 Flowability 125
3.4.2 Mixing or blending 126
3.4.3 Dry coating 128
3.4.4 Milling 129

4. Aspects of the influence of sample preparation on IGC measurements: the cases of silanised glass wool and column packing structure 133
4.1 Introduction 133
4.2 Experimental Methods 134
4.3 Results and discussion 136
4.3.1 Influence of silanised glass wool 136
4.4 Effects of packing 145
4.4.1 IGC measurements 145
4.4.2 Monte Carlo simulations 146
4.5 Conclusions 153
5. The importance of spreading pressure in the determination of surface energy via IGC measurements 155
5.1 Introduction 155
5.2 Experimental Methods 157
5.3 Results and discussion 158
5.3.1 IGC data 158
5.3.2 Wettability 162
5.3.3 Surface energy deconvolution 164
5.3.4 Expanding beyond p-monoclinic carbamazepine 167
5.3.5 Implications of this study on the previous chapter 170
5.4 Conclusions 170
6. The effects of amorphous interfaces in IGC measurements 172
6.1 Introduction 172
6.2 Materials 175
6.2.1 Recrystallisation of p-monoclinic carbamazepine 175
6.2.2 Copovidone 176
6.2.3 Properties of the solvent probes used in the measurements 176
6.3 HSP measurements 177
6.4 Results 178
6.4.1 Determining the T_g of copovidone 178
6.4.2 The effects of temperature on χ and HSP 180
6.4.3 The effect of flow rate on the measured value of χ and HSP of crystalline materials 184
6.4.4 Measuring the value of HSP at different flow rates for amorphous materials 185
6.4.5 Expanding measurement methodology to include the effects of carrier gas flow rate 189
6.5 Discussion 192
7. Anisotropic wettability of crystalline materials by aqueous solutions of non-ionic polymers 195

7.1 Introduction 195
7.2 Materials and Methods 197
7.2.1 Growth and characterisation of macroscopic p-monoclinic carbamazepine single crystals 197
7.2.2 XPS 199
7.2.3 Contact Angle Measurements 199
7.2.4 Polymeric Solutions 200
7.2.5 DLS 202
7.2.6 Langmuir balance tensiometry 202
7.3 Results 202
7.3.1 XPS analysis 202
7.3.2 Surface Energy Anisotropy 207
7.3.3 Wettability with polymeric solutions 210
7.4 Discussion 218
7.4.1 Anisotropic properties of p-monoclinic carbamazepine and implications on crystallisation 218
7.4.2 Wettability with polymer solutions 222
7.5 Conclusions 227
8. Interfacial phenomena in the dehydration of pharmaceutical channel hydrates 229
8.1 Introduction 229
8.2 Polymorphism 230
8.2.1 The importance of polymorphism in drug product development 232
8.3 The case of carbamazepine dihydrate 233
8.4 Experimental methodology 237
8.4.1 Materials used 237
8.4.2 Crystallisation and characterisation of macroscopic crystals of carbamazepine dihydrate via a bioinspired method 237
8.4.3 Producing carbamazepine dihydrate crystals with different aspect ratios 243
8.4.4 Structural changes associated with dehydration 246
8.4.4.1 Crack formation 246
8.4.4.2 Cracks are formed inside the crystal 250
8.4.4 Dehydration induced concomitant polymorphism 252
8.4.6 Polymorph quantification by means of IGC 253
8.5 Discussion 261
8.5.1 Crystallising macroscopic hydrates on an interface 261
8.5.2 Dehydration induced concomitant polymorphism and quantification 265

8.5.3 Structural changes during dehydration 266
8.5.4 Growth of whiskers 268
8.6 Conclusions 270
9. Conclusions 272
9.1 General conclusions 272
9.2 Criticism on aspects of this work 277
9.3 Directions for future work 280
References 288
Appendix 1: Supplementary information on the calculation of spreading pressure 305
A.1.1 The concept of spreading pressure 305
A.1.2 The roadmap for the correction of IGC data 308
Appendix 2: Pendant drop measurements 311

Acknowledgements

Pursuing a PhD can be a unique and adventurous endeavour. Similarly to all the great scientific endeavours, which have inspired us, such as "The Voyage of Beagle" and the conquest of space, this journey requires the researcher to go back and forth multiple times, to become obsessively passionate with every small bit of the project and show unprecedented commitment.

In this endeavour I had the privilege to work alongside numerous people worth mentioning. First and foremost, Dr Geoff Zhang, my industrial supervisor. Geoff is a model researcher, hardworking, passionate and with deep understanding of the fundamental laws underpinning the behaviour of complex systems. His influence shaped me as a researcher and I am proud that I had the opportunity Furthermore, I need to express my deepest gratitude to Dr Kyra Campbell, for her invaluable moral support during the first years of my PhD. I want to thank all my fellow PhD students at Imperial College and especially Mark-Antonin Isbell, Minos Skountzos, Giannis Tzouganatos, Naima Ali, Sabiyah Ahmed, Ziran Da and Clarence Chum. This work wouldn't have been possible without the support from Dr Jerry Heng.

My PhD was supported financially by the Department of Chemical Engineering of Imperial College, via the EPSRC DTP scholarship. I deeply acknowledge this and I am proud that I have been an active member of one of the world's most renowned institutions.

This work summarises the research efforts of the last four years. The results and the conclusions become ownership of the scientific community and they will be tested in the years to come. It was a research effort, that like any unique piece of research, required me to appreciate the idea proposed by Karl Marx in the preface of his in his work "A contribution to the Critique of Political Economy" 160 years ago. There, Marx suggests that at the gate of science, as at the gate of hell, the same demand (from Dantes' "Divine Comedy") should be inscribed:

Qui si convien lasciare ogni sospetto
Ogni vilta convien che qui sia morta.

Originality Declaration and Copyright

The work contained in this thesis is the original work of the author, except where noted by means of reference. No part this work has been submitted in support of an application for another degree or qualification in any other university, or institution of learning.

The copyright of this thesis rests with the author and is made available under a Creative Commons Attribution Non-Commercial No Derivatives licence. Researchers are free to copy, distribute or transmit the thesis on the condition that they attribute it, that they do not use it for commercial purposes and that they do not alter, transform or build upon it. For any reuse or redistribution, researchers must make clear to others the licence terms of this work

Peer Reviewed Journal Papers and Book Chapters

Journal papers

Published

1. **Eftychios Hadjittofis**, Mark-Antonin Isbell, Vikram A. Karde, Sophia Vargese, Chinmay Ghoroi, Jerry Y.Y. Heng, *Influences of crystal anisotropy in pharmaceutical process development.* Pharmaceutical Research, 2018, **35**(5); p. 100-122.
2. Wu, Jerry Y.Y. Heng, Senentxu Lanceros-Méndez, **Eftychios Hadjittofis**, Weiping Su, Junhong Tang, Hongting Zhao, Weihong Wu, *Comparative study of surface properties determination of colored pearl-oyster-shell-derived filler using inverse gas chromatography method and contact angle measurements.* International Journal of Adhesion and Adhesives, 2017, **78**(1); p. 55-59.
3. **Eftychios Hadjittofis**, Geoff G.Z. Zhang, Jerry Y.Y. Heng, *Influence of sample preparation on IGC measurements: the cases of silanised glass wool and packing structure*. RSC Advances, 2017, **7**(20), p. 12194-12200.
4. Zhitong Yao, Jerry Y.Y.Heng, Senentxu Lanceros-Méndez, Alessandro Pegoretti, Xiaosheng Jie, **Eftychios Hadjittofis**, Meisheng Xiae, Weihong Wu, Junhong Tang, *Study on the surface properties of colored talc filler (CTF) and mechanical performance of CTF/acrylonitrile-butadiene-styrene composite.* Journal of Alloys and Compounds. 2016, **676**; p. 513-520.

In preparation

1. **Eftychios Hadjittofis**, Geoff G.Z. Zhang, Jerry Y.Y. Heng, *Growth of macroscopic channel hydrates and investigation of their dehydration induced concomitant polymorphism.*
2. **Eftychios Hadjittofis**, Geoff G.Z. Zhang, Jerry Y.Y. Heng, *The importance of spreading pressure in adsorption based surface energy measurements; the case of IGC.*
3. **Eftychios Hadjittofis**, Mark-Antonin Isbell, Steven J. Hinder, Geoff G.Z. Zhang, Jerry Y.Y. Heng, *The anisotropic wettability of crystalline pharmaceutical solids by aqueous solutions of non-ionic polymers*.
4. **Eftychios Hadjittofis**, Geoff G.Z. Zhang, Jerry Y.Y. Heng, *The importance of interfaces in the determination of thermodynamic parameters of amorphous materials, using IGC*.

Book Chapters

1. **Eftychios Hadjittofis**, Shyamal C. Das, Geoff G.Z. Zhang, Jerry Y.Y. Heng, (2016) Interfacial Phenomena. In Yihong Qiu, Yisheng Chen, Geoff G.Z. Zhang, Lawrence Yu, Rao V. Mantri (Eds.), *Developing Solid Oral Dosage Forms* (p. 225-252). New York, NY: Academic Press.

Presentations in refereed conferences

1. **Eftychios Hadjittofis**, Geoff G. Z. Zhang Jerry Y. Y. Heng, "Inverse gas chromatography in Crystal Engineering", Crystal Engineering Gordon Research Conference, Newry, ME, 24–29 June 2018 (Poster presentation).
2. **Eftychios Hadjittofis**, Geoff G. Z. Zhang Jerry Y. Y. Heng, "The importance of spreading pressure on adsorption based surface energy measurements; the case of IGC", AICHE Annual Meeting, Minneapolis, MN, 29 October–3 November 2017 (Oral contribution).
3. **Eftychios Hadjittofis**, Geoff G. Z. Zhang Jerry Y. Y. Heng, "Assessing the impact of dry coating on the surface properties of pharmaceutical formulations", AICHE Annual Meeting, Minneapolis, MN, 29 October–3 November 2017 (Oral contribution).
4. **Eftychios Hadjittofis**, Geoff G. Z. Zhang Jerry Y. Y. Heng, "The importance of amorphous interfaces in the measurement of thermodynamic parameters, using inverse gas chromatography", AICHE Annual Meeting, Minneapolis, MN, 29 October–3 November 2017 (Oral contribution).
5. **Eftychios Hadjittofis**, Mark-Antonin Isbell, Geoff G. Z. Zhang Jerry Y. Y. Heng, "The influence of solution conditions on the self-assembly of pre-nucleation clusters", AICHE Annual Meeting, Minneapolis, MN, 29 October–3 November 2017 (Oral contribution).
6. **Eftychios Hadjittofis**, Geoff G. Z. Zhang Jerry Y. Y. Heng, "The importance of spreading pressure on adsorption based surface energy measurements; the case of IGC", UK Colloids, Manchester, UK, 10–12 July 2017 (Oral contribution).
7. **Eftychios Hadjittofis**, Mark-Antonin Isbell, Geoff G. Z. Zhang Jerry Y. Y. Heng, "The importance of interfaces in the measurement of thermodynamic parameters of amorphous materials, using inverse gas chromatography", UK Colloids, Manchester, UK, 10–12 July 2017 (Oral contribution).
8. **Eftychios Hadjittofis**, Geoff G. Z. Zhang Jerry Y. Y. Heng, "Growing macroscopic hydrates using a bioinspired approach and investigating dehydration induced polymorphism", AICHE Annual Meeting, San Francisco, CA, 13–18 November 2016 (Oral contribution).
9. **Eftychios Hadjittofis**, Geoff G. Z. Zhang Jerry Y. Y. Heng, "Aspects of good experimental practice in surface energy measurements, of particulate materials, using FD-IGC", AICHE Annual Meeting, San Francisco, CA, 13–18 November 2016 (Oral contribution).
10. **Eftychios Hadjittofis**, Geoff G. Z. Zhang Jerry Y. Y. Heng, "The effects of crystal size and habit on the dehydration induced polymorphism; the case of carbamazepine dihydrate", AICHE Annual Meeting, San Francisco, CA, 13–18 November 2016 (Oral contribution).
11. **Eftychios Hadjittofis**, Mark A. Isbell, Steven J. Hinder, Geoff G. Z. Zhang Jerry Y. Y. Heng, "The surface properties of organic crystalline solids and their interactions with polymeric excipients and binders", AICHE Annual Meeting, San Francisco, CA, 13–18 November 2016 (Oral contribution).
12. **Eftychios Hadjittofis**, Geoff G. Z. Zhang Jerry Y. Y. Heng, "Crystallisation of macroscopic carbamazepine dihydrate crystals and characterisation of their drying behaviour", Crystal Growth of Organic Materials Congress, Leeds, UK, 26–30 June 2016 (Oral contribution).
13. **Eftychios Hadjittofis**, Geoff G. Z. Zhang Jerry Y. Y. Heng, "Towards accurate predictions of the surface energy heterogeneity of crystalline pharmaceutical powders", American Association of Pharmaceutical Scientists Annual Meeting, Orlando, FL, USA, 25–29 October 2015 (Poster presentation).
14. **Eftychios Hadjittofis**, Jerry Y. Y. Heng, "Accurate mapping of energetic surface heterogeneity of crystalline materials", 10th European Congress of Chemical Engineering, Nice, France, 27 September–1 October 2015 (Poster presentation).
15. **Eftychios Hadjittofis**, Jerry Y. Y. Heng, "Towards accurate predictions of surface heterogeneity: phase transitions on the surface of energetically anisotropic crystalline materials", 5th UK-China and 13th UK Particle Technology Forum, Leeds, UK, 12–15 July 2015 (Oral contribution).

Figures and Tables

List of figures

Figure 2.1: Schematic representation of the three components of van der Waals forces.[3] 34
Figure 2.2: Schematic representation for the derivation of potential energy equation by Hamaker's approach A) top view, B) side view.[3] 36
Figure 2.3: Schematic depiction of the double surrounding a negatively charged particle. The graph at the bottom right provides a qualitative depiction of the decrease in the magnitude of the potential at increasing distances from the surface of the particle.[3] 41
Figure 2.4: Plot of the scatter intensity of laser (I_t) passing through a solution containing colloidal particles. The mean value of the intensity ($<I_t>$) can be seen on the vertical axis, as well as the boundaries of time intervals, which are shown with different colours. 45
Figure 2.5: Schematic representation of DLS correlograms. 48
Figure 2.6: Interactions for molecules in bulk and molecules on the surface of a material. For the resultant forces shown on one of the surface molecules with a red arrow, there is an equal magnitude and opposite direction force corresponding to the surface tension. 49
Figure 2.8: Schematic representation of the concept of advancing and receding contact angle measurements, indicating the relevant surface tensions, according to Young's equation and the spreading pressure. 57
Figure 2.9: Images depicting the operation mode of a Langmuir-Blodgett trough. At the first figure, on the top, the trough contains only water and callibration of the Wilhelmy plate is performed. In the figure in the middle, the surface active molecules have just been added and a weak surface activity is recorded. In the last figure, the barrier has moved, compressing the surface active molecules, increasing the surface coverage leading to an increase in the surface activity. 61
Figure 2.10: Schematic showing the Wilhelmy plate dimensions, as it is immersed in water, from A) side view, B) front view. 62
Figure 2.11: Schematic representations of A) the Schultz method and B) the Dorris and Gray method for the determination of surface energy, using IGC measurements. 75
Figure 2.12: Schematic depiction of the qualitative behaviour of a surface energy map obtained by FD-IGC measurements. 78
Figure 2.14: Schematic free energy of mixing A) no mixing; B) partial miscibility; C) mixing but with phase separation at some compositions; and D) complete miscibility. 90
Figure 2.15: Schematic depiction of the graphical construction used for the determination of HSP from IGC measurements. 96
Figure 3.1: A schematic depicting the Kossel model of crystal growth. The numbering signifies the steps undertaken by the molecule to move from the bulk to the surface (1), to diffuse on the solid surface until it reaches a kink (2), for the solute molecule to desolvate along with the surface (3), and finally for it to be incorporated into the solid shown with the black outline (4). The letters describe the following topographical features: a. the terrace, b. the step, and c. the kink site of preferred attachment. 103
Figure 3.2: Sorption desorption isotherms for different hysteresis cases. 121
Figure 4.1: Surface energy maps of α-lactose monohydrate (termed simply lactose in the legend) and glass wool at different combination ratios. 138
Figure 4.2: A) The calculated surface energy distributions of the silanised glass wool and α-lactose monohydrate, B) The calculated surface distribution obtained from the deconvolution of the surface energy map of a 1:4 wool to α-lactose monohydrate mixture, using the in silico tool developed. The theoretical distribution was obtained from the combination of the surface energy distributions of the constituent components of the mixture at the aforementioned ratio. C) The same as for B but for a 1:1 wool to α-lactose monohydrate mixture. 140

Figure 4.3: The deviation of the measurements at different loadings of silanised wool for the α-lactose monohydrate and the two simulated materials. 141
Figure 4.4: The surface energy distributions of the six in silico materials, investigated in this study. 143
Figure 4.5: The surface energy measurements obtained from pure carbamazepine, mannitol, and 1:1 mixtures of the two packed with different configurations. 146
Figure 4.6: Schematic depictions of the three different types of lattice employed in the Monte Carlo simulations; A) is for the physical mixture, B) is for the Janus and C) is for the zebra. The lattices are not in scale and the two different colours represent materials A and B. 148
Figure 4.7: Snapshot of the physical mixture lattice used in Monte Carlo simulations at the end of the simulation. The worm like blue structures are the adsorbates. 150
Figure 4.8: The results of the Monte Carlo simulations for decane on different types of lattice. 151
Figure 4.9: The change in the standard Gibbs free energy of adsorption calculated for octane and decane on the physical mixture lattice on similar values of surface coverage. 153
Figure 5.1: The surface energy measurements for p-monoclinic carbamazepine as obtained at the five different temperatures shown at the legend, the numbers in the legend correspond to the temperature, in degrees Celsius, of the experiment. 159
Figure 5.2: The values of spreading pressure obtained from the isotherms at five different temperatures, for the three alkanes of interest. 160
Figure 5.3: A) The Schultz's plot for the determination of the influence of spreading pressure at the temperatures of the study. B) The spreading pressure corrected surface energy measurements, the values in the legend indicates the temperature. 161
Figure 5.4: Stereoscopic image of a macroscopic p-monoclinic carbamazepine crystal, grown in methanol, with four facets of interest marked on it. 163
Figure 5.5: SEM images of carbamazepine recrystallised in ethanol resulting to a p-mononclinic polymorph. 164
Figure 5.6: A) The corrected dispersive component of the surface energy of p-monoclinic carbamazepine (dots) along with the simulated line corresponding to the predicted surface energy distribution. B) The surface energy distribution of the corrected IGC measurement at 25 ^{o}C. 166
Figure 5.7: A) The XRPD scan of the material produced by overnight thermal treatment of p-monoclinic carbamazepine at 140 ^{o}C. The peaks correspond to those of the triclinic polymorph. B and C) SEM images of the triclinic polymorph produced by overnight thermal treatment of p-monoclinic carbamazepine at 140 ^{o}C. 168
Figure 5.8: Surface energy maps for the triclinic polymorph of carbamazepine obtained at different temperatures (the number in the legend corresponds to the temperature of the experiment in degrees Celsius) before (A) and after (B) the spreading pressure correction. 169
Figure 6.1: Schematic showing the interaction of vapours with amorphous (above and below the T_g) and crystalline materials.[48] 174
Figure 6.2: Graphical construction for the determination of the T_g. The legend names the three alkanes used, as also a line corresponding to a common value of T_g found in literature. 179
Figure 6.3: Graphs showing A) The temperature variation of the χ interaction parameter, of three alkanes with copovidone, at a flow rate of 1 sccm, B) The variation of δ_d with temperature in both the glassy and the rubbery region, C) The variation with temperature of the entropic and the ethalpic component of the χ interaction parameter of three alkanes with copovidone at a flow rate of 1 sccm. 182
Figure 6.4: The graphical construction used for the calculation of the two components of the HSP, of p-monoclinic carbamazepine at a temperature of 30 ^{o}C and carrier gas flow rate 1 sccm. 184

Figure 6.5: Graphs showing A) The variation of the χ interaction parameter between three alkanes and copovidone at both the glassy and the rubbery region at different flow rates and B) The variation of δ_d for different flow rates in both the glassy and the rubbery region. 186
Figure 6.6: Graphs showing the variation of the enthalpic (χ_H) and the entropic (χ_S) component of the χ interaction parameter between three different alkanes and copovidone at different flow rates in A) the glassy and B) the rubbery region. 188
Figure 6.7: The extrapolation procedure to obtain the value of χ at a zero flow rate. The results for nonane in the glassy and the rubbery region are shown. 190
Figure 6.8: Graph showing the variation of δ_d, for two different temperatures, with flow rate, along with the corrected value of δ_d corresponding to a zero flow rate. 191
Figure 7.1: The molecular structure of carbamazepine. 198
Figure 7.2: Stereoscopic images, obtained at three different angles, of a macroscopic p-monoclinic carbamazepine crystal, grown in methanol with three facets of interest marked on it. 198
Figure 7.3: The skeletal structure of the copovidone used where the ratio between the vinylpyrrolidone (a) and vinyl acetate (b) in the copolymer is roughly 1:1.2. 201
Figure 7.4: The 5 local environments identified for the C1s in Carbamazepine. The three in blue are considered near identical in the deconvolution. The dashed double bonds represent the aromatic bonding of the two phenyl rings. 203
Figure 7.5: The deconvoluted C1s spectra for A) (101) facet, B) (010) facet and C) (001) facet, as also the N1s spectra for D) (101) facet, E) (010) facet and F) (001) facet. 206
Figure 7.6: Plot showing the correlation of hydrophilicity, measured as the cosine of the advancing contact angle of water on individual crystal facets, with the surface energy hydrophilicity factor, H, and with the C1s XPS polarity. The facets corresponding to every set of points are illustrated on the figure. 209
Figure 7.7: The variation of the surface activity of solution at different polymer concentrations. 210
Figure 7.8: The correlogram from the DLS measurement for different polymer solutions A) in the semi-dilute region and B) in the concentrated region. 212
Figure 7.9: The surface energy variation of the polymer solution for different amounts of polymer, the surface tension at no polymer content is shown at around 73 mJ/m^2. 213
Figure 7.10: The interfacial work and the two components of the surface energy of the polymer solution, at different polymer loadings. 216
Figure 7.11: A) The wettability of polymer solutions and B) The work of adhesion of the polymer solutions on the different facets. 217
Figure 7.12: Stereoscopic image, of a macroscopic crystal grew via top seeded solution growth, showing the dominant (101) facet. 221
Figure 7.13: The correlograms obtained for a polymer solution with $\varphi_p = 0.0157$ at three different temperatures. 226
Figure 8.1: Schematic representation of the variation of enthalpy, entropy and Gibbs free energy of a crystalline material, with temperature. The slope of the enthalpy curve provides the magnitude of the heat capacity of the material at the specified temperature. Similarly, the slope in the Gibbs free energy curve can be used to calculate the entropy of the system.[323] 231
Figure 8.2: Schematics describing, qualitatively the thermodynamics of A) a monotropic and B) an enantiotropic system.[323] 232
Figure 8.3: Schematic showing the thermodynamic stability of the four main anhydrous polymorphs of carbamazepine at ambient conditions. 234
Figure 8.4: BFDH morphology of carbamazepine dihydrate showing the water channels and having the major crystallographic planes. 235

Figure 8.5: Schematic summarising the anhydrous polymorphic outcomes obtained, by other investigators, via experiments at mild temperatures. 236
Figure 8.6: Schematic showing the crystallisation of hemozoin crystals, by a malaria parasite, inside a red blood cell. 238
Figure 8.7: Schematic showing the growth of a crystal in the bioinspired crystal growth system developed. 240
Figure 8.8: XRPD spectra for the crystals obtained from the bioinspired crystallisation system, verifying that the crystals are indeed carbamazepine dihydrate. The spectrum from material obtained via antisolvent crystallisation is used for comparison. 242
Figure 8.9: XRD spectra of the crystals obtained from the four different protocols compared with carbamazepine dihydrate obtained from antisolvent crystallisation. 244
Figure 8.10: Microscopy images showing the examples of the crystals obtained from the four different protocols, A) stereoscopic image of a macroscopic crystal from Protocol 1, B) SEM image of a needle shaped crystal of carbamazepine dihydrate obtained from Protocol 3, C) SEM image of crystals of carbamazepine dihydrate obtained from Protocol 2 and D) SEM image of carbamazepine dihydrate crystals obtained from Protocol 4. 245
Figure 8.11: A) A sections of the (100) facet before start dehydration. B) The same section, when the three types of cracks have appeared. C) The (100) facet of another crystal exposed in dehydration showing the similar types of cracks. 247
Figure 8.12: SEM image of the (100) facet of a carbamazepine dihydrate crystal, not exposed in dehydration, exhibiting the three types of cracks reported with optical microscope. The cracks are created from the vacuum induced dehydration. The image has been processed, post-capture, to enhance contrast. 248
Figure 8.13: SEM images of crystals from Protocol 4 dehydrated at 90 ^{o}C. 248
Figure 8.14: A) SEM image from the (100) facet of a crystal dehydrated partially at 50 ^{o}C. B) A magnified image of the area marked with the red circle, showing the whiskers growing on the facet. C, D) Images showing whiskers growing on (020) facet. 249
Figure 8.15: SEM images from crystals fully dehydrated under vacuum at ambient pressure, showing the absence of any long whiskers. 250
Figure 8.16: A-D) SEM images showing cracks that propagating from the core of the crystal towards the (100) facet. E) SEM image showing cracks propagated to the surface. F) Magnification of image (E). 251
Figure 8.17: Schematic summarizing the polymorph obtained from the dehydration of crystals obtained from different protocols under different dehydration temperatures. The triangle corresponds to the situations where only triclinic polymorph was observed, whereas the star corresponds to the cases were a mixture of p-monoclinic and triclinic polymorphs was observed. 253
Figure 8.18: A) The XRPD patterns obtained from the dehydration of carbamazepine dihydrate from Protocol 4 at two different temperatures compared with the patterns of two anhydrous carbamazepine polymorphs, the stable p-monoclinic and the metastable triclinic. B) The surface energy maps obtained from the IGC measurements on dehydrated crystals from Protocol 4; the dehydration temperatures are shown in the legend. 255
Figure 8.19: A) The surface energy map obtained for anhydrous triclinic carbamazepine. B) The surface energy distribution corresponding to the surface energy map, showing two major peaks. 257
Figure 8.21: A) The surface energy map obtained for material obtained from the dehydration of carbamazepine dihydrate crystals obtained from Protocol 4 at 90 ^{o}C. B) The surface energy distribution corresponding to the surface energy map, showing the peaks corresponding to the anhydrous triclinic and p-monoclinic polymorphs (one low and one high surface energy site was assumed for each of the anhydrous polymorphs, in order to decrease the computational complexities). 260

Figure 9.1: Schematic representation of the dry coating process, commencing with the deaggregation of silica nanoparticles and proceeding with the coverage of the surface of the host particle by primary silica nanoparticles. 282
Figure 9.2: Plot showing the variation of the total surface energy of hydrophilic silica nanoparticles, with RH, and the corresponding values of work of adhesion with water. 284
Figure 9.3: The spreading coefficient calculated for the materials used in this study. 285
Figure 9.4: SEM images of dry coated A-C) paracetamol and D-F) p-monoclinic carbamazepine...286
Figure 9.5: The surface energy maps of coated and uncoated A) mannitol and B)paracetamol 287
Figure A.1.1: Plot of a theoretical BET adsorption isotherm along with a two-term exponential fit.307
Figure A.1.2: The surface excess adsorption isotherms obtained for octane at two temperatures (30 and 40 ^{o}C) along with the fit lines obtained from two-term exponential fitting. The logarithmic plot in both axes enables better visualisation of the good agreement. The area below the curves shown in the figure above is used to calculate the magnitude of spreading pressure for octane at the two temperatures. .308
Figure A.1.3: Schematic showing the workflow for the determination of the corrected value of surface energy, using IGC data. 310
Figure A.2.1: Schematic depiction of a droplet hanging in a fluid. The schematic used cylindrical coordinates.....308

List of tables

Table 2.1: Summary of some of the most important adsorption isotherms available.[3] 66
Table 2.2: Calculated activity coefficients for n-hexane at infinite dilution in n-alkanes.[143].....93
Table 4.1: The properties of the alkanes used in the IGC measurements, which are relevant to this work.....136
Table 4.2: Depiction of the four different packing configurations tested experimentally; in the schematics carbamazepine is shown to have a yellow color, while δ-mannitol is shown with blue color; thus, the physical mixture of the two is naturally depicted green. 145
Table 4.3: The mean and the standard deviation of the experienced energy, calculated from the Monte Carlo simulations.....151
Table 5.1: The contact angle values and the calculated surface energy as they were measured on the four major facets of macroscopic p-monoclinic carbamazepine crystals. 164
Table 6.1: The values of the different components of the HSP at 30 ºC.[24] 177
Table 6.2: Summary of the values of HSP obtained for p-monoclinc carbamazepine at two different carrier gas flow rates at 30 ºC.....185
Table 6.3: The HSP for copovidone at two different temperatures, one in the glassy (30 ºC) and one in the rubbery (120 ºC) region. 192
Table 7.1: The surface tensions of the liquids used in the contact angle measurements at 25 ºC.[67]...200
Table 7.2: The elemental composition of carbamazepine's facets as measured with XPS. 207
Table 7.3: The equilibrium contact angles for the three polar solvents on the different facets calculated from the subsequent results of advancing and receding measurements. 208
Table 7.4: The surface energy values calculated from the averaged contact angles. 208

Nomenclature

Symbol	Description	Units
a_c	Number of successive segments of the polymer chain	-
a_{CH_2}	Surface area of a methyl group	m^2
a_{VdW}	Cohesive (van der Waals) interaction parameter of the van der Waals equation of state.	$Pa*m^6/mol^2$
A	Surface area	m^2
AN	Electron acceptor number	-
AN^*	Corrected electron acceptor number	-
A_{ij}	Hamaker constant between bodies i and j	J
A_{ijk}	Hamaker constant between bodies i and j through medium k	J
b_{VdW}	Repulsive interaction parameter of the van der Waals equation of state.	m^3/mol
B_{11}	Second virial coefficient	m^3/mol
c_p	Heat capacity	J/mol*K
C_A and C_B	Covalent contribution for acceptor (A) and donor (B)	$J^{0.5}/mol^{0.5}$
D	Distance between two bodies	m
DN	Electron donor number	-
e	Electron charge	C
E_A and E_B	Electrostatic contribution for acceptor (A) and donor (B)	$J^{0.5}/mol^{0.5}$
E_{BE} and E_{KE}	Binding energy	eV
f_i	Fraction of surface area	-
$f_{g,i}$	Fugacity of gas i	Pa

$f_{g,1}^{0}$	Fugacity of gas i at the standard state	Pa
g	Gravitational acceleration	m/s^2
$g_2(t)$	Normalised intensity correlation factor	-
$G_2(t)$	Intensity correlation factor	-
h	Planck constant	$m^2/kg*s$
h_i	Thickness of interfacial layer	m
I_t	Intensity	-
j	James-Martin pressure drop coefficient	-
k	Boltzmann constant	m^2*kg/s^2*K
K_A and K_B	Acid (A) and base (B) numbers of a surface	J/mol
K_R	Distribution coefficient	$m3/kg^2$
m	Number of segments of a polymer	-
m_{ads}	Mass of adsorbed molecule	kg
n	Number of molecules	-
n_0	Number of cells in a lattice	-
n_c	Concentration of surface adsorption sites	m^{-2}
n_i	Refractive index of material i	-
N_0	Number of solvent molecules in a lattice	-
N_A	Avogadro's number	mol^{-1}
N_p	Number of polymer molecules in a lattice	-
p	Pressure	Pa
Q_i	Charge of specie i	C
r	Intermolecular distance	m
R	Gas constant	J/mol*K
S	Entropy	J/mol*K

S_{ij}	Spreading coefficient for the spreading of j on i	J/m^2
t_R	Retention time	s
T	Temperature	K
T_{total}	Total time	s
U	Potential energy	J
U_S	Internal energy of solution	J
v	Molar volume	m^3/mol
v_0	Mean stay time of adsorbates on an adsorbent	s
v_f	Frequency of molecules' vibrations	s^{-1}
v_{N_p+1}	Number of segments a polymer chain can take	-
v_X	Frequency of X-rays	s^{-1}
V	Volume	m^3
V_n	Net retention volume	m^3/kg
w	Carrier gas flow rate	sccm (cm^3/min)
W	Work done	J
W_{AB}	Work of adhesion between surfaces A and B	J/m^2
W_C	Work of cohesion	J/m^2
W_{conf}	Total number of configurations of polymers in the lattice	-
z	Valency number	-
z_{nn}	Number of nearest-neighbour cells	-
β	Neumann constant	m^4/J^2
γ	Surface energy/Surface tension	J/m^2
$\gamma_{\mathrm{a,i}}$	Activity coefficient of substance i	-
γ_{ij}	Interfacial tension between surfaces I and j	J/m^2
γ_i^j	Component j of the surface tension of surface i	J/m^2

γ_{SV}^{0}	interfacial energy between the solid and the air, free of the influence of any adsorbed film	J/m^2
Γ	Amount adsorbed	mol/m^2
δ_i^j	Component j of the Hansen Solubility Parameter of substance i	MPa$^{0.5}$
ΔE_i	Enthalpy of vapourisation of substance i	J/mol
ΔG	Change in Gibbs free energy	J/mol
ΔG_{ad}^{0}	Change in the standard Gibbs free energy of adsorption	J/mol
ΔG_{de}^{0}	Change in the standard Gibbs free energy of desorption	J/mol
ΔG_{mix}	Change in the Gibbs free energy of mixing	J/mol
ΔH	Change in enthalpy	J/mol
$\Delta H_{\mathrm{ad}}^{0}$	Change in the standard enthalpy of adsorption	J/mol
ΔH^{AB}	Change in the acid-base component of enthalpy	J/mol
ΔH_{mix}	Change in the enthalpy of mixing	J/mol
ΔS	Change in entropy	J/mol*K
$\Delta S_{\mathrm{ad}}^{0}$	Change in the standard entropy of adsorption	J/mol*K
ΔS_{mix}	Change in the entropy of mixing	J/mol*K
ε_0	Vacuum dielectric permittivity	F/m
ε_i	Dielectric constant of material i	F/m
ε_{ij}	Descriptor of the interaction energy between i and j	-
$\bar{E}$	Experienced energy of adsorption	J/m^2
θ_A	Advancing contact angle	^{o}
θ_C	Equilibrium contact angle	^{o}

θ_e	Adsorption isotherm (non-dimensional)	-
θ_R	Receding contact angle	^{o}
λ	Wavelength	m
μ	Chemical potential	J/mol
π	Surface activity	J/m^2
π_e	Spreading pressure	J/m^2
Π_{osm}	Osmotic pressure	Pa
ρ	Density	kg/m^3
φ_0	Volume fraction of a solvent	-
φ_p	Volume fraction of a polymer	-
Φ	Work function	eV
χ	Flory-Huggins interaction parameter	-
χ_H	Enthalpic component of the Flory-Huggins interaction parameter	-
χ_S	Entropic component of the Flory-Huggins interaction parameter	-
$\chi(\varepsilon)$	Surface energy distribution	-
ψ	Electrostatic potential	J/C
ψ_{mid}	Electrostatic potential at the midpoint between two points	J/C

1. Introduction

1.1 Background

In his pioneering work "On the Equilibrium of Heterogeneous Substances", published between 1875 and 1876, in the Transactions of Connecticut Academy,[1] Professor Josiah Willard Gibbs, introduces for the first time the concept of surface energy, making the following statement:

"We started, indeed, with the assumption that we might neglect the part of the energy, etc., depending upon the surfaces separating heterogeneous masses. Now, in many cases, and for many purposes, as, in general, when the masses are large, such an assumption is quite legitimate, but in the case of these masses which are formed within or among substances of different nature or state, and which at their first formation must be infinitely small, the same assumption is evidently entirely inadmissible, as the surfaces must be regarded as infinitely large in proportion to the masses. We shall see hereafter what modifications are necessary in our formulæ in order to include the parts of the energy, etc., which are due to the surfaces"

In a few lines, well before any systematic investigation of surface phenomena in molecular scale, Professor Gibbs was able to appreciate that surface energy can be of great importance in the micro and nano scale. A lot of progress has been achieved since then. Micro and nano scale phenomena are exploited in various industrial sectors, enabling the development of innovative processes for the manufacturing of high value products.

Solid dosage forms constitute the backbone of the pharmaceutical industry and they are expected to retain this status in the years to come.[2] Owe to the size of the particles used in solid dosage forms, interfacial phenomena driven by, among other factors, surface energy are of crucial importance.[3] The in vivo behaviour of drug products relies heavily on the surface properties of the constituent components. In the majority of the manufacturing processes,

interfacial phenomena play an important role, as well. Despite the sophisticated equipment deployed, difficulties still exist in the development and implementation of mechanistic models accounting accurately for interfacial phenomena.

Surface energy anisotropy is a concept that has been established, in the context of pharmaceutical materials,[4-6] and it has been shown to influence pharmaceutical processes, [7-9] as well as the performance of the drug product.[10] Nevertheless, it has not fully implemented in the design and control of pharmaceutical processes and drug products. Instead, it is quite common to encounter models assuming spherical, energetically isotropic particles. The quantification of surface energy anisotropy, for macroscopic single crystals, via wettability measurements is a tedious process. In powder samples, surface energy anisotropy is manifested as surface energy heterogeneity. Establishing a robust framework for the determination of surface energy heterogeneity could have a great impact in both drug product development and pharmaceutical process development. Among other things, it would provide a robust quality control tool, enabling the determination of the effects of different process operations (milling, drying etc.) on the surface properties of materials.

Amorphous materials (such as polymers, amorphous APIs, and amorphous excipients) are of high importance in pharmaceutical industry and they are expected to gain more ground in the years to come.[11] Appreciating the distinct differences between crystalline and amorphous materials is crucial for the development of characterisation techniques, enabling the accurate determination of the surface properties of amorphous materials. In this context, it should be appreciated that techniques and protocols producing accurate results for crystalline materials will not necessarily provide accurate results for amorphous materials.

Accurate understanding of the surface properties of polymeric materials could shade light for the intriguing wettability behaviour of polymer solutions. The wettability of these

solutions is governed by the surface activity induced by the presence of polymer. The presence of polymer triggers a wettability mechanism, governed by the migration of polymer molecules to the three phase contact line.[12] This phenomenon leads to a solution with lower surface energy than that of the pure solvent. However, it is still unclear how the surface activity influences the van der Waals and the acid-base component of the surface energy of the liquid.

This concept of the different components of surface energy, introduced in early 1960's in a series of papers by Dr Frederick M. Fowkes,[13-14] is key in the understanding of phenomena happening at interfaces. Even though, this concept has not been unchallenged,[15] it still retains its status as the cornerstone of surface thermodynamics. The importance of long range van der Waals forces, in surface energy, is well understood. A lot of ambiguity exists in studies concerned with the investigation of short range acid-base interactions.[16-17]

Furthermore, issues exist with the experimental determination of the surface energy and surface energy heterogeneity of powder samples. As mentioned, the concept of surface energy anisotropy, existing in individual particles, is manifested as surface energy heterogeneity in powder samples, comprising by a large number of individual particles. Traditional wettability methods are incapable to capture surface energy heterogeneity. In this context, the use of Inverse Gas Chromatography (IGC), [18] coupled with *in silico* tools has emerged as a potential tool.[19-20] The cross validation of such a tool with complimentary techniques is, nevertheless, a prerequisite for its industrial implementation.

IGC is a versatile platform, enabling the characterisation of polymers.[21-23] However, despite the plethora of measurements found in literature, there is not a methodology taking into account the amorphous nature of polymers. For instance, the same protocol used for the measurement of the Hansen Solubility Parameter of a crystalline[24] material is used for the

measurement of a polymer. This is a fundamentally erroneous approach that can potentially lead to conclusions far from reality.

1.2 Objectives

In the context set from the previous section, it can be stated that the scope of this work is to use fundamental understanding of interfacial phenomena to improve the state-of-the-art IGC methodologies and use IGC, along with complimentary theoretical, experimental and computational approaches, to investigate intriguing phenomena of pharmaceutical interest.

Thus, the objectives from this project can be formulated as follow:

1) Perform a thorough literature review on the fundamentals of interfacial phenomena and their implications on the characterisation of pharmaceutical materials. Use the results of this investigation to identify gaps in the field which can be filled with the aid of IGC measurements.
2) Develop a theoretical background supporting the need for new methodologies in the measurement of material properties using IGC, for both crystalline and amorphous materials. In this context the following should be investigated:
    a. Improve the state-of-the-art protocols used for the measurement of the surface energy of crystalline materials via IGC measurements.
    b. Validate and expand the state-of-the-art methodology for the calculation of surface energy heterogeneity via the combination of IGC measurements and *in silico* tools. Use this approach to study a physicochemical phenomenon of pharmaceutical interest.
    c. Propose modifications required in the experimental protocols for the accurate prediction of the thermodynamic properties of amorphous materials, via IGC.

3) Use IGC measurements, in tandem with other experimental and *in silico* tools, to investigate the implications of interfaces in phenomena of pharmaceutical interest such as:
    a. The enhanced wettability driven by the presence of polymers in solution.
    b. Dehydration induced concomitant polymorphism.

2. Fundamentals of interfacial phenomena

2.1 Introduction

In an ingenious essay, published in 1873, under the title "Graphical methods in the thermodynamics of fluids",[1] by Professor Josiah Willard Gibbs, the following statement can be found:

"It may occur, however, in the volume-entropy diagram that the same point represent two different states of the body. This occurs in the case of liquids which can be vaporized."

This work, the first one providing a coherent mathematical description of an interfacial phenomenon, marks the birth of a new scientific field dealing with the investigation of phenomena at the boundaries between phases.

Interface is defined as the boundary between any two phases.[25] This definition implies that the two phases can be of the same state or they can even to be identical. For the sake of convenience, in this work, interfacial interactions are distinguished on the basis of the states of matter of the two contacting phases, solid, liquid and vapour. Therefore, six possible interfaces exist, as a result of the binary combination of contacting phases: solid-solid, solid-liquid, solid-vapour, liquid-liquid, liquid-vapour, vapour-vapour. It is obvious that not every type of interface is of tremendous relevance to every single development of manufacturing activity. For instance, the existence of an interface between two vapour phases is unlikely, thus it is omitted in this work and in a large portion of literature. Additionally, the liquid-vapour interface is of less practical importance in the development and manufacturing of solid oral dosage forms. Therefore, these two types of interfaces have not been a matter of investigation in this study.

Solid-solid interactions: The formation of a solid-solid interface plays a crucial role in the processability of pharmaceutical powders, used in both oral and inhalable drug products, influencing the flow of powders,[26-28] mixing[29] and blending operations (including dry coating),[8, 30] as well as milling and micronisation. In this context, it is important to appreciate

the concept of bidirectionality. The properties of materials are altered in processes such as dry coating and milling, but the properties, of the materials fed into these processes will affect the performance of the process as well.[31-34] Furthermore, the formation of solid-solid interfaces is crucial in downstream processes, such as tableting, where various components are formulated together.[35-37]

Solid-liquid interactions: These interaction are of particular importance for the design of operations such as wet milling and wet granulation,[34] where the solid-liquid interface plays a key role in the performance of process equipment. For instance, in wet granulation the affinity of the polymer solution to the solid determines, in a great extent, the formation of the initial granule nuclei, a prerequisite for a successful granulation process. Solid-liquid interactions will also affect the dissolution behaviour of solid dosage forms, both *in vitro* and *in vivo*.[10, 38-39]

Solid-vapour interactions: During processing or storage, pharmaceutical materials are exposed at different types of vapours, with moisture being the most obvious of them.[40-42] The mechanisms determining the interactions of vapours of with solid surfaces are heavily determined by surface properties, such as surface energy and roughness.[43-45] The accumulation of vapours on a material can cause changes in its topography and facilitate the crystallisation of amorphous materials.[46-47] Desolvation phenomena (when the solvent is water are called dehydration phenomena), during which bound and/or unbound solvent is removed, are equally important as solvent uptake phenomena. As the concept of polymorphism is crucial in drug product development, understanding the mechanisms of desolvation induced polymorphism, in other words which polymorph emerges from the desolvation of a solvate under certain conditions, is quite important.[48-50] In addition, adsorption based techniques provide a versatile platform for the characterisation of pharmaceutical materials. Thus, understanding their fundamentals could enhance the understanding of materials' properties.

Liquid-liquid interactions: These interactions, can be of high importance in cases were emulsions are employed to facilitate drug delivery. Furthermore, the interactions in systems such as amorphous solid dispersions, gaining ground in drug product development, is studied by means of liquid-liquid mixing models, with the Flory-Huggins one being the most well known.

2.2 Fundamentals of intermolecular forces

In his Nobel Lecture, delivered on the 12th of December 1910, the Dutch physicist Professor Johaness Diderik van der Waals[51] challenged Boyle's law stating:

"As you are aware the two factors which I specified as reasons why a nondilute aggregate of moving particles fails to comply with Boyle's law are firstly the attraction between the particles, secondly their proper volume".

This statement has been, later, interpreted mathematically (as no equations were provided in the original manuscript of the lecture) by the well-known equation of state, that later on was called van der Waals equation of state, honouring the great pioneer:

$$\left(p + \frac{a_{VdW}}{v^2}\right)(v - b_{VdW}) = RT \qquad \text{Eq. 2.1}$$

where a_{VdW} describes the attractive forces between the molecules, b_{VdW} represents the exclusion volume of a single molecule of the fluid and the rest of the parameters have the same meaning as in the ideal gas law equation. If one takes the limit where both a_{VdW} and b_{VdW} tend to zero, the above equation reduces to the infamous ideal gas law. This is because under these conditions, the system satisfies the two key assumption of the ideal gas law; that the molecules are volumeless and they do not interact. The attractive forces mentioned are the infamous van der Waals forces, which will be discussed in the next section.

2.2.1 Van der Waals forces

Based on the type of molecules involved in the interaction, van der Waals forces are categorised in: Keesom forces,[52] Debye forces[53] and London (or dispersion) forces.[54] These three types of forces are summarised schematically in **Figure 2.1**. For Keesom forces, two polarised molecules interact because of the existence of an inherent difference in charge distribution. In the case of Debye forces, a molecule with a permanent dipole induces charge redistribution to neighbouring molecules with no dipole moments. Finally, London forces arise in molecules without permanent dipoles. The fluctuations on the electron cloud lead to temporary changes in the charge distribution, inducing a charge redistribution, to neighbouring molecules. The mathematical formulation of all three components has the general form:

$$U(r) = -\frac{C}{r^6} \qquad \text{Eq. 2.2}$$

where C is a constant changing slightly for each component and *r* is the intermolecular distance. It should be noted that despite the fact that London forces is the weakest of the three types of van der Waals forces, they are the dominant type of forces arising in interactions involving solid state matter[55]; their importance is inversely proportional to their strength.

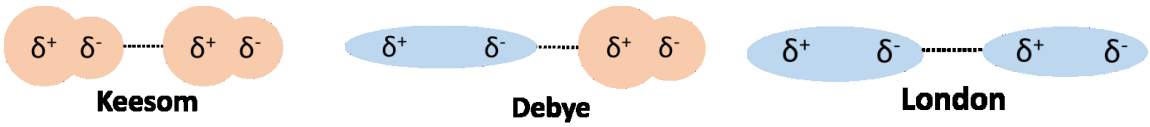


Figure 2.1: Schematic representation of the three components of van der Waals forces.[3]

Apart from van der Waals forces, there exists an interaction between electron poor and electron rich atoms, via the sharing of a lone pair of free electrons donated from the latter to the former, called dipole-dipole interactions. When a hydrogen atom is involved in this interaction, the interaction is called hydrogen bond.[56] Due to its nature, it is characterised by directionality and short-range action, meaning that the electron poor and the electron rich sites

should "face" one another at a close distance, for the interaction to be successful. Directionality leads to the formation of weak molecular structures, held together via dipole-dipole interactions. Owe to the nature of the interactions, their magnitude is affected by the proximity of the molecules, thus it changes depending on the state of the matter. The importance of hydrogen bond interactions is, as expected, more profound in the liquid and the solid state. The extraordinary behaviour of ice is, probably, the most striking manifestation of the effects of these forces.

2.2.2 Thermodynamics of van der Waals forces

Owe to the practical importance of van der Waals forces, a lot of efforts were directed towards the development of a coherent mathematical framework describing. In the following section, two main approaches for the derivation of van der Waal force will be introduced: Hamaker's and Lifshitz's approach.

2.2.2.1 Hamaker's approach

This approach was developed by the Dutch physicist Dr Hugo Christiaan Hamaker.[57] In his work, Hamaker employed an approach grounded on classical notions of quantum physics. If a single spherical molecule is suspended above a flat solid surface, like the one shown in **Figure 2.2**, the total interaction is given by the summation of all the intermolecular interactions between the molecule and the flat surface. Assuming ab n number of molecules on the surface then the potential energy of attraction between the sphere and the surface, U, can be written in terms of the following eqution:

$$\frac{dU}{dn} = -\frac{3\alpha^2 h v_f}{4(4\pi\varepsilon_0)^2 r_s^6} \qquad \text{Eq. 2.3}$$

where r_s is geometric term shown in **Figure 2.2**, α is the polarisability, h stands for the Planck constant, v_f is the frequency of fluctuation and ε_0 is the dielectric permittivity in vacuum.

If it is assumed that the molecules on the surface are spherical, then the number of molecules (n) of the surface can be easily calculated by integrating the following equation:

$$dn = 2\pi\rho \, a da \, dx \qquad \text{Eq. 2.4}$$

where ρ is the concentration of molecules on the surface.

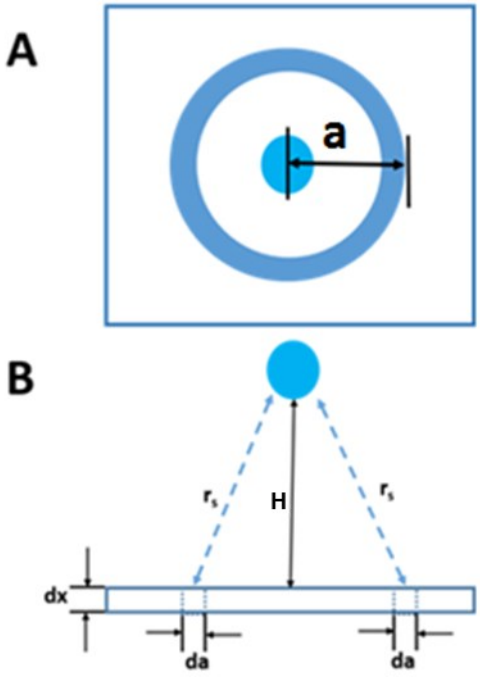


Figure 2.2: Schematic representation for the derivation of potential energy equation by Hamaker's approach A) top view, B) side view.[3]

Combining the equations 2.4 (with a slight modification by Pythagoras' theorem) and 2.5 and integrating in space, the following relation for the potential energy can be obtained:

$$U = \int_0^\infty \int_0^\infty -\frac{3a^2 h v_f}{4(4\pi\varepsilon_0)^2((H+x)^2+a^2)^3} \, 2\pi\,\rho\, a \, da \, dx = \frac{3a^2 h v_f}{4(4\pi\varepsilon_0)^2} \frac{\pi\rho}{6H^3} \qquad \text{Eq. 2.5}$$

As can be seen in **Figure 2.2** α is the radius of the flat solid surface, x is the variable used to measure the perpendicular distance between the molecule and the surface and finally H is the distance from the surface to the suspended molecule.

For a system of two parallel identical plates the number of molecules is given simply by $dn = \rho \cdot \mathrm{dh}$, so the potential is given by:

$$U = \frac{3a^2 h v_f}{4(4\pi\varepsilon_0)^2} \frac{\pi\rho^2}{12H^2} \qquad \text{Eq. 2.6}$$

Similar approach can be followed to include the other two types of van der Waals forces in a mathematical equation or to expand the analysis to different geometries.

On the ground of equation 2.6 Hamaker proposed the infamous constant (A_{ii}), named after him, to provide a measure for the strength of interactions between two similar bodies:

$$A_{ii} = \beta(\pi\rho)^2 \qquad \text{Eq. 2.7}$$

Using Berthelot's principle stating that the interactions between two different bodies interaction can be estimated in terms of a geometric mean, the following equation can be obtained for the Hamaker constant describing the interaction between two bodies:

$$A_{ij} = \sqrt{A_{ii}A_{jj}} \qquad \text{Eq. 2.8}$$

where A_{ii} and A_{jj} are the Hamaker constants of each material in vacuum.

On the same ground, the Hamaker constant describing the interaction between two unlike bodies (1, 2) via a third medium (3), can be calculated via:

$$A_{132} \approx A_{12} + A_{13} - A_{13} - A_{23} = \left(\sqrt{A_{11}} - \sqrt{A_{33}}\right)\left(\sqrt{A_{22}} - \sqrt{A_{33}}\right) \qquad \text{Eq. 2.9}$$

2.2.2.2 Lifshitz's approach

The Soviet physicist Professor Ilya Lifshitz developed a more refined approach, which accounts for all three types of van der Waals forces, to avoid the inherent problems associated with linear additivity of interactions, arising in Hamaker's analysis.[58] Lifshitz's approach ignores the atomic structure and treats the forces between large bodies as continuous media. The Lifshitz theory, developed using quantum mechanics, is grounded on the dielectric

constants and refractive indices of the materials. The Hamaker constant (A_{123}), for two unlike bodies (named 1 and 2) interacting in a medium (named 3), can now be evaluated according to Lifshitz's equation:

$$A_{132} = \frac{3}{4}kT\left(\frac{\varepsilon_1 - \varepsilon_3}{\varepsilon_1 + \varepsilon_3}\right)\left(\frac{\varepsilon_2 - \varepsilon_3}{\varepsilon_2 + \varepsilon_3}\right) + \frac{3h\nu}{8\sqrt{2}}\frac{(n_1^2 - n_3^2)(n_2^2 - n_3^2)}{\sqrt{(n_1^2 + n_3^2)(n_2^2 + n_3^2)}\left(\sqrt{(n_1^2 + n_3^2)} + \sqrt{(n_2^2 + n_3^2)}\right)} \quad \text{Eq. 2.10}$$

where n_i and ε_i stand for the refractive index and dielectric constant of material i respectively. The first term of equation 2.11 describes the Debye and Keesom interactions, where the right one describes London forces.

The Lifshitz's approach successfully overcomes the inherent limitations of Hamaker's approach. However, considering that the Lifshitz's approach is grounded on the continuum theory, it means that it also exhibits an inherent limitation. This limitation is that Lifshitz's theory holds true only when the interacting surfaces are further apart than their molecular dimensions. Furthermore, the practical use of this theory is dependent on the availability of the dielectric constant, for the materials of interest.

2.3 Thermodynamics of particles in solutions

2.3.1 DLVO theory

Let's now consider an electrolyte containing solution with negatively charged particles in it. For the sake of convenience, it is first assumed that only counterions (positive ions with respect to the negatively charged surfaces) exist in the solution. The surfaces of the particles are treated as flat, since in a microscopic point of view curvature effects can be neglected. The chemical potential of the ions described can be written as:

$$\mu = ze\psi + kT\log(\rho) \quad \text{Eq. 2.11}$$

where z corresponds to a particular valency number, e to the electron charge constant ($1.602*10^{-19}$ C), ψ stands for the electrostatic potential, ρ is the number density of ions with valency z at a distance x from the midpoint. Assuming that at the midpoint $\psi = \psi_0 = 0$ then $(d\psi/dx)_0 = 0$. Since the chemical potential at a particular value of x is the same throughout, then the concentration of counterions on that line is given according to Nernst equation as follow:

$$\rho = \rho_0 \exp\left(-\frac{z\varepsilon\psi}{kT}\right) \qquad \text{Eq. 2.12}$$

In this equation ρ_0 is the value of ρ at the midpoint and the rest of the terms have their usual meaning.

The behavior of the electrostatic potential is described by the Poisson-Boltzman (PB)[59] equation, which has the following one dimensional form:

$$\frac{d^2\psi}{dx^2} = -\frac{ze\rho}{\varepsilon\varepsilon_0} \qquad \text{Eq. 2.13}$$

Similarly to the Lifshitz equation introduced in the previous section ε stands for the dielectric constant of the solvent and ε_0 is the permittivity of the free space.

Instead of the simplistic case, with just one counterion described before, a more generic situation is now assumed, with n-number of different counterions, each with different valency, present in the electrolyte. So, at any point on the x-axis, the net charge is given by the summation of the contribution of all the ions.

$$\rho_x = \sum_{i=1}^{i=n} z_i e \rho_{x,i} \qquad \text{Eq. 2.14}$$

Substituting this more generic expression to the PB equation, the following differential equation is obtained, assuming that $ze\psi << kT$ (Debye-Huckel approximation):[53]

$$\frac{d^2\psi}{dx^2} = -\frac{e}{\varepsilon\varepsilon_0}\sum_{i=1}^{i=n} z_i\rho_{0,i}\, exp\left(\frac{ze\psi}{kT}\right) \approx -\frac{e}{\varepsilon\varepsilon_0}\sum_{i=1}^{i=n} z_i\rho_{0,i}\,\left(1-\frac{ze\psi}{kT}\right) \qquad \text{Eq. 2.15}$$

$$= \frac{\psi}{\varepsilon\varepsilon_0 kT}\sum_{i=1}^{i=n}(z_i e)^2\rho_{0,i} = \kappa^2\psi$$

The boundary conditions for the PB equation are that for $x \rightarrow 0$ then $\psi \rightarrow \psi_0$ and for $x \rightarrow \infty$ then $\psi \rightarrow 0$. These boundary conditions lead to a solution of the form:

$$\psi(x) = \psi_0 \exp(-kx) \qquad \text{Eq. 2.16}$$

If the Debye-Huckel approximation is not valid, there is still an analytical solution for the PB equation, provided that the electrolyte under consideration is symmetrical (e.g. KCl dissolved in water, giving K^+ and Cl^-). The symmetrical effect implies that equal number of positive and negative ions exist in the solution. Thus, the PB equation can be written as:

$$\frac{d^2\psi}{dx^2} = -\frac{e}{\varepsilon\varepsilon_0}\sum_{i=1}^{i=n} z_i\rho_{0,i}\, exp\left(\frac{ze\psi}{kT}\right) = -\frac{2ze\rho_{0,i}}{\varepsilon\varepsilon_0}\sinh\left(\frac{ze\psi_0}{kT}\right) \qquad \text{Eq. 2.17}$$

This can be solved analytically using the same boundary conditions as before to give the following general solution:

$$\tanh\left(\frac{ze\psi}{4kT}\right) = \tanh\left(\frac{ze\psi_0}{4kT}\right)\exp(-\kappa x) \qquad \text{Eq. 2.18}$$

where $\kappa^{-1}=(\varepsilon\varepsilon_0)\,/2ze\rho_{0,i}$ is the thickness of the electrical double layer, i.e. the thickness of the first two layers of ions attached on a surface as shown in the following figure:

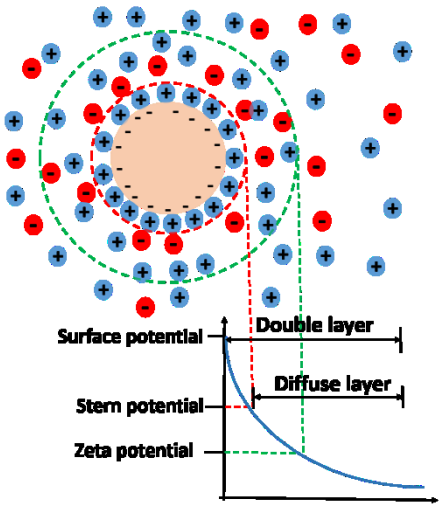


Figure 2.3: Schematic depiction of the double surrounding a negatively charged particle. The graph at the bottom right provides a qualitative depiction of the decrease in the magnitude of the potential at increasing distances from the surface of the particle.[3]

Besides the double layer interactions between the charged surfaces, the presence of ions gives rise to osmotic phenomena. In fact, osmotic pressure arises due to the change in ion concentration between the surface of the charged surfaces and the bulk electrolyte. The magnitude of the osmotic pressure is given simply as:

$$\Pi_{osmotic} = 2kT\rho_{0,i} \qquad \text{Eq. 2.19}$$

Combining the effects of the double layer and the osmotic pressure, the net repulsion force between two surfaces in the solution is given by:

$$F_{rep} = \rho\frac{d\psi}{dx} + \frac{d\Pi_{osmotic}}{dx} \qquad \text{Eq. 2.20}$$

At the midpoint between two charged surfaces, the gradient of electric potential is equal to zero, so repulsion is driven just by the osmotic pressure so:

$$F_{rep} = kT\left(\rho_{mid,cations} + \rho_{mid,anions} - \rho_{0,i}\right) \qquad \text{Eq. 2.21}$$

Substituting the Nernst equation on it, the following form is obtained:

$$F_{rep} = kT\left(\rho_{mid,cations} + \rho_{mid,anions} - \rho_{0,i}\right) = 2\rho_0 kT\left(\cosh\left(\frac{ze\psi_{mid}}{kT}\right) - 1\right) \approx \rho_0 kT\left(\left(\frac{ze\psi_{mid}}{kT}\right)^2\right) = \frac{\kappa^2\varepsilon_0\varepsilon_R}{2}(\psi_{mid})^2 \quad \text{Eq. 2.22}$$

Integrating the above relation with respect to the distance (D) between the two bodies, the interaction energy is obtained:

$$W_{rep}(D) = -\int_0^D F_{rep}\, dD = 2k\varepsilon_0\varepsilon_R\, \psi_0^2 \exp(-\kappa D) \quad \text{Eq. 2.23}$$

To account for the same system, but with spherical particles instead of flat surfaces the equation above can be modified as follow:

$$W_{rep}(D) = 2\pi R_s k\varepsilon_0\varepsilon_R\, \psi_0^2 \exp(-\kappa D) \quad \text{Eq. 2.24}$$

where R_s is the radius of the sphere.

The total interactions between particles in an electrolyte solution are given by adding the above repulsive component with an attractive van der Waals component:

$$W_{tot}(D) = -\frac{AR_s}{12D} + 2\pi R_s k\varepsilon_0\varepsilon_R\, \psi_0^2 \exp(-\kappa D) \quad \text{Eq. 2.25}$$

This equation constitutes the basis of the Derjaguin-Landau-Verwey-Overbeek (DLVO) theory, named after its pioneers. If the concentration of colloidal particles is high, the interparticle distances are small and hence repulsive forces dominate the system. The repulsive forces reach their maximum value at a point called primary minimum, corresponding to the case where $D \to 0$. As the distance increases, in other words are moderate concentrations, the behaviour of the system is determined by a combination of attractive and repulsive interactions. For instance, at high ψ_0 e.g. in strong electrolytes, the increase in attractive forces is such that it can lead to the formation of a minimum point called secondary minimum. In a similar fashion, for systems comprising of weak electrolytes or containing particles with low electrostatic potential, the repulsive forces are so weak that the primary minimum corresponds to a value of

$W_{tot}<0$. This phenomenon corresponds to a highly unstable system, exhibiting extensive flocculation.

DLVO remains one of the main pillars of colloidal research. Although, one should notice that is grounded on the assumption that van der Waals and electrostatic forces are linear additive.[60] Nevertheless, this assumption lacks any solid thermodynamic support. The Debye-Huckel approximation imposed in the PB equation, is the only one that satisfies the superposition principle of electrostatics:

$$-\frac{e}{\varepsilon\varepsilon_0}\sum_{i=1}^{i=n} z_i\rho_{0,i}\, exp\left(\frac{ze\psi}{kT}\right) \approx -\frac{e}{\varepsilon\varepsilon_0}\sum_{i=1}^{i=n} z_i\rho_{0,i}\left(1-\frac{ze\psi}{kT}\right) \qquad \text{Eq. 2.26}$$

As mentioned above, this approximation is valid if $ze\psi << kT$. However, this holds true only for dilute electrolyte solutions. For higher concentrations, the approximation collapses and the averaging of the electric fields on the basis of the Boltzmann distribution becomes increasingly non-physical. Furthermore, it is intuitive that for DLVO to hold true, it means that the ions are not subjected in any influence by any surface forces (such as van der Waals etc.). Obviously, this cannot be the case in any physical system. One could argue that low concentration and low ionic strength are key qualifications for DLVO-based experiments to produce accurate results. This limits the confidence on this type of experiments, investigating phenomena such as protein crystallisation.

2.3.2 Tracking the behaviour of particles in solution, using Dynamic Light Scattering

The experimental observation of the behaviour of particles in liquid media has been a subject of intense research for centuries. In observations performed in the summer of 1827, Professor Robert Brown[61] noted, among other things, that:

"This plant was Clarckia pulchelka, of which the grains of pollen, taken from antherae full grown, but before bursting, were filled with particles or granules of unusually large size, varying from nearly 1/4000th to about 1/3000th of an inch in length, and of a figure between

cylindrical and oblong, perhaps slightly flattened, and having rounded and equal extremities. While examining the form of these particles immersed in water, I observed many of them very evidently in motion; their motion consisting not only of a change of place in the fluid, manifested by alterations in their relative positions, but also not unfrequently of a change of form in the particle itself; a contraction or curvature taking place repeatedly about the middle of one side, accompanied by a corresponding swelling or convexity on the opposite side of the particle. In a few instances the particle was seen to turn on its longer axis. These motions were such as to satisfy me, after frequently repeated observation, that they arose neither from currents in the fluid, nor from its gradual evaporation, but belonged to the particle itself."

This paragraph summarizes, in essence, the main features of Brownian motion. The development of more advanced microscopy methods enabled the study of colloidal particles in solution. However, they were limited by the visible spectrum. Dynamic light scattering (DLS) emerged as a promising tool[62] as it uses a laser beam, with a much smaller wavelength than visible light (140-400 nm), to track the behaviour of particles in solution.

As particles are suspended in solution, moving in different velocities, a monochromatic laser beam passes through the solution. The beam scatters and the scattered light is directed to a photomultiplier. This process is repeated at intervals with a constant duration. The intensity of the scattered light (I_t), a unitless quantity, is plotted against time in a plot similar to the one depicted in **Figure 2.4**.

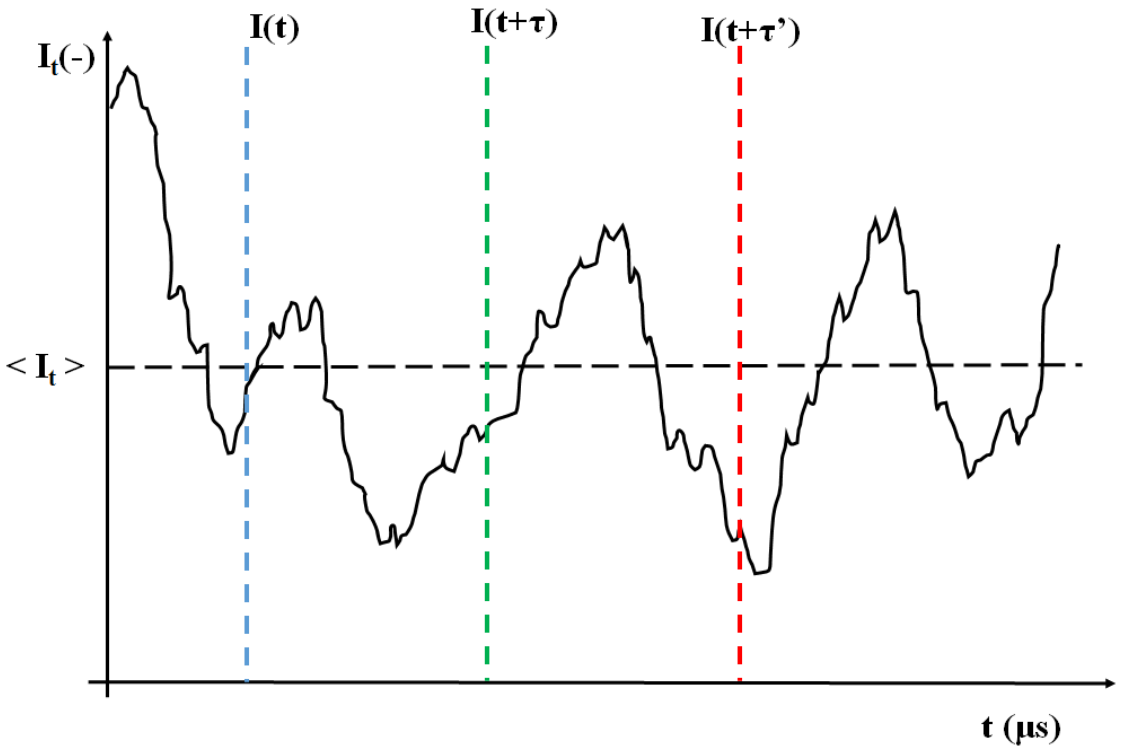


Figure 2.4: Plot of the scatter intensity of laser (I_t) passing through a solution containing colloidal particles. The mean value of the intensity ($<I_t>$) can be seen on the vertical axis, as well as the boundaries of time intervals, which are shown with different colours.

The change in scattering intensity with time is described by the intensity correlation function ($G_2(t)$). Its value is calculated by the following integration over the total time (T_{total}) of the experiment:

$$G_2(t) = \frac{1}{T_{total}} \int_0^T I(t) I(t+\tau) dt \approx \frac{1}{N} \sum_{i=1}^{N} I(t_i)\, I(t_i + \tau) \qquad \text{Eq. 2.27}$$

The normalised form of $G_2(t)$ is calculated by:

$$g_2(t) = \frac{< I(t) I(t+\tau) > - < I(t) >^2}{< I(t) >^2} = \frac{G_2(t) - < I(t) >^2}{< I(t) >^2} \qquad \text{Eq. 2.28}$$

Similarly, to the intensity correlation function, an electric correlation function ($G_1(t)$ and $g_1(t)$ for the normalised form), describing the measured fluctuations, exists and it is related with the intensity correlation function on the basis of the Siegert equation:[63]

$$G_2(t) = B(1 + \beta|g_1(t)|^2) \quad \text{Eq. 2.29}$$

where B and β are constants.

Then the following equation can be applied for the treatment of the experimental data:

$$C(t) = \frac{G_2(t) - B}{B} = \beta e^{-2\Gamma t} \quad \text{Eq. 2.30}$$

The value of Γ can be correlated with the diffusion coefficient of the particles (D) according to the following equation:

$$D = \frac{\Gamma}{\left(\frac{4\pi n_{liquid}}{\lambda} sin(\theta_{detector})\right)^2} \quad \text{Eq. 2.31}$$

where n_{liquid} is the refractive index of the liquid, λ is the wavelength of the laser and $\theta_{detector}$ is the angle at which the detector is located with respect to the sample. Then the classical Stokes-Einsten equation can be used to calculate the size of the particles in solution. It should be clear that owe to the polydispersity of different systems and/or the non-spherical nature of some particles, the calculated values of size obtained from the Stokes-Einstein equation, may not be representative.

By altering the solvent and/or the environmental conditions (e.g. temperature) and performing in situ measurements, one could track the interactions between the particles as they coalesce, grow or shrink. Similarly, to suspensions, DLS can be used to track the behaviour of polymers in solutions, as it enables to track aggregation and de-aggregation phenomena, of crucial importance in industry. In the case of polymer solutions, the study of aggregation and de-aggregation phenomena in different polymer loadings can provide indispensable information about the nature of the solvent.

Solvents can be classified, based on their interaction with polymers in three categories; namely theta, good and poor. In theta solvent conditions, it is assumed that the structure of the polymer chain in solution, resembles a random walk. In other words, the monomers coil

forming a random walk pattern. In good solvent conditions, the interactions between the polymer and the solvent molecules are favourable, promoting homogeneity. Contrary to that, under poor solvent conditions, the solvent-polymer conditions are unfavourable. These three types of solvent conditions can be described in terms of the infamous Flory-Huggins interaction parameter, χ, which will be discussed thoroughly in the 2.8 section of this chapter on "Liquid-liquid interfaces". As a brief mention, for theta solvent conditions, $\chi = 0,5$, for good solvent conditions $\chi < 0,5$ and for poor solvent conditions $\chi > 0,5$.

Plotting the value of normalised correlation function ($g_2(t)$) against τ one can obtain plots similar to those presented in **Figure 2.5**. The presence of two shoulders indicates the presence of a single shoulder as it happens with the continuous line you can see on the figure, corresponds to good solvent conditions, where light scattering occurs only on small delay times indicating the presence of very small entities in the solution. As the system moves away good solvent conditions, a second shoulder appears, corresponding to the occurrence of relatively larger entities in solution (i.e. aggregates). The presence of more than two shoulders indicates the presence of two distinct values of β and Γ. By fitting the experimental data appropriately, using equation 2.33, the relative abundance of large and small aggregates can be determined via the ratio of the corresponding β values.

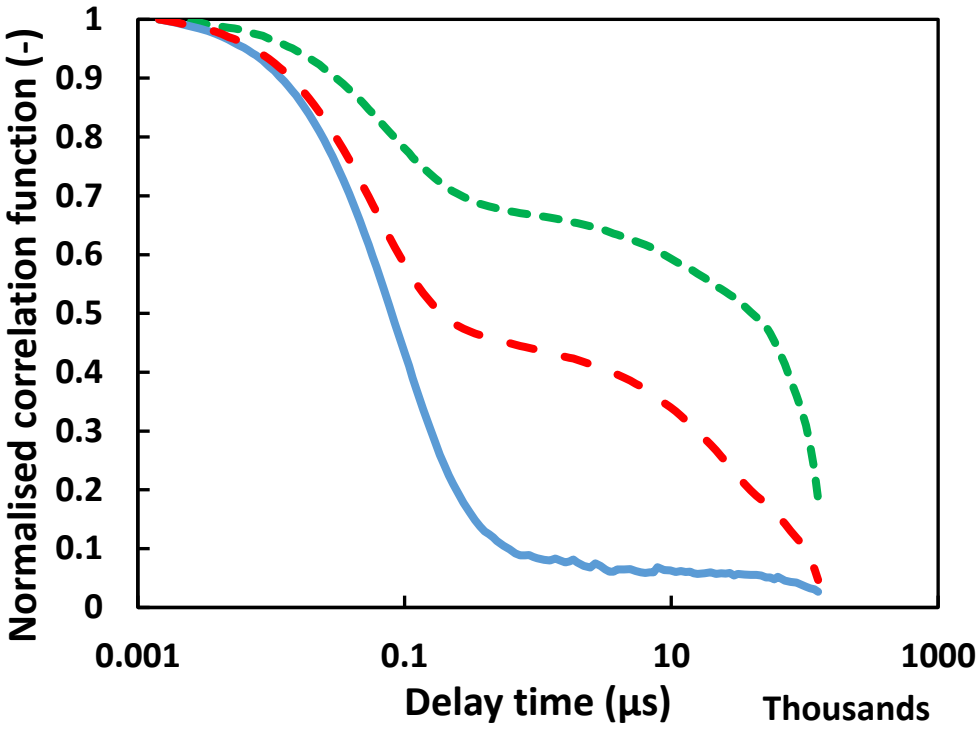


Figure 2.5: Schematic representation of DLS correlograms.

2.4 Surface Tension and Surface Energy

2.4.1 Fundamentals

The molecules, in the bulk of a substance, interact symmetrically with each other, by means of intermolecular forces, the fundamentals of which have been introduced earlier on. On the same time, molecules on the surface of the substance, consequentially at the interface with air, exhibit anisotropic interactions, with the molecules of the same substance, leading to a net force directed towards the bulk of the material. This concept is depicted in **Figure 2.6**. This imbalance in intermolecular interactions at the surface, gives rise to the concepts of surface tension (for liquids) or surface energy (for solids); effectively, a measure of the energy needed to create a unit area of a material.

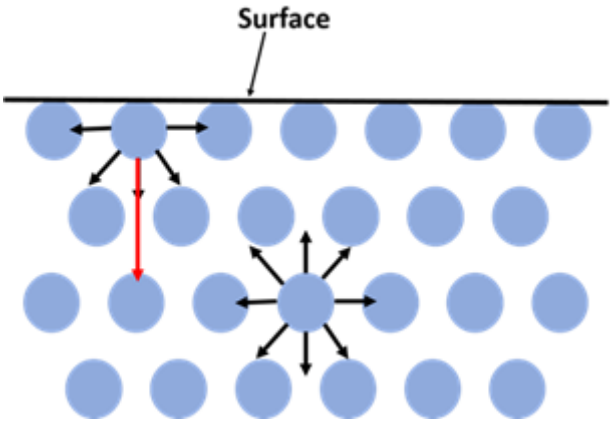


Figure 2.6: Interactions for molecules in bulk and molecules on the surface of a material. For the resultant forces shown on one of the surface molecules with a red arrow, there is an equal magnitude and opposite direction force corresponding to the surface tension.

The simplest interface of concern, examined in this work, is between a liquid and a vapour. If the height of the interface is h_i and its surface area is A, then its volume is given straightforwardly by $V = h_i \cdot A$. The work needed (W) to create a unit area of this interface should is a sum of the effects of surface energy and volume expansion:

$$dW = \gamma\, dA - P\, dV \qquad \text{Eq. 2.32}$$

where γ is the surface tension of the liquid and P is the pressure of the system.

The internal energy of the system is given by the sum of the work required and the change in heat of the system (dQ):

$$dU = dQ + dW = TdS + \gamma\, dA - P\, dV \qquad \text{Eq. 2.33}$$

Thus, the expression for the Gibbs free energy of the system takes the following form:

$$\begin{aligned} dG &= dH - d(TS) = dU + d(PV) - d(TS) \\ &= TdS + \gamma\, dA - P\, dV + PdV + VdP - SdT - TdS \\ &= \gamma\, dA + VdP - SdT \end{aligned} \qquad \text{Eq. 2.34}$$

If the system is isothermal and isobaric then the Gibbs free energy equation collapses further to:

$$\gamma = \left(\frac{\partial G}{\partial A}\right)_{T,P.V} \qquad \text{Eq. 2.35}$$

According to the equation, surface tension is defined as the change in Gibbs free energy per change in surface area at constant pressure, temperature and volume.

If constant pressure and surface area are assumed, instead, then the equation for the change in Gibbs free energy is taking the following form:

$$dG = -SdT \qquad \text{Eq. 2.36}$$

It is known that Gibbs free energy at the interface (dG^s) and surface tension are identical, thus the above equation can be rewritten as:

$$S = -\left(\frac{dG^s}{dT}\right)_P = -\left(\frac{d\gamma}{dT}\right)_P \qquad \text{Eq. 2.37}$$

The negative sign indicates that the surface free energy results to an attractive force between two interacting bodies. The amount of work required, for holding the two different interacting bodies together, is termed the adhesive work, W_A. If the two bodies are identhical then the amount of work is called the work of cohesion, W_c.

2.4.2 The deconvolution of surface energy

In the previous section it has been stated, the surface energy of a material can be defined as the energy required to create a unit area of it. According to Fowkes',[13-14] surface energy can be expressed as the sum of the intermolecular forces exhibited by a body or a surface. Mathematically this corresponds to equation 44, where n can be any surface energy contribution (dispersion forces, hydrogen bonds, dipole-dipole interactions, ion-dipole interactions etc.). This equation is usually written in a simplified form as proposed by Owens and Wendt,[64] with one term accounting for the dispersive interactions, γ^d, and one term accounting for the polar interactions, γ^P.

$$\gamma = \sum_n \gamma^n = \gamma^d + \gamma^P \qquad \text{Eq. 2.38}$$

The dispersive components, technically, includes only dispersion (London) forces, but not the forces induced by the orientation of the interacting molecules (Keesom forces) and by the interactions between a polar and a non-polar molecule (Debye interaction), while the polar component includes everything else. However, for the case of interactions in solid state matter, London interactions are dominating over the other two types of van der Waals interactions. Thus, it is an acceptable formalism to use, for convenience, γ^{LW} and call it the dispersive component of the surface energy.

Work of adhesion (W_{ij}) is the most usual way surface energy is expressed in macroscopic systems and it is effectively a measure of the work required to separate two dissimilar bodies. It's mathematical interpretation is given by:

$$W_{ij} = \gamma_i + \gamma_j - \gamma_{ij} \qquad \text{Eq. 2.39}$$

In the equation above, γ_i and γ_j, correspond to the surface energy of the surfaces i and j respectively where γ_{ij} stands for the surface energy of the interface. Using a geometric mean approximation, the value of the work of adhesion can be calculated by: [65]

$$W_{ij} = 2\left(\sqrt{\gamma_i^{LW}\gamma_j^{LW}} + \sqrt{\gamma_i^{P}\gamma_j^{p}}\right) \qquad \text{Eq. 2.40}$$

The geometric mean approximation is the most commonly used approach, to analyse surface energy data. However, in a model suggested by Wu,[66] harmonic mean approximation is used instead showing to accommodate data better, but posing more calculation challenges.:

$$W_{ij} = 4\left(\frac{\gamma_i^{LW}\gamma_j^{LW}}{\gamma_i^{LW}+\gamma_j^{LW}} + \frac{\gamma_i^{P}\gamma_j^{p}}{\gamma_i^{P}+\gamma_j^{p}}\right) \qquad \text{Eq. 2.41}$$

The polar component of equation 2.44, can be deconvoluted according to van Oss-Chaudury-Good (vOCG) approach. The polar component is separated in order to take in

account the electron acceptor (γ^+)/donor (γ^-) interactions between the two surfaces giving us the following:

$$W_{ij} = 2\left(\sqrt{\gamma_i^{LW}\gamma_j^{LW}} + \sqrt{\gamma_i^+\gamma_j^-} + \sqrt{\gamma_i^-\gamma_j^+}\right) \quad \text{Eq. 2.42}$$

In cases where polar interactions are negligible, the polar components get a zero value. When the surfaces i and j are the same, then $\gamma_i = \gamma_j$. In this situation the term energy of cohesion is used. In their work, the four pioneers propose a split for the acid-base component of the surface energy of different liquids. Water was used as the reference liquid and it was assumed that owe to its amphoteric nature, its acid and base component of the surface energy are equal. Later on, it was found that this approximation was resulting in clearly erroneous results, when it was used for the measurement of the surface energy of solids, by means of wettability measurements that will be presented later on in this chapter. Thus, Della Volpe and Siboni,[67] proposed that the ratio should be $\gamma_{H_2O}^+ = 6.5\gamma_{H_2O}^-$. This assumption resulted in the improvement of the calculated values of the acid-base component of the surface energy.

Despite the fact that the work of adhesion is usually considered to be reversible, meaning that is equal in absolute magnitude to the work required to disjoin the two objects, this has not been verified experimentally. In fact, measurements performed both on the solid-solid and the solid-liquid interface reveal that a number of different factors contribute to an inherent irreversibility of the process of adhesion-separation; meaning that is not the experimental procedure that leads to the irreversible behaviour, but the nature of the process per se.[68-71]

The concept of the Lifshitz-van der Waals component of surface energy is quite well established, however the exact nature of the acid-base component is a field of active discussion. The different approaches, such as the geometric mean approximation, used to describe acid-base interactions do not have a solid theoretical background and it has been adopted on the basis that it has a theoretical meaning for the Lifshitz-van der Waals component. These

theoretical weaknesses have been manifested in lack of consistency in the reported values of acid and base component of the surface energy of materials, reported in literature. These erroneous results are more profound for compounds as ethers, esters and aromatics.[72] Harmonic mean approximation has also been employed instead of the geometric mean one. Nevertheless, there is, also, a lack of theoretical explanation for why acid-base interactions can interact via means of a harmonic mean approximation. While for van der Waals forces the relation between the strength of the force and the distance is given by r^{-6}, for the short range acid and base interactions the strength of the interactions decays much faster, leading to a relation scaling according to r^{-10}.

2.4.2.1 Acid-base interactions

The use of the vOCG approach, including the geometric mean approximation and the even split between γ^+ and γ^- for water, for the determination of the magnitude of the acid-base interactions in certain types of molecules, was challenged. The use of the geometric mean approximation is not grounded to any solid theoretical evidences. Furthermore, doubts were casted owe to the appearance of hydrogen bonds in compounds such as ethers and esters, even though their structure does not permit the formation of such bonds (corresponding to $W_{\mathrm{AB}}^{\mathrm{hydrogen}} = 0$).[72] Instead of the erroneous geometric mean approximation, Fowkes and Mostafa[72] proposed the following relation to calculate the acid-base component of the work of adhesion between two bodies from the enthalpy change at the interface:

$$W^{\mathrm{AB}} = -f * N^{\mathrm{AB}} * \Delta H^{\mathrm{AB}} \qquad \text{Eq. 2.43}$$

In the above equation, ΔH^{AB} stands for the enthalpy of adhesion, N^{AB} for the number of acid-base pairs per unit area and f for a conversion constant used to normalise the units. This equation implies experimental calculation of ΔH^{AB}. In this direction, two different models have been proposed.

The first, developed by Drago[73] is a combination of Mulliken's work[74] on molecular complexes and of the Hard-Soft Acid-Base (HSAB) theory. According to this model, enthalpy can be measured in terms of the tendency of the acidic or the basic components to electrostatic interactions and covalent bonding. Mathematical formulation of it is given in the following form:

$$\Delta H^{\mathrm{AB}} = -(E_A E_B + C_A C_B) \qquad \text{Eq. 2.44}$$

To avoid any misconception, it is important to specify that for this equation the two terms with subscript A correspond to the electrostatic (E) and covalent (C) parameters for acceptor and those with B subscript to the same terms for the donor. The ratio of the two terms, E and C, of each component defines the hardness of the corresponding component. Iodine is used as the reference, giving a ratio equal to one. The validity of this method for solids with very high or very small hardness ratio has been disputed.

The second method for the determination of the acid-base component of the surface energy, was proposed by Gutmann.[75] This theory is represented mathematically as follow:

$$\Delta H^{\mathrm{AB}} = -(K_A DN + K_B AN^*) \qquad \text{Eq. 2.45}$$

in this equation, the *K*'s are parameters characterising the acidic (A) and the alkaline (B) capacity of the solid respectively. In addition, *DN* and *AN** stand for the donor and acceptor number respectively. The first one, *DN*, is a parameter measuring the electron donor characteristics. It is measured based on the heat of mixing of the compound in a solution of antimony pentachloride and dichloroethane. The corrected acceptor number (AN^*) is a parameter calculated indirectly from the acceptor number (*AN*). Acceptor number is measured based on the shifts the compound causes on the P-NMR spectrum of tri-ethyl phosphine. The correction was introduced to account for the effects of van der Waal forces on the shift. Using solvents with different acid/base properties, a plot of $\Delta H^{\mathrm{AB}}/AN^*$ against DN/AN^* can be constructed. The slope would correspond to K_A and the interception with the y axis is K_B

2.5 Thermodynamics of solid-liquid interfaces

2.5.1 Fundamentals

As shown in Section 2.4, the surface tension of a liquid can be defined as the change in the Gibbs free energy of a system of changing surface area at constant temperature, pressure and volume. The process of wetting of a surface (named j) from a liquid (named i) is governed by the formation of an interface (named ij). This process can be interpreted mathematically as the summation of the changes in the Gibbs free energy of each individual component of the system (solid, liquid and interface):

$$\partial G = \left(\frac{\partial G}{\partial A_{\mathrm{i}}}\right)_{\mathrm{T,P}} dA_{\mathrm{i}} + \left(\frac{\partial G}{\partial A_{\mathrm{j}}}\right)_{\mathrm{T,P}} dA_{\mathrm{j}} + \left(\frac{\partial G}{\partial A_{\mathrm{ij}}}\right)_{\mathrm{T,P}} dA_{\mathrm{ij}} \qquad \text{Eq. 2.46}$$

During the wetting process, the following relationship for the change in the surface area of the individual components holds true:

$$dA_i = dA_{ij} = -dA_j \qquad \text{Eq. 2.47}$$

Thus, using the definition of surface energy/tension, the above equation can be written as:

$$-\left(\frac{\partial G}{\partial A_{\mathrm{i}}}\right)_{\mathrm{T,P}} = S_{\mathrm{ij}} = \gamma_{\mathrm{j}} - \gamma_{\mathrm{i}} - \gamma_{\mathrm{ij}} \qquad \text{Eq. 2.48}$$

where S_{ij} is the so called spreading coefficient, relating the work of cohesion between the molecules of the spreading liquid with the work of adhesion between the liquid and the solid. Since the work of cohesion can be expressed in terms of surface tension by the equation $W_{\mathrm{C}} = 2\gamma_{\mathrm{i}}$, then a derivation for the work of adhesion can be obtained as follow:

$$S_{\mathrm{ij}} = W_{\mathrm{ij}} - W_{\mathrm{C}} = \gamma_{\mathrm{j}} - \gamma_{\mathrm{i}} - \gamma_{\mathrm{ij}} \qquad \text{Eq. 2.49}$$

$$W_{\mathrm{ij}} - 2\gamma_{\mathrm{i}} = \gamma_{\mathrm{j}} - \gamma_{\mathrm{i}} - \gamma_{\mathrm{ij}} \qquad \text{Eq. 2.50}$$

$$W_{\mathrm{ij}} = \gamma_{\mathrm{j}} + \gamma_{\mathrm{i}} - \gamma_{\mathrm{ij}} \qquad \text{Eq. 2.51}$$

If the spreading coefficient is positive, then spontaneous spreading occurs and the solid is covered by the liquid. Otherwise, the liquid sits on the solid forming a spherical cap, the

dimensions of which are determined by the balance of forces between the liquid and the solid, as it will be presented in the next section. The measurement of the contact angle between the spherical cap and the solid, constitutes the bases for wettability measurements that they are outlined in the next section.

2.5.2 Experimental techniques

2.5.2.1 Sessile drop contact angle

As mentioned, when the spreading coefficient for the spreading of a liquid droplet on a solid is negative then the droplet does not spread instantaneously but it forms a spherical cap instead. Contact angle measurements enable the calculation of the surface energy of a solid via the measurement of the contact angle of different solvents, with known properties, with it. These measurements exploit the observation described in Young's pioneer essay on "The cohesion of fluids":[76]

"It is necessary to premise one observation, which appears to be new, and which is equally consistent with theory and with experiment; that is, that for each combination of a solid and a fluid, there is an appropriate angle of contact between the surfaces of the fluid exposed to the air, and to the solid"

This statement is depicted schematically in **Figure 2.8**. Let's assume the droplet of a liquid i sitting on a surface j and the corresponding value of the spreading coefficient is negative. If the mass of a droplet is not big (its radius (r) should, in fact, satisfy the condition $r < \sqrt{\frac{\gamma_{LV}}{\rho g}}$, where γ_{LV} is the surface tension of the liquid, ρ is the density of the liquid and g is the gravitational acceleration), the gravity effects can be omitted and the forces determining the shape of the spherical cap are those illustrated in **Figure 2.8.** In this case γ_{SL} stands for the solid-liquid interfacial energy, γ_{SV}^{0} is the interfacial energy between the solid and the air (the one that needs to be determined usually) free of the influence of any adsorbed film on the solid,

γ_{LV} is the surface tension of the liquid and θ_c is the equilibrium contact angle between the solid and the liquid. If the sitting drop is in its equilibrium state then the net resultant force of the system should be zero, as the droplet is not moving. Then assuming, also, that the effects of the three phase contact line are negligible, a force balance analysis can be conducted resulting to the infamous Young's equation:

$$\gamma_{SV}^{0} = \gamma_{SL} + \gamma_{LV} cos\theta_c \qquad \text{Eq. 2.52}$$

In mid-30's Bangham and Razouk,[77-79] in their pioneer work on gas-solid adsorption showed that in the case that the droplet sitting on a surface is in equilibrium with its vapour, then molecules from the vapour phase adsorb on the surface leading to a reduction on the value of solid vapour surface energy. This phenomenon, described in **Figure 2.8**, and is expressed mathematically by the equation:

$$\gamma_{SV} + \pi_e = \gamma_{SL} + \gamma_{LV} cos\theta_c \qquad \text{Eq. 2.53}$$

The reduction in the solid vapour surface energy is indicated by the equilibrium spreading pressure, πe. The value γ_{SV} is in this case the values of the solid vapour surface energy in the presence of an adsorbed film.

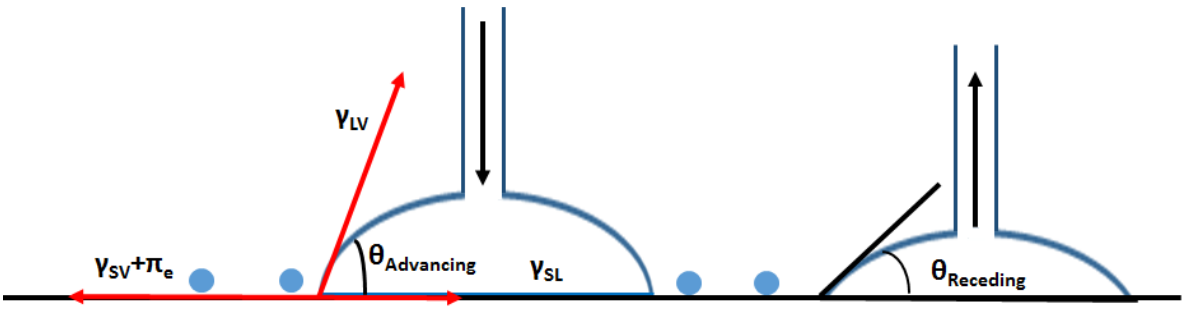


Figure 2.8: Schematic representation of the concept of advancing and receding contact angle measurements, indicating the relevant surface tensions, according to Young's equation and the spreading pressure.

Combining the two equations above, one could, intuitively, derive the following equation for the definition of spreading pressure.

$$\pi_e = \gamma_{SV}^0 - \gamma_{SV} \qquad \text{Eq. 2.54}$$

The determination of accurate values for π_e was a task challenged numerous prominent researchers in the past. A number of studies revealed that for relatively high surface tension and low vapour pressure liquids, including water, spreading on surfaces with relatively low surface energy, where the contact angle is relatively high, the effect of spreading pressure can be neglected.[80-84]

Theoretically, a clean and perfectly smooth ideal surface would lead to a single equilibrium position. Experience lead to the conclusion that droplets do not exhibit a unique contact angle, corresponding to a unique equilibrium position but they experience a range of contact angles. Studies revealed that this spectrum of contact angles is related to the structural[85-87] and chemical heterogeneity[88-91] of the material. The effects of structural heterogeneity on wetting have been investigated in depth, with an example application in the development of biomimetic surfaces.[92-95] Contact angles on non-ideal surfaces can exhibit a maxima or minima, referred to as the advancing and receding contact angle respectively, shown in **Figure 2.9**.

Advancing and receding contact angle measurements have been proposed as an alternative, to capture the true equilibrium contact angle value.[96] The droplet is placed on the surface and is inflated through pumping liquid into it, via a needle. Simultaneously, measurements of the advancing contact angle are taken at regular, constant time intervals. It is important not to overinflate the droplet, because the effects of gravity become significant and it may collapse (stick-slip phenomenon) under its own weight. When the droplet reaches a sufficiently large volume, the contact angle should plateau at a value named the advancing contact angle (θ_A). Then liquid is removed, gradually, from the droplet. At the point where the droplet reaches its minimum possible size and it is about to detach from the needle, it is

expected that its contact angle has reached a minimum value termed the receding contact angle (θ_R). The values of the advancing and receding contact angles are fed in the equations 61-63 to calculate the "real" contact angle (θ_c). The difference between advancing and receding contact angle, is the contact angle hysteresis.

$$r_{\mathrm{A}} = \left(\frac{sin^3\theta_{\mathrm{A}}}{2 - 3cos\theta_{\mathrm{A}} + cos^3\theta_{\mathrm{A}}}\right)^{\frac{1}{3}};\ r_{\mathrm{R}} = \left(\frac{sin^3\theta_{\mathrm{R}}}{2 - 3cos\theta_{\mathrm{R}} + cos^3\theta_{\mathrm{R}}}\right)^{\frac{1}{3}};$$

Eq. 2.55-2.57

$$\theta_{\mathrm{c}} = arccos\left(\frac{r_{\mathrm{A}}cos\theta_{\mathrm{A}} + r_{\mathrm{R}}cos\theta_{\mathrm{R}}}{r_{\mathrm{A}} + r_{\mathrm{R}}}\right)$$

2.5.2.2 Surface roughness and wettability

As mentioned a few paragraphs before, in section 2.4.2, the work of adhesion is not reversible. Thus, inevitable advancing and receding contact angles cannot fundamentally be equal. Nevertheless, structural and chemical heterogeneity of a surface reinforce contact angle hysteresis The effects of structural and chemical heterogeneity have been first addressed by Cassie[97-99] and Wenzel[100] respectively. Wenzel suggested a linear equation to relate the measured (or actual) contact angle with the actual (or theoretical) contact angle, the liquid should take on that specific surface. This was done through the introduction of an roughness coefficient ($r_{\mathrm{w}} > 1$):.

$$r_{\mathrm{w}}\cos(\theta_{\mathrm{actual}}) = \cos(\theta_{\mathrm{measured}}) \qquad \text{Eq. 2.58}$$

If the surface energy of the material results to an angle $\theta_{actual} > 90^{\mathrm{o}}$ then increasing the roughness parameter (rougher surface) would result in an increase in the measured contact angle. The opposite happens with surfaces where $\theta_{actual} < 90^{\mathrm{o}}$. This is a very interesting notion used for the design of hydrophobic surfaces, very important in industrial applications.

The Cassie-Baxter equation was developed to assess the effects of chemical heterogeneity on the contact angle. It is widely used for the characterisation of composite surfaces. It assumes

that the contact angle of a composite surface, wetted by a liquid, can be predicted by the following equation:

$$\cos(\theta) = \sum_{i=1}^{n} f_i \cos(\theta_i) \qquad \text{Eq. 2.59}$$

where f_i stands for the relative surface coverage of component i on the surface of interest and θ_i is the contact angle of the liquid on pure surface i.

2.5.2.3 Solutions containing surface active molecules – Langmuir-Blodgett trough

In the presence of surface active molecules, such as polymers and surfactants, the wetting behaviour of a solution does not obey the notions imposed by the Young's fundamental work. Instead, a fundamentally different wettability mechanism, based on the migration of the surface active molecules on the three phase contact line, emerges.[12, 101-102] This gives rise to the concept of surface activity. This phenomenon leads to improvement of wettability by decreasing the work of cohesion term of the spreading coefficient, shown in equation 2.49. In terms of the force balance, one could envisage surface activity as a component decreasing the surface tension of the wetting fluid. Owe to its similarity to spreading pressure, the Greek letter π is ften used in literature to describe surface activity.

Intuitively, it can be hypothesised that surface activity can, similar to surface tension, be decomposed to a van der Waals and an acid-base component. Nonetheless, no studies exist showing the variation in these two components, upon addition of the surface active molecules. Such a finding would be quite interesting as it will shade light on the importance of the polymer properties, on its macroscopic behaviour in solution.

For the experimental study of solutions containing surface active molecules, the Langmuir-Blodgett trough. This is an ingenious apparatus, first designed by Professor Irving Langmuir[103-104] and Professor Neil Kensington Adam[105-106] to study monolayers. Its use gained a lot of popularity thanks to the work of Professor Katharine Blodgett[107] on multilayer films.

The fundamentals of this apparatus, as it is used today, can be seen in **Figure 2.9**, whereas one should look in literature for the original drawings.

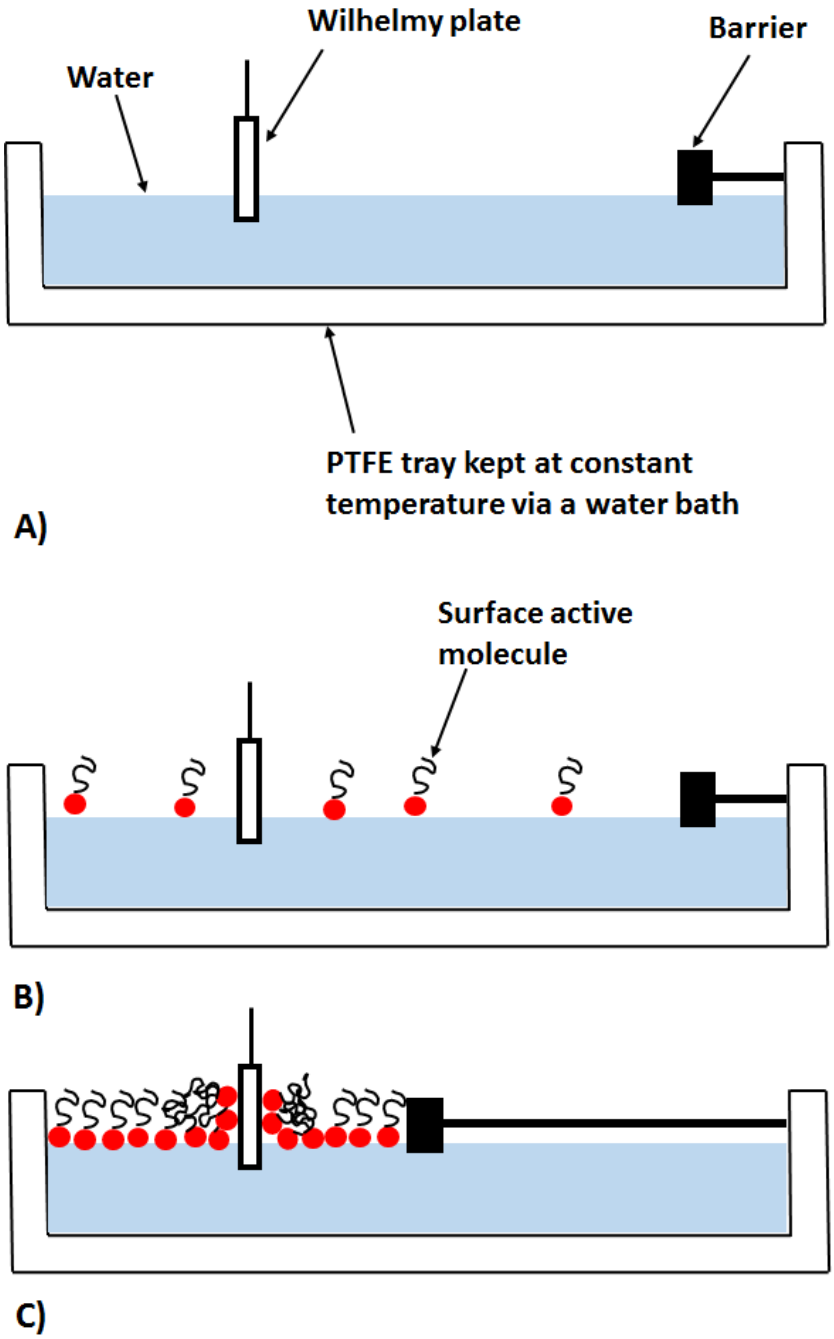


Figure 2.9: Images depicting the operation mode of a Langmuir-Blodgett trough. At the first figure, on the top, the trough contains only water and callibration of the Wilhelmy plate is performed. In the figure in the middle, the surface active molecules have just been added and a weak surface activity

is recorded. In the last figure, the barrier has moved, compressing the surface active molecules, increasing the surface coverage leading to an increase in the surface activity.

In the first frame, one could see the system as is it in the absence of any surface active molecule. A known amount of water is loaded in a temperature controlled tray. Then the Wilhelmy plate is calibrated for the surface tension of the water.

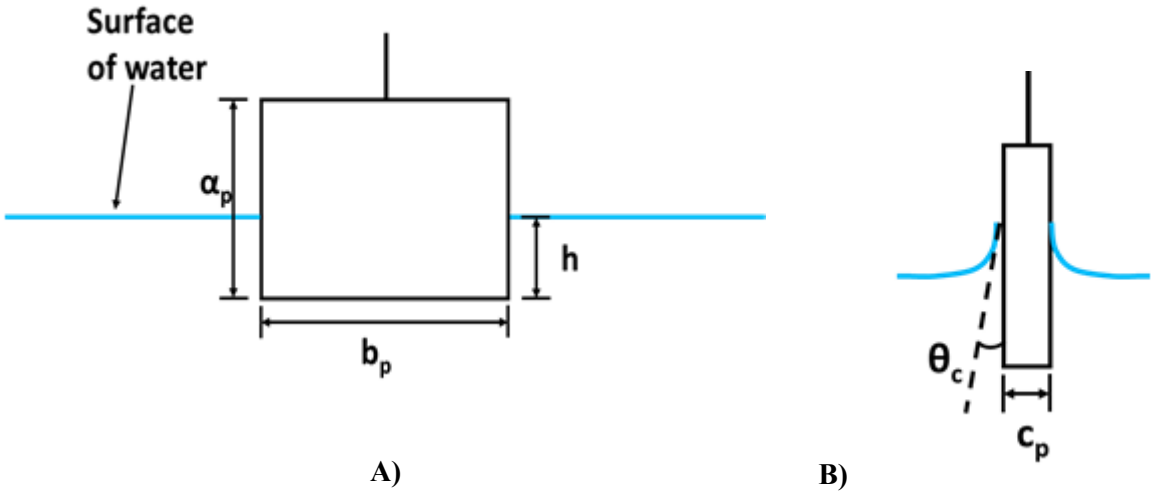


Figure 2.10: Schematic showing the Wilhelmy plate dimensions, as it is immersed in water, from A) side view, B) front view.

For a rectangular parallelepiped Wilhelmy plate with dimensions α_p, b_p and c_p (please refer to **Figure 2.10** as well), immersed in a liquid the following equation describes the force balance of the system:

$$F_p = \rho_p g a_p b_p c_p + 2\gamma_{LV,Water} b_p c_p \cos(\theta_c) - \rho_l g h b_p c_p \qquad \text{Eq. 2.60}$$

in the above equation, the first component on the right hand side of the equation, accounts for the gravitational forces acting on the Wilhelmy plate (ρ_p is the density of the plate and g is the gravitational acceleration), the second one accounts for the interfacial interactions between water ($\gamma_{LW,\ Water}$ is the surface tension of water) and the third component accounts for the effects of buoyancy (ρ_l is the density of the liquid).

A known amount of the polymer or surfactant, dissolved in an extremely volatile solvent, is added in different points of the tray. Since the solvent is extremely volatile, the system is left for a few minutes for it to evaporate. The amount of polymer in the water is known, so as the volume of the water, so the concentration can be calculated.

After the solvent is evaporated, the barrier starts to move at a speed of a few millimetres per minute. As the barrier moves, it pushes the molecules on the surface of the water with it. Thus the surface area available for the active molecules to be spread decreases, increasing the coverage of the surface of water with them. This induces a force on the Wilhelmy plate, which is recorded by means of the equation described above. The experiment proceeds until the recorded value plateaus, indicating the formation of the monolayer. Assuming that the parameters of the system remains constant, then at this point, the surface activity of the solution can be calculated, as follow:

$$\pi = -\frac{\Delta F}{2(b_p + c_p)} \qquad \text{Eq. 2.61}$$

It should be appreciated, that, similarly to the spreading pressure, the measured value of the surface activity, is a relative quantity, measured with respect to a specific surface, in this case the Wilhelmy plate. Thus, it is not used extensively for the design of surfaces or solutions but as a mean to describe the behaviour of active molecules in solutions.

2.6 Solid-vapour interface

2.6.1 Introduction

Adsorption based techniques provide a versatile platform for materials characterisation. They are more reliable than wettability methods and they can provide more insights than their wettability counterparts. Thus, it is not a coincidence that they gain ground in the measurement of the surface energetics of various types of materials.[18, 43] In this section, the readers are

introduced the fundamental concepts of adsorption, with emphasis in heterogeneous adsorption in non-porous materials. The IUPAC definition of adsorption is given as follow:

"An increase in the concentration of a dissolved substance at the interface of a condensed and a liquid phase due to the operation of surface forces. Adsorption can also occur at the interface of a condensed and a gaseous phase"

This definition is grounded theoretically on Gibb's work on "Equilibrium of Heterogeneous Substances".[108] In a footnote in this work, the great pioneer makes the following statement:

"If liquid mercury meets the mixed vapors of water and mercury in a plane surface, and we use μ_1 and μ_2 to denote the potentials of mercury and water respectively, and place the dividing surface so that $\Gamma_i = 0$, i.e., so that the total quantity of mercury is the same as if the liquid mercury reached this surface on one side and the mercury vapor on the other without change of density on either side, then $\Gamma_{2(1)}$ will represent the amount of water in the vicinity of this surface, per unit surface, above that which there would be, if the water-vapor just reached this surface without change of density, and this quantity which we may call the quantity of water condensed upon the surface of the mercury) will be determined by the equation

$$\Gamma_{2(1)} = -\frac{d\sigma}{d\mu_2}$$

(In this differential coefficient as well as the following, the temperature is supposed to remain constant and the surface of discontinuity plane. Practically, the latter condition may be regarded as fulfilled in the case of any ordinary curvatures.)"

Noting that in the above statement σ stands for the surface tension of liquid mercury and Γ for the surface excess, the equation, provided there, is the first mathematical interpretation of adsorption. It is clear from the script that it refers to the phenomenon of the adsorption of vapours on a liquid; no solid is mentioned.

In 1937, three seminal papers were published by Bangham and Radzouk,[77-79] pioneering the studies of vapour-solid adsorption systems. In this work, they make the argument that this isotherm proposed by Gibbs can be utilised for "the case where only one gas is present at the surface of a solid or liquid in which it is nearly insoluble".

As discussed in the section on "sessile drop contact angle", Bangham and Razouk were the first to provide a mathematical framework for the effect of adsorbed vapour on a solid surface. They summarised this framework in terms of the Gibbs adsorption isotherm in the form resembling to the definition of the spreading pressure outlined, as well, in the "sessile drop contact angle":

$$\pi_e = \gamma_{SV}^0 - \gamma_{SV} = RT \int_0^{P_0} \Gamma \, d(\ln(P)) \qquad \text{Eq. 2.62}$$

In the above equation, π_e stands for the spreading pressure, γ_s and γ_{sv} are the surface energy of the solid and of the solid vapour interface respectively, Γ is the surface excess, R, T and P have the same meaning as in the ideal gas law. This equation suggests that when the influence of spreading pressure is negligible, the surface energy of the solid is the same as the solid-vapour interfacial energy.

Following these publications, a lot of work was devoted work on the development of new mathematical models to describe adsorption isotherms corresponding to different conditions. The following table summarises some of the most well-known isotherms describing their main attributes (chronological order is followed, going from the oldest to the most recent).

Table 2.1: Summary of some of the most important adsorption isotherms available.[3]

Name	Equation	Comments
Freudlinch (1909)	$\theta_e = K_0 P_e^{\frac{1}{n}}$	Developed for the investigation of chemisorption on activated carbon.
Langmuir (1918)	$\theta_e = \frac{Q_0 b P_e}{1 + b P_e}$	Emblematic equation, used for the study of monolayer chemisorption.
Brunauer–Emmett–Teller/BET (1938)	$\theta_{monolayer} = \frac{C P_e}{(1 - P_e)(1 + (C - 1)\, P_e]}$	The most widely used isotherm. Employed for the investigation of multilayer adsorption.
Fowler-Guggenheim (1939)	$K_{FG} P_e = \frac{\theta_e}{1 - \theta_e} \exp\left(\frac{2\theta_e W}{RT}\right)$	One of the first attempts to introduce non-idealities in an adsorption isotherm.
Temkin (1940)	$\theta_e = \frac{RT}{\Delta Q} \ln(K_0 P_e)$	One of the first attempts to introduce the concept of surface energy heterogeneity in an adsorption isotherm.
Kiselev (1958)	$K_1 P_e = \frac{\theta_e}{(1 - \theta_e)(1 + k_n \theta_e)}$	Similar to the BET equation, used in the characterisation of mesoporous materials.
Elovich (1962)	$\frac{q_e}{q_{monolayer}} = K_E P_e \exp\left(-\frac{q_e}{q_m}\right)$	A more advanced equation for the investigation of multilayer adsorption.
Hill-de Boer (1968)	$K_1 P_e = \frac{\theta_e}{1 - \theta_e} \exp\left(\frac{\theta_e}{1 - \theta_e} - \frac{K_2 \theta_e}{RT}\right)$	Similar to Fowler-Guggenheim, derived from van der Waals equation of state.

2.6.2 Heterogeneous adsorption

The aforementioned isotherms describe the adsorption phenomena in energetically homogeneous surfaces. Nevertheless, populations of pharmaceutical particulate solids (as well as other materials used in engineering applications) are characterised by energetic heterogeneity. To account for heterogeneity, the following equation has been suggested:[109]

$$\int_0^\infty \chi(\varepsilon)\, d\varepsilon = 1 \qquad \text{Eq. 2.63}$$

The term $\chi(\varepsilon)$ is the probability distribution of having an energy site with energy ε on the surface of a given material. Combining the aforementioned equation with any isotherm equation, the fundamental equation of adsorption on heterogeneous surfaces is derived [77].

$$\theta(T,p) = \int_0^\infty \theta_e(\varepsilon,T,p) * \chi(\varepsilon)\, d\varepsilon \qquad \text{Eq. 2.64}$$

In equations 2.64 and 2.65, θ denotes for the surface coverage and θ_e for the adsorption isotherm.

Similarly, an integral equation can be developed for the mean experienced surface energy of adsorption:

$$\bar{E} = \int_0^\infty \varepsilon * \theta_e(\varepsilon,T,p) * \chi(\varepsilon)\, d\varepsilon \qquad \text{Eq. 2.65}$$

Considering that for a vapour to condensate on a solid surface, sufficient energy should be provided by the latter to overcome the condensation energy of the fluid. In this context, the integration should not be performed from zero to infinity. Instead, the integrals should be rewritten as follow:

$$\theta(T,p) = \int_{\varepsilon_{condensation}(T,P)}^\infty \theta_e(\varepsilon,T,p) * \chi(\varepsilon)\, d\varepsilon \qquad \text{Eq. 2.66}$$

$$\bar{E} = \int_{\varepsilon_{condensation}(T,P)}^{\infty} \varepsilon * \theta_e(\varepsilon, T, p) * \chi(\varepsilon)\, d\varepsilon \qquad \text{Eq. 2.67}$$

In the above equations, the $\varepsilon_{condenstion}$ is the condensation energy, which depends on the adsorption conditions.

Considering that the values of θ and $\bar{E}$ can be determined experimentally, then the above equations can be solved in order to obtain the surface energy distribution $\chi(\varepsilon)$. However, owe to the nature of the equations, there is not a universal analytical solution for these equations. As IGC is a tool of particular interest in the characterisation of pharmaceutical materials, it is quite important that solution schemes have recently been developed for the treatment of IGC data. These efforts have been materialised in the *in silico* tools presented in the works of Jefferson et al. and Smith et al., which constitute the pillars of this field.[19-20, 43]

In Jefferson's work, on the deconvolution of surface energy distributions from IGC measurements, the Henry's law model was used to model heterogeneous adsorption phenomena. According to this model surface coverage increases linearly with vapour pressure. Even though this approximation sounds over simplistic and it was challenged by Smith,[110] in reality Henry's law approximation is quite valid as IGC measurements are generally performed at low partial pressures. In fact, as can be seen, in **Table 2.1**, BET equation at low pressure reduces to Henry's law.

Using the kinetic model proposed for gas adsorption on crystalline solids, Henry's constant (C) was given in the following terms:

$$C = \frac{v_0}{n_c\sqrt{2\pi m_{ads} kT}} \exp\left(\frac{-\Delta G_{\text{ads}}}{kT}\right) \qquad \text{Eq. 2.68}$$

In the definition of Henry's constant given in the above equation, v_0 corresponds to the mean stay time of an adsorbed molecule on the surface, n_c stands for the concentration of surface

adsorption sites, m_{ads} is the mass of an adsorbed molecule, ΔG_{ads} is the change om Gibbs free energy of adsorption, k is the Boltzmann constant, and T the temperature.

Assuming that the adsorbent molecule is an alkane, then the change in the Gibbs free energy of adsorption is given as follow:

$$\Delta G_{\text{ads}} = -2a_{\text{m}}\sqrt{\gamma_{\text{surface}}^{\text{LW}}\gamma_{\text{adsorbent}}^{\text{LW}}} \qquad \text{Eq. 2.69}$$

On the surface of a crystal a finite number of patches/facets exists. Each facets carries a specific surface energy value, depending on the corresponding facet specific surface chemistry. The relative affinity of an adsorbent towards the two different patches is given by the ratio of the Henry's constant corresponding to each facet. In this context, it can be assumed that the concentration of surface sites is facet independent, as it is determined by the crystal lattice parameters. The adsorption of van der Waals fluids is driven only by the dispersive component of surface energy (physisorption). The mean stay time, in this case, is approximately 10^{-2} seconds. Taking into account these two assumptions, the mathematical formulation of the relative surface coverage takes the following form:

$$\frac{C_1}{C_2} = \exp\left(\frac{-\Delta G_{\text{ads},1} + \Delta G_{\text{ads},2}}{kT}\right)$$

$$= \exp\left(\frac{2a_{\text{m}}\sqrt{\gamma_{\text{adsorbent}}^{\text{LW}}}\left(\sqrt{\gamma_{\text{surface},1}^{\text{LW}}} - \sqrt{\gamma_{\text{surface},2}^{\text{LW}}}\right)}{kT}\right) \qquad \text{Eq. 2.70}$$

2.6.2.1 Mapping of energetic surface heterogeneity

Smith et al. used the analysis conducted above to solve the integral equations to obtain de-convoluted representations of the surface energy heterogeneity profiles of crystalline powders, assuming Gaussian distribution of surface energies. The integral equations were solved using the point-by-point integration scheme suggested by Thielmann.[43] The underlying

idea of this method is that the integral equations are solved for different combinations of the surface energy density distribution function ($\chi(\varepsilon)$), until agreement is reached between model and experimental data. For example, let's assume a sample of powder X containing crystals with four different facets A − D, each one with a different surface energy value (let's call it μ). Assumptions are made for the relative contribution of each of the facets to the total surface area (this fraction would be called w) of the sample. If a Gaussian distribution of the energetic sites is assumed then the following equation for the $\chi(\varepsilon)$ can be formulated:

$$\chi(\varepsilon) = \sum_{\mathrm{i=A}}^{\mathrm{D}} \frac{w_{\mathrm{i}}}{\sigma_{\mathrm{i}}\sqrt{2\pi}} e^{-\frac{1}{2}\left(\frac{\gamma_{\mathrm{i}}^{\mathrm{d}}-\mu_{\mathrm{i}}}{\sigma}\right)^2} \qquad \text{Eq. 2.71}$$

In fact, since the values for μ are known from contact angle experiments, only the values of w's can be varied in this equation. By inspection of the IGC data, is possible to obtain some good predictions for them.

This, deterministic, approach for the solution of adsorption problems is grounded on two main assumptions. The first one is that a Boltzmann distribution is adequate to describe the behaviour of gas molecules in microscopic level. The second, is that each adsorption site corresponds to a certain energetic threshold value, determined by the surface energy of the sites. If the adsorbent particles carry enough energy to overcome this threshold, then this site will be definitely filled.

Employing notions similar to those Einstein[111] used to explain the stochastic nature of Brownian motion, adsorption phenomena can be classified as stochastic processes. The stochastic nature of adsorption implies that even if the energy of an adsorbent particle does not exceed the threshold value of the adsorption site, there are still probabilities to adsorb on it. A stochastic description can shade more light in the study of adsorption phenomena, even though the computational complexity scales significantly. In a similar manner, the codes developed by Jefferson[19] and Smith,[20] could be modified. For instance, a Monte Carlo approach can be used

to solve equation 2.71. This has been done by Smith,[110] but has not been published in peer reviewed journals. These stochastic models, were more computationally expensive than the deterministic and thus, they were not very practical for engineering applications.

More advanced Monte Carlo schemes, can also be used.[112-113] However, this requires computationally expensive simulations to be performed on large lattices, making them even less practical for engineering applications than the stochastic models developed by Smith. Nevertheless, these are very powerful simulations that they can be used to investigate, from a more fundamental perspective, adsorption phenomena.

2.6.3 Inverse gas chromatography (IGC)

Powders are energetically heterogeneous and adsorption based methods provide an attractive platform for the determination of surface energy and surface energy heterogeneity. Inverse gas chromatography is the main method developed in this direction. As implied by its name IGC, operates the opposite way conventional chromatography, developed by the Russian botanist Mikhail Tswett[114] at the beginning of the 20th century, does. The stationary phase is the unknown component and solvent probes with known properties are the mobile phase. The retention time, the time required for a solvent to pass through the column of the packed solid, determines the strength of the interactions between the adsorbent and the adsorbate and as it will be shown in the next section, it can be used to measure surface energy.

At its infinite dilution mode of IGC, a relatively small amount of solvent is injected, covering only the high surface energy sites of the stationary phase under investigation. In this mode, the chromatograms obtained are usually Gaussian. In the finite dilution mode, higher amounts of solvents are injected covering larger sections of the stationary phase. In this case, the chromatograms can be skewed. A chromatogram exhibiting back tailing, indicates strong interactions between the adsorbent and the adsorbate, corresponding to the type II and type IV isotherms of IUPAC classification. On the other hand, when fronting is observed, then the

interactions between the adsorbent and the adsorbate are weak, corresponding to the type III or type V isotherms of IUPAC classification. For non-Gaussian isotherms, the retention time (t_R) is not estimated from the maximum of the peak, but from the centre of mass of the chromatogram. Then the retention volume (V_N) can be calculated as follow:

$$V_N = \frac{j}{W_s} w(t_R - t_0) \left(\frac{T}{T_{Ref}}\right) \quad \text{Eq. 2.72}$$

In the above equation, j stands for the James–Martin pressure drop correction factor, accounting for the compressibility of the injected probes. The coefficient W_s stands for the specific surface area of stationary phase. The parameter w is the carrier gas flow rate. In chromatographic processes, this is usually given in Standard Cubic Centimeters per Minute (sccm), which is effectively how many cubic centimeters of gas are passing per minute at standard (reference) conditions of 273.15 K and 1 atm. Then, t_0 stands for the dead time, which is the time required for an inert molecule to travel through the stationary phase. For its determination methane injections are usually employed. Finally, T corresponds to the experiment's temperature and T_{Ref} stands for the reference temperature, which, as mentioned before, is usually at 273.15 K.

2.6.3.1 Thermodynamics of IGC

In the context of IGC, the interaction between the sorbate and the sorbent is determined by a distribution coefficient K_R, which is given by the following ratio:

$$K_R = \frac{V_N}{W_S} = \frac{\Gamma RT}{P} \quad \text{Eq. 2.73}$$

Where V_N is the net retention volume, a measure of the strength of the interaction between the sorbate and the sorbent. The parameter W_S stands for the specific surface area per unit mass of the stationary phase. It can, also, be assumed that the behaviour of solvent molecules, inside IGC, can be described in terms of the ideal gas law. Assuming that $P=P_0$, then from the

definition of the spreading coefficient it can be deduced that π_e=ΓRT. Thus, K_R can be written as:

$$K_R = \frac{\pi_e}{P_0} \qquad \text{Eq. 2.74}$$

From classical thermodynamics, it can be recalled that the standard Gibbs free energy change of adsorption (ΔG_{ad}^0) and desorption (ΔG_{de}^0), at constant temperature, can be expressed according to the classical equation:

$$\Delta G_{ad}^0 = -\Delta G_{de}^0 = -RTln\left(\frac{P_G}{P_0}\right) \qquad \text{Eq. 2.75}$$

where P_G is the pressure of the adsorbate and the terms R and T have the same meaning as in the ideal gas equation. By introducing the relationships derived for the distribution coefficient the above equation takes the following form:

$$\Delta G_{ad}^0 = -\Delta G_{de}^0 = -RTln\left(\frac{V_N P_G}{\pi_e W_S}\right) \qquad \text{Eq. 2.76}$$

Applying fundamental mathematics, the above equation can be rearranged to a linearised form as follow:

$$\Delta G_{ad}^0 = -\Delta G_{de}^0 = -RTln(V_N) + C_1 \qquad \text{Eq. 2.77}$$

The standard enthalpy change of adsorption (ΔH_{ad}^0) can be, similarly, be obtained, in terms of VN, using the well established van Hoff's equation:

$$\Delta H_{ad}^0 = -R\frac{d(\ln(K_R))}{d\left(\frac{1}{T}\right)} = -R\frac{d\left(\ln\left(\frac{V_N}{W_S}\right)\right)}{d\left(\frac{1}{T}\right)} \qquad \text{Eq. 2.78}$$

Thus, the standard entropy change of adsorption (ΔS_{ad}^0), at constant temperature, can be calculated according to the fundamental thermodynamic equation:

$$\Delta G_{\mathrm{ad}}^0 = \Delta H_{\mathrm{ad}}^0 - T\Delta S_{\mathrm{ad}}^0 \qquad \text{Eq. 2.79}$$

The thermodynamic analysis conducted above combined with the relationship between change in standard Gibbs free energy and work of adhesion per molecule constitutes the basis of the two graphical methods used for the determination of surface energy, using IGC; the Schultz method[115] and the Dorris and Gray method.[116-117] The fundamentals of these graphical constructions are outlined in **Figure 2.11**.

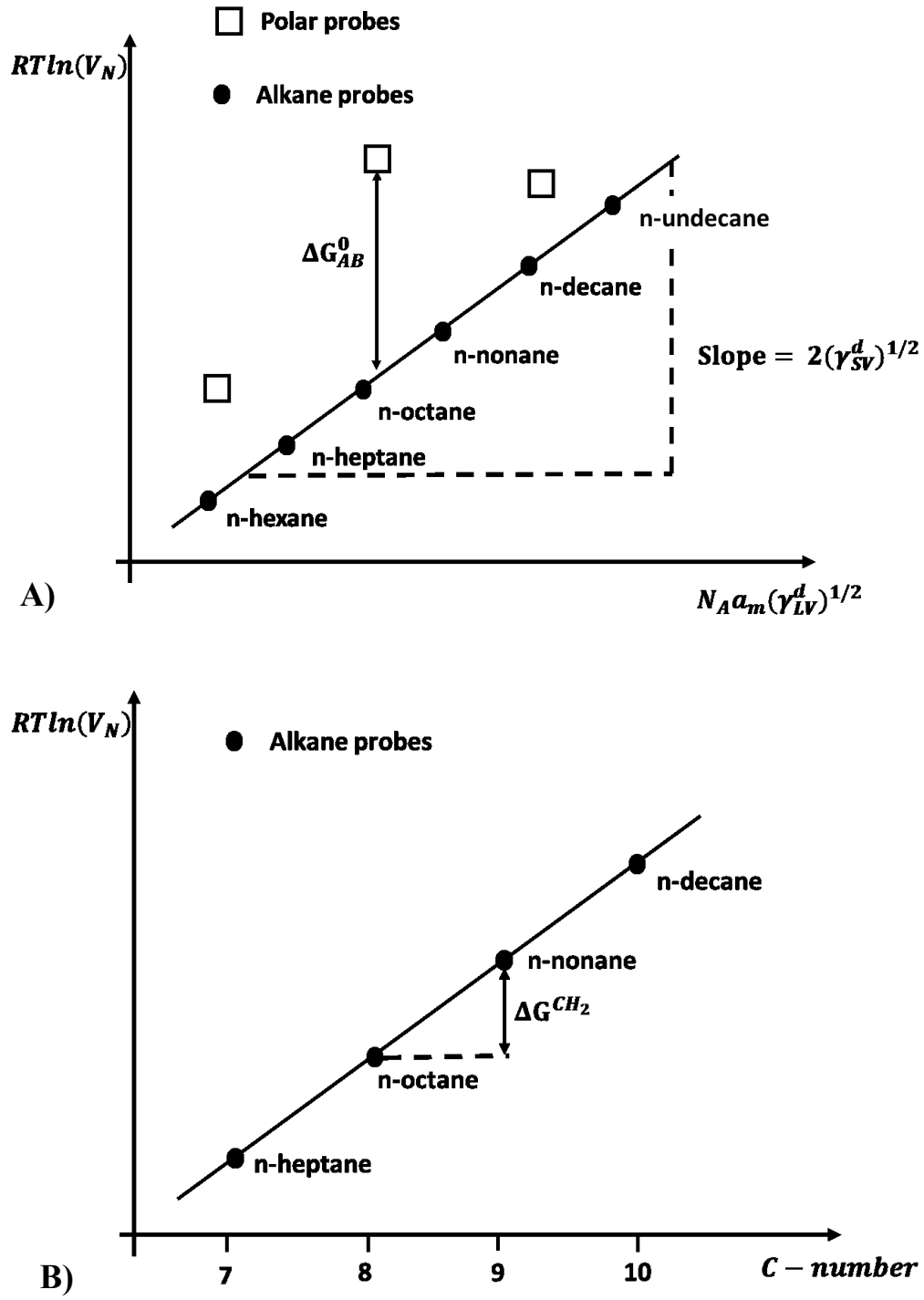


Figure 2.11: Schematic representations of A) the Schultz method and B) the Dorris and Gray method for the determination of surface energy, using IGC measurements.

Chain alkanes are used, in both methodologies, for the determination of the van der Waals component of surface energy. The Schultz method, assumes that the value of the intercept C_1, of equation 2.78, is constant for every solvent probe; neglecting in this way the effect of

spreading pressure. On the ground of this assumption a graphical construction as the one shown in **Figure 2. 12 A**, can be generated. From the slope of the line formed by the van der Waals probes, the van der Waals component surface energy can be calculated.

In the Dorris and Gray approach the concept of the methylene group, as the constituent component of normal chain alkanes is used in the calculation. Using the results from a series of chain alkanes, the change in the standard free energy of adsorption for a methylene group (ΔG^{CH_2}) can be calculated from the retention volumes of two consecutive alkanes. Then the van der Waals component of the surface energy can be calculated according to the following linearised equation:

$$\gamma_{SV}^{d} \approx \gamma_{SV}^{LW} = \frac{1}{4\gamma_{CH_2}}\left(\frac{-\Delta G^{CH_2}}{N_A a_{CH_2}}\right) = \frac{1}{4\gamma_{CH_2}}\left(\frac{RTln\left(\frac{V_{N,n+1}}{V_{N,n}}\right)}{N_A a_{CH_2}}\right) \qquad \text{Eq. 2.80}$$

In the above equation, N_A is the Avogadro's constant, α_{CH2} is the surface area of a methylene group, γ_{CH_2} is the surface tension of the methylene group, $V_{N,n}$ is the retention volume of n alkane and R and T have the same meaning as in the ideal gas equation. Dorris and Gray approach does not have a solid physicochemical background. Thus, even though it is quite common to give similar results with the Schultz approach, it is not extensively used in literature.

The Schultz plot can be used for the calculation of the acid-base component of the surface energy, via the retention volumes of polar probes. The difference between the change in the Gibbs free energy of adsorption of a polar solvent data point and the chain alkanes' regression line provides a measure for the change in the acid-base component of Gibbs free energy of adsorption. This value can be used along with the values of the acid and the base component of the surface tension of the polar solvents to calculate the acid-base component of the surface energy of the solid. The calculations are performed using the notions developed in section 2.4.2.1 of Chapter 2, using a geometric mean approximation to describe the interaction between the adsorbent and the adsorbate. Thus, they are subjected to the limitations discussed there.

Monopolar polar probes such as toluene and dichloromethane are usually employed in these measurements.[118]

As mentioned, the Schultz's construction, even though it has some physical basis, omits the fundamental concept of the spreading pressure, which has been introduced in the very early days of solid-vapour adsorption. It is well documented that the spreading pressure of a gas adsorbing on a solid, with surface energy higher than its surface tension, is positive. Thus, the assumption, that the value of the spreading coefficient is negligible, is not very robust.

The development of Finite Diliution IGC (FD-IGC) enables experiments to be performed at different and relatively high concentrations of the solvent probes. This means that relatively large surface coverage of the packed material can be achieved. By performing experiments at different concentrations, with different solvents, one can construct a surface energy map of the material under investigation. **Figure 2.12** depicts the general form of a surface energy map. Two very distinct region can be identified. At low values of surface coverage, the injected molecules adsorb preferentially on high energy sites, mainly defects, present on the surface of the material. These defects constitute a relatively very small amount of the total surface area and thus, as the surface coverage increases their effect, rapidly, becomes less prominent. When the material is well into the finite dilution zone, corresponding to values of surface coverage higher than 0.03 the surface energy map plateaus. This means that in the finite dilution zone, the energy experienced by the injected molecules is relatively constant. In this context, the surface energy at the plateau is usually regarded as the true surface energy of the material under investigation.

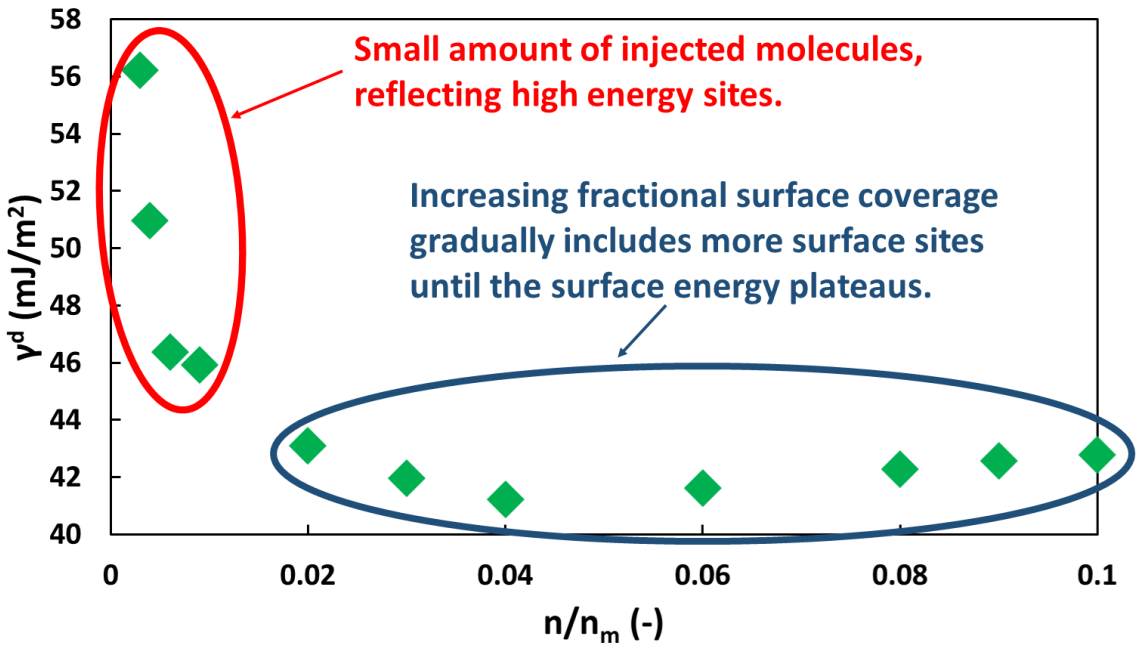


Figure 2.12: Schematic depiction of the qualitative behaviour of a surface energy map obtained by FD-IGC measurements.

Using the notions described in 2.6.3.1 section of this work on the mapping of surface energetics, one could recreate, *in silico*, the FD-IGC experiment and then use an optimisation algorithm to determine the surface energy distribution better describing its experimental data. Considering that crystalline materials have facets, each one carrying a specific value of surface energy, the resulting surface energy distributions, for crystalline powders, would provide an estimate of the relative abundance of each facet in the powder sample under investigation. Theoretically, a robust optimisation algorithm can identify both the relative abundance of each facet and its surface energy. Nevertheless, owing to the highly non-linear nature of heterogeneous adsorption and the need for faster computation times, this can lead to erroneous results. Thus, wettability measurements, on macroscopic single crystals, can be used to measure the facet specific surface energy of the different facets. Facet specific surface energy is an increasing property, meaning that it will be the same for a macroscopic crystal and a micron

sized crystal. Thus, the wettability measurements can be fed into the *in silico* tool in order to enhance its performance.[19-20]

2.7 Solid-solid interface

2.7.1 Fundamental thermodynamics

Surface properties have a critical role in the determination of the contact mechanics. In this context all the types of forces discussed in the first sections of this chapter, including but not limited to van der Waals forces and acid-base interactions are involved in the formation of solid-solid interfaces. Similarly to before, London (dispersion) forces have the lion's share in these interactions. These forces dominate cohesive interactions between particles of the same material or adhesive interactions between particles of different materials. Environmental factors, especially relative humidity, have a major role in the formation of solid-solid interfaces.[119] It should also be mentioned that electrostatics, heavily influenced by both the surface properties of the materials and the relative humidity, play a key role in particle-particle interactions, but they are not studied in this work.[120-123] As discussed in the section on solid-vapour interfaces, hydrophilic materials are more susceptible to the effects of relative humidity.

The mechanisms via which moisture influences adhesive/cohesive interactions are quite though provoking. For instance, the presence of a moisture layer, adsorbed on the surface of a solid, increases the effective distance between adjacent particles, diminishing the effects of surface forces. Similarly, it will contribute to the rapid dissipation of the surface charge, contributing further to the reduction of attractive interactions.

As a rule of thumb, capillary forces are not generally significant when the RH is less than 50%. However as the RH climbs above 65%, capillaries can become the dominant mechanism determining adhesion.[124] For hydrophilic materials, liquid bridges is an important mechanism via which moisture can influence interparticle interactions.[125-127] These bridges are formed by the condensation of moisture in the gaps between particles. These structures start gradually to

dissolve the material and if they remain for prolonged periods of time undisturbed, then they will consume significant amounts of a hydrophilic material. Then, during drying, the evaporation of this moisture will cause the recrystallisation of the dissolved material leading to the formation of solid bridges.[128-129] Solid bridges increase the adhesive/cohesive interactions, between particles, significantly. The formation of solid bridges can be attributed to other factors, such as chemical reactions between adjacent particles of different materials. These reactions can be, of course, facilitated by the presence of moisture. The presence of high level of moisture can develop capillary forces which can enhance adhesive/cohesive interactions.

As it will be discussed in the next chapter, dry coating is a downstream process gaining ground in pharmaceutical industry, used for the improvement of the flowability of cohesive. The surface of cohesive micron-sized particles is coated with sub-micron particles, increasing the roughness. Rough particles have less contact points, hindering the formation of van der Waals interactions. Nevertheless, topographical changes, associated with increased roughening can be induced by milling, as well. In this case, topographical features, such as holes and crevices may induce mechanical interlocking. This will enhance attractive interactions between particles.

2.7.2 Experimental techniques

For the quantitative determination of adhesion/cohesion forces, atomic force microscope can be used. However, as this tool has not been used in the experimental section of this thesis, no section was devoted to it. The interested reader can be referred to literature where abundance of studies exists. Inverse gas chromatography, the operation of which has already been discussed extensively, can be used to calculate adhesion/cohesion forces by measuring surface energy. However, scanning electron microscope and other imagining techniques are also used to understand the interparticulate interactions qualitatively. Spectroscopic techniques such as

X-Ray Photoelectron Spectroscopy (XPS) have also been employed to quantify surface chemistry, critical in the determination of adhesive/cohesive interactions.

2.7.2.1 Scanning Electron Microscope (SEM)

SEM is a microscopy technique enabling the imaging of submicron particles. Owe to the size of particles used in pharmaceutical industry, SEM is an indispensable tool for drug product development. It exploits electron scattering to create images of objects, thus a strong SEM can achieve a theoretical maximum magnification of up to 10^6 times, enabling a resolution of up to 2 nm. SEM is a technique relying on electron scattering, so when a non-conductive material is examined, it appears as a dark shade owe to poor scattering. Thus, non-conducting materials are coated, via vapour deposition, with a thin film of a conducting material, such as gold, prior to SEM examination. The introduction of environmental SEM in 1980s has made now possible to study powder sample in relative humidity ranging from 0 to almost 100%.[130]

2.7.2.2 X-Ray Photoelectron Spectroscopy (XPS)

XPS is a surface probing technique enabling the quantification enabling of the surface chemistry of a solid surface in terms of the different functional groups consisting it. X-ray photons, emitted usually from an anode material bombarded by electrons generated from a tungsten source, are bombarding a surface. The absorption of high energy X-rays, with photon energy between 200 and 2000 eV, leads to the ejection of core electrons, as described by the fundamentals of the photoelectric effect. The kinetic energy of the ejected electrons is recorded and then the electron binding energy can be calculated using the classical quantum mechanical equation:

$$E_{BE} = h_p v_X - E_{KE} - \Phi \qquad \text{Eq. 2.81}$$

Where E_{BE} and E_{KE} is the ejected electron's kinetic energy and the electron binding energy, h_p is Planck's constant, v_X is the frequency of the X-rays and Φ is the work function.

Using simple Newtonian intuition, it is easy to realise that the product of h_p and v gives the energy of the incident X-rays and the work function is the minimum amount of energy required for the ejection of one electron, the cornerstone of the photoelectric effect.

The ejected electron's current density is plotted against calculated electron binding energy to provide a quantitative plot for the frequency of each binding energy. Considering that the binding energy for each individual element is unique, describing not only the pure state of the element but its chemical functionality as well, the XPS plots can provide accurate mapping of the functional group on the measured surface. Utilising reference materials, it was possible to develop huge databanks summarising the binding energy corresponding to a wide range of functionalities. Using these databanks is possible to accurately deconvolute, via optimization, the relative abundance of each functional group.

2.8 Liquid – liquid interface

Contrary to crystalline materials, amorphous materials do not exhibit long range order. This lack of long range order gives rise to the non-equilibrium character of amorphous materials. Thus, amorphous materials are energetically higher than their crystalline counterparts. Amorphous materials are gaining momentum in the development of solid dosage forms. For instance, new strategies for the formulation of poorly soluble amorphous active pharmaceutical ingredients, with the aid of polymers, are currently under investigation. Thus, understanding of the interaction of amorphous materials with fluids is of crucial importance, as it will open new boulevards in the study of the dissolution and bioavailability of drug products and it will allow the development of new characterisation techniques. Thankfully, amorphous materials have been a subject of study, thanks to their versatility making them suitable for a wide range of applications in numerous industries. Thus, a plethora of theoretical, computational and experimental approaches are available for the study of the properties of amorphous materials. The concepts of miscibility and phase separation, both dictated by the

thermodynamics of mixing have been in the epicentre of the efforts of understanding of the behaviour of amorphous materials.

Between 1934 and 1935, Professor Lawrence Bragg and Professor James Williams published a series of three papers[131-133] on the phase transitions in alloys, discussing numerous intriguing topics such as phase separation and metastability. The milestone of this work is the statistical mechanical analysis for the change in the standard free energy of mixing of alloys. In this analysis, the authors introduce, for the first time, the concept of interaction between the atoms of a binary alloy, both similar and non-similar atoms, a concept that has been discussed by other investigators in the same period. This statistical mechanical model constitutes the basis of all the modern computational tools used for the study of phase transitions in complex systems, as it can be generalised in a wide range of systems, introducing more sophisticated types of interactions, to accommodate more intriguing phase transitions.

A few years later, in April 1941, Professor Maurice Huggins[134] published his work on "Solutions of Long Chain Molecules" arguing that the interactions between the long chain molecules and between long chain molecules and solvent molecules influences the osmotic pressure of the system. A few months later, in October, Professor Paul John Flory[135] published a papers providing a more generalised statistical mechanical treatment of the ideas proposed by Huggins. Using arguments similar to those proposed by Bragg and Williams, Flory proposed the implementation of a heat of mixing term, to account for the interactions between the different components of the solution. Later on, this heat of mixing parameter was manifested in terms of a dimensionless parameter, χ, called Flory-Huggins interaction parameter, to honour the pioneers of the field.

In this section a thorough derivation of the classical lattice based Flory-Huggins equation, for a system comprising of a solvent molecule and a macromolecule, is presented, aiming to

provide an understanding of the key assumptions and limitations of the model. Then, it will be shown how the concept of Flory-Huggins interaction parameter can be employed to characterise amorphous materials, via IGC.

2.8.1 The Flory-Huggins theory

One should recall that the change in the Gibbs free energy of mixing is given as follow:

$$\Delta G_{mix} = \Delta H_{mix} - T\Delta S_{mix} \qquad \text{Eq. 2.82}$$

For an ideal solution, where no interaction between the molecules are taking place the value of ΔH_{mix} is equal to zero. This implies that the thermodynamics of mixing are solely governed by the entropy of the system. Furthermore, it is implied that an increase in temperature will favour solubility as it leads to an even smaller value of ΔG_{mix}.

In the classical derivation of the Flory-Huggins equation a binary system comprising of solvent molecules and linear polymer molecules was used. A Meyer type lattice was considered to describe the binary system; a quasi-solid lattice, which enables the interchangeability of the polymer chain with solvent molecules in the lattice cells and where the lattice parameters are independent of the polymer composition.

The lattice comprises of n_0 cells and it is populated by solvent and polymer cells only. The number of solvent molecules is N_0 and the number of polymer molecules is N_p. Each polymer molecule consists of m segments. Each lattice cell can be populated either by a solvent molecule or one segment of a polymer molecule, in order to fulfil the equation:

$$n_0 = N_0 + mN_p \qquad \text{Eq. 2.83}$$

The number of nearest-neighbour cells available for each cell on the lattice is annotated by z_{nn}.

It was assumed that the polymer is well dispersed in the matrix, in other words that the concentration of polymer segment containing cells next to solvent containing cells is the same as the overall polymer concentration.

Following that, intuitively it can be deduced that the number of conformations (α_c) for each successive segment of the polymer chain is given by:

$$a_c = (z_{nn} - 1)\frac{(n_0 - mN_p)}{n_0} \qquad \text{Eq. 2.84}$$

However, the careful reader should notice that the aforementioned number includes a number of impossible conformations such as the case when two segments of the same polymer chain, separated by two or more intervening segments, occupy the same cell. Thus, it can be deduced that the number of conformations that a single polymer chain can take is given by:

$$\begin{aligned} v_{N_p+1} &= \frac{1}{2}(n_0 - mN_p)\left(\frac{z_{nn}}{z_{nn}-1}\right)\left((z_{nn}-1)\frac{(n_0 - mN_p)}{n_0}\right)^{m-1} \\ &\approx \frac{1}{2}(n_0 - mN_p)^m (z_{nn}-1)^{m-1} \end{aligned} \qquad \text{Eq. 2.85}$$

Since there are N_p polymer molecules in the lattice, the total number of their possible configurations is given by:

$$W_{conf} = \frac{1}{N_p!}\prod_{N_p=1}^{N_p} v_{N_p} \qquad \text{Eq. 2.86}$$

The first term on the right hand side of the equation above acts as an operator removing the redundant configuration, differing only by one interchange of one or more pairs of polymer chains. To simplify the equation, the Stirling approximation can be introduced which has the form:

$$N_p! = \left(\frac{N_p}{e}\right)^{N_p} \quad \text{Eq. 2.87}$$

Thus, the equation for the total number of possible configurations of N_p polymer molecules becomes:

$$W_{conf} = \left(\frac{z_{nn}-1}{e}\right)^{(z-1)N_p}\left(\frac{1}{2}\right)^{N_p}\left(\frac{\left(N_0+mN_p\right)^{N_0+N_p}}{{N_0}^{N_0}{N_p}^{N_p}}\right) \quad \text{Eq. 2.88}$$

Then applying the infamous equation written on Professor Ludwig Boltzmann's tombstone the following relationship is obtained:

$$\Delta S_{mix,linear} = -k\left(N_0 \ln\left(\frac{N_0}{N_0+mN_p}\right)+N_p \ln\left(\frac{N_p}{N_0+mN_p}\right)\right)+k(m - 1)N_p((\ln(z_{nn}-1)-1) - kN_p \ln(2) \quad \text{Eq. 2.89}$$

In real solutions, the polymer molecules are not linear, but entangled. The change in entropy associated with the transition from a state of perfect orientation to a state of random entanglement can be calculated by setting the number of solvent molecules equal to zero (N_0=0).

$$\Delta S_{mix,entanglement} = kN_p \ln\left(\frac{z}{2}\right)+kN_p(z_{nn}-1)(\ln(z_{nn}-1)-1) \quad \text{Eq. 2.90}$$

hen to obtain the entropy change for mixing, the following operation is performed:

$$\begin{aligned}\Delta S_{mix} &= \Delta_{mix,linear} - \Delta S_{mix,entanglement} \\ &= -k\left(N_0 \ln\left(\frac{N_0}{N_0+mN_p}\right)+N_p \ln\left(\frac{mN_p}{N_0+mN_p}\right)\right) \\ &= -k\left(N_0 \ln(\varphi_0)+N_p \ln(\varphi_p)\right)\end{aligned} \quad \text{Eq. 2.91}$$

where φ_0 and φ_p are the volume fractions of the solvent and the polymer respectively. As mentioned, for an ideal solution, the enthalpy of mixing is considered to be zero. Thus, the change in the Gibbs free energy of mixing is given by:

$$\Delta G_{mix} = kT\left(N_0 \ln(\varphi_0) + N_p \ln(\varphi_p)\right) \quad \text{Eq. 2.92}$$

This equation, corresponding to a parabolic curve, excludes the possibility of any phase separation as it gives only negative values of ΔG_{mix}.

So, to introduce the concept of enthalpy of mixing, Flory and Huggins used the idea that the molecules in the solution interact with their neighbouring molecules. On the framework of the lattice, this is manifested by the introduction of parameters accounting for the interactions of cells with their nearest-neighbouring cells. In the cell there are solvent containing cells and cells containing polymer segments, so there are three possible types of interactions: interactions between solvent molecules, between polymer segment molecules and interactions between solvent molecules and polymer segments. It has been assumed that the probability of finding, let's say a polymer segment cell next to a solvent cell is proportional to the concentration of the polymer. In addition, they assumed that the polymer solution is incompressible, such as $\Delta H_{mix} \approx \Delta U_{mix}$. So they derive the following expression for the internal energy of the solution:

$$U_S = kT\left(\frac{1}{2}N_0\left(\varepsilon_{00} z\varphi_0 + \varepsilon_{0\mathrm{p}} z\varphi_p\right) + \frac{1}{2}mN_p\left(\varepsilon_{\mathrm{pp}} z\varphi_p + \varepsilon_{0\mathrm{p}} z\varphi_0\right)\right) \quad \text{Eq. 2.93}$$

In the above equation the term ε_{ij} describes the interaction energy between phase i and j. The ½ coefficient was added to eliminate double counting of bonds.

Following the same notions, the total change in the enthalpy of mixing is calculated according to the following relationship, which includes the internal energy of the solvent (U_0^0) and the polymer (U_p^0) and the polymer segments:

$$\Delta H_{mix} = U_S - U_0^0 - U_P^0 = kT\left(\frac{1}{2}N_0\left(\varepsilon_{00} z\varphi_0 + \varepsilon_{\mathrm{op}} z\varphi_p\right) + \frac{1}{2}mN_p\left(\varepsilon_{pp} z\varphi_p + \varepsilon_{0\mathrm{p}} z\varphi_0\right) - \frac{1}{2}N_0\varepsilon_{00} z - \frac{1}{2}mN_p\varepsilon_{pp} z\right) \quad \text{Eq. 2.94}$$

After some mathematical treatment the equation takes the following form:

$$\Delta H_{mix} = kT(N_0 + mN_p)\chi\varphi_p\varphi_0 \qquad \text{Eq. 2.95}$$

Where the χ interaction parameter takes the following form

$$\chi = \frac{z}{2}(2\varepsilon_{0\mathrm{p}} - \varepsilon_{00} - \varepsilon_{pp}) \qquad \text{Eq. 2.96}$$

One should notice that the value of χ, from the classical derivation, is independent of the concentration of the solution. Nevertheless, this is not the case in physical systems, where it was found to have a non-linear correlation with the polymer concentration. Even though χ is a parameter accounting for the heat of mixing, one should understand that the bond formation, occurring during mixing, involves a change in the entropy of the system. The formation of bonds inherently changes the vibrations of a particular molecule around its equilibrium position in the lattice. Thus, the ε parameters should not be regarded as purely enthalpic parameters, but as free energy parameters. To cope with this situation, Guggenheim suggested that the χ parameter could be divided in an enthalpic and an entropic component as follow:

$$\chi = \chi_H + \chi_S \qquad \text{Eq. 2.97}$$

Hildebrand[136-138] suggested that the enthalpic component can be described in terms of the solubility parameters of the system. Solubility parameters are metrics of the cohesive density of a substance, which is given as follow:

$$\delta_i = \left(\frac{\Delta E_i}{V_i}\right)^{1/2} \qquad \text{Eq. 2.98}$$

Where, δ_i, ΔE_i and V_i are the solubility parameter, the enthalpy of vapourisation and the molar volume of compound i. Hence, the χ_H can be formulated, in terms of the analysis conducted for the Flory-Huggins equation, as follow:

$$\chi_H = \frac{V_0}{RT}\left(\delta_0 - \delta_p\right)^2 \qquad \text{Eq. 2.99}$$

So substituting in the fundamental equation, the change in the Gibbs free energy of mixing is given by:

$$\Delta G_{mix} = kT\left(N_0 \ln(\varphi_0) + N_p \ln\left(\varphi_p\right) + (N_0 + mN_p)\chi\varphi_p\varphi_0\right) \qquad \text{Eq. 2.100}$$

This is the infamous Flory-Huggins equation. Empirical studies, show that the classical Flory-Huggins equation holds well for concentrated and dilute polymer solutions, lacking accuracy in intermediate regimes.

Considering that there are no restrictions in the value of the χ, it could be either positive or negative, a number of possible miscibility cases can be observed. Four of them are illustrated in figure. In the first schematic of **Figure 2.14** figure, the value of $\chi >> 0$, indicating strongly repulsive interactions. Thus, the enthalpic component dominates the system, the value of ΔG_{mix} is constantly above zero and hence no mixing is expected to occur.

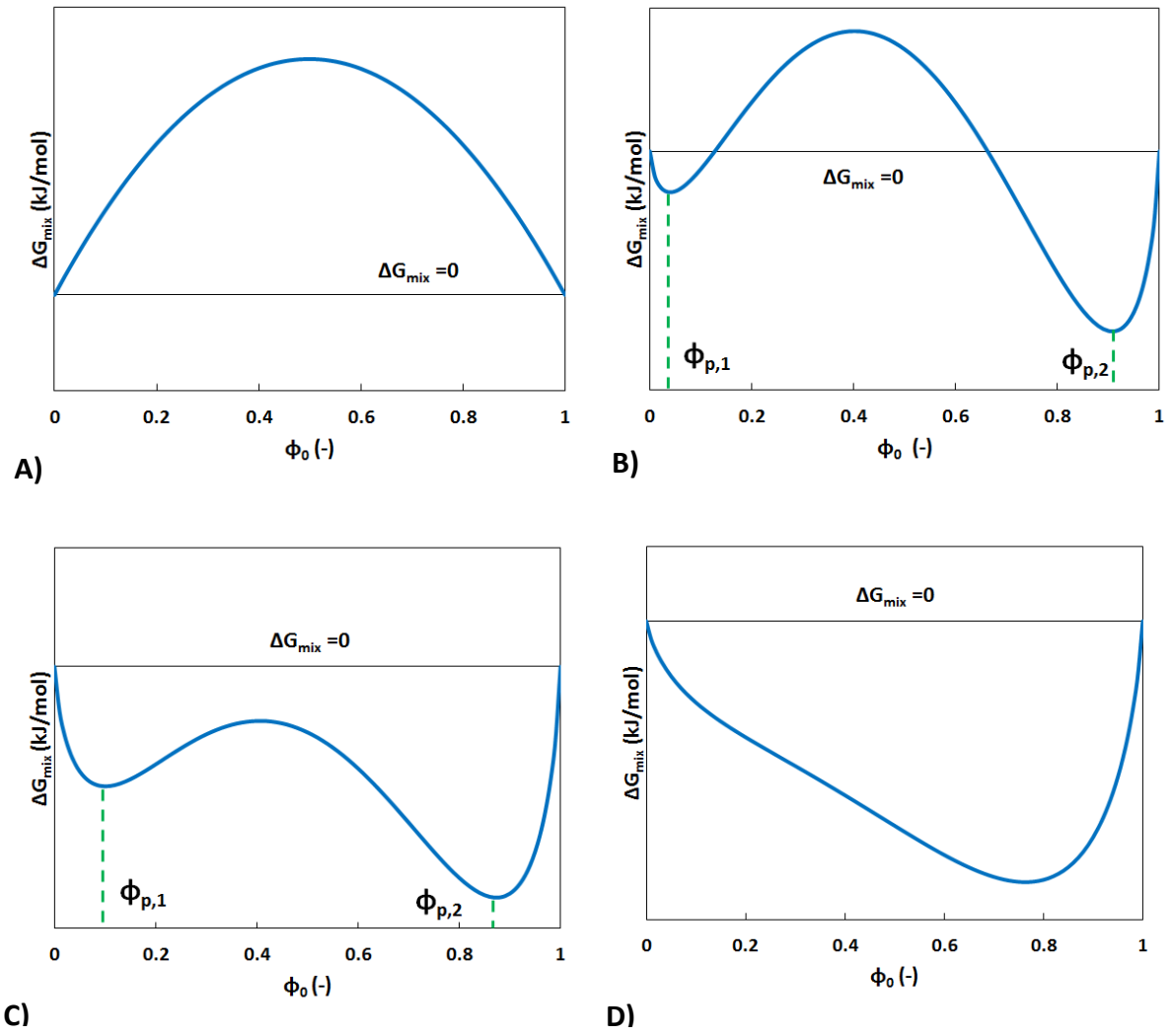


Figure 2.14: Schematic the change in free energy of mixing between a polymer and a solvent depicting the four main cases observed A) no mixing between the two components; B) partial miscibility; C) mixing but with phase separation at some compositions; and D) complete miscibility.

In the second schematic, the system is miscible only for $\varphi_p < \varphi_{p1}$ and $\varphi_p > \varphi_{p2}$. For $\varphi_{p1} < \varphi_p < \varphi_{p2}$, the system will phase separate in a solvent rich phase and a polymer rich phase, the composition of which can be deduced graphically from the curve. In the third schematic, even though $\Delta G_{mix} < 0$, the system does not exhibit miscibility for every single composition. Instead for $\varphi_{p1} < \varphi_p < \varphi_{p2}$ the system will decompose to the two local minima φ_{p1} and φ_{p2}.

Finally, for the last case, full miscibility is expected as the curve does not exhibit any maxima or minima.

2.8.2 Using IGC to measure the χ interaction parameter and beyond

Flory-Huggins equation, has been employed for the study of various systems, beyond polymer solutions, mainly thanks to its simple form. For instance, it has been used in the study of the behaviour of surfactants and amorphous solid dispersions. Owe to its inherent limitations stemming from weak assumptions such as that the polymer segments and the solvent molecules are equal in size, Flory-Huggins equation was subjected to various modifications in order to become more robust. Further modification were proposed in order to capture some more exotic phenomena, like the appearance of Lower and Upper Critical Solution Temperatures and the formation of closed loop phase diagrams.[139-140] Some of the modifications, attempted to model the evolution of the value of χ over different concentrations of polymer. Others, attempted to introduce some additional terms, describing entropic phenomena upon physical bond formation.[141-142]

In 1971, in a paper published in "Macromolecules", Patterson[143] proposed a framework for the measurement of the χ interaction parameter using IGC. He assumed that for a polymer sample packed in a chromatographic column, interacting with a gas, the partition coefficient of is given by:

$$K_R = \frac{N_{polymer}}{V_{polymer}} \frac{V_{gas}}{N_{gas}} = \frac{V_N}{V_{polymer}} \qquad \text{Eq. 2.101}$$

Where, $N_{polymer}$ and $V_{polymer}$ stand for the number of polymer molecules and the molar volume of the polymer respectively. Similarly, N_{gas} and V_{gas} stand for the number of the probe molecules in the vapour phase and the molar volume of the gas respectively. Finally, V_N stands for the retention volume, similarly to what it has been described before for the interaction between a gas and a solid.

The activity coefficient for the probe gas ($\gamma_{a,1}$) in this system is given by the well-known equation:

$$\gamma_{a,1} = \frac{a_1}{x_1} = \frac{f_{g,1}}{x_1 f_{g,1}^0} \quad \text{Eq. 2.102}$$

In the above equation α_1 is the activity of the gas, $f_{g,1}$ is the fugacity of the gas, $f_{g,1}^0$ is the fugacity at the standard state. Finally, x_1 stands for the mole fraction of the gas. Assuming that the concentration of the gas probe is very small compared to the volume of the carrier gas, then $x_1 \rightarrow 0$. Under these conditions, the activity coefficient at infinite dilution (γ_1^∞) can be written as follow:

$$\gamma_{a,1}^\infty = \frac{P_1}{P_1^0} \quad \text{Eq. 2.103}$$

Where P_1 is the gas pressure and P_1^0 is the saturation pressure of the gas. Assuming ideal gas behaviour and using the equation for the partition coefficient the following expression for the activity coefficient at infinite dilution can be obtained:

$$\gamma_{a,1}^\infty = \frac{N_1}{V_1}\frac{RT}{P_1^0} = \frac{RT}{P_1^0}\frac{N_{polymer}}{V_N} \quad \text{Eq. 2.104}$$

By introducing the second-virial coefficient (B_{11}) to account for the non-idealities in the behaviour of the probe gas, one could obtain the following equation:

$$\ln(\gamma_{a,1}^\infty) = \ln\left(\frac{RT}{P_1^0 V_N M_p}\right) - \frac{P_1^0}{RT}(B_{11} - V_1) \quad \text{Eq. 2.105}$$

In this equation, it is counterintuitive the fact that as $M_p \rightarrow \infty$, the activity coefficient $\gamma_{a,1}^\infty = -\infty$. This suggests that the activity coefficient is not a suitable reference quantity for a system where the value of the molecular weight of the polymer M_p, can still be determined accurately. In the same direction, it is obvious that a composition based quantity such as the activity coefficient at infinite dilution, is inadequate to describe the interactions in a

concentrated polymer solution. So, an alternative thermodynamic quantity was selected on the ground of these limitations. The weight fraction of the gas phase (1) was picked as an ideal candidate. **Table 2.2** presents a comparison of the activity coefficient for n-hexane at infinite dilution in different n-alkanes, as calculate using the classical definition of γ_1^∞ and the alternative one proposed on the ground of the weight fraction. It is evident that the latter gives more realistic quantities. Thus, it will be used for the rest of this derivation.

Table 2.2: Calculated activity coefficients for n-hexane at infinite dilution in n-alkanes.[143]

n-Alkane	$\ln(\gamma_{a,1}^\infty)$	$ln\left(\frac{a_1}{w_1}\right)^\infty$
C_{20}	-0.10	0.90
C_{40}	-0.39	1.25
C_{60}	-0.65	1.39
C_{100}	-1.03	1.50
C_{1000}	-3.14	1.67
C_∞	-∞	1.69

Thus, the equation for the activity coefficient at infinite dilution is now written as follow:

$$ln\left(\frac{a_1}{w_1}\right)^\infty = \ln\left(\frac{RT}{P_1^0 V_N M_p}\right) - \frac{P_1^0}{RT}(B_{11} - V_1) \qquad \text{Eq. 2.106}$$

The classical Flory-Huggins equation can be differentiated, with respect to the number of solvent molecules, and slightly modified to get the following form for the change in the molal Gibbs free energy of mixing:

$$\Delta\bar{G}_{mix} = \text{RT} * ln\left(\frac{a_1}{w_1}\right)^\infty = \text{RT}\left(\ln\left(\frac{v_1}{v_p}\right) + \varphi_p\left(1 - \frac{V_1}{M_p v_p}\right) + \chi\varphi_p^2\right) \qquad \text{Eq. 2.107}$$

where v_1 and v_2 stand for the specific volume of the solvent and the polymer respectively.

For a concentrated polymer solution, $\varphi_p \to 1$, resulting to the following equation:

$$\chi^{\infty} = \ln\left(\frac{RTv_2}{P_1^0 V_N M_p V_1}\right) - \frac{P_1^0}{RT}(B_{11} - V_1) - \left(1 - \frac{V_1}{M_p v_p}\right) \quad \text{Eq. 2.108}$$

Thus, an equation has been derived enabling the determination of χ using IGC. One should stand critically on the key assumption that this equation is valid only for the case of a concentrated polymer solution. Thus, it is important to understand, that, contrary to the surface energy measurements described in the section on "Solid-Vapour interfaces", it is not reasonable to run IGC experiments at the finite dilution mode, as the fundamental equations do not support them theoretically.

2.8.3 Hansen Solubility Parameters

The concept of the Hildebrand solubility parameters was expanded by Hansen,[24] who proposed that the cohesive forces contributing to the vapourisation energy can be deconvoluted in a similar manner as the surface energy. The following equation was proposed for the cohesive energy (E_{coh}):

$$E_{coh} = E_d + E_p + E_h \quad \text{Eq. 2.109}$$

Where E_d, E_p and E_h correspond to the dispersive, the polar and the hydrogen bond component of the cohesive energy. In a similar manner, the solubility parameter is deconvoluted as follow:

$$\delta^2 = \delta_d^2 + \delta_p^2 + \delta_h^2 \quad \text{Eq. 2.110}$$

In the above equation δ_d, δ_p and δ_h stand for the dispersive, the polar and the hydrogen bond component of the solubility parameter.

Recalling Equation 2.99 and combining it with the recently derived Equation 2.108 one should obtain the following equation linking HSP with the χ interaction parameter:

$$\frac{\delta_1^2}{RT} - \frac{\chi^{\infty}}{V_1} = \frac{2\delta_2}{RT}\delta_1 - \frac{\delta_2^2}{RT} \qquad \text{Eq. 2.111}$$

In the above equation, δ_1 and δ_2 stand for the total HSP of the probe molecule and the stationary phase, respectively. The parameter V_1 is the molar volume of the probe molecule, χ^{∞} is the interaction parameter calculated directly from IGC data via Equation 2.109. Finally, R and T have the same meaning as in the ideal gas equation. Using the same notions used for the development of graphical constructions, such as the Schultz's plot, for the calculation of the surface energy of a material, a graphical construction has been developed for the calculation of HSP using multi-solvent IGC measurements. By performing infinite dilution measurements, using alkanes, aprotic polar molecules and alcohols one could create a graphical construction, like the one depicted in **Figure 2.15**, on the ground of Equation 2.111. From this graphical construction one could calculate the slope of the lines resulting from alkanes ($m_{n\text{-}Alkanes}$), aprotic polar molecules ($m_{Aprotic}$) and alcohols ($m_{Alcohols}$). On this ground, the different components of the HSP of the stationary phase (δ_2) are calculated according to the following equations:[23]

$$\delta_{d,2} = \frac{m_{n-Alkanes}RT}{2}$$

$$\delta_{p,2} = \frac{(m_{Aprotic} - m_{n-Alkanes})RT}{2} \qquad \text{Eq. 2.112 – 2.114}$$

$$\delta_{h,2} = \frac{(m_{Alcohols} - m_{n-Alkanes})RT}{2}$$

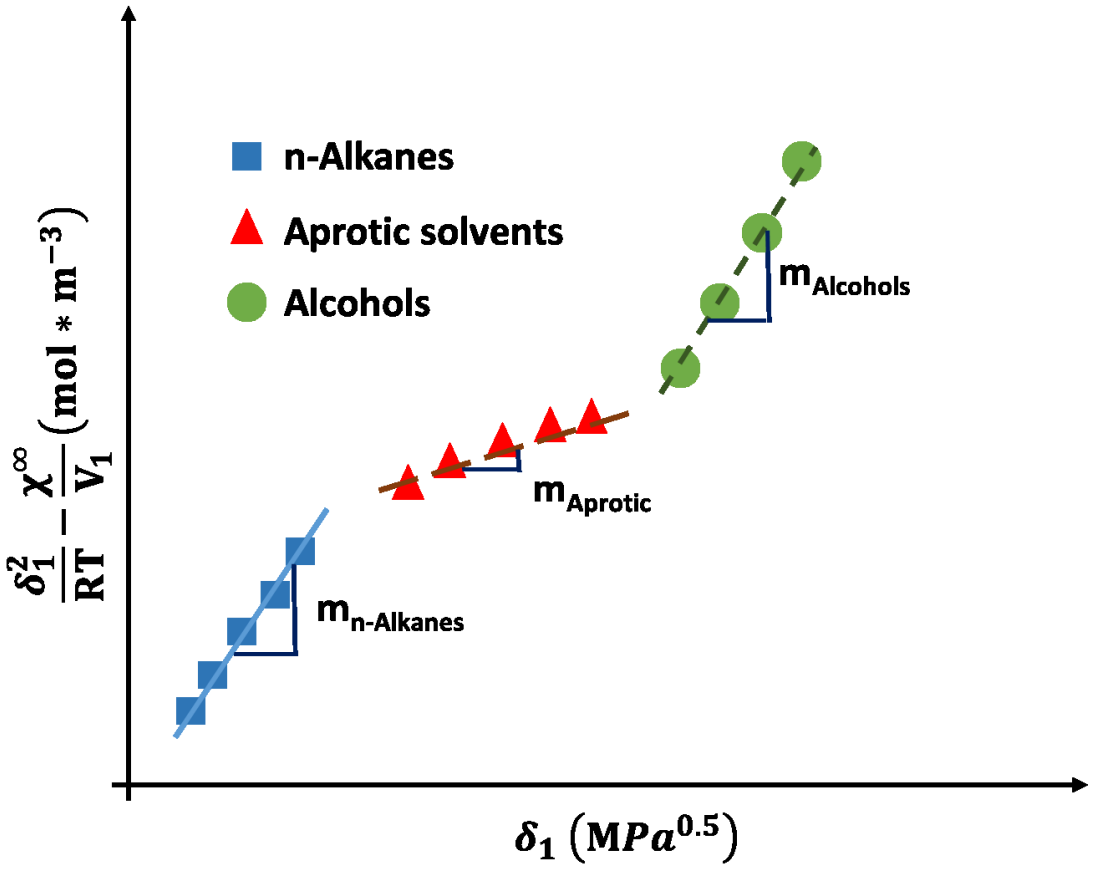


Figure 2.15: Schematic depiction of the graphical construction used for the determination of HSP from IGC measurements.

3. Implications of interfacial phenomena in drug product development and pharmaceutical process development.

3.1 Introduction

As it becomes clear from the previous chapter, the importance of interfacial phenomena varies at different length scales. In addition, as it happens in every scientific field, a number of conditions had to mature, before the community to be able to tackle complex problems associated with interfacial phenomena in pharmaceutical industry. Considering that the first scientific breakthroughs in the field took place in the late 19th century, it is not surprising that it was not until 1970's that people started to extensively employ the scientific tools required for the study of interfacial phenomena. The development of more sophisticated and diverse pharmaceutical formulations, including multicomponent drug products and sub-micron based formulations, created the need for the use of these tools in pharmaceutical industry. It remains a matter of discussion why some of the biggest breakthroughs (such as AFM, IGC, XPS etc.), currently in use for the study of interfacial phenomena in pharmaceutical industry, have developed for the study of phenomena in other disciplines.

The diverse nature of drug products and pharmaceutical processes does not allow a thorough description of all the associated interfacial phenomena in a single chapter. In this direction, this chapter aims to shade light in aspects of the influence of interfacial phenomena associated with the development of solid oral dosage forms. Solid oral dosage forms constitute the backbone of drug products marketed around the world. They are expected to retain this status in the years to come, thanks to the unprecedented advantages they pose. In particular, solid oral dosage forms, are easily administered, they enable accurate dosing, they are robust upon storage and it is easy to package and distribute them.

A structure similar to the one followed in the previous chapter is used in this one, as well. Phenomena from the four main interfaces are presented, starting from the solid-liquid

interface, moving to the solid-vapour and the liquid-liquid interface and closing with the solid-solid interface. The structure was picked in order to make the flow of the material more coherent; in line with the previous chapter.

For the solid-liquid interface the emphasis is given on crystal nucleation, growth and dissolution. These three key phenomena constitute the backbone of the operations of numerous biopharmaceutical organisations. In the solid-vapour and the liquid-liquid interfaces, the emphasis is given on vapour sorption phenomena and then for the solid-solid interface a wide range of downstream processes such as milling, micronisation and granulation are discussed here.

3.2 Implications of Solid-Liquid Interfaces

The first part of this section discusses the implications of interfacial phenomena in crystal nucleation and growth in solution. A number of fundamental concepts of particular importance for crystal growth will be addressed quite early on, to facilitate the discussions concerning the effects of solvents and additives in crystallisation. Particular emphasis will be given on the importance of anisotropic interactions in crystal growth. Then, the focus of the section will be shifted towards crystal dissolution. In this context, the effects of additives will be discussed. Furthermore, the influence of interfacial phenomena, in crystal engineering and post crystallisation strategies employed for the improvement of crystal dissolution, will be addressed. As the field of crystal dissolution is quite extensive, this work would remain focused on the dissolution of crystals and little emphasis will be given on the dissolution of drug products. At the end of the "Solid-Liquid Interfaces" section, a number of more advanced topics are discussed, such as the use of surface active molecules for the control of crystal growth and dissolution, in the light of the topics presented in the previous chapter, on the importance of surface activity on the solid-liquid interface.

3.2.1 Crystal nucleation and growth

3.2.1.1 Crystal nucleation in solution

Crystallisation commences with the formation of a crystalline nucleus. According to the classical nucleation theory (CNT), the crystallisation conditions determine the thermodynamics and kinetics of nucleation. In this context, according to CNT,[144] the solid-liquid interfacial tension is the major barrier for nucleation. On the other hand, the supersaturation of the solution is the driving force for it. Solution conditions determine the critical diameter of a nucleus, the point above which the nucleus is growing spontaneously.

CNT provides an easily digestible framework for the investigation of crystallisation. However, it was proved to be not very reliable in the prediction of crystallisation kinetics, deviating orders of magnitude from the experimentally measured data. In this direction, research efforts non-classical nucleation schemes were investigated. At the epicentre of these non-classical models is the idea that the solid nucleus does not emerge directly from solution, but from a metastable amorphous precursor droplet.[145] This concept was first proposed for proteins, the size of which make the emergence of a crystalline nuclei directly from solution thermodynamically expensive. However, the two-step nucleation model was later verified in the context of small molecules experimentally for both small molecules[146, 147] Besides the amorphous precursor mediated two step nucleation, more exotic non-classical nucleation schemes have been discussed, especially in the context of biomineralisation.[148]

The emergence of non-classical nucleation schemes creates new challenges in the direction of understanding of the influence of macromolecular additives in the formation of a nucleus inside a precursor droplet or otherwise. For instance, it was shown that, in the field of biomineralization, the process used by biological entities to create minerals, the presence of an intermediate liquid-like phase, termed polymer induced liquid phase, is of high importance in the regulation of the mineralisation process. As has been speculated in a review paper by

Professor John Spencer Evans, the this phenomenon may be applicable in the macromolecules assisted crystallisation of small organic molecules.[149-150]

Nucleation is a phenomenon taking place in the nanoscale. Inevitably, interfacial phenomena play a key role in nucleation. From a classical nucleation perspective, interfacial tension is the thermodynamic quantity opposing the formation of a nuclei. In this sense, it is a key factor in the determination of the thermodynamic barrier required for nucleation to take place and the critical nucleation size. Furthermore, for heterogeneous nucleation,[151-152] for the case, where the nuclei are formed on a solid surface immersed in the solution, the contact angle of the nuclei with the solid surface, determined by the work of adhesion between the two, decides the geometric factor that lowers the thermodynamic barrier and the critical nucleation size, making heterogeneous nucleation more energetically favourable. [153-156]

On the other hand, the importance of interfacial phenomena in two step nucleation[157] is still a topic of active research. As mentioned a metastable liquid droplet constitutes the backbone of the two step nucleation theory. It has been suggested by MD simulations[158-159] and very recently verified by in situ TEM experiments,[160] that the nuclei are not formed generally somewhere inside this metastable droplet, but instead they are formed on the walls of the droplet. This suggests, that as long as the behaviour of a system is described by two step nucleation, then every single nuclei is a product of heterogeneous nucleation. Concurrently, in some more fundamental studies, it was shown the two step nucleation pathway is chosen over the classical nucleation one because it offers a lower surface energy barrier. Similar to bigger crystals, nuclei are anisotropic in nature and, as mentioned before, for their formation of which is influenced a solid-liquid interfacial energy barrier. It remains unclear whether crystallisation conditions will influence the crystal anisotropy of the primary nucleus or if all the nuclei exhibit the same anisotropy.

The size and the timescales associated with nucleation make the fundamental study of nucleation phenomena an intellectually challenging field. In this direction, a lot of the concepts are studied in conjunction with crystal growth. In fact, topics that will be discussed later on in this chapter, such as the influence of additives in crystal growth, have direct applicability in crystal nucleation in solution.

3.2.1.2 Introduction to crystal growth in solution

Crystal growth is the process following, chronologically, the nucleation of a stable primary particle, where a crystalline solid will form and continue to grow, via incorporation of solute molecules from the supersaturated solution surrounding it until equilibrium, with the surrounding solution, is achieved. From a thermodynamic perspective this means that crystal growth proceeds as long as the free energy of the molecules on the surface of the solid is lower than that of those in the solution. In a footnote in his pioneering essay on the "Equilibrium of Heterogeneous Substance", published in 1878, Professor Josiah Willard Gibbs[1] made the following statement highlighting the possibility for the growth of perfect crystals, where the term 'perfect' refers to crystals where there only defects are their surfaces, via a layer by layer nucleation mechanism:

"Single molecules or small groups of molecules may indeed attach themselves to the side of the crystal but they will speedily be dislodged, and if any molecules are thrown out from the middle of a surface, these deficiencies will also soon be made good; nor will the frequency of these occurrences be such as greatly to affect the general smoothness of the surfaces, except near the edges where the surfaces fall off somewhat, as before described. Now a continued growth on any side of a crystal is impossible unless new layers can be formed."

In the decades to follow, numerous prominent members of the crystal growth community investigated the growth of perfect crystals, via the nucleation of layers on the surface of the

crystals. It was soon realised that in the range of supersaturation, typically employed, where crystals usually grow, two dimensional nucleation is not easily achievable. Thus, the possibility topographical features of the crystal surface to dictate crystal growth was explored. by researchers such as Frenkel, Burton, Cabrera,[161] and Frank.[162] These works verify that in for low and intermediate levels of supersaturations, surface defects are necessary for the development of a quantitative framework for the study of crystal growth.

Defects can be distinguished in three large categories on the basis of their properties. These categories can include more than one cases of defects:

1. Point defects: In this case, vacant sites appear in the lattice, as atoms or molecules are missing, from the positions they should be. In addition, this category includes the cases when atoms or molecules appear on random sites of the crystal lattice, where they were not supposed to be.
2. Line defects: This category includes the defects associated with groups of atoms or molecules that they are misplaced in the crystal lattice. This phenomenon gives rise to screw or edge dislocations, that they are essential in crystal growth, as it will be discussed later on.
3. Plane defects: This category includes the cases where interfaces appear between homogeneous crystal planes, abruptly changing the direction of the crystal lattice. Grain boundaries are pobable the most well perceived case of planar defects. However, by definition, even the interface between the crystal and air is a plane defect. This argument makes evident that there is not such a thing as a defect-less crystal, as the crystal facets are inherently a type of defect.

As mentioned, surface defects are an inherent part of any modern crystal growth mechanism. These defects can be induced during crystal growth or by thermal or mechanical stresses.

Generally speaking, they are characterised by a higher surface free energy thus, they act as preferential reaction sites (either via van der Waals or chemical interactions).

Crystal growth models effectively describe the addition, onto the crystal surface, of solute molecules, becoming a part of the lattice. A qualitative crystal growth model, termed Kossel model, was developed to interpret the importance of defects, such as dislocations in crystal growth. This model comprises of four mains steps it is schematically depicted in **Figure 3.1**.

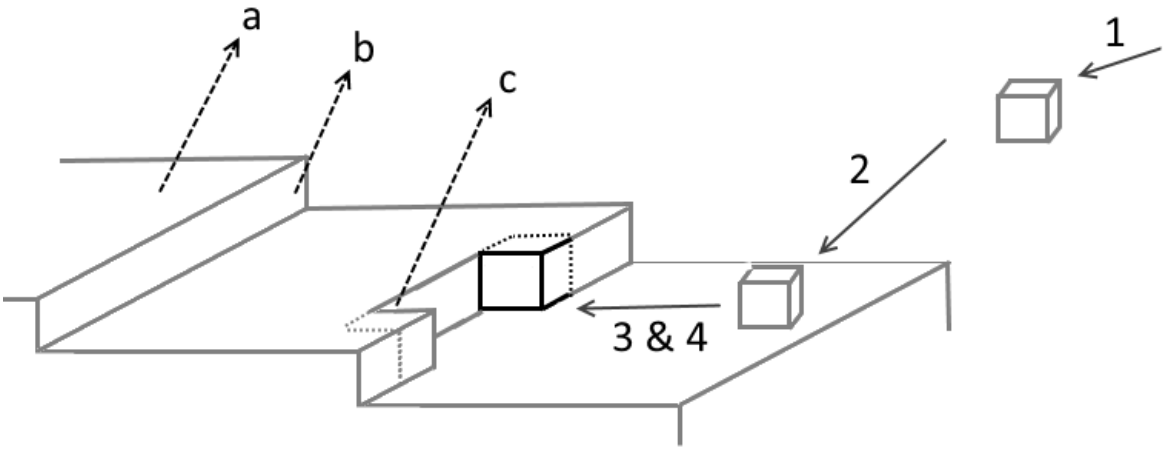


Figure 3.1: A schematic depicting the Kossel model of crystal growth. The numbering signifies the steps undertaken by the molecule to move from the bulk to the surface (1), to diffuse on the solid surface until it reaches a kink (2), for the solute molecule to desolvate along with the surface (3), and finally for it to be incorporated into the solid shown with the black outline (4). The letters describe the following topographical features: a. the terrace, b. the step, and c. the kink site of preferred attachment.

It is critical for the reader to understand that, in the range of conditions typically used, surface diffusion the rate limiting step of crystal growth. In addition, it should be clear that the attachment frequency of a molecule onto a perfectly flat surface is a very energetically expensive process. Thus, crystal growth on a flat surface is a very slow process. In his ground-breaking work, Gibbs, shows that once a molecule is attached on a flat surface, it forms a point defect greatly, contributing to the diminish of the energetic barrier and speeding up growth.

These defects, facilitating crystal growth, are illustrated **Figure 3.1**. This process of layered growth, mediated by the two dimensional nucleation on a flat surface, is highly unlikely to occur as long as the supersaturation is not high. Nevertheless, in reality, experimental data reveal that crystal growth could occur despite low degrees of supersaturation.

Crystal growth at relatively low supersaturations allowed researchers to understand that a mechanism should exist, forcing flat monolayers to roughen, facilitating, in this way, crystal growth. In the model developed by Burton, Carbrera, and Frank (BCF), a cornerstone in the field, the concept of spiral growth was introduced. According to it, crystal facets grow in the form via the spiral movement of a plane dislocation, regenerating in every turn of the spiral. Thus, the perpendicular growth rate of a facet (R_{hkl}) should be given by the following equation:

$$R_{hkl} = {}^{h_s v}/_{y} \qquad \text{Eq. 3.1}$$

where h_s is the height of the dislocation, v is the velocity of the rotation and y is the interstep distance (all of these parameters vary at different experimental conditions and they can be determined experimentally, mainly with the use of AFM). BCF model is grounded on the Kossel lattice shown in **Figure 3.1**, assuming that the solute molecules attaching on the lattice are isotropic cubes. In the work conducted by Chernov,[163-164] this concept was re-examined in the context of anisotropy.

A novelty introduced, by the spiral growth model, was the implementation of the concept of critical length (L_c) for the crystallographic steps. It was proved experimentally that for a step to flow parallel to the facet, so to effectively have crystal growth, it must be of a certain length and above. Otherwise, no movement occurs, the spiral mechanism is not taking place and crystal growth is hindered. Using AFM measurements, on protein crystals, it was proved experimentally, that the critical length is a function of the chemical potential difference ($\Delta\mu$) of the solution (which provides a measurement of the driving force for crystallisation), the liquid-

solid interfacial tension (γ_{SL}) between the bulk solution and the newly formed nucleus (which is effectively a measure of the energetic barrier required for this process), and the volume occupied by a single molecule in the crystal lattice (ω).[165-167] The mathematical interpretation of this, is given by:

$$L_c = {}^{\gamma_{SL}\omega}/_{\Delta\mu} \qquad \text{Eq. 3.2}$$

If there are strong interactions between the fluid and the crystal facet, the magnitude of the interfacial tension is large. As this parameter is at the numerator it means that the stronger the interactions between the fluid and the crystal facet the larger the critical step and hence the there is a larger thermodynamic barrier for growth (for the creation of new solid surface).

A more coherent approach on the crystal growth mechanism problem, focusing on growth kinetics and the solid-liquid interface, was pioneered by Boek and Bennema.[168-170] A modified BCF mechanism was proposed to incorporate the process of solutes' diffusion towards the kinks on the surface of the crystal. On the same work the authors incorporated, on the BCF model, the free energies required for both the desolvation of the solute and its incorporation at the solid interface. This phenomenon is depicted in **Figure 3.1** by the third step. In the same work, the rate of attachment/detachment of solutes was presented, enabling the investigation of the kinetics of the process of molecular re-orientation prior to the incorporation in the crystal lattice.

More advanced studies were conducted with the aid of molecular simulations. Gilmer and Bennema,[171] used Monte Carlo simulations, to study crystal growth at various conditions. They showed that at low supersaturations, their mechanistic model was in good agreement with the Monte Carlo simulations. Using urea as the model compound, Boek deployed Molecular Dynamics (MD) simulations[168-169] to understand the importance of hydration shell in crystal growth. The results of this work revealed the importance of facet specific surface chemistry on

the structure of the hydration shell surrounding a crystal. These results highlight the importance of facet specific interfacial phenomena in the development of accurate mechanistic models for crystal growth.

3.2.1.3 The influence of solution conditions in crystal growth

Snowflakes, quite abundant in different regions of the planet, were probably the first system for which crystal habit was investigated, as a function of different parameters. As liquid water crystallises to ice (the occurrence of amorphous ice, is highly improbable), the crystals could be easily collected and examined, while the temperature, pressure and ambient humidity could be very easily measured, using thermometers and manometers. From the early 17th century, scientists were already investigating their crystal habits, but it was not until 1932 that a systematic study, correlating crystal habit with crystallisation conditions, was performed. At that time, Professor Ukichiro Nakaya started examining the crystal habit of snowflakes produced at different temperatures and different values of water vapour saturation. His results were tabulated in the Nakaya diagram,[172] depicting the crystal habits obtained at different temperatures and different supersaturations of the atmosphere with water.

In the field of industrial crystallisation, the crystal habit of urea, a compound of great importance in the manufacturing of fertilisers and explosives, was one of the first to be studied. A publication from 1936[173] reports that the urea produced in the USA, crystallised, on that time, in alcohol, was rhombus like, contrary to the needle shaped imported urea, crystallised in water. In the same publication, it was mentioned that the rhombohedral crystal habit offers great advantages in terms of flowability over the needle shaped imported urea. Even without advanced knowledge of crystal growth it can be claimed, that the strength of the interactions between the different crystal facets on one hand and the solvent and solute molecules on the other, determines the observed crystal habit. Thus, slow growing facets, having high affinity

towards the solvent molecules, dominate the crystal habit compared to the faster growing facets.

The first attempts to understand this phenomenon were done with the aid of a mechanistic models based on the BCF approach. The model was parameterised using the results from force field simulations and it was able to capture the needle shaped structure of urea crystals grown in water and the cuboid habit of crystals grown in polar solvents. A similar model was successfully implemented for the investigation of the crystal habit of amino acids.[174-175]

The implementation of the concept of solid-liquid interfacial interactions in the modelling methodology, signified an important advancement in the understanding of crystal growth. In this direction, MD simulations were performed investigating the interaction of individual facets with different solvent. These data, were, later introduced into a model, based on the Wulff-Chernov formalism, to construct diagrams accurately predicting the crystal habit of different compounds growing in different solvents at different supersaturations.[176] Despite their unprecedented accuracy MD simulations require, occasionally, excessively long simulation times. Thus, the investigation of more complex phenomena, such as the influence of additives, in crystal growth, via MD simulations, becomes a non-trivial problem.

The improved understanding of the rate of attachment/detachment of solute molecules on/from kink sites of a crystal facet, lead to the development of mechanistic models for the study of spiral growth on individual facets, and the influence of solvents.[177-178] The latest version of these models is the ADDICT algorithm.[179] ADDICT was tested with different molecules of pharmaceutical interest (acetaminophen, lovastatin, δ-mannitol, and glycine) and solvents and it was able to accurately reproduce their steady state crystal habits.

The surface energies of both the solvent and the solid surface are key components of the algorithm. Nevertheless, these surface energy-based approaches come with certain

compromises, with the most notable one being that the acid-base component of the surface energy of a crystal facet is assumed to be equal to zero if no hydrogen bonds are formed. Further doubts are casted owing to the empirical nature of the geometric mean approximation proposed to study acid-base interactions. In addition, certain aspects of the behaviour of fluids at interfaces could be implemented. This could include the formation of "clathrate cages" by water molecules around strongly hydrophobic molecules, where the average number of hydrogen bonds is higher than in the bulk.[180] Finally, an experimental validation of the proposed values for both the surface energies of individual facets, as well as their corresponding work of adhesions with different solvents, could provide guidelines for the enhancement of the predictive power of the algorithms.

The importance of solvent polarity in the determination of the steady state crystal habit, was investigated, from a purely experimental perspective, by Shah et al., using mefenamic acid as the model compound.[181] A range of solvents was used, showing that mefenamic acid can crystallise in a broad spectrum of habits, ranging from needles to thick plates. In this study, it was possible to correlate the aspect ratio of the crystals with the polar component of the solubility parameter of the solvent. However, the work did not investigate the influence of degree of supersaturation, which can have a profound effect, influencing via different mechanisms the crystal habit. Similar studies, investigating the effect of solvent polarity on crystal habit were conducted using acetaminophen.[182] The high affinity of polar protic solvents towards facets favouring the formation of hydrogen bonds diminished the growth rate of these facets. Solvent molecules were interacting much stronger with the crystal, compared with the solute molecules. For polar aprotic solvents, not favouring hydrogen bonding, the correlation was more ambiguous.

Attempts have been made to understand the importance of more exotic phenomena like π-π stacking in crystallisation.[183-186] In this direction hybrid modelling – experimental

approaches have been employed. The α polymorph of para-amino benzoic acid (α-PABA) was picked as the model compound thanks to its ability to interact via to π-π stacking interactions. The conclusion of this investigation suggest that for the case of α-PABA crystal nucleation is governed by the hydrogen bonding, associated with the carboxylic acid functional group. On the other hand, the process of crystal growth is governed by the π-π stacking interactions. The authors proposed a a poly-nucleation roughening mechanism to explain crystal growth. According to this mechanism solute molecules diffuse on the $(01\bar{1})$ facet and they attaching on it by means of π-π interactions. This attachment process creates a rough surface resembling crystal growth at high supersaturations. This mechanism appears to dominate the process independently of the supersaturation. Aspects of π-π stacking are still a matter of debate in literature,[187] hence it can argued that beyond π-π stacking, a number of other phenomena, including interfacial phenomena, could influence crystal growth of α-PABA.

3.2.1.4 The influence of additives in crystal growth

The studies described in the previous section enable the construction of a robust framework for the determination of steady state crystal habit of small molecules at different superaturations, in different solvents. The effect of solute additives in crystal growth emerged as a new challenge; additives influence crystal growth via interacting anisotropically, depending on their structure, with the different crystal facets, competing with both the solvent molecules and the solute molecules of the crystallising material. In other words, additives can adsorb on specific facets, inhibiting the attachment rate of the molecules of the crystallised compound, slowing down the growth, changing in this way the steady state crystal habit.

The pillars for this field have been set by the works of Chernov, Cabrera and Vermilyea investigating the influence of solute impurities on the development of surface dislocations dictating crystal growth.[163, 188-189] More accurate models have been developed over the years,

incorporating the accumulated experience of mechanistic modelling of crystal growth.[190-191] The concept of structurally similar additives emerged through these studies. Solute molecules posing structural similarities with the crystallising molecules were found to act as crystal habit modifiers. These additives interact with the crystal facets by means of adsorption and thus it was not a surprise that their effect was found to be a function of their concentration. Amino acids, have been a very attractive additive in different formulations, on the same time they exhibit numerous challenges in their crystallisation. In experiments conducted, α-glycine was crystallised in the presence of l-alanine. It was shown that l-alanine has strong affinity towards the (020) facet of α-glycine, making the dominant facet of the resulting crystal habit. [190, 192] Similar experiments were conducted with acetaminophen, using p-acetoxyacetanilide as the additive.[193] In this case, the additive was found to have a strong affinity towards the (110) facet of acetaminophen.

This concept, of structurally similar additives, has been implemented towards the development of therapeutic strategies against a certain type kidney stones; kidney stones are biominerals growing in tissues.[194-195] In a very elaborate study the effectiveness of a plethora of additives was explored. The growth velocities of different facets of kidney stones in supersaturated solutions, containing different additives, were measured via AFM. In most of the cases, as expected, inhibition of crystal growth was reported. The binding energy between the solute and the crystal was found to provide a good metric for the extent of inhibition of each imposter. However, a very intriguing case of crystal growth acceleration, owing to the presence of additives was reported as well.[196-197] The same phenomenon was observed during the crystallisation of l-alanine in the presence of another amino acid, l-valine.[198] This counterintuitive observation has been associated with the strong solvation of the crystal surface by water molecules owe to the very strong hydrophobicity of the additive. Because of the strong solvation the additive was not able to interact with the surface.

The same concept, of structurally similar additives, has been used for the development of treatments for malaria, a life-threatening disease, used to eradicate populations in equatorial countries. The heme present in red blood cells is toxic to the malaria parasites residing there. To avoid eradication, malaria parasites were found to use heme molecules to crystallise hemozoin in their digestive vacuole.[199-203] Hemozoin crystals were grown, *ex vivo*, and their structure was resolved. Using the structures obtained, the facet specific attachment energies of hemozoin crystals were calculated. These results were used to explain the mechanism via which quinoline, a compound present in tonic, is an effective anti-malarial drug. Quinoline acts as inhibitor, preventing the growth of hemozoin crystals. Thus, the concentration of heme in the digestive vacuole remains high killing the parasites.

It has been demonstrated that polymers and surfactants can be employed to control crystal growth.[204-206] In this direction, investigators explored the applicability of polymers and surfactants to for the development of therapeutic applications, associated with pathological crystallisation. The influence of ionic polymeric additives in the inhibition of kidney stones has been investigated and it was found that polyanions were interacting much better with crystal surfaces compared to polycations.[167, 195] Furthermore, it was shown that beyond crystal growth, polymeric additives contribute to the aggregation of crystals. In fact, it was demonstrated that in the presence of a mixture of polyanions with polycations, the polymer aggregates formed were mediating the formation of crystal aggregates.

Seeding is used extensively, in industry, for the control of crystallisation processes.[207-209] From the hitherto discussion and from intuitive understanding of the mechanisms of crystal growth, it becomes obvious that as long as crystal growth is going to be allowed to reach steady state, the initial habit of the seed should not influence the steady state crystal habit. This was proved experimentally, using sucinic acid as the model compound.[210] The steady state crystal habit was found to be independent of the habit of the seed crystals. In addition, MD simulations

crystallisation have shown that the presence of seeds facilitates the formation of metastable precursor droplets, having the potential to give birth to crystal nuclei. This is an intriguing phenomenon that has not been implemented in the development of mechanistic models for seeding crystallisation.[211]

3.2.1.5 Interfacial phenomena in the crystallisation of amorphous materials

The study of the mechanisms determining the transformation of amorphous materials to crystalline is an intriguing field, gaining attention, thanks to the growing influence of amorphous materials in drug product development. For instance, active ingredients are formulated in amorphous form as they improve the bioavailability of purely soluble molecules. A field exhibiting thought provoking phenomena is that of crystallisation of organic compounds from their amorphous organic glasses.[212-213] Experimental studies suggest that even for organic glasses below their glass transition temperature glasses e below its glass transition temperature the molecular mobility could be sufficient to support crystallisation.[214-215] However, the most intriguing experimental observation is that the rate of growth, of the crystalline phase from an organic glass, can be up to several orders of magnitude higher at the surface of the material than in the bulk.[216-217] Considering that the intermolecular forces, and consequentially the molecular mobility, at the surface are different from the bulk, different mechanisms have been proposed in this context to explain this phenomenon.

Contrary to crystallisation in solution, the organic glass to crystal transition occurs via the expansion of the crystalline phase towards the glassy phase. The advancing crystalline phase must move fast enough to overcome the fluidity barriers, hindering the formation of an ordered phase. The ratio of the diffusivity of the amorphous glass to the rate of expansion of the crystalline front is the critical quantity determining the feasibility of glass to crystal transition. If its magnitude is more than seven picometers ($7 * 10^{-12}$ m), then crystallisation ceases.[218]

3.2.3 Crystal dissolution

3.2.3.1 Funamentals

Dissolution is a multistep process during which a homogeneous solute-solvent solution is created owe to the mass transfer from particles (or any other solid material) surrounded by an undersaturated liquid. Both interfacial and hydrodynamic phenomena can be of crucial importance depending on the solids, the solvents and the dissolution system (reactor or tissue). As this study focuses on interfacial phenomena and considering that the majority of the dissolution studies in industry are performed under well controlled laminar regimes, this chapter will not discuss the effects of hydrodynamics in dissolution.

Dissolution commences by the wetting of the solid and the formation of the solid-liquid interface. Molecules at the surface of a particles are solvated and move to the solid liquid interface. On the interface a diffusion controlled mechanism, the behaviour of which is determined by means of the second law of thermodynamics, transfers the material to the bulk. As discussed in Chapter 2, the change in the Gibbs free energy of dissolution can be decomposed to an enthalpic and an entropic component. The enthalpic component provides a measure for the energetic penalties associated with the solvation, stemming, mainly, from the average potential energy interactions between solute and solvent molecules. On the other hand, the entropic component describes the effects of the spatial conformation of the molecules taking part in dissolution process. These concepts have been summarised in the Flory-Huggins theory, in the previous chapter.

As mentioned the breakage of the bonds, leading to the formation of the solid-liquid interface, involves large enthalpic penalties. On the other hand, for the dissolution in aqueous media, the solvation of molecules requires the formation of hydrogen bonds. Owe to the short range of these bonds, this phenomenon exhibits specific spatial arrangement. Thus, for the dissolution in water the entropic interactions have a crucial role in dissolution.[219] The spatial

orientation of the molecules in a solid particle affects the dissolution process. This phenomenon can be better understood in the context of single crystals. As crystals exhibit anisotropic surface chemistry, it was shown, with the aid of single crystals, that facets exhibiting greater tendency towards the formation of hydrogen bonds dissolve faster in water.[220] Thus, similarly to surface energy, it is expected that the χ interaction parameter is facet specific.

The change in Gibbs free energy at the interface between a spherical and isotropic, solute molecule and the bulk solvent, consisting of solvent molecules much smaller than the solute molecules, is described mathematically with the following expression:

$$\frac{\Delta G}{4\pi R^2} \approx \frac{pR}{3} + \gamma\left(1 - \frac{2\delta}{R}\right) \qquad \text{Eq. 3.3}$$

where R is the radius of the solute molecule, p is the pressure of the system, γ is the interfacial tension at the solute-solvent interface and δ is a length scaling parameter indicating the asymptotic behaviour of the surface tension, depending on the nature of the solute and the solvent molecules. Theoretical studies, based on this equation, suggest that for solute molecules (or clusters of molecules) with radius smaller than one nanometer (these is effectively the case encountered in the dissolution of small APIs) the change in Gibbs free energy increases proportionally with the solute size (R^3). However, as the size of the solute goes to $R > 1$ nm a qualitative shift is observed, leading the change Gibbs free energy to grow, proportionally to the surface area of the solute (R^2), approaching a limiting value. This qualitative shift marks the formation of an interface between large solute molecules solute and the solvent. MD simulations conducted on aqueous systems to shade light on the origins and the evolution of this interface.

It was revealed that entropic phenomena dominate the interface formation. In particular, it was shown that the tendency of water molecules, held together by hydrogen bonds, to increase their distance from the solute molecule, so as to reduce the number of unformed hydrogen

bonds and hence the entropic penalty on the system, drives the formation of the interface. Using results from numerous *in silico* studies it was shown that, on average, about less than one hydrogen bond (out of the four a water molecule can form) is lost, due to this structural shift in the vicinity of large solute molecules. These *in silico* findings are in line with the ideas proposed by Professor Frank Stillinger,[221] who among other things stated that:

"Although liquid water might properly be described as a random, three dimensional, hydrogen-bond network, it surely cannot have invariant fourfold coordination. Instead, some of the hydrogen bonds must be broken and others severely strained in length and direction".

Different properties of crystalline solids influence the dissolution rate via different mechanisms, affecting one or more of its steps. This includes both surface properties, such as such as crystal defects, surface chemistry and surface energetics, and bulk properties, such as surface area to volume ratio and physiochemical stability (polymorphism and the propensity of forming hydrates or solvates). Crystal engineering approaches exploiting synergistic phenomena between different properties offer an attractive platform for the improvement of dissolution rates. The following sections discuss some of the aspects associated with the effects of interfacial phenomena in dissolution.

3.2.3.2 Anisotropy wettability of crystalline materials

The anisotropic nature of properties, such as surface energy, of crystals influences their dissolution. Lippold and Ohm performed dissolutions experiments to assess the effect of surface energy in dissolution.[222] The experiments were conducted at constant agitation rate; the initial effective surface area of the dissolved particles was, also, kept constant. Aqueous solutions of isopropanol at different concentrations were used as probe liquids, in wettability measurements, for the determination of a metric for the surface energy of the solids. The results of this study show a correlation of dissolution rate with the surface energy of the solid. In a

series of similar studies performed by Modi et al. an attempt for the determination of crystal anisotropy in dissolution was performed. The results suggest that as the concentration of high energy crystal facets promote bioavailability.[38, 223]

In the aforementioned studies, it was attempted to assess the importance of surface energy and surface energy anisotropy in crystal dissolution. Even though macroscopic single crystals could provide an attractive platform for such studies, powder compacts were used instead. The preparation of compacts induces defects on the crystalline particles, owe to the mechanical stress imposed. The mechanical properties of crystals are anisotropic[224-226] and hence the compaction induced modifications are anisotropic as well. Thus, the extent of defect formation is different on each facet, whereas the surface energy of individual facets, resulting from compaction is difficult to be determined. As the post-compaction surface energy of individual facet is unknown, doubts are created for the validity of wettability measurements. Adsorption based techniques such as IGC may be more suitable for such an investigation. In the absence of such a tool, wettability measurements performed on the ground of the Wenzel and Cassie-Baxter equations, may provide more robust results.

3.2.3.3 The importance of defects in dissolution

Defect formation can potentially impact, significantly, the dissolution of pharmaceutical crystals. Precise control of the defect formation during crystal growth is a non-trivial operation, thus it is not easy to perform a systematic investigation of the effects of the different types of defects in dissolution. It can be hypothesised that in a defect-less crystal, dissolution rate is greatly determined by surface properties, thus from the crystal habit. In preliminary experiments conducted with acetaminophen it was verified that it was not possible to correlate facet specific dissolution rates with the attachment energies of the corresponding facets.[220] In the light of these results, it was hypothesised that defects are responsible for this lack of correlation. In order to validate this hypothesis, X-ray topography was employed.

Acetaminophen crystals with two distinct crystal habits were generated for the purposes of this study; needle shaped particles were obtained at low supersaturations, and prismatic shaped particles were obtained at elevated supersaturations. The X-ray topography data acquired suggest that the abundance of defects incorporated within the crystal lattice of acetaminophen lead to the accumulation of strain. This phenomenon is expected to promote dissolution. However, it is not clear the exact mechanism via which the strain affects specific facets.

Defects introduced during crystallisation are inherent. However, the importance of defects induced by mechanical processing is more often discussed in literature. This is because, such defects are of higher industrial relevance and in addition they can be investigated with common analytical techniques. The investigation of milling induced defects is of particular interest, as milling is one of the most common downstream processes in pharmaceutical industry. Milling induced defects create disorder into the crystal lattice. The effects of this disorder are manifested in changes which can be tracked via DSC and XRPD measurements. Solution calorimetry is another experimental platform providing a more accurate measure of disorder.[227-228] The effects of cryogenic milling on brivanib alaninate was studied recently. It was revealed that milling at cryogenic temperatures leads to higher disorder in the crystal lattice, compared with milling at ambient temperature. This result suggests that even for crystalline materials, cooling at cryogenic temperatures can make the material quite brittle.[229]

3.2.3.4 Crystal engineering approaches for enhanced dissolution

The importance of surface area and surface energy in dissolution kinetics, makes crystal habit and crystal size critical factors in dissolution. Sometimes the physicochemical changes in surface characteristics, such as defects and surface chemistry, may contribute as well. Employing crystal engineering strategies to tune crystal habit may enable the design of drug substances with improved dissolution rates. Different solvents and polymeric additives were used to investigate the effects of crystal habit in the dissolution rate dipyridamole crystals. [230]

More sophisticated strategies taking advantage of the synergistic relation of surface area and hydrophilicity have been employed as well. In a very elaborate study, the dissolution rate of doped phenytoin crystals was improved by a strategy involving the manipulation of the crystal habit and the doping of the surface of the crystals with hydrophilic dopants.[231] The hydrophilic dopants are expected to provide the mean for a faster wetting. Similarly to other works presented in this section, contact angle measurements were used to assess the effectiveness of doping. However, it remains unclear how dopes interact with different facets and how the extent of coverage of a facet with dope is determined.

Besides doping, a wide range of techniques have been used to enable the control of the surface chemistry of pharmaceutical powders. Surface functionalisation is a quite attractive technique, as it enables the introduction of functional groups with very tailored structure. Functional polymeric coatings from solvents are the most commonly used approach to obtain APIs with desirable dissolution properties.[232] Besides improvement in dissolution rate, it was shown that functionalisation with polymer coatings enable the controlled release of the drug. Other wet functionalisation techniques, such as silanisation, can be explored in the future to tune wettability.

As mentioned, improvement in dissolution can be achieved by the manipulation of more than one of particles' properties, such as the crystal habit and the hydrophilicity. In this direction, designing processes enabling the simultaneous modification of more than particle properties, in a direction improving dissolution, it will be an important advancement. In a recent study, a method combining micronisation and surface modification to improve dissolution, was presented. In this study ibuprofen particles were co-grinded with a hydrophilic polymer in a continuous fluid energy mill.[31] Using this process, it was possible to achieve the simultaneous decrease of the particle size and the enhancement of the hydrophilicity. The processed particles were showing improved dissolution behaviour. In a similar study, Tay et al. performed the

mechanofusion of poorly water-soluble indomethacin with MgSt and NaSt.[233-234] An increase in the dissolution rate of the NaSt coated drug substance was reported. In this case, the coating was enhancing wettability, while on the same time it was promoting drug dispersion during dissolution. Better dispersion prevents coagulation in solution, favouring dissolution. In a study published by Karde and Ghoroi,[235-236] dry coating of cohesive particles with functionalised silica nanoparticles was performed. The results of this study suggest that by tuning the functionalities of the host particles, the hydrophilicity of the coated particles can be tuned.

3.2.3.5 The effects of surface active additives in crystal growth and dissolution

The presence of additives, such as surfactants and polymers, in solution, gives rise to surface activity, changing the wetting behaviour of the solution. In this case, the wetting behaviour of the solution is driven by the migration of the surface active molecules to the three phase contact line.[101, 237] As crystal growth is heavily influenced by the solid-liquid interface, this phenomenon can lead to intriguing changes in the steady state crystal habit. As a matter of fact, surfactants were used to modify the crystal habit of carbamazepine dihydrate,[238] a compound usually crystallising in needle shaped crystals or elongated plates. The interactions between the hydrophilic component of sodium taurocholate (a surfactant) with the (111) facet of the carbamazepine dihydrate, facilitated by the hydrogen bond network existing there, limits the growth of that facet, diminishing the rapid increase of the aspect ratio of carbamazepine dihydrate crystals. Similar studies have been conducted with aspirin and nifedipine.

Similarly to crystallisation, the presence of additives affects crystal dissolution, as well. The influence of a wide range of polymers in the dissolution rate of pharmaceutical crystals has been investigated. Experimental studies, in the absence of polymers, have revealed the existence of a lag time between the contact of a tablet with a solvent and the start of drug release.[35, 239-241] This lag phase, was found to be determined by the work adhesion between the undersaturated fluid and the surface of the dissolving API crystal, under investigation. Higher

wettability, linked with the presence of the polymers, decreases lag time. Increasing the amount of polymer used and its physicochemical properties, one can alter the surface tension and therefore the lag time. Dissolution experiments are usually performed with the use of tablets, hence great importance should be given in the preparation of the tablets, especially as the experiments aim to study the aforementioned lag time. In the preparation of the experiment, any traces of unbound powder on the surface of the tablet should be removed. These "untabletted" particles dissolve faster than the rest of the tablet owe to their small size. This makes the measurement of the true value of the lag period difficult.

Numerous studies have established the fact that additives have a profound effect on the surface tension of solution. Nevertheless, there are no studies suggesting a detailed mechanism on how the surface activity, induced by the additives, influences the different components of surface tension. It can be hypothesised that thermodynamic parameters, of the additives, such as the HSP,[24] could provide a metric for the influence of each additive on the different components of the surface tension. For instance, a polymer with a relatively high van der Waals component of the HSP, it could induce a large decrease in the van der Waals component of the surface tension of its solution.

3.3 Implications of Solid-Vapour Interfaces

In this section, implications on the solid-vapour interface will be discussed. At first, issues associated with the moisture content of pharmaceutical materials will be addressed. Then some aspects associated with the influence of interfacial phenomena in drying processes are presented. Emphasis will be given in the molecular mechanisms triggered during desolvation processes. Finally, some aspects of vapour sorption in non-equilibrium materials will be discussed. The careful reader may notice that this topic, strictly speaking, belongs to the field of liquid-liquid interfacial phenomena. However, when non-equilibrium/amorphous materials, such as amorphous drugs are under investigation, the separating lines are thin and it is not

uncommon this kind of topics to be addressed in literature on solid-liquid interfacial phenomena.

3.3.1 Moisture content in pharmaceutical materials

Pharmaceutical materials, either pure or in formulations, are quite often exposed to different humidities, during processing and/or storage. In crystalline materials, water is present in two main states; bound and unbound.[40-42] Bound or stoichiometric water is incorporated in the crystal lattice. On the other hand, unbound water can be either adsorbed on the crystal facets or trapped in voids. This classification is useful in distinguishing water containing pharmaceutical materials, but can be misleading.

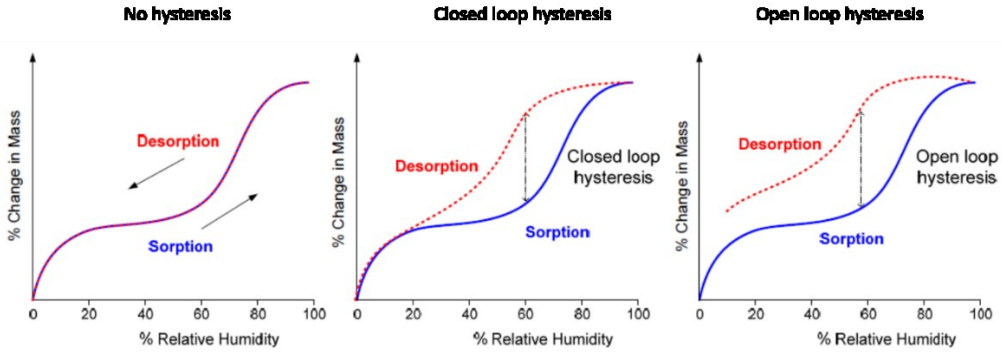


Figure 3.2: Sorption desorption isotherms for different hysteresis cases.

Sorption studies are used in materials characterisation. Both the adsorption and the desorption behaviour are investigated. Interfacial phenomena associated with the Kelvin equation can lead to a hysteretic behaviour during the adsorption-desorption process.[242] The shape of the hysteretic loop can provide invaluable data for the nature of the porosity of the material under examination. Macroporous crystalline materials exhibit limited hysteretic behaviour, porous materials have a larger hysteresis loop and amorphous materials can exhibit an open loop hysteresis. The open loop indicates that the water bound in the bulk of the material cannot be released by just decreasing the relative humidity. This phenomenon may be associated with the recrystallisation of a solvate/hydrate.

For systems dominated by multilayer adsorption, BET and Hill de Boer adsorption isotherms were found to provide good fitting of the data obtained. On the other hand for systems where monolayer adsorption prevails (systems dictated by short-range chemical forces), Langmuir-type of isotherms[243] would provide a more realistic description of the process. In any case, the investigators should always be aware of the physical interpretation of these isotherms. For instance, it is common to encounter pieces of literature where the investigators are attempting to fit sorption data from amorphous materials in the van der Waals equation, and use the coefficients obtained to draw conclusions. Considering that for amorphous materials, absorption plays an important role, which becomes even more important with increasing amount of sorbed vapours.

Equilibrium models, such as the Flory-Huggins and the Vrentas and Vrentas[244] models, have been employed, as an alternative to adsorption isotherms, for the interpretation of sorption data from amorphous materials. However, these models, fail to capture the inherently non-equilibrium character of the phenomenon. Furthermore the χ interaction parameter and the rest of the thermodynamic quantities, appearing in these models, are of little practical importance.

Only the combined relaxation-diffusion models,[245] describing the sorption phenomenon on the basis of the two fundamental processes involved provide physically meaningful data, including the diffusion and relaxation coefficients. Nevertheless, a multiparametric fitting of experimental data is required, prone to inaccuracies. Emerging techniques such as QCM may provide the framework for the isolation of relaxation and diffusion phenomena, via the casting of very thin films and the correlation of the relaxation phenomena with the dissipation mode of the QCM.

3.3.2 Drying

Moisture or solvent removal is a dynamic process including both heat and mass transfer phenomena; energy is transferred from the surroundings to the particle leading to the removal

of moisture (bound or unbound) in the form of vapours. Due to the different states at which moisture can be bounded in the solid, drying occurs at different stages. An initial heating period exists, where the fluid is heated to evaporation. In the next phase moisture removal occurs at a constant drying rate. During this phase, the moisture adsorbed on the surfaces is evaporated until a critical moisture content value corresponding to the tightly bound water content; in other words, the water confined in capillary structures or bound in the material stoichiometrically or not. The vapour pressure of the moisture bound in capillary structures can be significantly lower owe to capillary effects.

In the case of crystalline solids, with bound water, exposure to ambient moisture may induce changes on the surface patterning or increase in the nucleation density of the anhydrous phases.[246] The increase in surface roughness, arising from the nucleation of new phases is a common feature of hydrated compounds. However, no literature findings support the facet specific dependence of this process, although crystal defects can affect this process.

During desolvation, the nucleus of the anhydrous crystalline form is expected to initially be formed in the vicinity of a high energy site, quite often a dehydration induced crack and/or defect. In the case of catastrophic desolvation, when the removal of the solvent is very fast, the stress induced may lead to the collapse of the crystal lattice and the formation of an anhydrous amorphous form. Owe to its nature this amorphous, non-equilibrium, material has the propensity to recrystallise towards an anhydrous crystalline polymorphic form, upon exposure to conditions providing sufficient molecular mobility. The vapours released during the desolvation provides the molecular mobility to facilitate the nucleation and growth of the crystalline anhydrous phase. The amount of molecular mobility provided may determine which anhydrous polymorphic form will emerge upon desolvation. It is not uncommon, for cases were the molecular mobility is not sufficient, the process of recrystallisation not to be directed towards the most stable anhydrous form, but towards the one with the energy minimum of

closest proximity. Thus, it could turn to a metastable form which would then turn to the most stable one, under the effect of Ostwald's rule,[247] which can be summarised by the words of the Nobel laureate Professor Wilhelm Ostwald:

"At a sufficiently high supersaturation the first form that crystallises is the most soluble form. This transient state then transforms to the more stable form through a process of dissolution and crystallisation."

One should notice that the kinetics of this transformation, depending on the conditions, can be quite slow, enabling the metastable form to remain for long periods.

Spray drying and freeze drying allow moisture removal combined with transition from crystalline phase to amorphous. Thus, they gained a lot of ground recently. Amorphisation significantly impacts the properties of the anhydrous form. However, the studies found in literature are limited in the application of infinite dilution IGC for the determination of the surface energetics of spray and freeze dried materials. Infinite dilution measurements are not sensitive enough, as they account solely for high energy sites of the material.[248-249] It is not a coincidence that the data obtained from these studies show negligible changes in the surface energy. If the material prior to drying was having extensive high energy sites, will not be uncommon to have a lot of them post drying. In fact, it will be expected. More advanced studies employing finite dilution IGC, can provide more detailed maps of the surface energy shading light to the mechanisms determining molecular rearrangement upon dehydration.

3.4 Implications of Solid-Solid Interfaces

This section starts with an introduction to flowability, a field where solid-solid interactions play an important role. Following that, some key processes, where solid-solid interactions are of particular importance, will be discussed. Particular importance is given to

the examination of the influence of these processes on the surface energetics of the processed material. A number of studies, showing the applicability of IGC in the field will be discussed.

3.4.1 Flowability

Flowabilty is an important bulk powder characteristic. The term 'flowable' refers to an irreversible deformation causing a powder to flow under the influence of an external force. Various parameters such as angle of repose, Carr's index, Hausner ratio, flow function (ff) are used to quantify flowability.

The flow of powders is influenced by interparticulate interactions, a term summarising various phenomena including adhesion and cohesion interactions, friction forces and mechanical interlocking. A range of other factors, including but not limited to the particle size and particle size distribution, the particle shape and the shape distribution, the bulk and skeletal density, the moisture uptake capacity and the ambient temperature and moisture, also influence the flowability of powders. As this work has dealt a lot with adhesion and cohesion interactions, it will be useful to mention that the lower the adhesion or the cohesion forces exhibited by the particles in a powder sample, the smaller the barrier needed to overcome for flow.

Flowability can be improved via coating of the particles with both hydrophilic guest particles (such as Aerosil) and hydrophobic guest particles (such as magnesium stearate, sodium stearate, magnesium silicate and calcium silicate etc.). In both cases, coating increases roughness, reducing the surface area available for interaction between particles.[241, 250-251] Owing to their lower surface energy hydrophobic additives can increase flowability of powders by decreasing the strength of interparticle adhesive interactions. The use of low cohesive, hydrophobic lubricants has been attractive to improve flowability of powders. These types of coating have already been explained, a few pages before, can be beneficial for the dissolution performance of the particles, as well.

One of the challenges of increasing flowability by using flow additives is to disperse the flow additives on the surface of host particles, creating a thin layer. Flow additives are added either by mixing or by mechanofusion. The processes of mixing and mechanofusion are to be discussed in the following sections.

3.4.2 Mixing or blending

Mixing or blending is a widely used process enabling the creation of homogeneous blends of multi-component particulate systems. This is of high interest in the development of manufacturing processes for different types of solid dosage forms, such as tablets, capsules, dry powders for inhalation and powders for reconstitution. For instance, in tablet manufacturing, active ingredients are mixed with excipients before granulation, to create homogeneous granules. Following that, the granules are mixed with glidants and lubricants, before the final tableting step. Different types of blenders/mixers are currently in use such as v-mixers, cone mixers and rotating cylinders.

There are three main mechanisms of solid mixing: diffusive mixing, convective mixing and shear mixing. In diffusive mixing, individual particles move relative to each other in a random way, resembling a random walk process. In this mechanism, particle size and density determine the effectiveness of mixing in a great extent. Diffusive mixing is common for free-flowing particles. It is easy to understand that for example for a binary system comprising of two types of powders, with similar particle size and shape distribution and similar density, achieving a uniform mixture is extremely difficult, especially when the concentration of one of the components is very low.[252] Thus, mechanisms relying more on the use of mechanical energy, to facilitate mixing, are required.

As implied by the name of the mechanism, during convective mixing a fraction of one of the materials is moved, by means of convection to another, from one position to another. Finally, during high shear mixing, mechanical force is used to force aggregates of particles to

move the one past the other and break down. The mechanical properties of the individual particles and the aggregates, as well as the amount of input energy, influence the effectiveness of shear mixing. High shear mixing is very important for the mixing of fine powders. As has been discussed, particles with smaller size have the tendency to be more cohesive and the have the tendency to form aggregates. In this case, for the efficient mixing of fine particles, the mixing equipment should be able to provide sufficient mixing energy to break down the aggregates and then force them to disperse, creating an evenly distributed mixture.

De-mixing (segregation) is a phenomenon taking place concurrently with mixing but also during storage. The factors driving segregation include the sharp differences in particle size, particle habit and density.[253-254]

IGC has emerged as a potential technique for quality control of mixing and blending processes. Sampling could be performed from batches, obtained from mixing or blending processes. The surface energy of the harvested sample could be measured by means of FD-IGC. Having prior knowledge of the surface energy of the constituent components of the mixture, the degree of mixing can be calculated. However, this type of measurements is subjected to severe limitations, imposed by the adsorption nature of the technique. Let's consider a binary mixture comprising of two powders, one with high and one with low surface energy. The solvent probes interact preferentially with the particles exhibiting higher energy, leaving the adsorption sites of the lower energy material empty. Thus, especially at low values of surface coverage, only one of the materials is effectively taking part the measurement. The development of computational tools enabling the determination of the surface energy distributions from IGC data, can boost the applicability of IGC as a quality control tool for mixing and blending. IGC measurements can potentially be employed to identify the differences between mixed and coated samples can be identified, but special care needs to be

taken, to make sure that in the coated samples the guest particles are mechanically locked on the surface.

In one of the pioneering studies showing the applicability of FD-IGC in quality control of pharmaceutical processes, the mechanism of interaction between salbutamol sulphate and magnesium stearate particles, upon mixing was investigated.[233] FD-IGC measurements reveal that the van der Waals surface energy profile of the mixture was almost identical to that of the magnesium stearate. The authors combined these results with complimentary techniques, such as SEM to suggest that the magnesium stearate creates a coating layer around the salbutamol sulphate particles. Nevertheless, they have not reported control experiments were a physical mixture of the two compounds was measured using IGC. Considering the range of surface energies exhibited by the two materials, it can be expected that IGC experiments alone, would have not been sufficient to shade light to the mechanism. Thus, FD-IGC measurements should be complimented in advanced studies. In similar studies, the surface energy maps of two blends of fine lactose (LH210) and large lactose (LH250) at different ratios were found to be exhibit similar behaviour with the mixtures of salbutamol sulphate with magnesium stearate.[255]

AFM has been deployed for the investigation of multicomponent mixtures. The accuracy provided by the AFM enabled the elucidation of one of the mechanisms via which fines can improve the performance of dry powder inhalers. It was shown that upon mixing, the fines are attached to the more energetically active sites of the carrier particles, making them less accessible for drug particles. Thus, upon aerosolisation, the drug particles are released more easily.[256]

3.4.3 Dry coating

Dry coating is the process where submicron-sized guest particles directly attach onto relatively larger, micron-sized host particles, by means of mechanical forces, in the absence of

a liquid medium. Mechanofusion has been used to modify the surface properties of powders by coating powders with guest particles with different surface chemistries.

Dry coating can be performed via equipment such as the magnetic assisted impaction coater (MAIC) and mechanofusion apparatus.[250, 257] Magnesium stearate, a well-established lubricant, has been widely used in coating by mechanofusion. Previous studies have revealed the versatility of magnesium stearate as a guest particle, improving the properties of various host particles, such as acetonide, fine lactose, salbutamol sulphate, salmeterol xinafoate and triamcinolone.[258-259] In fact, dry coating of α-lactose monohydrate with magnesium stearate was found to be much more effective compared with conventional mixing via a turbular mixer.[260]

Recently, Resonant Acoustic Mixer (RAM) has been proposes as a promising technique to improve mixing and mechanofusion. A high intensity acoustic field to transmit energy into a mixing vessel containing both the host and the guest particles. The current technology enables the particles to be accelerated with a force equal up to 100 times that of Earth's gravitational acceleration. RAM was found in proof of concept studies to be able to handle pharmaceutical particles quite well.[261] Furthermore, owe to its design it can be easily scaled up and it can be easily shifted from a batch mode to a continuous one. Thus, it has a number of attributes making it an attractive technique for future applications.

3.4.4 Milling

Micronisation and milling are commonly used pharmaceutical processes for reducing particle size of pharmaceutical materials.[262-263] A reduction in size is extremely important in the development of dry powder inhaler, since particles of < 5 μm size can reach the lower respiratory tracts which are the primary sites of drug delivery through inhalation. In tablet manufacturing, APIs are micronised before wet granulation with excipients. Micronisation is often carried out using high energy air jet mill while ball milling is, also used. The process is

influenced by many factors, which are quite often omitted. Most importantly, little attention is given to the properties of the feed material (particle size and particle habit), reducing the efficiency of the process.

Micronisation creates new interfaces by fracturing or breaking a particle, by creating lattice defects, or by producing amorphous sites on a crystalline material. The new crystalline interfaces may correspond to new, facets, not exposed in the initial sample. Therefore, this process may increase or decrease the surface energy of powders based on the nature of the newly created interfaces. However, in practice the high energy sites occurring in the form of defects dominate the surface energy of the final product. Heng et al. used acetaminophen to assess the changes in surface energy upon milling.[264] The milled material was sieved and the dispersive component of surface energy was measured by means of vapour sorption. The van der Waals components of the surface energy was found to increase with decreasing particle size of sieved fractions. This was attributed to the surface energy of the weakest attachment energy plane for the acetaminophen crystals. Using contact angle measurements on macroscopic crystals, it was shown that the weakest attachment energy plane, with a relatively small acid-base component of surface energy, compared to the van der Waals one.

In general, an increase in dispersive or non-polar surface energy was observed upon micronisation of compounds, such as form I paracetamol, salbutamol sulphate, salmeterol xinafoate, and crystalline α-lactose monohydrate. Increase in surface energy may result in increased aggregation due reinforced cohesive interactions, overcoming the gravitational forces. Milling of DL-propranolol was found to result in an increase of the van der Waals component of the surface energy, until a particular point, called the brittle to ductile transition point. After this point the milled material was found to exhibit a decrease in the van der Waals component of the surface energy with further milling.[265] A similar behaviour was reported for the milling of ketoconazole and griseofulvin, again with the use of IGC measurements.[266]

However, micronisation of compounds showed to lead to more intriguing changes on the acid-base component of the surface energy. For example, the acidic component of surface energy appears, upon micronisation to decrease for DL-propranolol, salbutamol sulphate, salmeterol xinafoate and α-lactose monohydrate, but to increases for acetaminophen. On the other hand the alkaline component of surface energy appears, upon micronisation, to increase for DL-propranolol,[265] salbutamol sulphate,[267] and α-lactose monohydrate,[268] but to decrease for acetaminophen.[264] This peculiar behaviour can similarly to before be attributed to the fact micronisation exposes new surfaces. Unfortunately, only the study for acetaminophen employs wettability measurements to verify its results, in the context of surface energy anisotropy. In any case, one should keep in mind a number of issues associated with the measurement of the above changes. In all these studies, surface energy was determined via infinite dilution IGC and the results correspond to a small, very limited, amount of the material. Furthermore, the issues associated with the accuracy of the currently existing methodologies for the experimental determination of the acid-base component of the surface energy, should be taken in account and create scepticism.

A limited number of finite dilution IGC studies exists, showing more robust results, compared to those from infinite dilution measurements. It has been shown that the distribution of the acid-base component of the surface of milled α-lactose monohydrate is more heterogeneous compared with that of untreated α-lactose monohydrate.[44] Nevertheless, one should keep in mind that the deconvolution performed in order to calculate the distribution of surface energy sites, is not the one described in the previous chapter, that is based on the mechanistic modelling of the adsorption process.[19-20] Instead an empirical method, based on the surface area below the surface energy map was used. Infinite dilution measurements showed that milled α-lactose exhibits a more profound acid-base component of surface energy than untreated α-lactose monohydrate at infinite dilution. However, finite dilution measurements

showed that at higher surface coverages, the milled α-lactose monohydrate carries lower surface energy than the unmilled α-lactose monohydrate. In another study, with ibipinabant as the model compound, a more complex behaviour was reported upon milling.[269] The acid-base component of surface energy after micronisation was measured to be smaller, compared to before micronisation, at low surface coverages whereas it was larger at bigger coverages. This result, it is subjected to the limitations discussed before, associated with the very fundamental nature of the measurements of the acid-base component of surface energy. However, it suggests a redistribution of the surface energy sites upon milling.

From the hitherto discussion, it is clear that the use of in silico tools, enabling the deconvolution of surface energy distributions from surface energy maps, can be highly beneficial. Especially for the case of milling these models, can be highly successful. Defects occupy a small portion of the surface area of the material. Thus, their contribution influences mainly the left-hand side of a surface energy map, as the one shown in Figure 2.12, but it also has effects to higher coverages. Using wettability measurements on macroscopic crystals, the facet specific surface energies can be determined. Then these data can be used for the deconvolution of the surface energy distributions of the same material milled at different conditions. This would allow the simultaneous identification of the formation of new facets and the creation of high energy defects.

4. Aspects of the influence of sample preparation on IGC measurements: the cases of silanised glass wool and column packing structure

4.1 Introduction

Inverse Gas Chromatography (IGC) emerged in the mid-70's as an attractive technique for the characterisation of the particulate materials.[22, 270] The fundamentals of this technique have been outlined extensively in Chapter 2. As it was shown, in its finite dilution mode, IGC produces a surface energy map showing the value of surface energy measured at a variety of surface coverages. These maps can then be used in conjunction with *in silico* models[19-20] to enable the construction of surface energy distributions describing the surface energy heterogeneity.

Nowadays, IGC is widely used in both academia and industry, contributing to the characterisation of different materials. However, cases exist where different researchers record different data for the same material. Similarly, cases also exist where researchers raise questions regarding the effect of packing on raw chromatographic data and the corresponding results. In the literature, detailed analyses are provided for the accurate analysis of IGC data, however no systematic work, investigating the importance of sample preparation or good experiment practice in general, is reported. This work deals with two important aspects of IGC experiments focusing on the column preparation. The first is the amount of silanised glass wool used in the packing of IGC columns. The second examines the effect of column packing pattern. The experimental data presented are rationalised by the findings on *in silico* studies.

Silanised glass wool is a commercially available fibrous, amorphous material, used to assist the package of powders in IGC columns, ensuring no powder movement during the measurements. Silianised glass wool carries some surface energy and thus it could potentially influence the measurements, as the injected probe molecules, interact with

it, as well. However, it was not possible to identify, in literature, a reliable code of good experimental practice which includes some data on how to identify what is the maximum amount of silanised glass wool that can be used without influencing the quality of the measurements. Intuitively, one could think that this would be a function of the specific surface area of the material and its surface energy; neither of the two are reported in literature.

As it has been outlined in the previous chapter, powder blending is an important process in pharmaceutical process development. Nevertheless, the quality control methods for it are not always very robust; IGC can provide an alternative for some cases. However, as it is an adsorption-based method the interpretation of the data is not necessarily straightforward. An IGC based quality control protocol for the blending of a binary (or an arbitrary) system of powders, should commence with baseline measurements of the surface energy of the two components at different ratios. In this direction, the second section of this chapter investigates whether the packing structure of a binary powder system would influence the IGC measurements.

4.2 Experimental Methods

The silanised wool, used in the experiments described in this chapter, was acquired commercially (Sigma Aldrich, Poole, UK); the material was used as received. During packing the fibrous material is introduced in the glass column with the aid of some sort of stick. Usually a small amount of the material is introduced in one side of the column and the weight of the column with it is measured. Then the powder of interest is added, with the aid of a funnel, and the mass of the column is measured again to find the amount of powder added. Then the column is sealed with the addition of silanised glass wool on

its other side. In this work, the importance of silanised glass wool is under investigation, thus known masses of it are used.

α-Lactose monohydrate, a sugar used as a pharmaceutical excipient, was used as the model material in the experimental studies investigating the impact of silanised glass wool in surface energy measurements via IGC. α-Lactose monohydrate was acquired commercially (Sigma Aldrich, Poole, UK) and was recrystallised. Cooling crystallisation, under stirring, was used in the recrystallisation.

For the studies, investigating the influence of packing, anhydrous p-monoclinic carbamazepine, a common antiepileptic drug, and δ-mannitol, another sugar used as an excipient, were employed. Carbamazepine was purchased from Apollo Scientific, Stockport, UK, and was recrystallised from methanol, under stirring, to obtain fine powder. δ-Mannitol were obtained commercially (Sigma Aldrich, Poole, UK), and was recrystallised from a mixture of deionised water and ethanol, under stirring, as well. The active pharmaceutical ingredient (carbamazepine) and the two excipients (δ-mannitol and α-lactose monohydrate) used in this study are not only studied in this chapter but elsewhere in this work. In particular, a lot of emphasis is given on carbamazepine, in Chapters 5, 7, 8 and 9.

The surface areas of the aforementioned materials, both the powders and the silanised wool, were measured using two alkane probes, octane and nonane. The surface energy measurements were carried out using three alkane probes, octane, nonane, and decane; at surface coverages ranging from 0.003 to 0.1. The Schultz's construction was used in surface energy calculations. The results presented in this study exhibit an R^2 agreement greater than 0.999.[271] The study did not expand to higher values of surface coverage to avoid encountering complexities associated with the effects of lateral

interactions, scaling with increasing surface coverage. In the case of strong lateral interactions, the chromatograms exhibit fronting. At this regime, the instrument is not effectively measuring adsorbate-adsorbent interactions, but only the interactions between solvent molecules, making the measurement inaccurate. The properties of the alkane probes used in this study are summarised in the following table.

Table 4.1: The properties of the alkanes used in the IGC measurements, which are relevant to this work.

Alkane	**Molecular cross sectional area (Å^2) at 20 ^{o}C[115]**	**Surface tension at 20 ^{o}C (mJ/m^2)**	**Change in surface tension for 1 ^{o}C increase in temperature (mJ/m^2)**
Octane	64.9	21.62	-0.0951
Nonane	69.6	22.72	-0.0936
Decane	74.4	23.83	-0.0920

4.3 Results and discussion

4.3.1 Influence of silanised glass wool

This section outlines a simple set of experimental and *in silico* studies, used to determine the influence of silanised glass wool. The results obtained were used to propose a road map for the optimum selection of the amount of silanised glass wool used in the measurement of materials with different surface energies.

The surface area of the silanised glass wool was determined, as mentioned in the "Experimental Methods" section, to be about 0.27 ± 0.02 m^2/g. The dispersive surface energy map of silanised glass wool was then determined using the three alkanes mentioned in the previous section. The next step was to determine the surface energy maps of α-lactose monohydrate sample. About 2.5 g of α-lactose monohydrate were packed with about 0.1 g of wool and measurements of surface area (found to be about

0.4 m^2/g) and surface energy were conducted. This first measurement of surface energy was used as the baseline for α-lactose monohydrate. In later experiments silanised glass wool was added on top of this 0.1 g. Inarguably, this minor addition of wool can, theoretically, influence the data. Nonetheless, it would become clear from the *in silico* experiments, presented later on in this chapter, that such an amount of wool, packed with a material like α-lactose monohydrate, does not have a measurable impact in the measurement. The surface energy distributions were determined, using a multi-solvent system site filling model based on Boltzmann statistical distribution, under the assumption that it comprises from the sum of four Gaussian distributions, each one at a different ratio, each one representing an adsorption site of different surface energy. Aspects of this model have already been presented in Chapter 2. The surface energy distributions obtained for the pure glass wool and the almost pure α-lactose monohydrate would be the surrogate for the development of a quantitative study of the importance of silanised glass wool in IGC measurements.

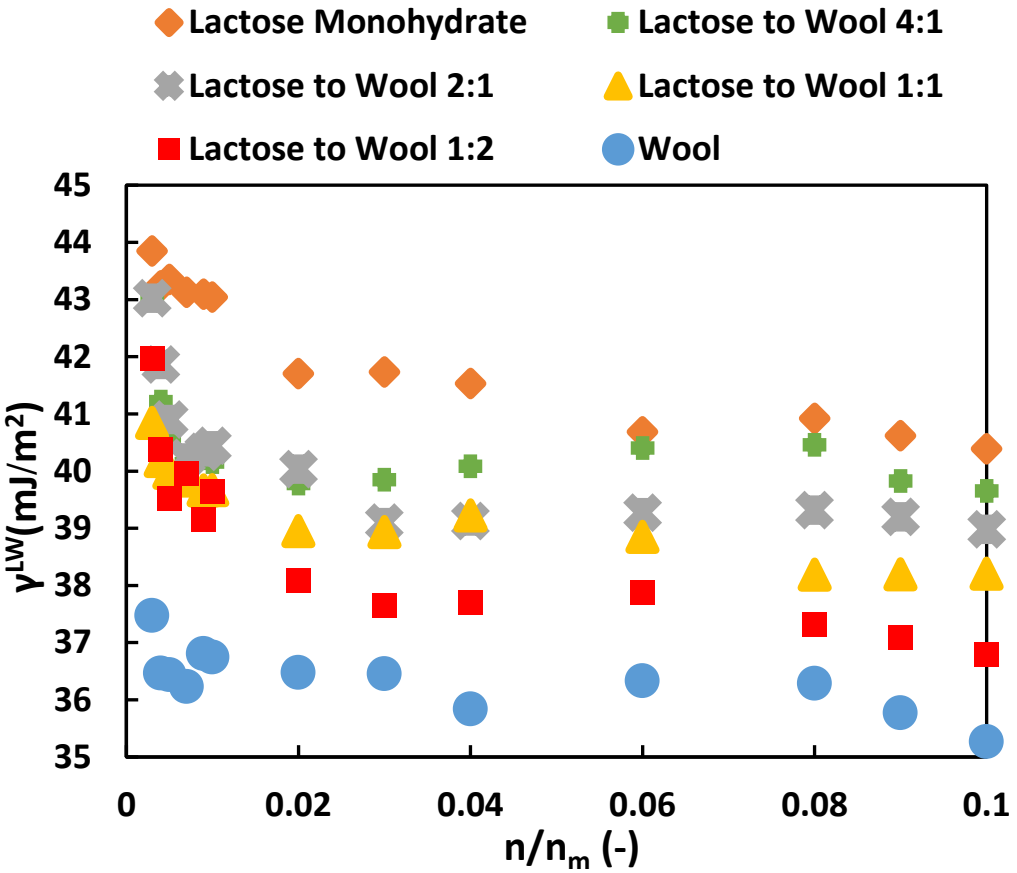


Figure 4.1: Surface energy maps of α-lactose monohydrate (termed simply lactose in the legend) and glass wool at different combination ratios.

The next step was to pack silanised glass wool (W) and α-lactose monohydrate (L) at a series of surface area ratios (the ratio of the surface area of the silanised glass wool to the surface area of the α-lactose monohydrate baseline), L:W =1:2, 1:1, 2:1, 4:1. The mixtures were examined and the curves of dispersive surface energy as a function of surface coverage are shown in **Figure 4.1** for these samples. It is important to note that the two baseline measurements act as the boundaries, α-lactose monohydrate is the higher boundary while silanised glass wool is the lower boundary. Data for all mixtures lie in-between the two boundaries. Considering that the surface area of the silanised glass wool is about 65% of the α-lactose monohydrate and that the silanised glass wool is fibrous in nature, an experienced IGC operator would immediately realise that the

amount of silanised glass wool used in the aforementioned mixtures is much higher than the amount is frequently used. This was done intentionally in order to examine the limits of the influence of silanised glass wool. The surface energy maps of the mixtures of wool with α-lactose monohydrate were determined. It is important to clarify, that for the calculation of the surface coverage, only the α-lactose monohydrate content was taken in account. The reason for this was to highlight the erroneous results associated from the use of excess amount of wool. In other words, the experiment was trying to reproduce conditions were an IGC operator, unaware of the importance of the amount of silanised glass wool in the measurements, is packing the samples using excessive amounts of the fibrous material.

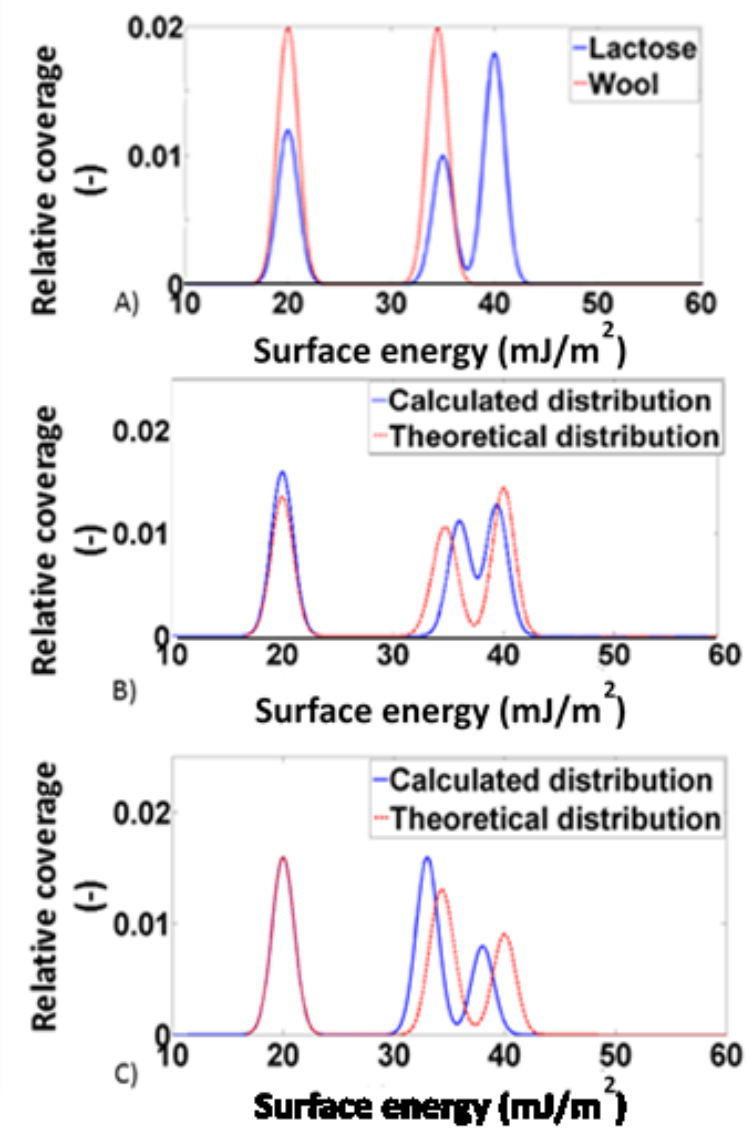


Figure 4.2: A) The calculated surface energy distributions of the silanised glass wool and α-lactose monohydrate, B) The calculated surface distribution obtained from the deconvolution of the surface energy map of a 1:4 wool to α-lactose monohydrate mixture, using the *in silico* tool developed. The theoretical distribution was obtained from the combination of the surface energy distributions of the constituent components of the mixture at the aforementioned ratio. C) The same as for B but for a 1:1 wool to α-lactose monohydrate mixture.

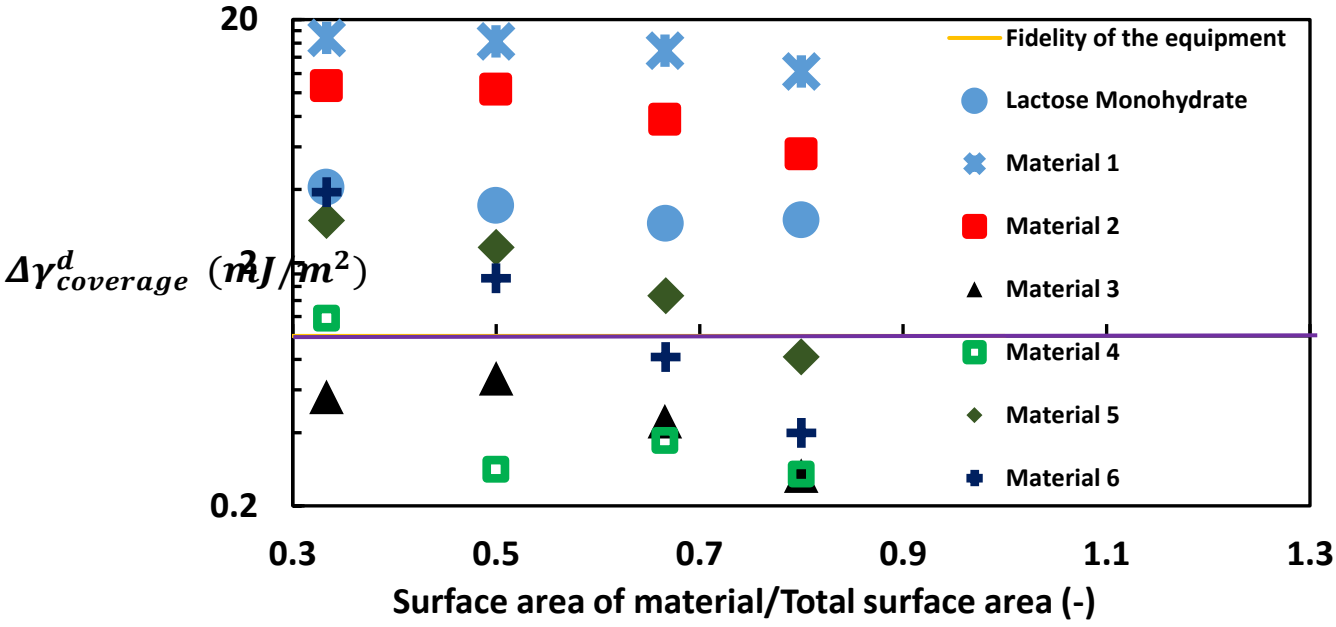


Figure 4.3: The deviation of the measurements at different loadings of silanised wool for the α-lactose monohydrate and the two simulated materials.

Using *in silico* tools,[20] it was possible to calculate the surface energy distributions of the samples by fitting their surface energy distributions in a mathematical model describing heterogeneous adsorption. In these calculations, the surface areas of the columns was fixed, in order to obtain a meaningful distribution; contrary to the previous paragraph, where the aim was to highlight the erroneous results, that will be obtained from the excess amount of silanised glass wool. Theoretical surface energy distributions were determined by appropriate combinations of the surface energy distributions of α-lactose monohydrate and wool. For instance, for the column containing equal amount, by surface area, of α-lactose monohydrate and silanised glass wool the theoretical surface energy distribution was calculated by multiplying the distributions of the two individual components (wool and α-lactose monohydrate) by 0.5 and adding the two products together. In **Figure 4.2**, these theoretical surface energy distributions are depicted, along with the surface energy distributions obtained from the fitting of the

experimental data, using the *in silico* tool. By inspection, one could see that in both cases illustrated in this figure, the theoretical and the actual surface energy distributions are quite similar. This is a very promising result, as it verifies the accurate execution of the experiment and the robustness of the *in silico* tool employed. Furthermore, it indicates that there is no formation of new interfaces, upon mixing of the two materials, that can alter the measurement.

The quantification of the effects of the silanised glass wool requires the use of an approach taking into account all the surface energy map. Thus, the following equation was developed measuring the deviation of a point at coverage x of a mixture of α-lactose monohydrate with silanised glass wool, with the corresponding point obtained from the surrogate column:

$$\boldsymbol{\Delta\gamma^{d}_{coverage\ x} = \gamma^{d}_{coverage\ x\ of\ lactose} - \gamma^{d}_{coverage\ x\ of\ sample\ x}} \qquad \text{Eq. 4.1}$$

where α-lactose monohydrate stands for the baseline α-lactose monohydrate column and sample x for the combinations of α-lactose monohydrate with different amounts of silanised glass wool. The largest value of $\Delta\gamma^{d}_{coverage\ x}$ for each column, was found and plotted against the corresponding ratio of surface area of material to the total surface area of the packed material in the column, given by the summation of the surface area of the material with that of the silanised glass wool. The results of this operation are illustrated in **Figure 4.3**. One should observe that for the case of the α-lactose monohydrate even when the surface area of the sugar is four times bigger than that of the silanised glass wool packed, the deviation from the real surface energy can be up to three times larger than the fidelity of the instrument (~ 1 mJ/m^2).

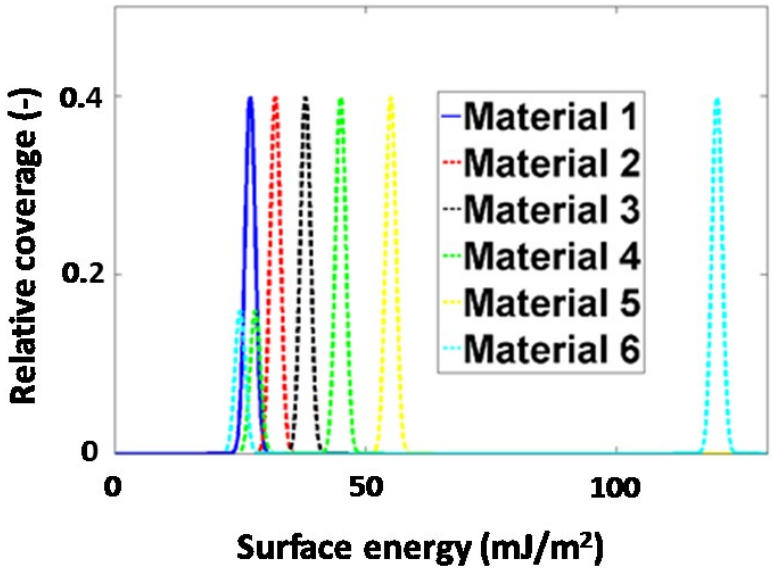


Figure 4.4: The surface energy distributions of the six *in silico* materials, investigated in this study.

As the influence of silanised glass wool was verified experimentally, *in silico* studies were deployed to investigate the limits of this influence. Six model materials with a wide range of surface energies were simulated. The surface energy distributions of these materials are shown in **Figure 4.4**. These are in silico created material, with specific surface energy distributions. They do not correspond to specific materials used in pharmaceutical industry or elsewhere. The range of values was chosen to be in realistic limits encountered in commercial materials, while providing sufficient breadth of values, so to explore different possible scenario. The same procedure for the calculation of the maximum deviation was employed and the results obtained are shown in **Figure 4.3**. The most intrinsic finding of this analysis is that the materials can be categorised in three main categories. The first category includes Materials 1 and 2. These materials exhibit surface energy smaller than silanised wool (γ^d < 30 mJ/m^2), corresponding to hydrophobic polymers like polytetrafluoroethylene (PTFE). When these materials are investigated, the surface area of the packed material should be much

larger than silanised wool because. In fact, as it can be seen from **Figure 4.3**, even when material's surface area is four times larger than that of silanised glass wool, the error in the measurement can be up to five times the standard equipment error (approximately 1 mJ/m^2). The second category involves Materials 3 and 4, with surface energy similar to silanised wool ($30 < \gamma^d < 40$ mJ/m^2). The surface energy of these materials is similar to this of the wool, the effects of silanised wool are camouflaged and are not manifested in the measurement. The last category includes materials similar to Material 5 and 6, exhibiting high surface energies ($\gamma^d > 50$ mJ/m^2). The affinity of an adsorbate molecule towards two different adsorption sites can be determined by means of equation 2.70. In the context of this equation it is not a surprise that for high surface energy materials the measurements is not affected even if the surface area of the material under investigation is equal to that of the silanised glass wool. However, heterogenous adsorption is a non-linear phenomenon, the non-linearity of which is driven by the surface energy heterogeneity. Thus, it would not have been possible to attempt to generalise further the results of this study, as the amount of computational complexity will very easily culminate.

The findings of this section are important as they highlight the need for complimentary techniques in surface energy measurements. In order for an IGC operator to select the optimum amount of silanised wool for a specific material, prior knowledge of the order of magnitude of surface energy is required. Furthermore, the importance of this section is that it provides with numerical data for the surface energetics of silanised wool which can be used in the design of experiments. Finally, the computational framework described can be used as a tool for researchers to assess previous measurements in the light of the findings of this paper.

4.4 Effects of packing

4.4.1 IGC measurements

Mixtures of carbamazepine and δ-mannitol were used in this study. The materials were prepared as described in the Experimental Methods section. Their surface area was found to be quite similar (about 0.35 m^2/g). Chromatographic columns were packed, using four different ways, with the aforementioned materials, at a 1:1 surface area ratio. The four different ways of packing are outlined in **Table 4.2**. The surface energy of each of the columns was measured and the results were plotted in **Figure 4.5**. Similarly with the wool analysis, the surface energy distributions of the two materials were calculated.

Table 4.2: Depiction of the four different packing configurations tested experimentally; in the schematics carbamazepine is shown to have a yellow color, while δ-mannitol is shown with blue color; thus, the physical mixture of the two is naturally depicted green.

Packing name	Description	Schematic
Physical mixture	Powders are physically mixed together	
Janus	Two layers of powder; a carbamazepine and a δ-mannitol one on each side of the column.	
Tapir	Three layers of powder; the upper and the bottom layers are δ-mannitol, and the middle layer is carbamazepine	
Zebra	Six layers of powder, alternating between δ-mannitol and carbamazepine	

From **Figure 4.5**, it can be seen that there is not a large variation in the measured surface energy of the mixtures, indicating that the packing of the material does not influence the IGC measurements. In addition, the deconvoluted surface energy distribution of the mixture agrees with the theoretically distribution predicted from the combination of the surface energy distributions of its constituent components. From a

formulation perspective, this is a quite important finding. It indicates that the influence of the solid-solid interfaces is negligible. Thus, no mechanical interlocking or particle coating is observed. In turn, this suggest that IGC can be used as a quality check technique for processes such as dry coating. The powder is expected to give different profile in the case where mechanical interlocking, between two types of powders, is observed compared with cases where only dispersion of the two powders occurs.

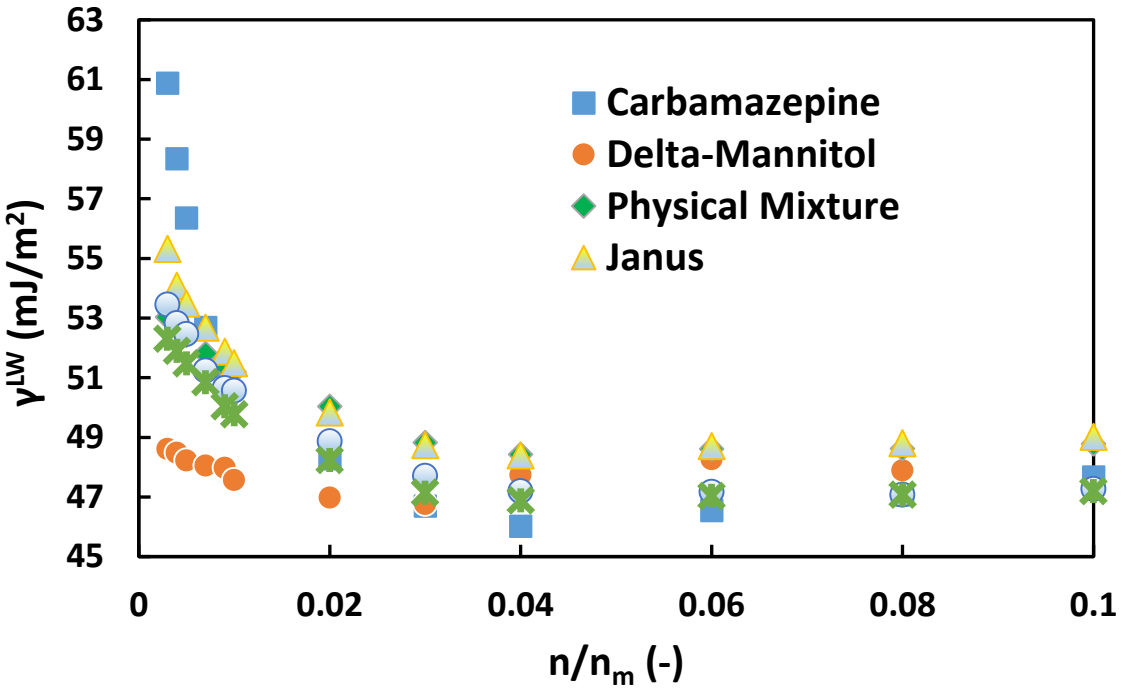


Figure 4.5: The surface energy measurements obtained from pure carbamazepine, mannitol, and 1:1 mixtures of the two packed with different configurations.

4.4.2 Monte Carlo simulations

The fundamentals of the *in silico* tool used for the deconvolution of surface energy heterogeneity used in the previous section of this chapter, has been discussed in Chapter 2, as well as in literature. It is a deterministic model, where no randomness is involved. However, as has been mentioned in Chapter 2, using arguments similar to those Professor Albert Einstein[111] used to classify Brownian motion as a stochastic process,

adsorption processes can be classified stochastic as well. In other words, the adsorption phenomenon can be understood as an agglomeration of smaller and simpler interactions, during which individual gas molecules interact with a solid. By repeating the same simple gas solid interaction over a large number of times, the equilibrium behaviour of the system could be determined, along with the variability associated with every stochastic phenomenon.

In this context, the surface energy heterogeneity is not described, anymore, by an equation, but by a two dimensional lattice. For the case of heterogeneous adsorption, each site of the lattice can carry a different values of surface energy. A square type of lattice was chosen, instead of a hexagonal one, in order to keep the computation times in a reasonable time frame.

A Grand Canonical Monte Carlo ensemble is used for the simulations, presented in this work.[112-113] This means that the aforementioned lattice is in thermodynamic equilibrium with a sink of particles. In this case, the particles are chain entities resembling the chain alkanes used in IGC measurements. These particles are going to interact with the lattice during the simulation. In IGC is assumed that the changes in the Gibbs free energy of adsorption are due to adsorption/desorption phenomena and that no surface diffusion occurs. Thus, for the purposes of these simulation, the particles interacting with the lattice can either attempt to adsorb on it or if they are already adsorbed they can attempt to desorb. However, no movement of particles on the lattice can be performed. The Metropolis criterion was used to calculate the probability of adsorption/desorption phenomena. This is a detailed process that has been extensively discussed in literature.

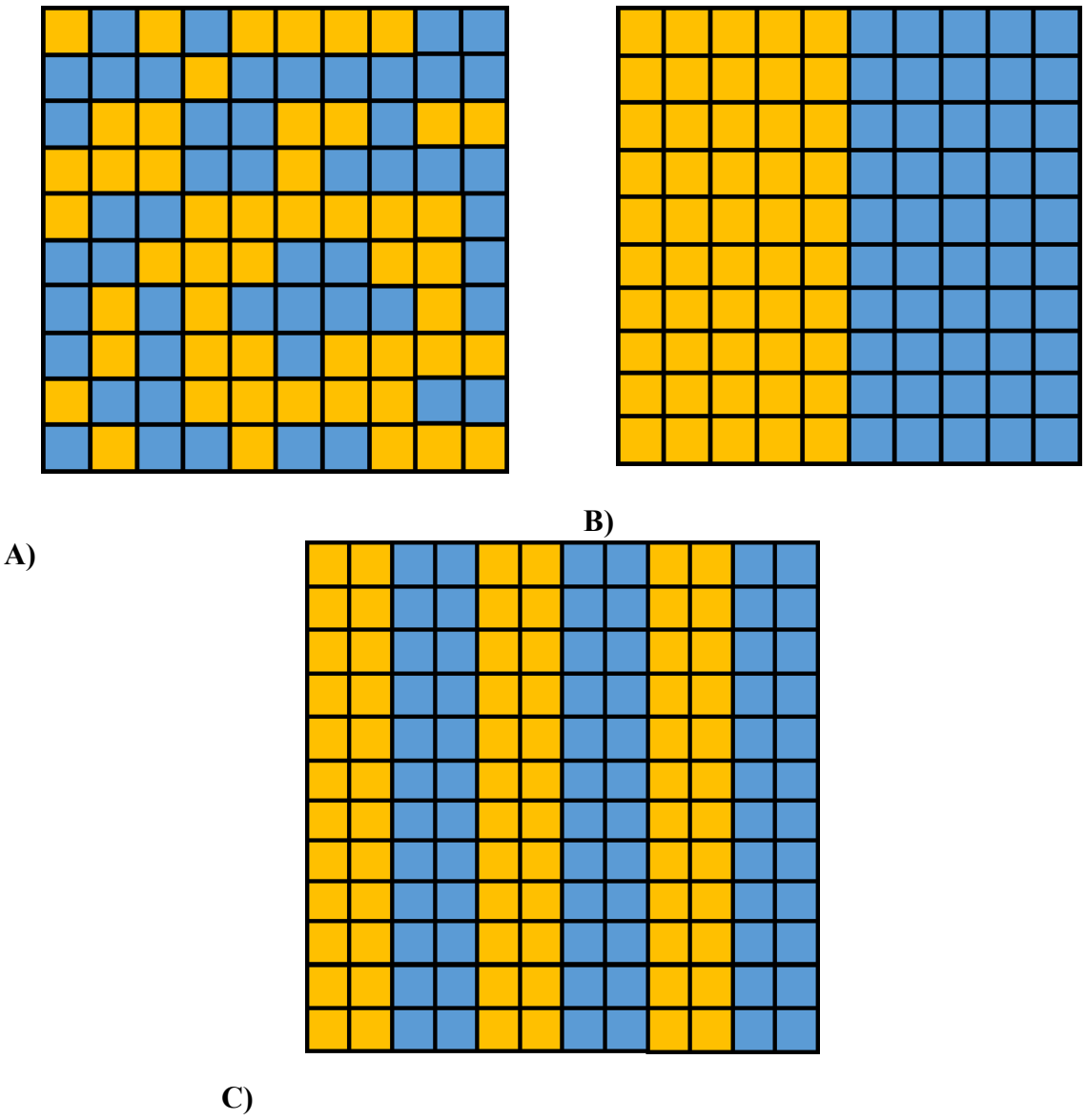


Figure 4.6: Schematic depictions of the three different types of lattice employed in the Monte Carlo simulations; A) is for the physical mixture, B) is for the Janus and C) is for the zebra. The lattices are not in scale and the two different colours represent materials A and B.

Monte Carlo simulations based on the works conducted were done on 500 x 500 square lattices. Three different types of lattice arrangements (depicted qualitatively in **Figure 4.6**) were used in order to verify the results obtained from the surface energy measurements on materials packed at different ways, as shown in **Table 4.2**:

a) Physical mixture lattice: The adsorption sites predicted by the energy distributions are allocated randomly throughout the lattice
b) The two side lattice: In this case the lattice was divided in two sections each with dimensions 500 x 250, the adsorption sites for material A were distributed on one side and those for material B were distributed on the other side.
c) The zebra lattice: It is similar with (b), but it has six sections each with dimension 500 x 83 (apart from one which is 500 x 84).

The schematics in Figure, qualitatively describe the three types of lattice. Material A was given a surface energy of 45 mJ/m2 and material B was given a surface energy of 25 mJ/m2. In addition a small amount of high energy sites with surface energy of 100 mJ/m2 were distributed randomly around the lattice to account for the high energy defects. The experiments were conducted at a relative pressure leading to small coverage in order to minimise effects associated with the orientiation of the adsorbates. **Figure 4.7** depicts a section of the physical mixture lattice at the end of the simulation. The worm like structures appearing in the image at the right correspond to the decane adsorbate. One should notice that the total coverage is not high in order to avoid issues with the orientation of the adosrbate molecules.

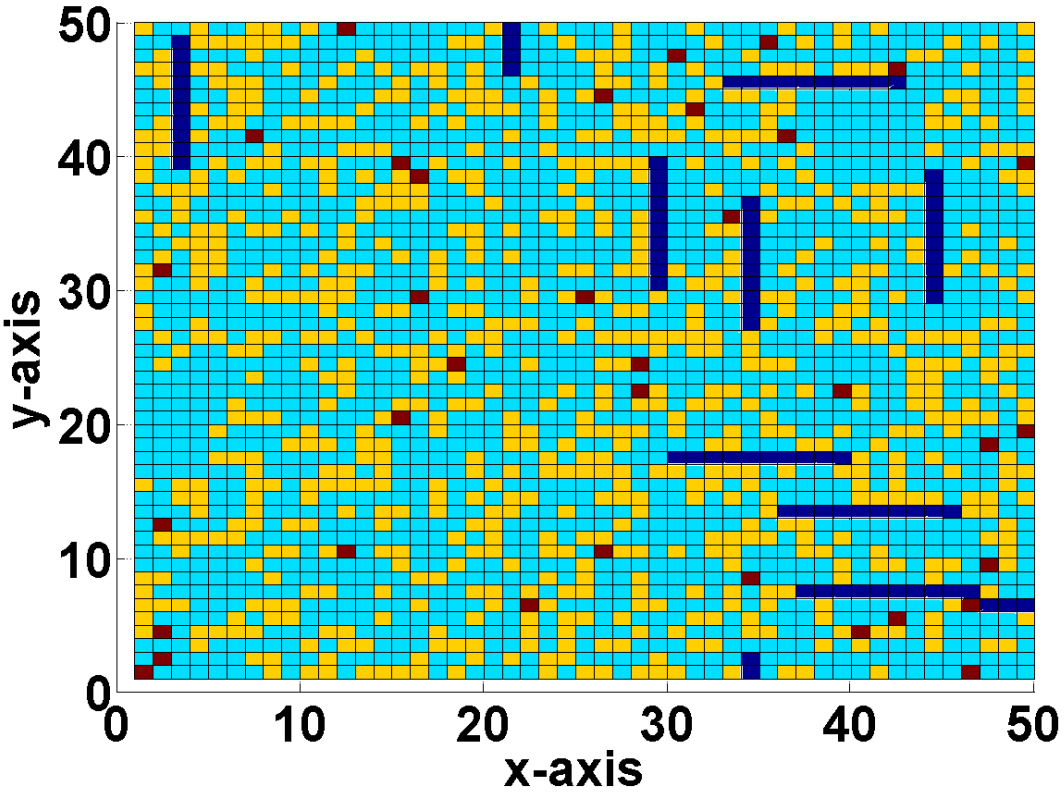


Figure 4.7: Snapshot of the physical mixture lattice used in Monte Carlo simulations at the end of a simulation. The worm like blue structures are the adsorbates.

The results obtained, from the Monte Carlo simulations, for the experienced surface energy of decane on the three different types of lattice are shown in **Figure 4.8**. The systems behave similarly in all three lattices meaning that no significant differences are identified for different lattice arrangements. In **Table 4.3**, the mean and the standard deviation of the experienced energy calculated for each case is shown. The results are quite similar and in the vicinity of the standard experimental error for IGC (~1 mJ/m^2). Thus, they are in agreement with the experimental findings for the influence of packing structure. The simulations are performed using adsorption sites with quite distinct values of surface energy (25 and 45 mJ/m2). If values corresponding to the surface energies of the materials used in the experimental section of this paper, the proximity of the results obtained from the simulation was going to be even smaller.

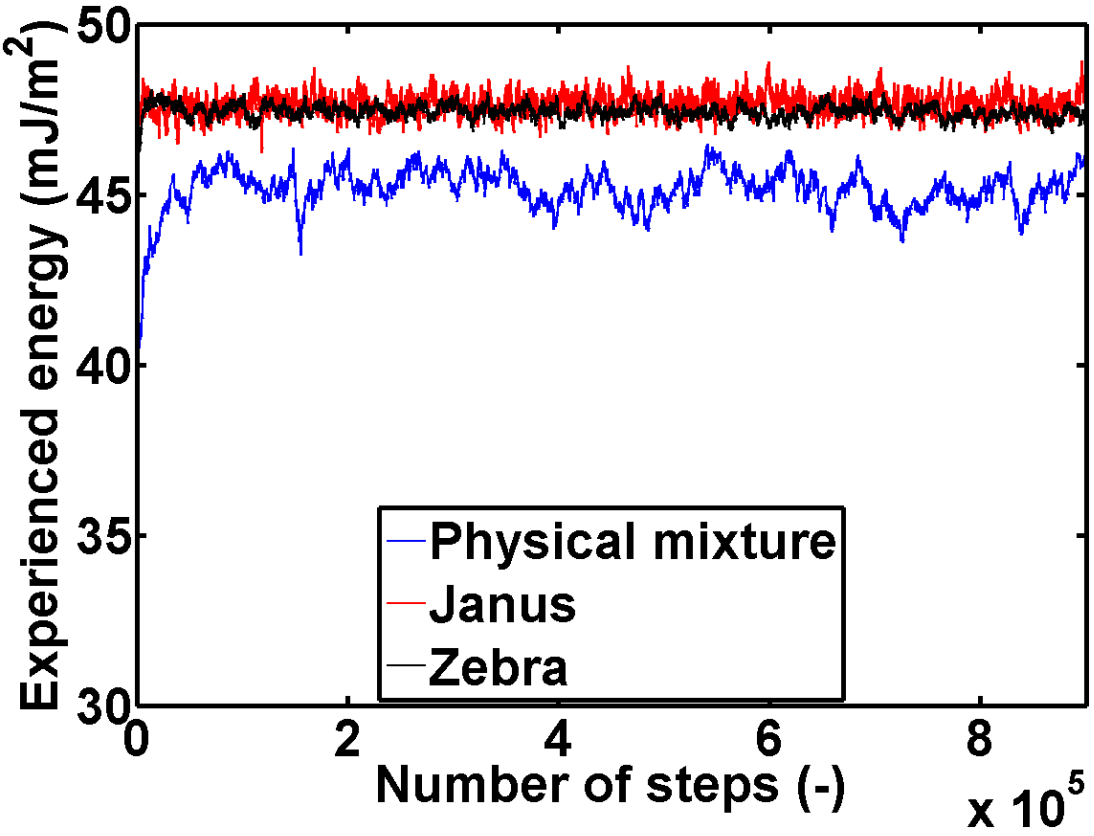


Figure 4.8: The results of the Monte Carlo simulations for decane on different types of lattice.

Table 4.3: The mean and the standard deviation of the experienced energy, calculated from the Monte Carlo simulations.

Lattice	**Mean experienced energy (mJ/m^2)**	**Standard deviation of experienced energy (mJ/m^2)**
Physical mixture	45.18	0.49
Janus	47.66	0.30
Zebra	47.41	0.18

Simulations were performed with octane as well showing the same qualitative behaviour. Using the results of the simulations, one could calculate the change in the Gibbs free energy (ΔG^0) of adsorption for both alkanes using the equation:

$$\Delta G^0 = \alpha_m N_A W_{AB}^0 \qquad \text{Eq. 4.2}$$

where α_m is the molecular cross-sectional area of the alkane, N_A is the Avogadro number and W_{AB}^0 is the work of adhesion. The results of simulations performed on the physical mixture lattice, for octane and decane at similar values (0.017 and 0.018 respectively) of surface coverage, are shown in **Figure 4.9**. As expected from the experimental results, the change in Gibbs free energy of decane is higher than for octane. As decane has a higher surface tension, a bigger change in the Gibbs free energy is required to cover the same amount of surface. This results for the change in Gibbs free energy of adsorption may not shade additional light in the effects of packing, nevertheless they act as sanity checks for the simulations.

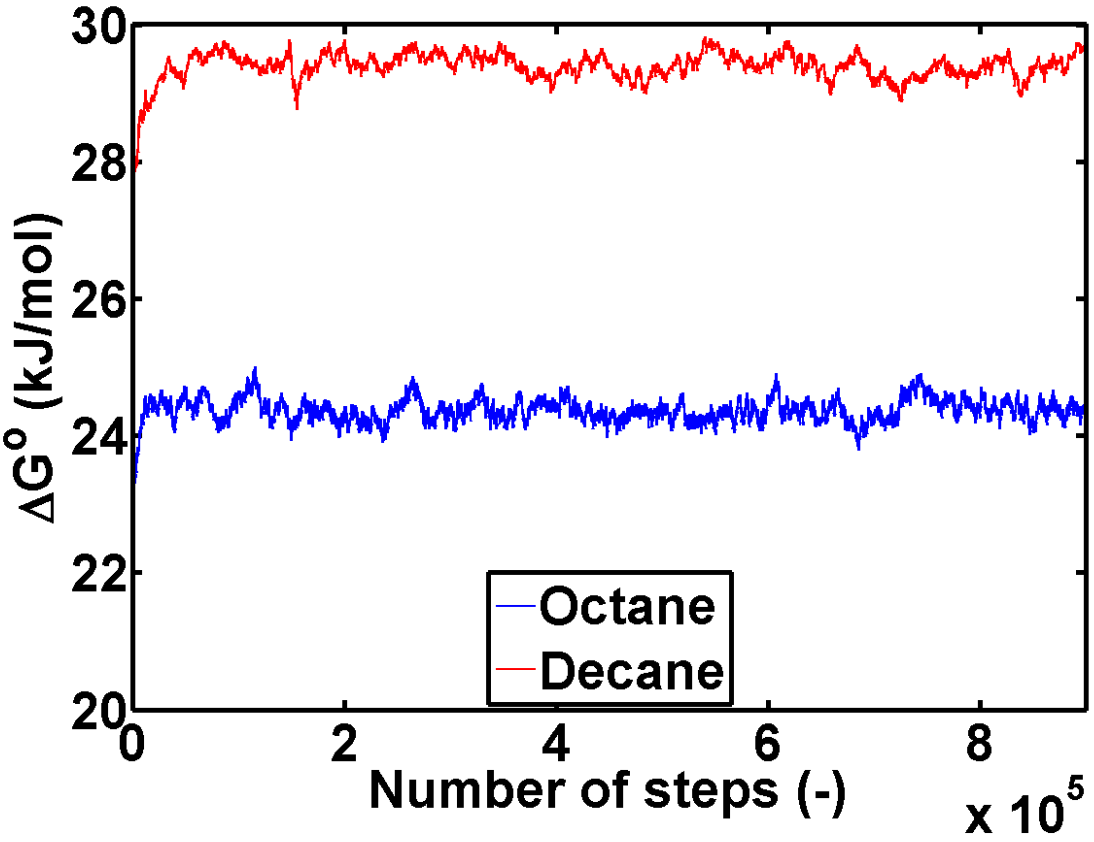


Figure 4.9: The change in the standard Gibbs free energy of adsorption calculated for octane and decane on the physical mixture lattice on similar values of surface coverage.

4.5 Conclusions

A combination of experimental and computational approaches was applied to investigate the influence of the amount of silanised wool and of column packing patterns on IGC measurements. For the case of silanised wool the surface energy of the material was examined using IGC measurements and computational models. The recommendation is that care should be taken especially for low surface area and/or low surface energy materials. The presented data could be used for guidance to determine how much material or wool should be packed in the chromatographic column and the computational models provide a versatile toolbox guiding researchers in the selection of the appropriate amount of silanised wool.

In addition, it was shown that the packing of mixtures of particulate materials does not significantly influence the experimental data and the surface energy results. All the experimental measurements were supported by state-of-the-art computational approaches, highlighting the importance of in-depth computational analysis of IGC data. The Monte Carlo simulations can be a powerful tool, for the understanding of various phenomena in gas-solid adsorption processes. Nonetheless, owe to their computational cost they cannot substitute other, deterministic, *in silico* tools developed for the deconvolution of the surface energy distribution of powders. Following the publication of the results of this study, at least one independent study has been published verifying the results presented in this chapter.[272]

In general this study verifies IGC as a powerful characterisation technique able to detect even small variations in surface energy between different samples. It reaffirms the importance of *in silico* tools for the in depth understanding of IGC results. In an era where multicomponent mixtures gain ground in pharmaceutical process development, the tools employed in this chapter, along with the corresponding outcomes, provide a robust framework for the investigation of processes, involving different types of powders such as mixing and dry coating.

5. The importance of spreading pressure in the determination of surface energy via IGC measurements

5.1 Introduction

In his work on "The Spreading of Fluids on Glass", published in 1919, Sir William Bate Hardy[273] argues that:

"Whether primary or secondary spreading does or does not occur on a fluid face depends mainly upon the relative value of the surface tensions, but on a clean solid face it must depend wholly upon the value of vapour tension."

Considering that the term vapour tension is directly related to spreading pressure, this constitutes the first scientific statement highlighting the importance of spreading pressure in wetting (for reasons of clarity it should be noted that the term clean solid surface does not refer to a molecularly smooth surface, but on a clean surface of normal glass). Nonetheless, the concept of spreading pressure has been discussed, by Hardy and other prominent members of the then scientific community, well before 1919, in the context of its importance in the spreading of oils on water.[274-276]

In 1937 Bangham and Razouk[77-79] applied Gibb's isotherm in gas-solid adsorption, in a work where they addressed the importance of spreading pressure. In fact, the mathematical interpretation for the influence of spreading pressure in adsorption was first proposed in these publications. This mathematical interpretation is still used in the following form:

$$\pi_e = \gamma_{SV}^0 - \gamma_{SV} = RT \int_0^{P_0} \Gamma \, d(\ln(P)) \qquad \text{Eq. 5.1}$$

In the above equation, π_e stands for the spreading pressure, γ_S and γ_{SV} are the surface energy of the solid and of the solid vapour interface respectively, Γ is the surface excess, R, T and P have the same meaning as in the ideal gas law. This equation suggests that when the influence of

spreading pressure is negligible, the surface energy of the solid is the same as the solid-vapour interfacial energy.[277]

In adsorption-based techniques developed for surface energy measurements, in the years followed the publication of this work, the importance of spreading pressure was omitted, on the basis that its value can be considered negligible. One such technique is Inverse Gas Chromatography (IGC), a widespread technique used since 70's. The fundamentals of the technique have been thoroughly discussed in Chapters 2 and in literature. IGC's paramount importance in the advancement of surface energy measurements is more than evident through the constantly growing number of operators in a wide range of disciplines both in academia and in industry.

Nonetheless, a limited number of publications have addressed the issue of good experimental practice of IGC. IGC measurements are usually performed in temperatures ranging from 25 ^{o}C to 150 ^{o}C, however in the majority of the published work the measurements are performed at around 30 ^{o}C. Situations exist where the researchers want to examine the behaviour of the material of interest under different conditions, however it is not unusual for operators to perform measurements at temperatures well above the aforementioned usual value in order to speed up the experiment.

From a fundamental physicochemical perspective it is expected that at higher temperatures the majority of the materials would have a lower surface energy; even though Lifshitz equation proposes that, theoretically, the opposite scenario is possible.[58, 278] The influence of temperature varies with the type of material, crystalline solids for example are less susceptible compared to amorphous materials.

The work presented in this chapter stemmed from some peculiar results obtained while measuring the surface energy of p-monoclinic carbamazepine, using IGC. This clear deviation

from theory, could be explained in terms of the influence of spreading pressure. Spreading pressure increases with temperature, owe to the higher tendency of the molecules to be in the vapour phase. Using tailored experiments, the spreading pressure was measured. By incorporating the values of spreading pressure on the surface energy measurements, it was possible to obtain corrected values of surface energy. The new results suggest a decrease in surface energy with increasing temperature, agreeing with theory. The results obtained were verified with the aid of SEM images and surface energy distribution calculations. Then the study was expanded for the case of carbamazepine's triclinic polymorph. This work provides a road map for the correction of IGC measurements at different temperatures. In addition, the findings, presented, can be used by fellow investigators to re – examine their results in the light of this work. In this direction, the main outcomes of Chapter 4 are re – examined.

5.2 Experimental Methods

Carbamazepine powder was purchased from Apollo Scientific, Stockport, UK, and was recrystallised in ethanol, acquired commercially (VWR, Radnor, PA, USA). The recrystallisation was performed under stirring in order to ensure the conversion of all the material to the p-monoclinic polymorph. Powder X-ray diffraction measurements on the resulting powder did not reveal the presence of any other polymorph.

The surface area of carbamazepine was measured using two alkane probes, octane and nonane. The surface energy measurements were carried out using three alkane probes, octane, nonane, and decane; at surface coverages ranging from 0.003 to 0.1. The measurements were performed at five temperatures; 25, 30, 40, 50 and 60 ^{o}C. The temperature in this study was kept relatively low, as carbamazepine has the tendency to sublime. The properties of the alkane probes used in this work are the same as those presented in **Table 4.1**, from the previous chapter. The Antoine's equation for each alkane was obtained from NIST thermophysical data

bank. The molecular cross-sectional area was assumed to increase, with increasing temperature, the same way the molar volume was increasing.

The Schultz's approach was used to determine surface energy at individual values of surface coverage, with the R^2 agreement being greater than 0.999. For the calculation of the surface excess, the isotherms were measured to higher values of surface coverage and then extrapolation was performed in order to be able to integrate over the 0 to P_0 range. The measurements were conducted using an IGC-SEA (Surface Measurement Systems, London, UK).

Macroscopic crystals of p-monoclinic carbamazepine were grown in methanol. The detailed description of this process is reported elsewhere. Seeds for macroscopic single crystal growth were prepared via a two-step cooling crystallisation of a methanol (VWR, Radnor, PA, USA) solution supersaturated with as received carbamazepine (Apollo Scientific, Stockport, UK). The seeds were then suspended in a supersaturated methanol solution, evaporating slowly at ambient conditions. The crystals were left to grow for a few weeks. Fresh supersaturated solution was added to ensure sufficient amount of liquid in the vessel. The dispersive component of the surface energy, for each of the major facets expressed, was determined using sessile drop contact angle method; diiodomethane, also acquired commercially (VWR, Radnor, PA, USA), was used as the probe liquid.

5.3 Results and discussion

5.3.1 IGC data

The first results from the measurements of the surface energy of p-monoclinic carbamazepine are shown in **Figure 5.1**. It can be seen that the data show an increasing tendency. To tackle this peculiar result, the concept of spreading pressure was employed.

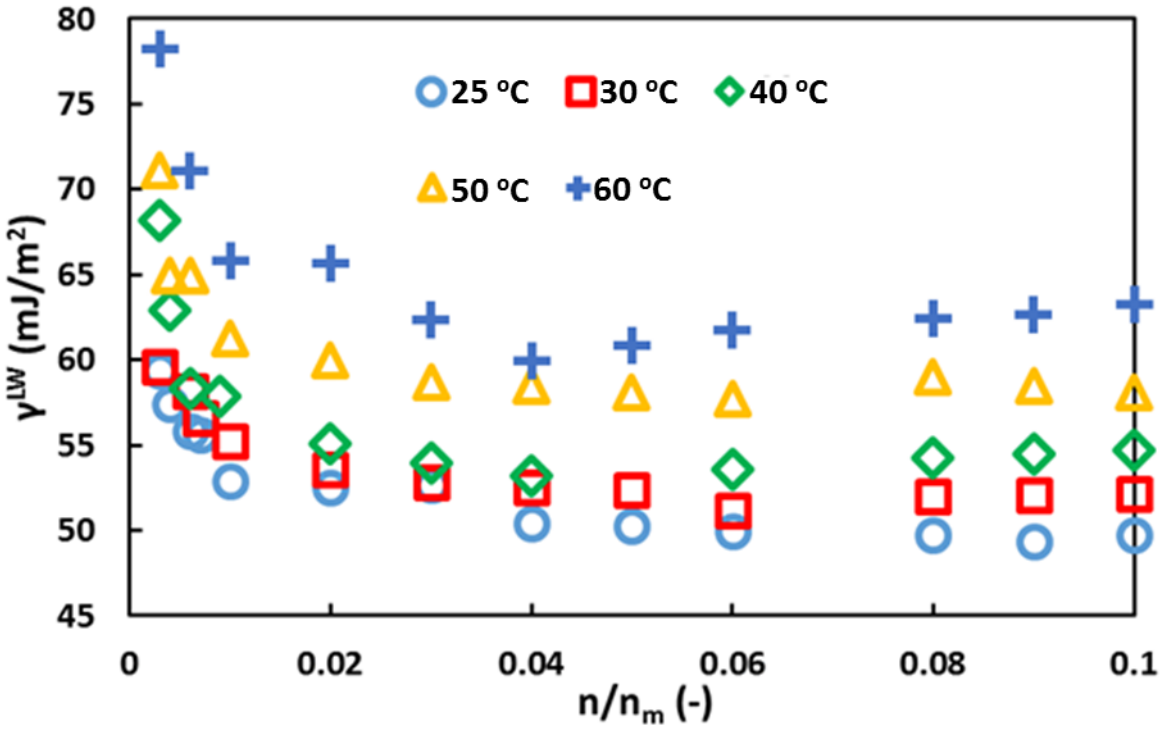


Figure 5.1: The surface energy measurements for p-monoclinic carbamazepine as obtained at the five different temperatures shown at the legend, the numbers in the legend correspond to the temperature, in degrees Celsius, of the experiment.

By extrapolation of the isotherms obtained at five different temperatures, for all three alkanes, it was possible to perform numerical integration to calculate the corresponding values for the spreading pressure; the results are shown in **Figure 5.2** (a more detailed analysis of these calculations, with some example isotherms can be found in Appendix 1). The data points, as expected, follow the trajectories of the corresponding vapour pressures as they are determined from Antoine's equation. The magnitude of the spreading pressures compare quite well with similar measurements, obtained with the same instrument, if they are adjusted for the differences in the surface energy.[116, 279-281]

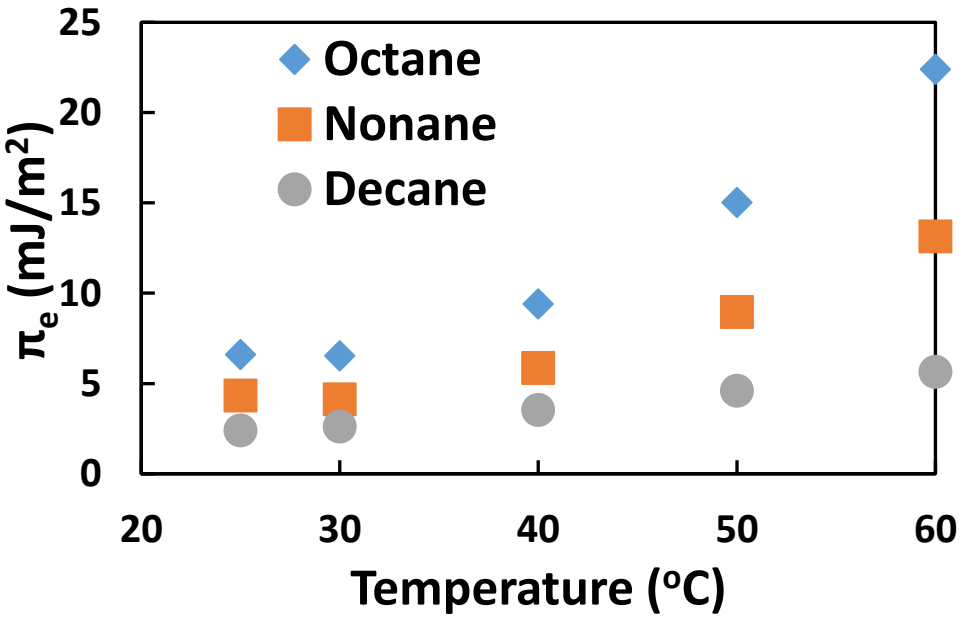
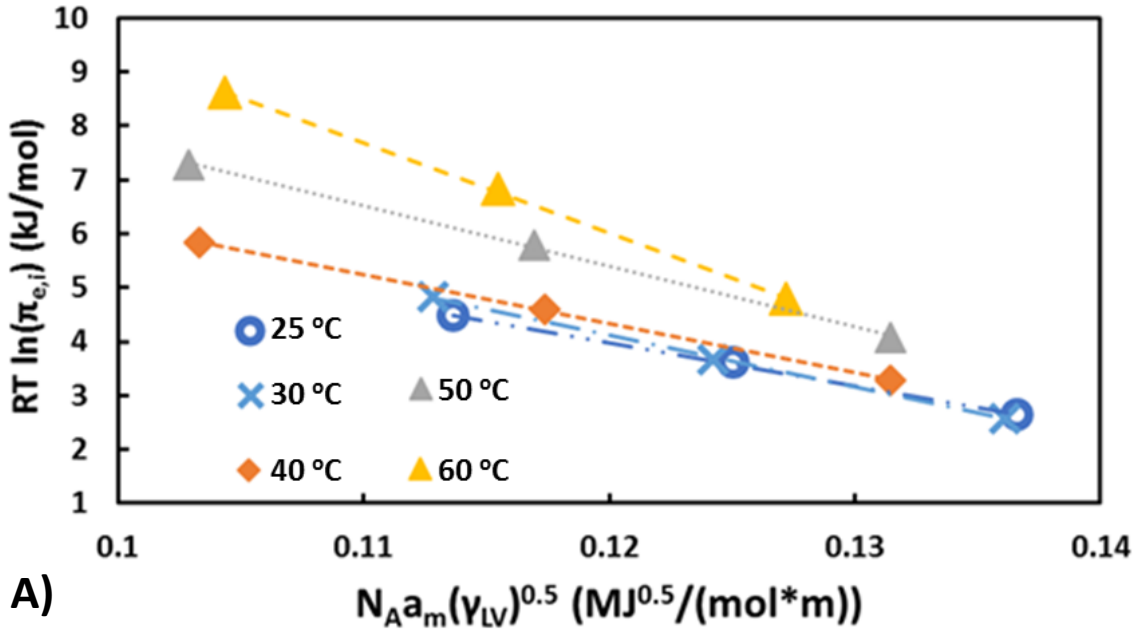


Figure 5.2: The values of spreading pressure obtained from the isotherms at five different temperatures, for the three alkanes of interest.

The data were implemented on Schultz's[115] plot in order to determine the overall influence of spreading pressure on the measurement; a single value was obtained for each temperature. The Schultz's plot used is shown in **Figure 5.3**. Then, the value obtained for each temperature was subtracted from every single point of the surface energy plot. Thus, a second surface energy plot, shown in **Figure 5.4**, was obtained depicting the corrected values of surface energy. The new surface energy plots correctly depict the decrease in surface energy of the material. As expected, owe to the crystalline nature of the material, decrease in surface energy is not massive. In fact, this decrease can be associated, partially, with the adsorption nature of IGC measurements.



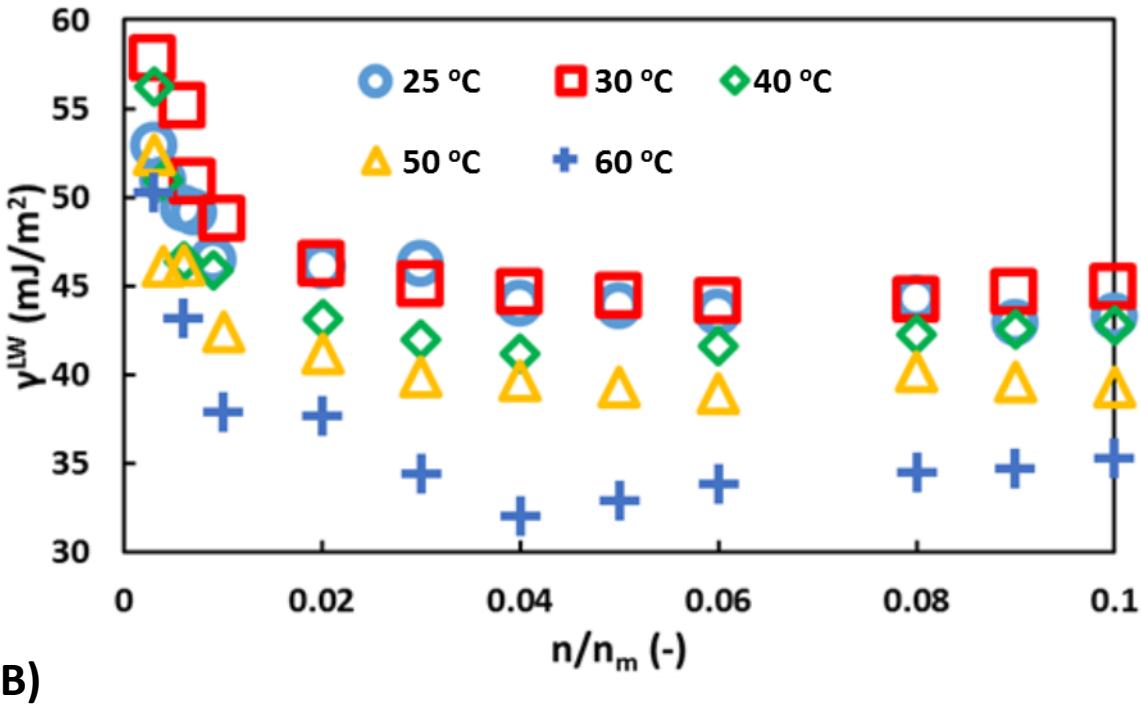


Figure 5.3: A) The Schultz's plot for the determination of the influence of spreading pressure at the temperatures of the study. B) The spreading pressure corrected surface energy measurements, the values in the legend indicates the temperature.

5.3.2 Wettability

Images of the macroscopic crystals of p-monoclinc carbamazepine are shown in **Figure 5.4**. Indexing has been performed and the indixes of the most important facets are shown on the images.[282] Protractor measurements were used to confirm literature findings. For instance, the dihedral angle between the (101) and the (001) facets was measured to be 65.3 º, comparable to the theoretical value of 64.9 º.[283]

The Kruss Drop Shape Analysis instrument (Kruss Gmbh, Hamburg, Germany), along with the corresponding software, was used for the contact angle measurements. The sessile drop contact angles were determined using the circle profile method. Each measurement performed had 4 repeats, each on clean facets, where the initial drop volumes ranged from 3 to 6 μL in volume. The measurements were performed in a temperature controlled room at about 24 ± 2 ºC.

Both advancing ($\theta_{Advancing}$) and receding ($\theta_{Receding}$) contact angle measurements were performed, following the procedure described in section 2.5.2.1 on "Sessile drop contact angle measurements".[96] The method proposed by Tadmor[28] has been used to determine the equilibrium contact angle from advancing and the receding contact angle measurements. Diiodomethane is a liquid exhibiting only van der Waals interactions; thus, $\gamma_{LV}^{+} = \gamma_{LV}^{-} = 0$. The work of adhesion ($W_{SL}$) for the formation of a solid-liquid interface is given by:

$$W_{SL} = \gamma_{SV} + \gamma_{LV} - \gamma_{SL} \qquad \text{Eq. 5.2}$$

where γ_{SV} is the surface energy of the solid, γ_{LV} is the surface tension of the liquid and $\gamma_{SL}$is the surface energy of the interface. Combining equation 5,2, with the definition of Young's equation, and taking into consideration the assumption about the nature of the interactions exhibited by diiodomethane the following equation can be obtained:

$$\gamma_{LV}\,(1+\cos(\theta_c)) = 2\left(\sqrt{\gamma_{LV}^{LW}\gamma_{SV}^{LW}}\right) \qquad \text{Eq. 5.3}$$

This equation was used to directly calculate the surface energy of a solid, using contact angle measurements from diiodomethane. In **Table 5.1** the results of the contact angle measurements are summarised along with the calculated values of surface energy.

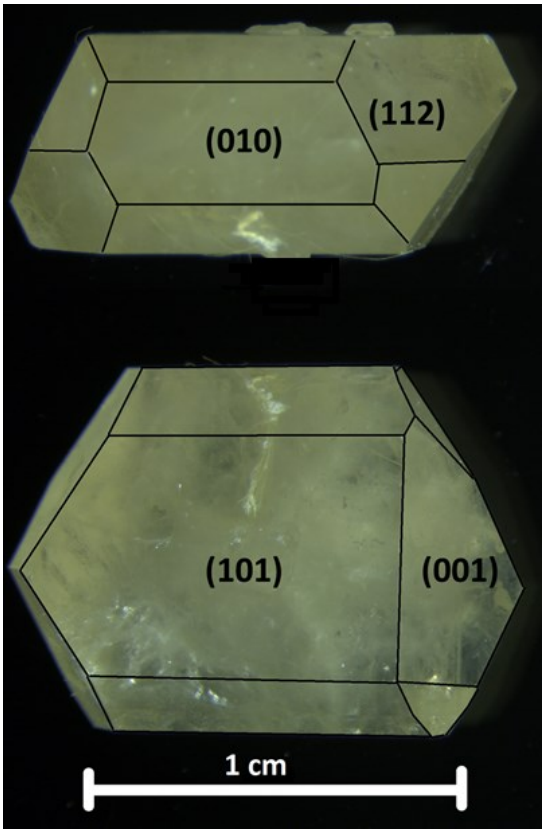


Figure 5.4: Stereoscopic image of a macroscopic p-monoclinic carbamazepine crystal, grown in methanol, with four facets of interest marked on it.

Table 5.1: The contact angle values and the calculated surface energy as they were measured on the four major facets of macroscopic p-monoclinic carbamazepine crystals.

Facet	$\theta_{Advancing}$ (°)	$\theta_{Receding}$ (°)	γ_i^{LW} (mJ/m^2)
(101)	35.1 ± 0.3	24.9 ± 1.0	44.2 ± 2.3
(001)	52.6 ± 1.2	38. ± 1.1	36.6 ± 3.0
(010)	50.8 ± 2.9	39.2 ± 1.0	37.0 ± 1.0
(112)	45.2 ± 0.2	38.9 ± 0.8	38.6 ± 0.3

5.3.3 Surface energy deconvolution.

In **Figure 5.5**, SEM images of the recrystallised p-monoclinic carbamazepine are shown. Similarly to the macroscopic crystals, the (101) facet dominates the surface of the particles. The reasons why the particular facet dominates have been explained exhaustively in Chapter 3, even though interesting work heavily lying on the concept of surface energy has been published recently.[30-33]

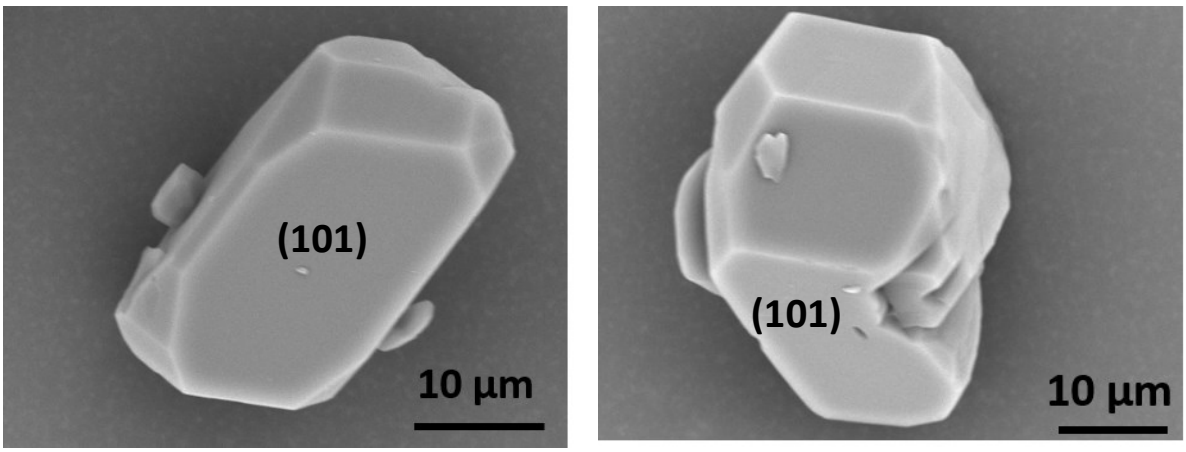
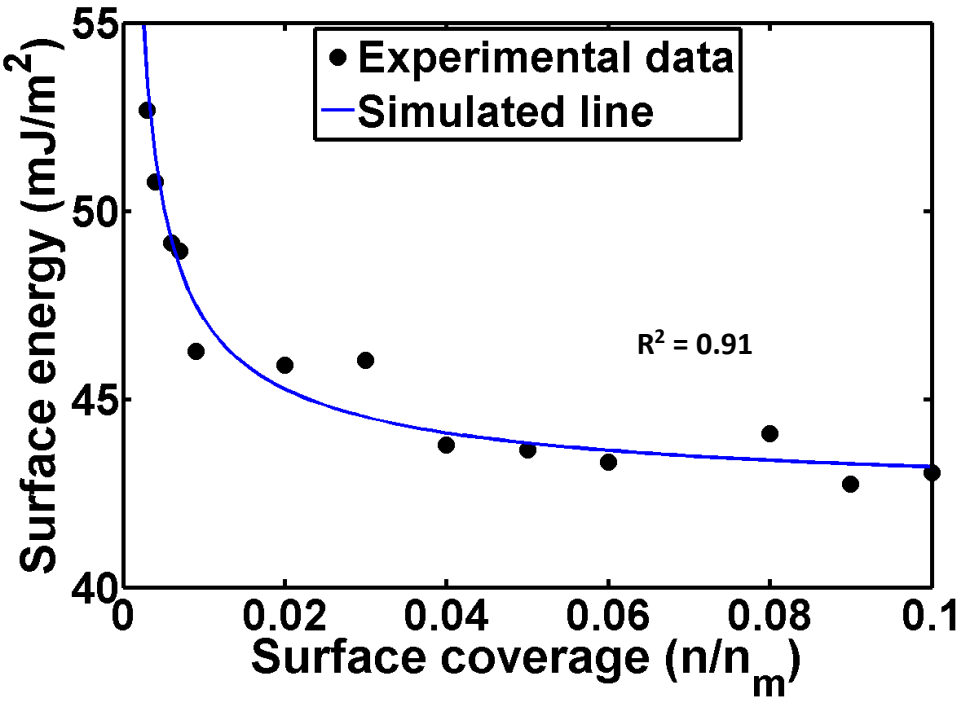


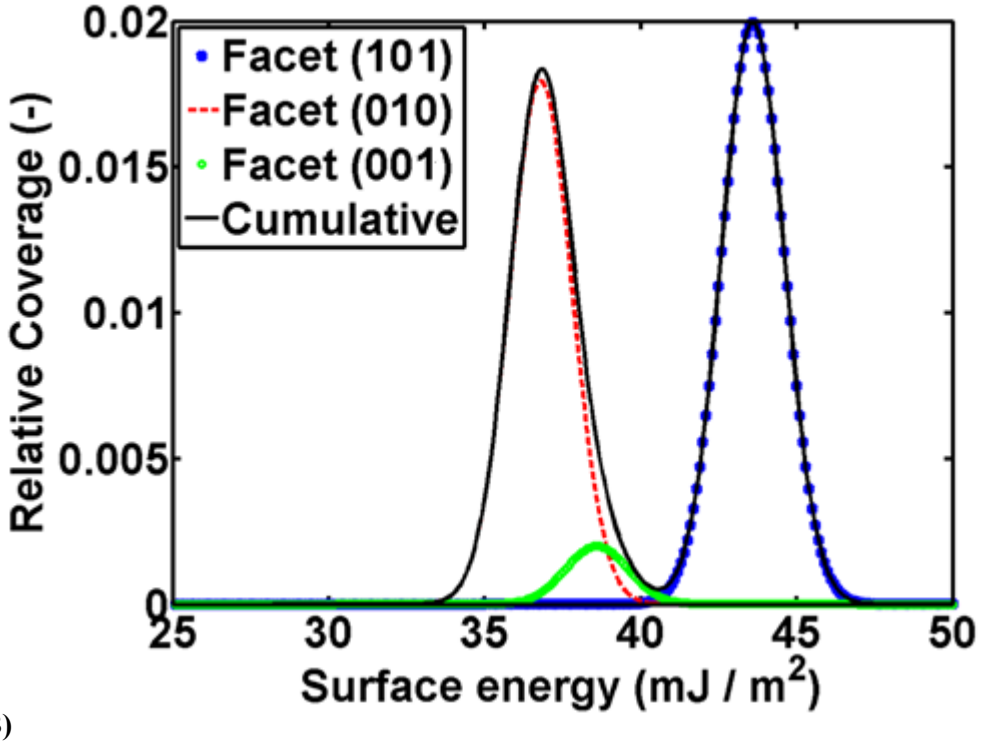
Figure 5.5: SEM images of carbamazepine recrystallised in ethanol resulting to a p-mononclinic polymorph.

In silico tools[19-20] deployed in the previous chapter, based on previous works, were implemented to obtain the surface energy distributions of the powder at 25 °C. A BET type of

isotherm is employed to fit the data. The contact angle values were used as inputs in the model. In **Figure 5.6 A** one could see the corrected experimental data for p-monoclinic carbamazepine at 25 ^{o}C and the simulated line, corresponding to the surface energy distribution show in **Figure 5.6 B**. The deconvoluted surface energy distribution shown in **Figure 5.6 B**, clearly reflects the dominance of the (101) facet; which is calculated to account for about 50 % of the surface area of the sample.



A)



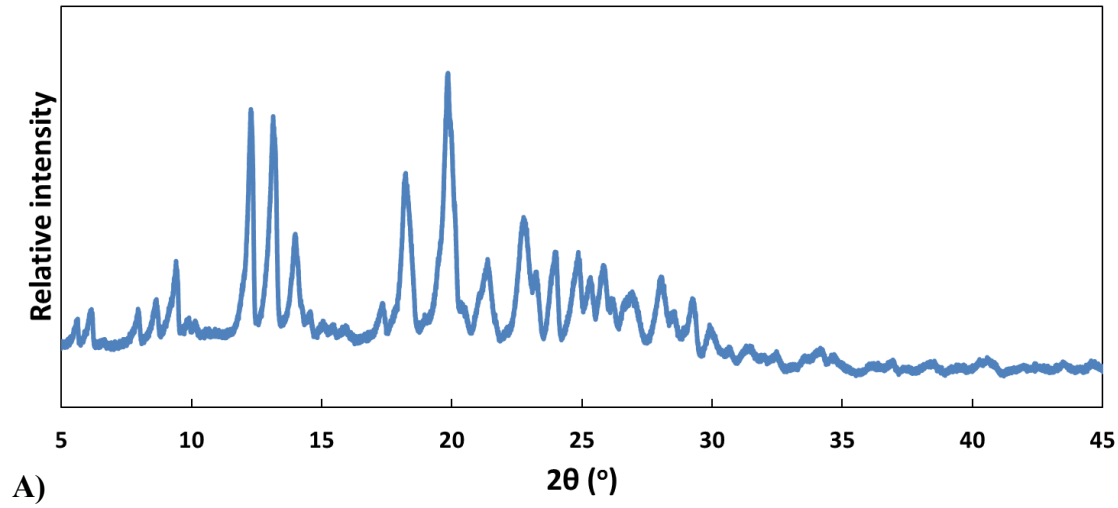
B)

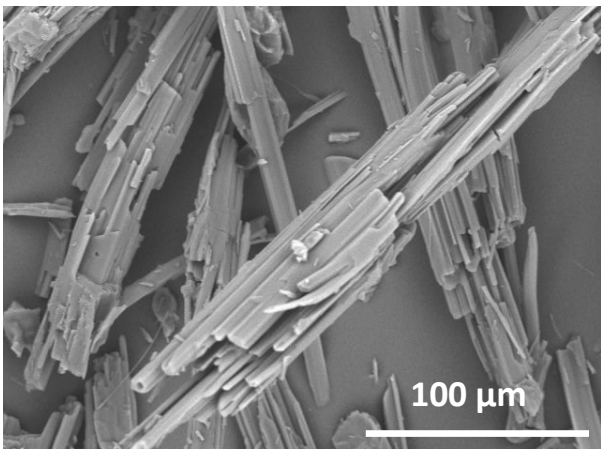
Figure 5.6: A) The corrected dispersive component of the surface energy of p-monoclinic carbamazepine (dots) along with the simulated line corresponding to the predicted surface energy distribution. B) The surface energy distribution of the corrected IGC measurement at 25 ºC.

The simulations were repeated at 60 ºC, assuming that the surface energy of the material is immune to the influence of the temperature. The surface energy plot obtained did not change greatly from the one determined at 25 ºC. A small decrease in the measured surface energy was attributed to the adsorption nature of the process, but the value at a surface coverage of 0.1 was found to be around 42 mJ/m^2, well different from what has been measured experimentally, shown in **Figure 5.3B**. Thus, all the surface energy change measured can be attributed to the influence of temperature on surface energy. This gives a surface energy change of about 7 mJ/m^2 for a change of 35 ºC.

5.3.4 Expanding beyond p-monoclinic carbamazepine

The same notions, described in the hitherto analysis of Chapter 5, have been applied for the case of another carbamazepine's polymorph; the triclinic one. In thorough discussion of the polymorphic behaviour of carbamazepine will be conducted in Chapter 8. Nevertheless, for the purposes of this chapter, it is important to mention that triclinic polymorph exhibits enantiotropic behaviour with respect to the p-monoclinic polymorph. The transition temperatures is at around 78 ºC. Triclinic carbamazepine was prepared by heating p-monoclinic carbamazepine prepared with the method described in the "Experimental methods" section of this chapter at 140 ºC overnight.[284] In **Figure 5.7 B** and **C**, one can see SEM images of the triclinic carbamazepine obtained. Previous DSC studies have shown that the polymorphic transition occurs via the melting of the p-monoclinic carbamazepine and the subsequent recrystallisation of the melt towards the triclinic polymorph. The crystals obtained exhibit a distinct acicular habit, deviating significantly from the prismatic shape of the p-monoclinic carbamazepine. The triclinic nature of the material was verified with XRPD scans as well.





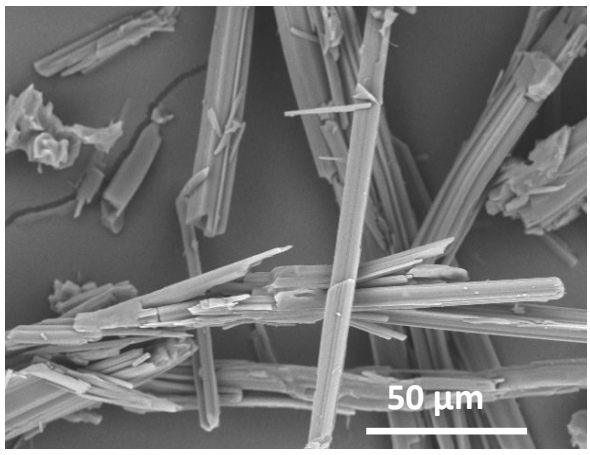


Figure 5.7: A) The XRPD scan of the material produced by overnight thermal treatment of p-monoclinic carbamazepine at 140 ºC. The peaks correspond to those of the triclinic polymorph. B and C) SEM images of the triclinic polymorph produced by overnight thermal treatment of p-monoclinic carbamazepine at 140 ºC.

The same procedure used for the measurement of the surface energy of p-monoclinic carbamazepine was used in the case of triclinic carbamazepine. The specific surface area of the material was measured using octane. The surface energy maps for triclinic carbamazepine, before it was corrected are shown in **Figure 5.8 A**. One could observe the same peculiar behaviour suggesting an increase in surface energy with increasing temperature. Then in

Figure 5.8 B the corrected version of the measurements is presented, showing a trend in accordance with the theory.

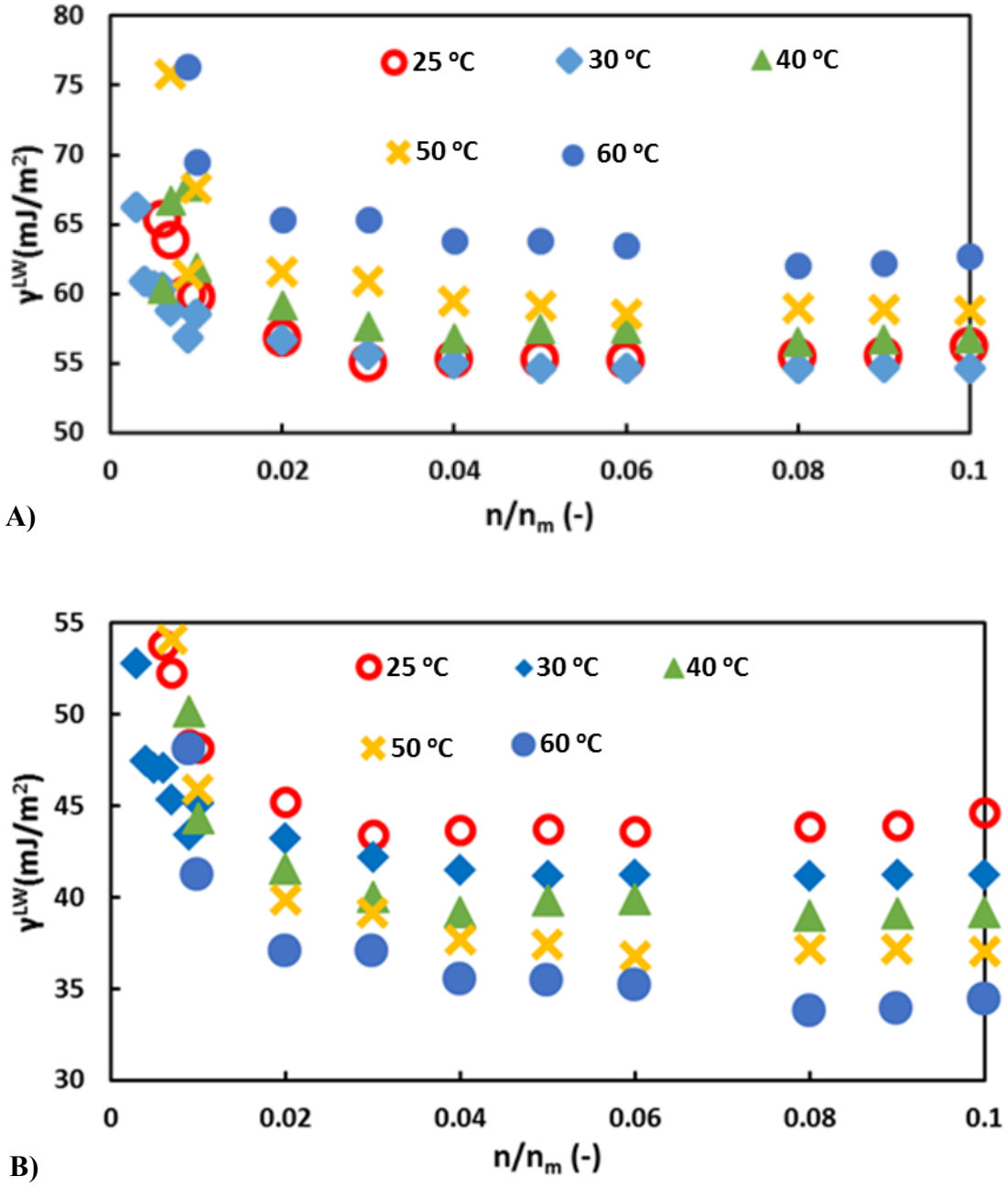


Figure 5.8: Surface energy maps for the triclinic polymorph of carbamazepine obtained at different temperatures (the number in the legend corresponds to the temperature of the experiment in degrees Celsius) before (A) and after (B) the spreading pressure correction.

5.3.5 Implications of this study on the previous chapter

In the previous study, elaborated experiments have been employed to show the influence of silanised wool and powder packing on IGC measurements. Whilst the experiments of this chapter take into account the precautions suggested on the amount of silanised wool, the results presented in Chapter 4 do not take into account the effects of spreading pressure. The implementation of the findings on spreading pressure do change the results on the influence of silanised glass wool quantitatively. The surface energy of silanised glass wool upon correction was found to exhibit a decrease of around 6 mJ/m^2, landing to the area of around 30 mJ/m^2. Corrections were imposed to the rest of the measurements, as well. The qualitative findings, suggesting the ability of the *in silico* model to identify mixtures of two different materials, were verified once more.

The new findings do not suggest a qualitative shift from the basic conclusions on the influence of silanised glass wool. The new surface energy of silanised glass wool, obtained upon correction, is lower than before. However, the classification of the materials, proposed in Chapter 4 will not change. The materials can still be classified as low surface energy materials severely affected by the amount of wool, materials with surface energy similar to that of silanised wool where the effects of the wool are masked and high energy materials, not severely influenced.

5.4 Conclusions

Overall, this study contributes to the building of a set of good experimental practice in the field of IGC. Its importance spans in two different levels. It revealed the importance of spreading pressure in the correction of surface energy measurements performed via chromatographic methods. In this context, it provides a detailed method, grounded on well-established theoretical approaches, to correct the results in order to be able to directly compare measurements obtained at different temperatures. Furthermore, from the results presented it is

clear that if operators want to minimise the influence of spreading pressure should use probe molecules with high vapour pressure. It should also need to be clear that these measurements would not be completely accurate, but they would be less susceptible to the effects of temperature.

This study reaffirms the importance of spreading pressure in adsorption, based processes. It shows that the magnitude of spreading pressure, directly related to the temperature, is not negligible. A road map for the implementation of the influence of spreading pressure in IGC measurements is proposed. Furthermore, it is showcased that surface energy measurements, obtained with IGC, should be critically assessed with the aid of SEM images, wettability measurements and surface energy distributions. The use of complimentary tools is paramount, as they can provide more rational to the results obtained.

6. The effects of amorphous interfaces in IGC measurements

6.1 Introduction

Hansen Solubility Parameters (HSP)[24] have been established as thermodynamic quantities of crucial importance for the understanding of the behaviour of materials of industrial importance; primarily polymers, but also minerals and nano-materials. The corresponding theory has been addressed in Chapter 2 on the "Fundamentals of Interfacial Phenomena". Further studies can be found in literature, along with theoretical, experimental and computational investigations of the topic,[285-289] some directly relevant to pharmaceutical industry.[290-293] Contrary to surface energy, solubility parameters, have been considered, not to be hindered by the surface area to volume ratio of the system and that's why they are quite convenient for the characterisation of amorphous materials. Thus, accurate determination of HSP interests a wide spectrum of investigators both in academia and industry.

Traditionally, the measurement of HSP was performed by tedious experiments involving the use of large quantities of materials and solvents. IGC came in mid-70s as a game changer, providing a less labour and cost intensive route for the measurement of HSP. The development of the methodology underlying the use of IGC in the determination of HSP should be credited to a number of investigators, such as Voelkel, DiPaola and Ito.[21-23] The corresponding theory, which can be found in great detail in the chapter on the "Fundamentals of Interfacial Phenomena", is built around IGC's ability to determine the, infamous, χ mixing parameter, predicted by the Flory-Huggins theory. This is achieved by measuring the retention time and hence the interaction energy between, presumably, the surface of a stationary polymer phase and a solvent of known properties. The value of χ can be, then, introduced to appropriate geometric constructions to determine the three components of the HSP, namely the dispersive, the polar and the hydrogen bonding.

One should remember that χ is an interaction parameter, accounting mainly for the enthalpy changes associated with interactions between molecules upon mixing. Thus, it is, in essence, describing an interfacial phenomenon. The occurrence of any form of interaction requires the presence of an interface. Numerous materials of pharmaceutical interest, mainly polymers, are amorphous, hence during an IGC experiment the probe molecules have the potential to diffuse through them. Considering that the flow rate of the carrier gas (usually Helium) influences the retention time of a probe molecule a number of arguments can be made. For high carrier gas flow rates, the retention time is small and the probe molecule interacts mainly with the surface of the amorphous material. It does not have sufficient time to diffuse in the material. Thus, the measured value of χ accounts for the interactions with molecules on the surface of the material. On the other hand, for high retention times, corresponding to low carrier gas flow rates, the diffusion is more prominent. The probe molecules interact with molecules in the bulk of the stationary phase; an interface is formed between the probe molecules and the molecules of the amorphous material.

Literature findings suggest that a difference should exist between the bulk and the surface value of χ. For amorphous materials, the difference between the bulk and the surface magnitude of properties such as molecular diffusivity, surface composition is a well-established concept in literature. This difference has been reported for the first time in the study of crystallising metallic glasses.[212-213] In those studies it has been reported that metallic glasses tend to nucleate faster on the surface. Similarly, crystal growth was faster on the surface compared to the bulk. Similar studies are nowadays conducted on organic glasses.[215, 217] A more extensive discussion on this can be found in the section 3.2.1.5 on the "Interfacial phenomena in the crystallisation of amorphous materials".

Taking into account these arguments and considering the existing status of literature, it can be concluded that is important to study the extent of the influence of carrier gas flow rate

on the measured values of χ. Considering that the interactions at the molecular level, hence the magnitude of χ, are influenced by temperature, it is obvious that an investigation of the imfluence of Helium gas flow rate, should not be considered complete unless it provides a thorough overview of the influence of temperature on the measured values of χ. **Figure 6.1**, summarises the discussion of this paragraph with a simple schematic. On the right-hand side there is a crystalline material. No diffusion occurs in crystalline materials and the measured value of χ should be the same for amorphous and crystalline materials. For amorphous materials in their glassy state, some diffusion occurs. As the temperature rises above the T_g of the material, diffusion is more prominent.

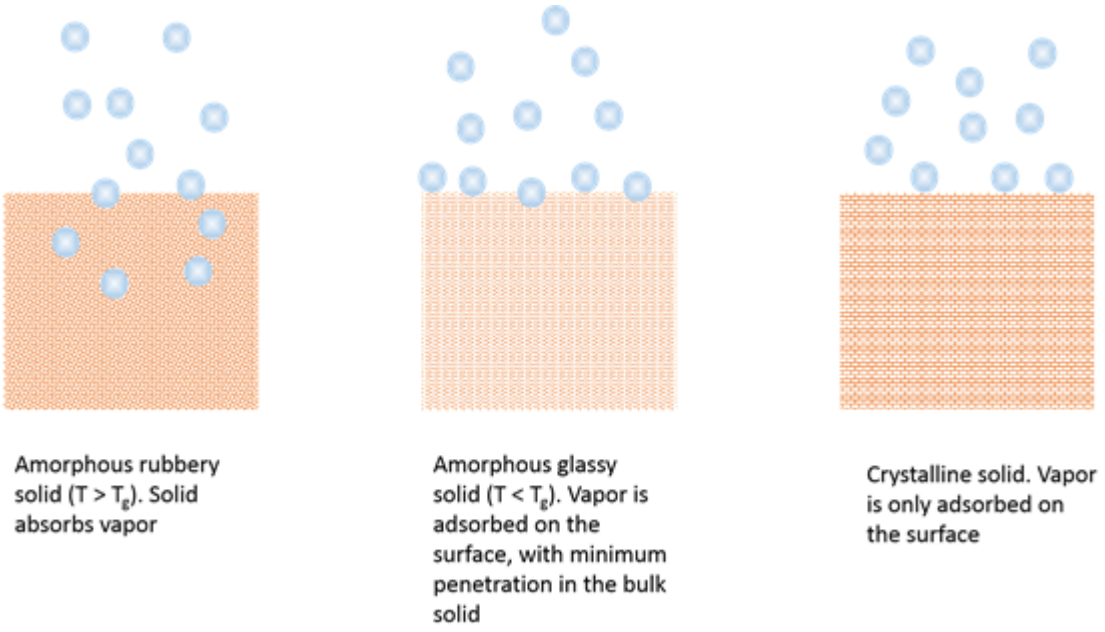


Figure 6.1: Schematic showing the interaction of vapours with amorphous (above and below the T_g) and crystalline materials.[48]

This chapter addresses the importance of carrier gas flow rate and temperature on the determination of the HSP. The study commences with an investigation of the effects of temperature. The T_g of copovidone was measured using IGC and the value obtained, compared with the results obtained from DSC. Then the variation of the value of χ with temperature and

the consequent implications to the measured values of HSP are studied. The second part deals with the importance of carrier gas flow rate on the measurements. The HSP for a crystalline material, p-monoclinic carbamazepine, are measured at two different flow rates. The results are identical, verifying that for crystalline materials where the diffusion of solvent in the crystal lattice is negligible the measurement is independent of the flow rate. Then, copovidone was used to expand the investigation in amorphous materials. The results, at 30 ^{o}C, suggest increase of the magnitude of δ_d with decreasing gas flow rate, in the glassy state. The same measurements were performed at 100 ^{o}C, showing small variations with gas flow rate, owe to the increased molecular mobility of the polymers at the rubbery state. For materials at the glassy state, a methodology was proposed to decouple the effects of the flow rate and obtain the actual value of χ. On this ground, it can be argued that amorphous materials in their glassy state exhibit two main χ parameters; a surface and a bulk one. The bulk one is that predicted by the Flory-Huggins theory. The surface one may be significant when assessing kinetic phenomena, such as the wettability of the surface of a polymer during dissolution. In this case, the formation of the liquid-polymer interface on the may be described better in terms of the surface value of χ. The results of this section constitute an important improvement in the field, as they enable the measurement of thermodynamic properties with higher accuracy.

6.2 Materials

6.2.1 Recrystallisation of p-monoclinic carbamazepine

P-monoclinic carbamazepine powder was purchased from Apollo Scientific, Stockport, UK, and was recrystallised under stirring in ethanol, acquired commercially (VWR, Radnor, PA, USA). The recrystallisation was performed under stirring in order to ensure the conversion of all the material to the p-monoclinic polymorph. Powder X-ray diffraction measurements on the resulting powder did not reveal the presence of any other polymorph.

6.2.2 Copovidone

Copovidone (Kollidon VA-64) was provided by BASF and used in all the measurements of this study as received.

6.2.3 Properties of the solvent probes used in the measurements

In Chapter 2 a thorough derivation of the equations used for the determination of HSP via IGC, was performed. The resulting equations contain numerous thermodynamic quantities, characterising the properties of the solvents used. As measurements will be performed at various temperatures, the variations of the thermodynamic quantities with temperature are required. Thermophysical quantities such as the molar volume, the partial pressure, the molecular weight and the second virial coefficient (B_{11}) are tabulated in NIST thermophysical database.

As for the HSP of the solvents, **Table 6.1** provides a summary of them at 30 ^{o}C. One could calculate their value at different temperatures using the equations provided in literature.

Table 6.1: The values of the different components of the HSP at 30 °C.[24]

Solvent	δ_d (MPa$^{0.5}$)	δ_p (MPa$^{0.5}$)	δ_h (MPa$^{0.5}$)	δ_T (MPa$^{0.5}$)
Hexane	14.9	-	-	14,9
Heptane	15.3	-	-	15,3
Octane	15.5	-	-	15,5
Nonane	15.7	-	-	15,7
Decane	15.7	-	-	15,7
Dichloromethane	18.2	6.3	6.1	20,2
Ethyl Acetate	15.8	5.3	7.2	18,2
Toluene	18.0	1.4	2.0	18,2
Ethanol	15.8	8.8	19.4	26,5
Propan-2-ol	15.8	6.1	16.4	23,6

6.3 HSP measurements

The measurements were performed using an IGC-SEA (Surface Measurement Systems, London, UK), equipped with flame ionisation detector (FID). The geometric construction proposed by Voelkel,[23] as an improvement to the model proposed by DiPaola,[21] was used for the determination of the components of HSP. As has been mentioned, in Chapter 2, the split of the HSP in three components is arbitrary. For instance, for surface energy, people have proposed to treat hydrogen bonds in terms of a separate surface energy parameter, in a similar manner as with the HSP. As the number of solvents available is limited, an alternative approach

was used in this study and the HSP was splitted in a way resembling the splitting of surface energy:

$$\delta_T^2 = \delta_d^2 + \delta_{AB}^2 \qquad \text{Eq. 6.1}$$

where δ_T stands for the total HSP and δ_d and δ_{AB} are the dispersive and the acid-base components respectively. For the determination of δ_d chain alkanes were used; namely heptane, octane, nonane and decane. For the determination of δ_{AB} five polar molecules were used; namely toluene, dichloromethane, ethyl acetate, ethanol and propan-1-ol. It is important to notice that the focus of this chapter is to provide a more in depth understanding of the influence of amorphous interfaces on the measured values obtained via IGC. On the other hand using a large number of solvents to calculate the HSP of copovidone does not constitute a significant step forward in the field.

The material was packed in the glass IGC column and preconditioned at the appropriate temperature for three hours before each measurement. At each measurement the amount of solvent injected corresponded to a surface coverage of 3 %. The injected amount was kept low in order to be in line with the assumption presented in Chapter 2, that $\varphi_p \rightarrow 1$. In the majority of the literature studies, no mention is made on the injected amount of solvents. This is problematic, as the development of new injection systems enable the use of high concentrations of solvents. However, the use of high concentration injections violates the aforementioned assumption, leading to a collapse of the mathematical formulae enabling the calculation of the χ interaction parameter by means of IGC measurements.

6.4 Results

6.4.1 Determining the T_g of copovidone

An IGC column was packed with a small amount (50-80 mg) of silanised glass wool and placed in the machine. The sample was pretreated for three hours at 30 ºC and 0 % RH. Then

injections of hexane, heptane and octane were performed. After the elution of the solvents, the temperature was raised to 40 °C and pretreated at this temperature for another three hours. Measurements were performed with the same three alkane probes. The process was repeated in 10 °C increments up to a temperature of 130 °C. The logarithm of the retention volume for each alkane was plotted against the inverse of temperature (in Kelvin), in **Figure 6.2**. This graphical construct, resembling the well known Van't Hoff plot.[294] The T_g for the polymer can be determined graphically, from the onset of the non-linear behaviour as the plot moves from right (low temperatures) to the left (high temperatures).

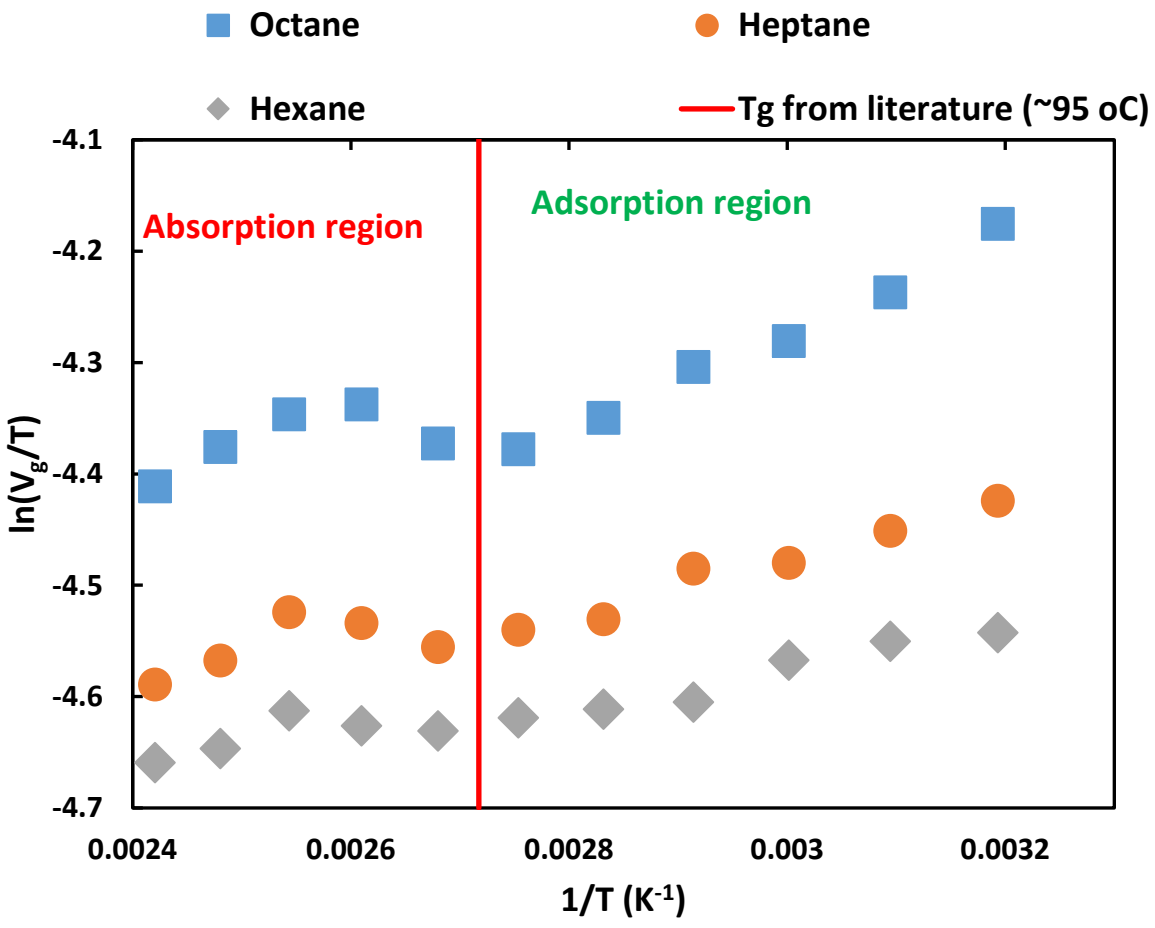
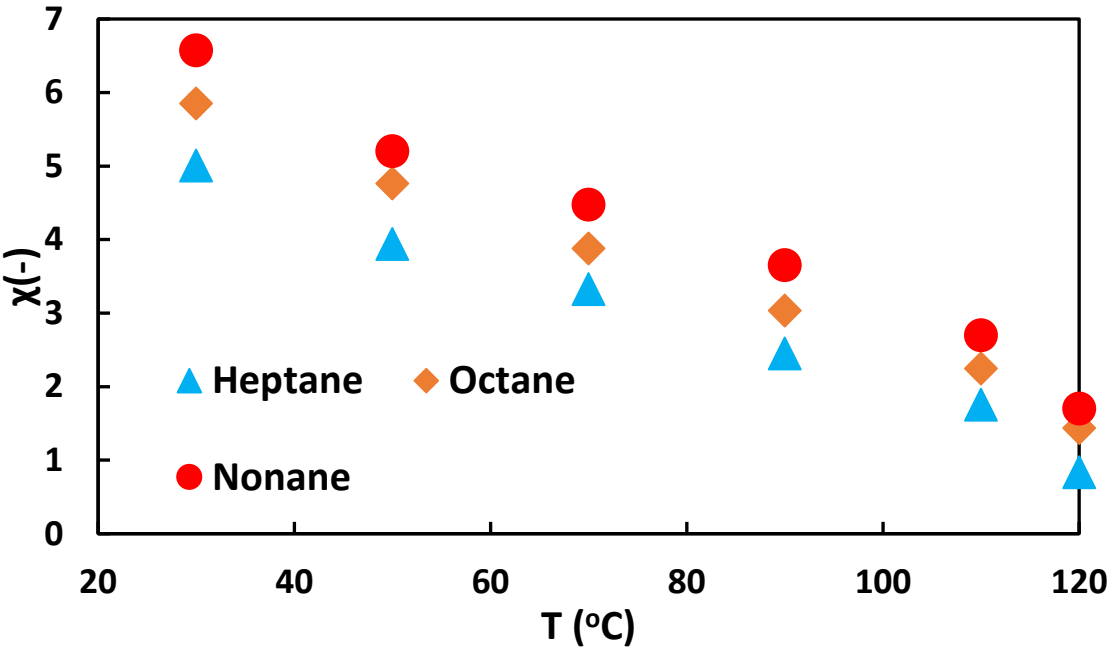


Figure 6.2: Graphical construction for the determination of the T_g. The legend names the three alkanes used, as also a line corresponding to a common value of T_g found in literature.

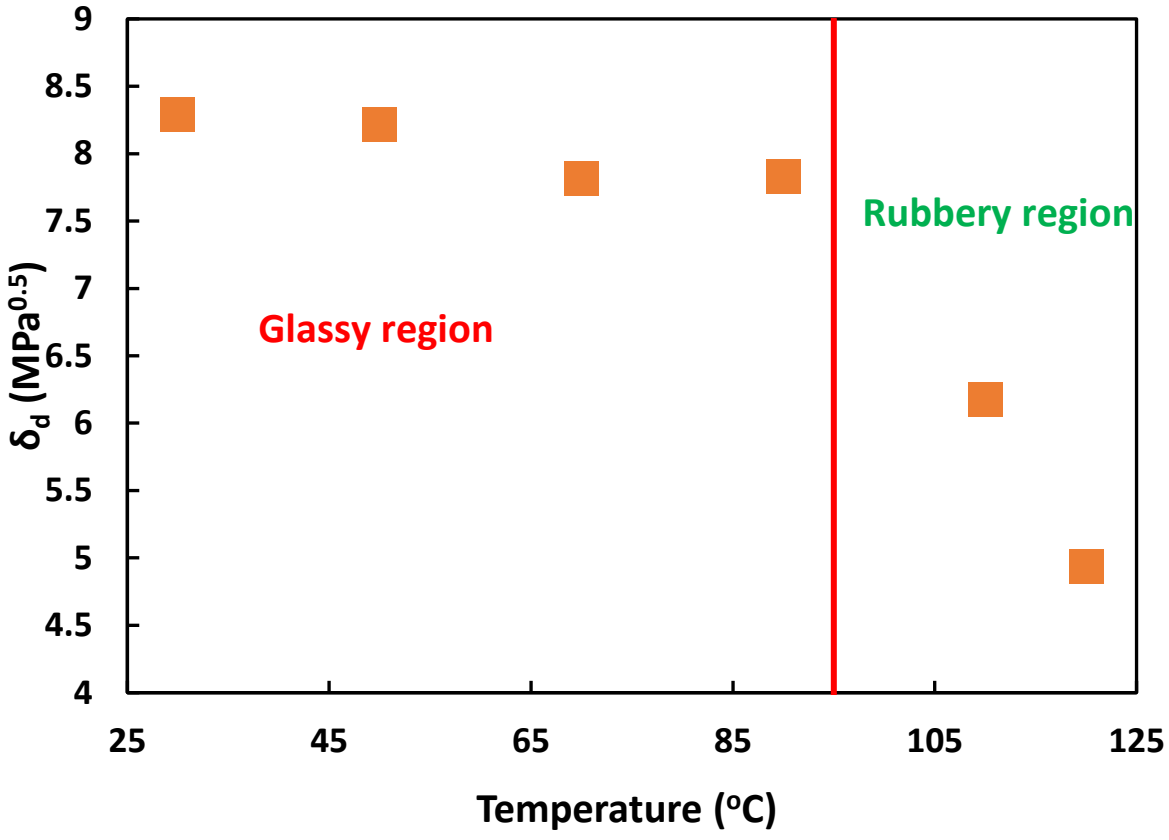
The T_g is determined to be around 95 ^oC, close to the literature values for this material and DSC measurements (~100 ^oC).[295] As can be seen heavier hydrocarbons give a sharper image of the behaviour of the system. The region right to the red line, corresponds to temperatures below the T_g, where adsorption is the dominant interaction mechanism between the hydrocarbon and the polymer. On the T_g, this behaviour starts to shift, owe to the shift in the molar volume of the polymer. This behaviour indicates a zone of non-equilibrium absorption. From thereafter absorption dominates the system. It is interesting that heavier hydrocarbons provide a sharper image of the process. This is attributed to the larger diffusion coefficient of smaller molecules. Because of that, smaller molecules diffuse much more easily in the polymer thus, the shift associated with the T_g is not that profound for them. This, very sharp, difference in the diffusion coefficients, observed in this **Figure 6.2**, highlights the importance of a study as that presented in this chapter.

6.4.2 The effects of temperature on χ and HSP

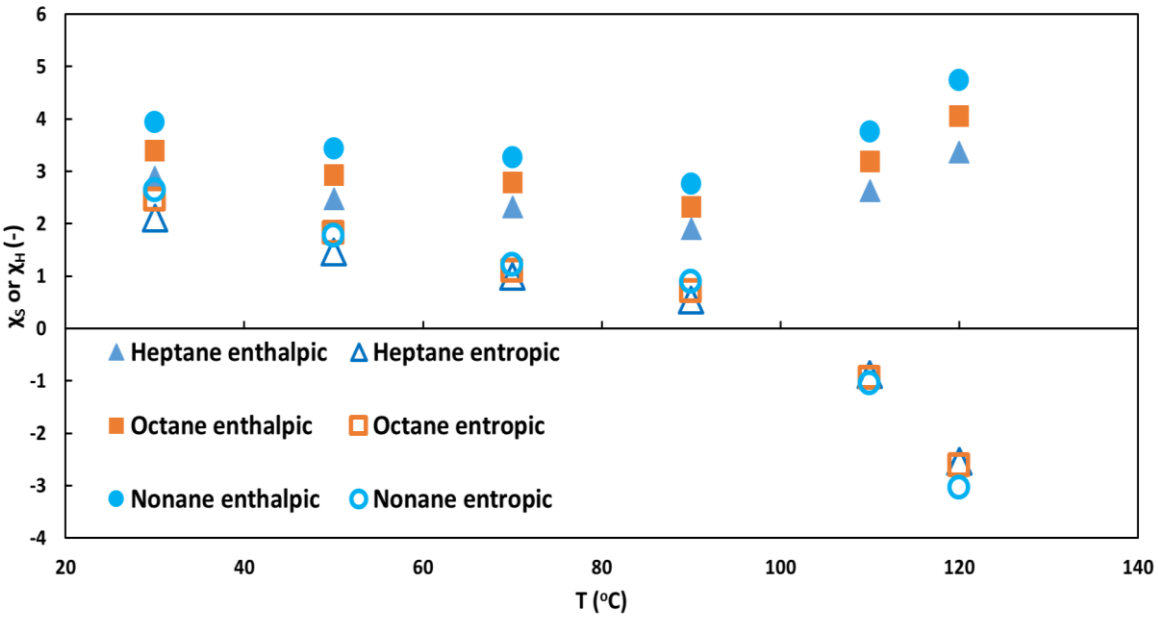
In the previous section of this chapter, the ability of the IGC to determine the T_g of an amorphous material was determined. Thus, the next step is to use different solvent probes to understand the influence of temperature on the measured values of the χ interaction parameter and its constituent components, χ_S and χ_H, as well as of the HSP, in both the glassy and the rubbery region. The measurements were performed using the methodology described in section 6.2 of this chapter, and some indicative values of χ obtained are plotted in **Figure 6.3 A**. The flow rate of the carrier gas was 1 sccm. The values of δ_d were then calculated and plotted on **Figure 6.3 B**. Using the definition of χ, the values of χ_S and χ_H were calculated and some indicative values are plotted in **Figure 6.3 C**.


χ(-)
T (°C)
Heptane
Octane
Nonane

A)


δd (MPa0.5)
Temperature (°C)
Glassy region
Rubbery region

B)



C)

Figure 6.3: Graphs showing A) The temperature variation of the χ interaction parameter, of three alkanes with copovidone, at a flow rate of 1 sccm, B) The variation of δ_d with temperature in both the glassy and the rubbery region, C) The variation with temperature of the entropic and the ethalpic component of the χ interaction parameter of three alkanes with copovidone at a flow rate of 1 sccm.

According to the classical formulation of the Flory-Huggins theory an increase in temperature will lead to a decrease of the entropic component of the Flory-Huggins equation, favouring solubility. However, for the enthalpic component, things can be more intriguing, especially when hydrogen bond is involved. In literature, a semi-empirical general equation was found to describe quite well the variation of χ with temperature, for a lot of cases. The general form of the equation is:[296]

$$\chi = A + \frac{B}{T} \qquad \text{Eq. 6.2}$$

in this equation, A and B are empirical constants, determined experimentally, and T is the temperature. The results obtained in this study are in agreement with the proposed equation. The decrease in the value of χ with increasing temperature suggests favourable dissolution. The results obtained do not show an abrupt change in the value of χ during the glass transition.

However, a more careful observation of the data shows that for temperatures above the T_g, there is a qualitative change in the values of χ measured. The difference in the χ parameter between different alkanes becomes smaller. The values of χ appear to converge.

This qualitative change is manifested in the values of δ_d. The abrupt decrease in the rubbery region, is in agreement with the idea that in this region the molecular mobility of the material increases, leading to a decrease in the cohesive forces between the molecules and an increase in the molar volume of the polymer. Using the values of δ_d obtained, the deconvolution of the value of χ in its two constituent components was performed, giving some intriguing results. As the temperature increases in the glassy region, both the value of χ_S and χ_H decrease. The decrease in the value of χ_H can be explained intuitively by the fact that the rate of decrease of the value of δ_d of the probe molecule, with temperature, is higher than that of the polymer. This is because the probe molecule is liquid and the cohesive forces are not as strong as for a soft material like a polymer.

In the rubbery region, both components of χ exhibit an inflection. The value of χ_H appears to increase with increasing temperature. This suggests that in the rubbery region, an increase in temperature does promote mixing, from an enthalpic point of view. As the temperature increases above the T_g, the rate of decrease of the value of the δ_d, with temperature, becomes faster, approaching that of the solvent. As the value of the δ_d of the two phases approach, the affinity between the molecules of the two decreases. On the other hand, the entropy component exhibits an inflection to the opposite direction as the enthalpic. Because of the temperature, the conformational changes associated with mixing may become more vigorous, favouring the mixing of the two phases. On the same time, as the temperature increases the film mass transfer coefficient at the surface of the polymer decreases, favouring diffusion. These two mechanisms are not decoupled the one of the other; they are interrelated.

6.4.3 The effect of flow rate on the measured value of χ and HSP of crystalline materials

The have been measured for p-monoclinic carbamazepine at two different flow rates, at 30 °C. **Table 6.2** summarises the findings (with δ_T being the total value of HSP). As can be seen the values are quite similar, suggesting that the crystalline nature of the material does not enable any diffusion. Thus, the measurement is conducted purely on the surface of the material. The results of this table suggest that for crystalline materials the measurement is purely interfacial. No bulk mixing occurs. Thus, the next step would be to investigate the behaviour of amorphous materials, where diffusion can, actually, occur.

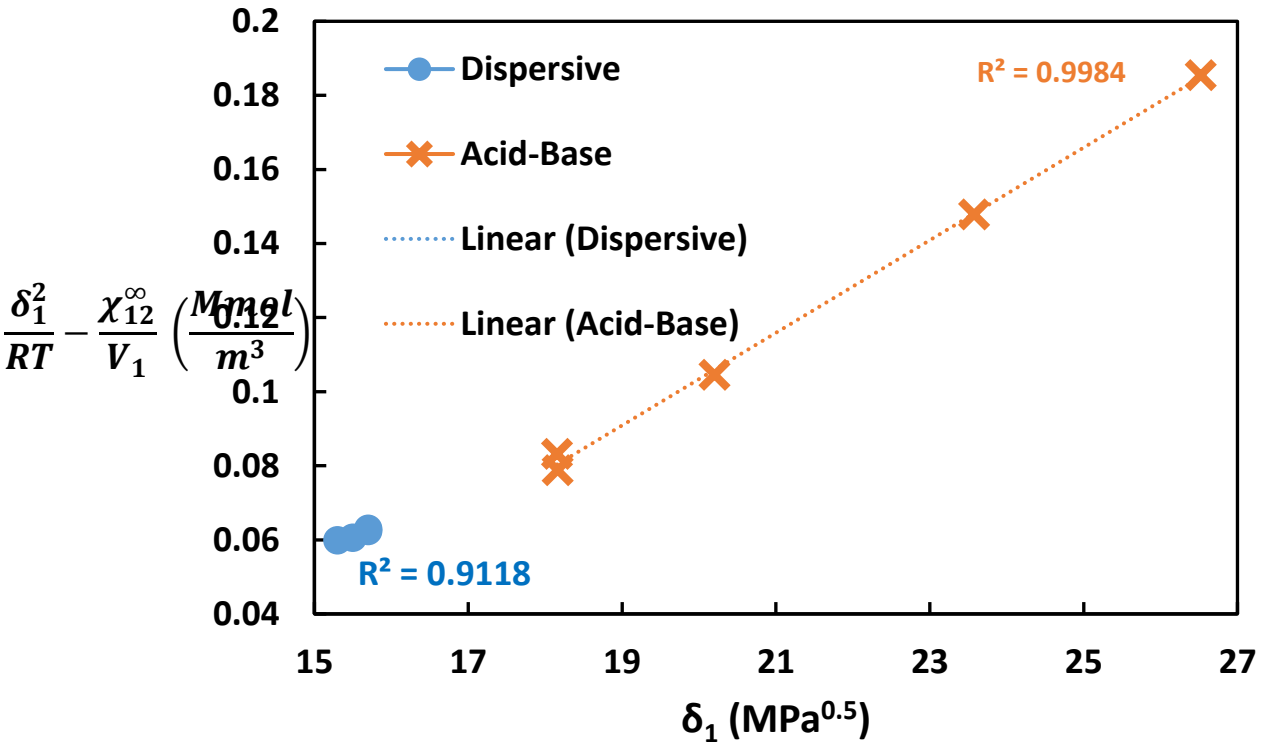


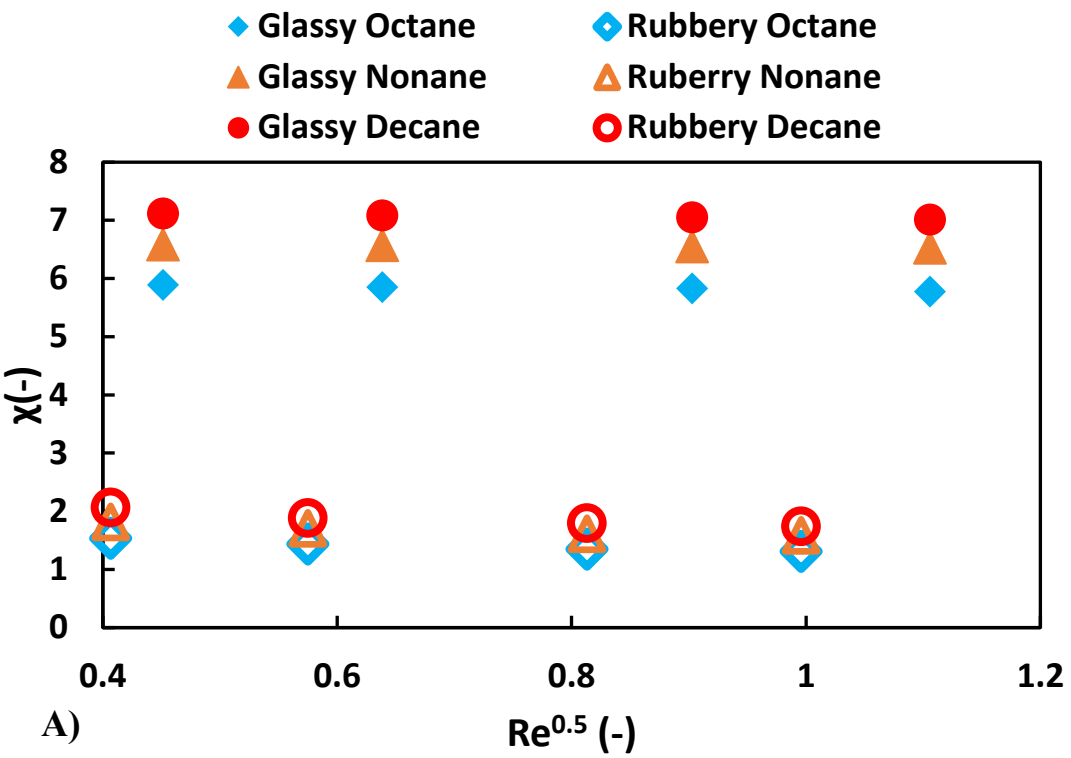
Figure 6.4: The graphical construction used for the calculation of the two components of the HSP, of p-monoclinic carbamazepine at a temperature of 30 °C and carrier gas flow rate 1 sccm.

Table 6.2: Summary of the values of HSP obtained for p-monoclinc carbamazepine at two different carrier gas flow rates at 30 ^{o}C**.**

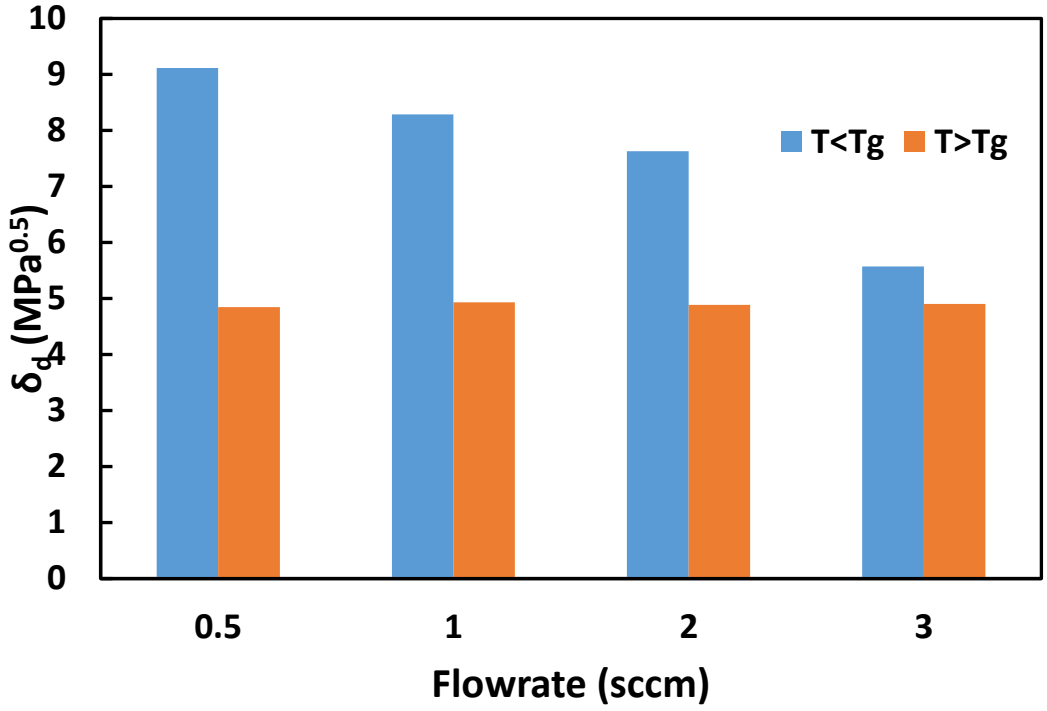
Flow rate (sccm)	**δ_d (MPa$^{0.5}$)**	**δ_{AB} (MPa$^{0.5}$)**	**δ_T (MPa$^{0.5}$)**
1	9.49	6.06	11.26
3	9.24	6.51	11.30

6.4.4 Measuring the value of HSP at different flow rates for amorphous materials

Before commencing the presentation of the results of this section and the corresponding discussion, there is a point that should be highlighted. The flow rate in chromatographic equipment is usually measured in standard cubic centimetres (sccm). This unit is effectively, the volumetric flow rate in cubic centimetres per minute, standardised at 1 bar and 0 ^{o}C. This means, that as the temperature of the measurement increases, the flow rate increases as well. Fundamentally, all the measurements performed at different temperatures and same flow rates, in sccm, are effectively performed at different flow rates as well. Considering that the behaviour of the carrier gas, can be described in terms of the ideal gas law, one should immediately notice that this change is not necessarily profound. In fact, as it was shown in the previous section, for crystalline materials is negligible.



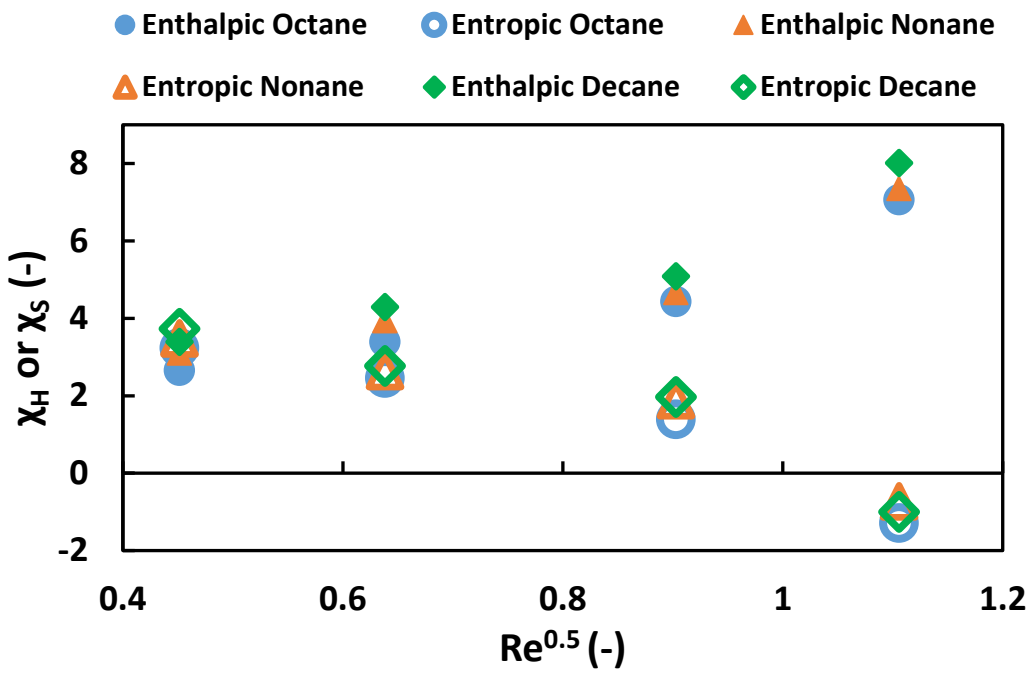
A)



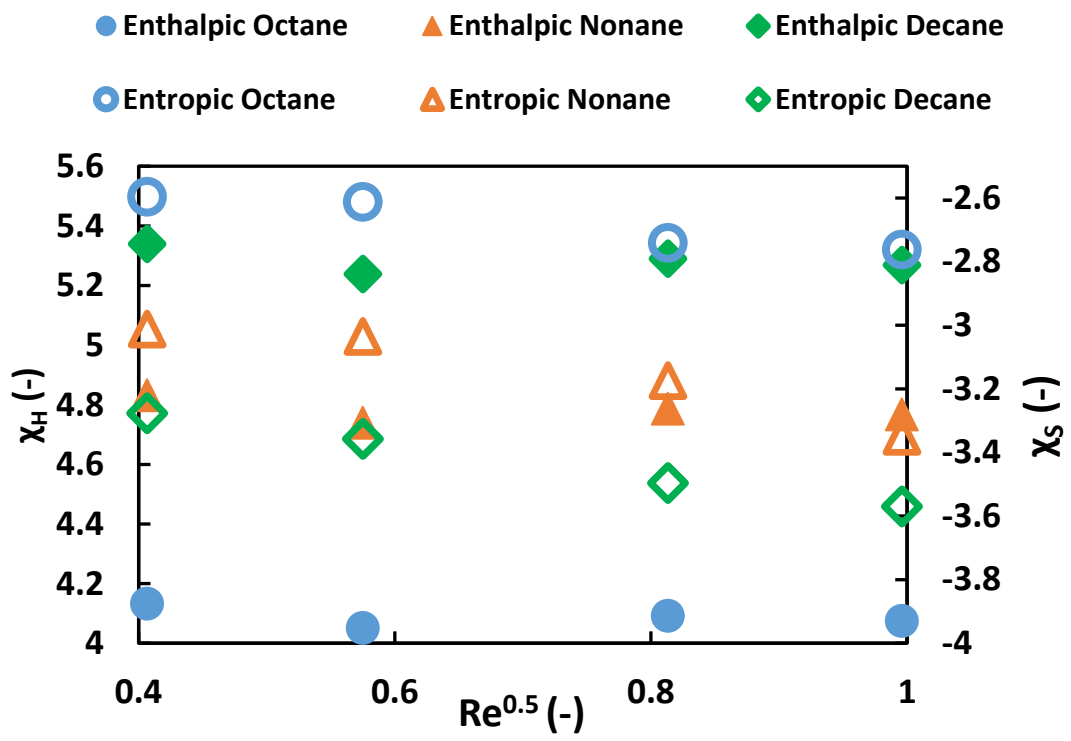
B)

Figure 6.5: Graphs showing A) The variation of the χ interaction parameter between three alkanes and copovidone at both the glassy and the rubbery region at different flow rates and B) The variation of δ_d for different flow rates in both the glassy and the rubbery region.

For the purposes of this section, measurements were performed at both the glassy and the rubbery region, at 30 and 120 ^{o}C respectively. The measurements were performed at four different flow rates for both temperatures. The results of the measured values of χ for the same three alkanes presented before are shown in **Figure 6.5**, along with the corresponding values of δ_d. Similarly to before the deconvoluted values of χ_S and χ_H, for the glassy state, are presented as well. The values of χ were plotted against the square root of the Reynolds number, which enables the comparison of results obtained at different temperatures and from IGC columns of different diameter.



A)



B)

Figure 6.6: Graphs showing the variation of the enthalpic (χ_H) and the entropic (χ_S) component of the χ interaction parameter between three different alkanes and copovidone at different flow rates in A) the glassy and B) the rubbery region.

The results at the glassy state indicate a decrease in the value of δ_d with increasing flow rate, for the material in the glassy state. This change is manifested on the deconvoluted values of the entropic and enthalpic component of χ. As the flow rate increases the enthalpic component of χ increases, making mixing more and more unfavourable. Increasing flow rate leads to a decrease in the retention time, indicating that the probe molecules mainly interact with the surface of the polymer; diffusion is not prominent, as the molecules do not stay in the column for long. Considering that the value of δ_d of the solvent does not change with flow rate, simple intuition can be used to understand that there two types of δ_d (as also the values of χ, χ_S and χ_H), an interfacial and a bulk one. The former should be smaller than the latter. This change in magnitude is manifested on the value of χ_H. The decrease in the value of χ_S, can be explained in similar terms to the case of increasing temperature. Higher flow rate decreases the mass transfer film resistance. On the same time it facilitates conformational changes favouring mixing.

In the rubbery state the value of δ_d does not seem to be affected by the flow rate. It remains almost constant. In the rubbery state, the molecular mobility of the polymer is higher, thus the importance of interfaces is not prominent, as in the glassy state.

6.4.5 Expanding measurement methodology to include the effects of carrier gas flow rate

The results, presented in the previous section, suggest that the carrier gas flow rate influences the measured values of χ and δ. These effects are more prominent in the rubbery state, owe to the stronger effects of diffusion (higher diffusion coefficient). However, the results obtained in the glassy region are more intriguing, as absorption phenomena are sometimes neglected in the study of glassy materials. It is evident that there are effectively two types of χ an interfacial (two dimensional) and an actual/bulk (three dimensional) one; similarly, two values of δ exist. The interfacial values are those obtained from IGC measurements at high

carrier gas flow rates, where the solvent interacts only with the surface of the polymer. The bulk value is the one predicted by the Flory-Huggins theory. For the determination of the bulk value of χ, an extrapolation approach is proposed.

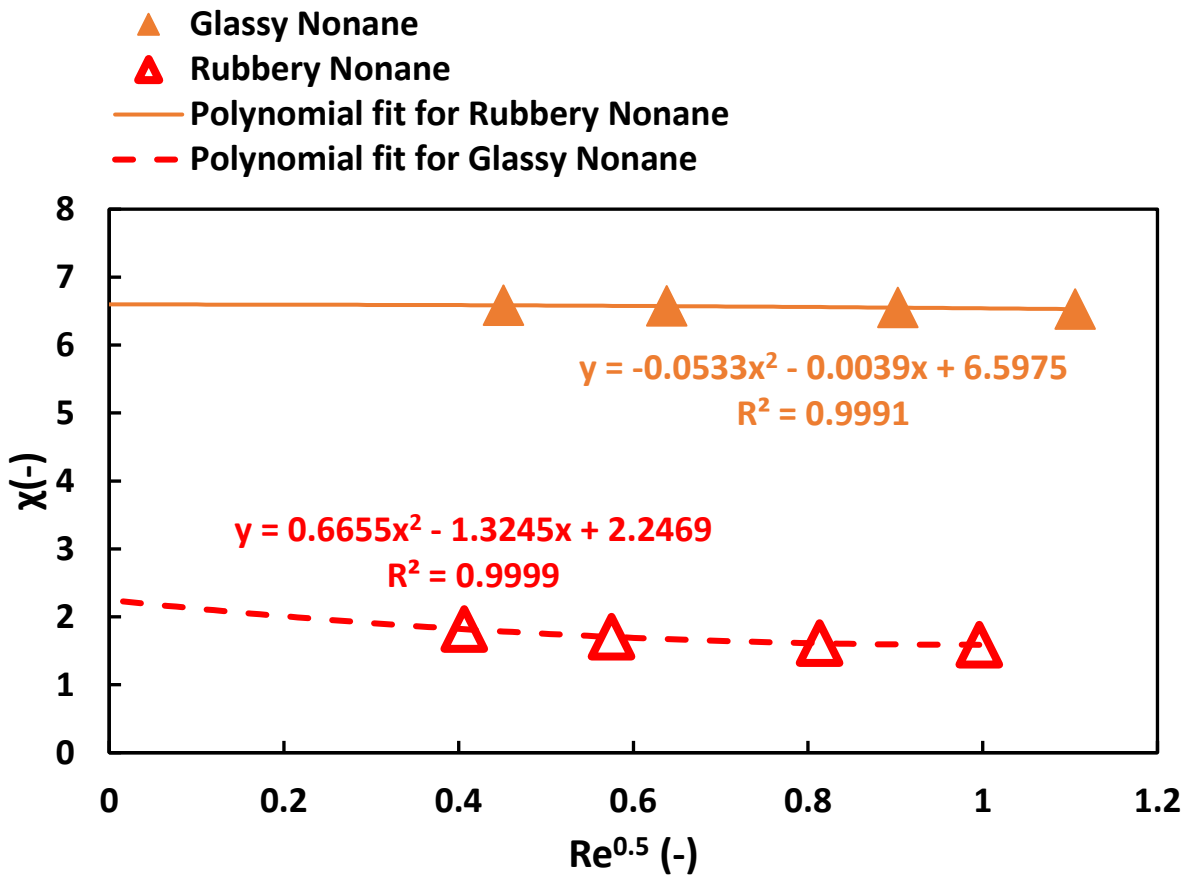


Figure 6.7: The extrapolation procedure to obtain the value of χ at a zero flow rate. The results for nonane in the glassy and the rubbery region are shown.

As shown in **Figure 6.7**, the values of χ are extrapolated to a value of flow rate equal to zero. A second order polynomial fitting was found to fit the data well and to give reasonable values of χ. It is expected, that the extrapolated value of χ corresponds to the situation where only diffusive phenomena are determining the interactions and the advective phenomena, owe to the carrier gas flow rate, are negligible. Then using the extrapolated values of χ, the corrected value of δ_d was calculated for both the glassy and the amorphous polymer, the calculated values

are shown in **Figure 6.8**. As expected from the trend, values in both the glassy and the rubbery state are higher than those under flow rate.

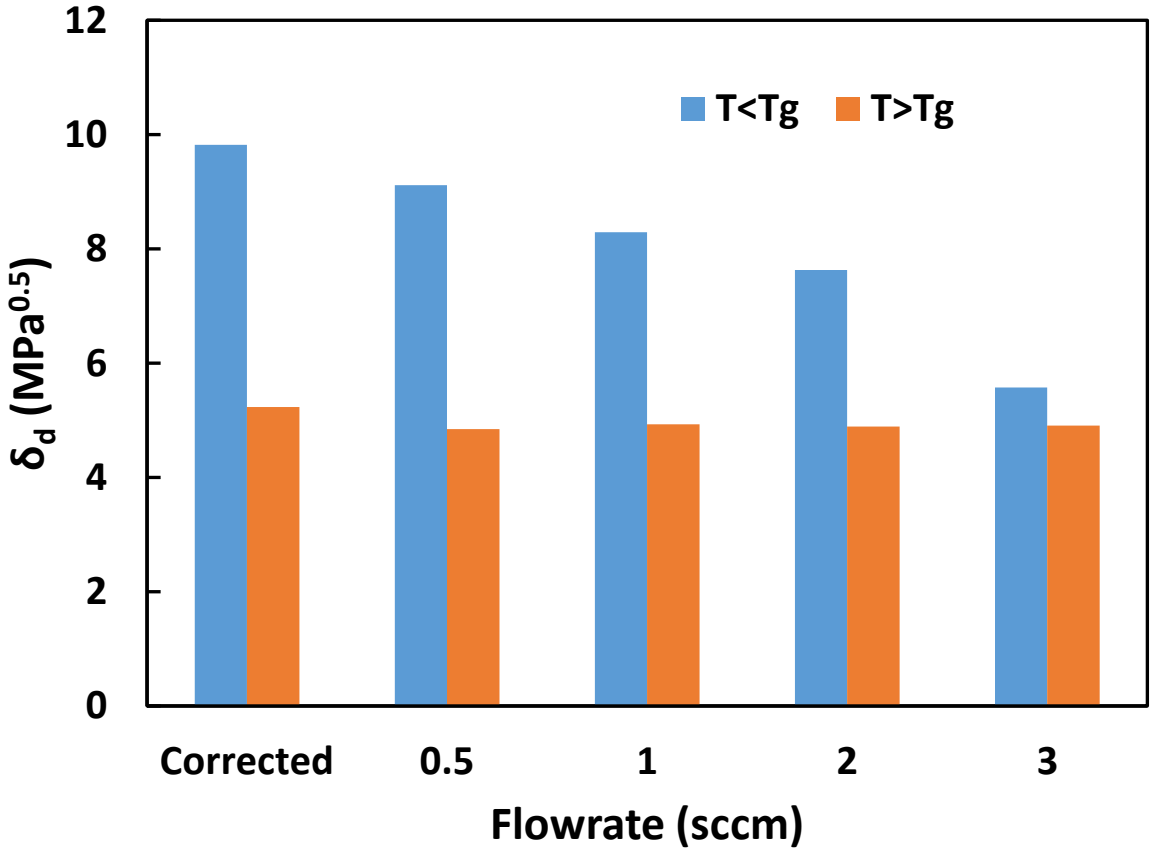


Figure 6.8: Graph showing the variation of δ_d, for two different temperatures, with flow rate, along with the corrected value of δ_d corresponding to a zero flow rate.

The same approach can be used to calculate the values of δ_{AB}. The results for the glassy and the rubbery state are summarised in **Table 6.3**. One could see that all the components of the HSP exhibit a decrease upon the glass transition.

Table 6.3: The HSP for copovidone at two different temperatures, one in the glassy (30 ^{o}C) and one in the rubbery (120 ^{o}C) region.

Temperature (^{o}C)	**δ_d (MPa$^{0.5}$)**	**δ_{AB} (MPa$^{0.5}$)**	**δ_{Total} (MPa$^{0.5}$)**
30	9.82	6.74	11.91
120	5.23	3.81	6.47

6.5 Discussion

The results of this study verify the applicability of IGC as a useful tool for the characterisation of amorphous materials. Most importantly, they demonstrate that IGC can be used to study bulk and surface properties of amorphous materials. For the first time, IGC is deployed to investigate the difference between surface and bulk properties of amorphous materials. Thus, the results of this study, create new opportunities for the faster measurement of the variation of different thermodynamic quantities in the bulk and the surface of a material.

For a number of engineering applications, it is important to have an understanding of the interfacial value of χ, especially when these processes involve the formation of an interface as a key step. Translating the values of χ to HSP it will give better flexibility in the rigorous selection of solvents for process design. Since χ is a concentration dependent quantity, it becomes clear that IGC is able to provide measurements for a limited range of values and with a certain amount of solvents. However, this IGC based study is important, as it uses an established technique to prove the variation of χ in the bulk and on the surface. The results can spark further studies on this field, primarily *in silico*. Some very sensitive surface probing instruments, such as QCM can also provide experimental data.

This study is part of a greater effort presented in this thesis, to improve the accuracy of IGC measurements. It is crucial to appreciate that there is a sharp boundary between surface

energy and χ interaction parameter measurements. This sharp boundary arises from the fundamental theory behind the calculations performed with the measured value of the retention volume. In the former case, a set of equations, leading to the Schultz's plot have been developed assuming surface adsorption. In the latter, the corresponding equations are grounded on the Flory-Huggins mixing theory. Of course, the same data can be studied both ways however, the usefulness of the different measured quantities varies. For instance, someone measuring the solubility parameters of PTFE, would hardly find any interest, as the material is quite immiscible to almost everything. On the other hand, the surface energy of the PTFE is a very useful quantity to be measured, as it enables the design of non-sticking surfaces. Of course, the necessary precautions should be taken, so as the retention time to be as small as possible to minimise the effects of diffusion and ensure that the measurement will be a result of mainly interfacial interactions and not diffusion.

Using the same intuition as before, it is easy to see why the study conducted on the influence of spreading pressure on surface energy measurements, is not relevant to the work of this section on the accurate measurement of χ. As there is no coherent thermodynamic framework linking the two phenomena, adsorption and mixing, in the context of IGC measurements, then the two studies should be examined separately. Some work has been conducted in the field, trying to relate diffusion with spreading pressure. Nevertheless, the work was limited in liquid-liquid interfaces. These studies were focused in the kinetics of wetting and thus their notions it was not possible to be implemented for the derivation of an analytical equation relating the χ interaction parameter and the spreading pressure with the change in Gibbs free energy of the system.

One could speculate that the results of this chapter may have implications on the results of Chapter 4. This is because silanised glass wool is an amorphous material, thus the flow rate may influence the measurements conducted. However, considering how high is the Tg of glass

fibers (~800 – 1000 ºC), one could assume that the effects of flow rate in the glassy state will be negligible. Similarly, it seems not possible the moisture sorption upon storage by glass wool to have caused any form of glass transition. If this has happened, it will have been manifested in a change in the texture of the material; no such change has been observed.

7. Anisotropic wettability of crystalline materials by aqueous solutions of non-ionic polymers

7.1 Introduction

Wettability has intrigued investigators for centuries. For instance, in his groundbreaking work "Discourses and Mathematical Demonstrations Relating to Two New Sciences" published in 1638,[297] Galileo admits the following:

"There is one great difficulty of which I have not been able to rid myself, namely, if there be no tenacity or coherence between the particles of water. How is it possible for those large drops of water to stand out in relief upon cabbage leaves without scattering or spreading out?"

It was Thomas Young who first provided a coherent approach to this phenomenon.[76] In the years following Young's work, a large number of studies have been published approaching wettability from either a theoretical, an experimental, or a computational perspective. Very interesting works on the hydrophobicity and oleophobicity of surfaces highlight, amongst others, the importance of the van der Waals and the acid-base interactions in wettability.[13, 55, 298-299]

Nowadays, wettability is quite important in a wide range of industries. Processes like wet granulation, liquid assisted grinding, and wet coating are the pharmaceutical processes heavily dependent on the wettability of the components involved.[34, 300] Especially within the pharmaceutical industry, the wet coating of active ingredients (API) with polymeric excipients is of great importance to the drug products processability, flowability, and bioavailability.[232]

Previous studies have revealed the anisotropic nature of crystalline pharmaceutical materials and have highlighted its direct implication on properties such as cohesion and adhesion.[7-9] It is, consequentially, clear that crystal anisotropy influences wettability-based

processes. However, the findings in the area of crystal anisotropy have, as of yet, not been translated into mechanistic models for a more in depth understanding of wettability-based processes.

In this chapter, the concept of surface anisotropy for p-monoclinic carbamazepine, a common antiepileptic drug, was established. Macroscopic single crystals of this compound were grown to study this, as they express sufficiently large facets.[4-6] A variety of techniques were employed to quantify the crystalline anisotropy. X-ray phoroelectron spectroscopy (XPS), a technique used extensively in the characterisation of polymeric materials, was used to determine the abundance of each different functional group on each of the major facets. Dynamic contact angle measurements were performed, using different solvents, to determine the different components of the surface energy for each facet.

With the concept of surface anisotropy established, aqueous solutions of copovidone, a common polymeric excipient, were prepared. The surface activity for each solution was determined using dynamic light scattering (DLS), and Langmuir balance tensiometry. DLS has been established, in previous studies, as a means for investigating the behaviour of polymers in solutions.[301-304] In those studies, the instrument successfully determined the aggregation behaviour of polymers under different regimes. In this study, DLS is used to verify that the surface activity of the polymer solution stems from the influence of the dissolved polymer. The Langmuir balance, a technique developed for the measurement of monolayer films, was used to determine the relative magnitude of the solutions surface activity and also to reveal the different regimes of the water–copovidone system (dilute, semi-dilute and concentrated). The data between the two techniques showed good correlation and agreement with those found in literature for the behaviour of non-ionic polymer in aqueous systems.

Following the establishment of the concept of surface activity for the polymeric solutions, the density and the surface tension were determined. The solution density showed an increase upon addition of polymer. On the other hand, the total surface tension, measured using pendant drops, appeared to decrease. Contact angle measurements were used, to determine the work of adhesion between the polymer solution and the different crystal facets.[12, 305] These measurements showed that even a tiny amount of polymer is sufficient to lead to a substantial change in the wettability of crystalline facets with aqueous solutions of copovidone.

7.2 Materials and Methods

7.2.1 Growth and characterisation of macroscopic p-monoclinic carbamazepine single crystals

Seeds for macroscopic single crystal growth were prepared via a two-step cooling crystallisation of a methanol (VWR, Radnor, PA, USA) solution supersaturated with as received carbamazepine (Apollo Scientific, Stockport, UK). The seeds were then suspended in a supersaturated methanol solution, evaporating slowly at ambient conditions. The crystals were left to grow for a few weeks. Fresh supersaturated solution was added to ensure sufficient amount of liquid in the vessel. **Figure 7.2** is a stereoscopic image showing an indexed crystal obtained from this procedure. The indexing was performed using previous literature work[282] and the CCDC Mercury software (Cambridge Crystallographic Data Centre, Cambridge, UK). The surface energy of three major crystal facets and their elemental composition were determined using the same experimental procedure described in the literature.

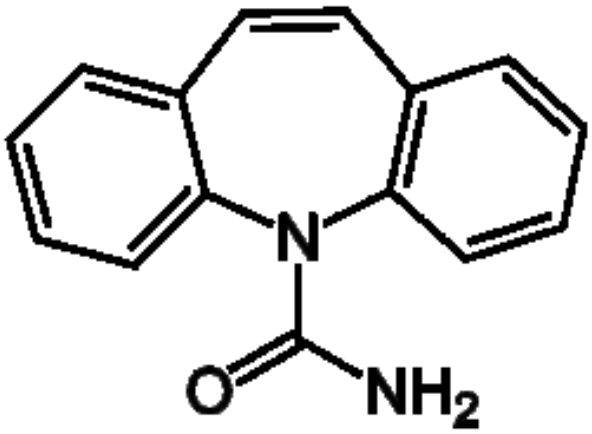


Figure 7.1: The molecular structure of carbamazepine.

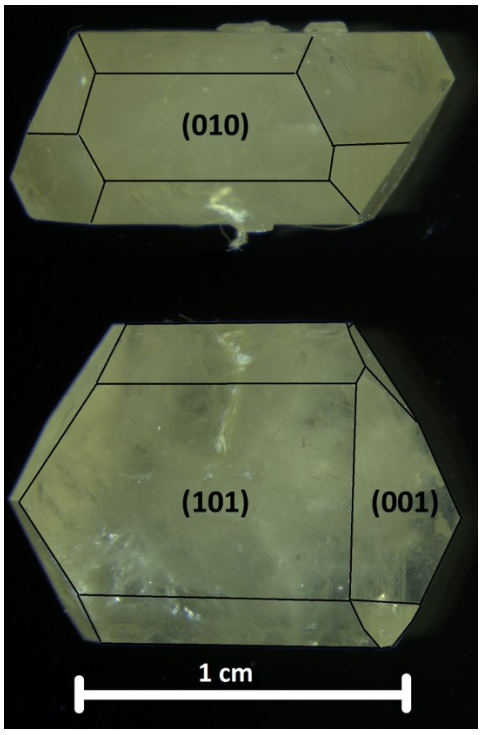


Figure 7.2: Stereoscopic images, obtained at three different angles, of a macroscopic p-monoclinic carbamazepine crystal, grown in methanol with three facets of interest marked on it.

7.2.2 XPS

XPS analyses on the three available facets of the macroscopic CBZ crystal were performed on a Theta Probe spectrometer (ThermoFisher, East Grinstead, UK). The XPS spectra were acquired using a monochromatic Al Kα X-ray source ($h\nu$ = 1486.6 eV) and the anode voltage was set at 16 kV. An X-ray spot of ~200 μm diameter was employed in the acquisition of all spectra. The survey spectra were acquired using a pass energy of 300 eV and the high resolution, core level, spectra were acquired with a pass energy of 50 eV, for C1s, N1s and O1s. Quantitative surface chemical analyses were calculated from the high resolution, core level spectra following the removal of a non-linear (Shirley) background. The manufacturer's Advantage software was used which incorporates the appropriate sensitivity factors and corrects for the electron energy analyser transmission function.

7.2.3 Contact Angle Measurements

The Kruss Drop Shape Analysis (Kruss Gmbh, Hamburg, Germany) instrument, along with the corresponding software, was used for the contact angle measurements. The sessile drop contact angles were determined using the circle profile method. Each measurement performed had 4 repeats, each on clean facets, where the initial drop volumes ranged from 3 to 6 μL in volume. The measurements were performed in a temperature controlled room at about 24 ± 2 ^{o}C. Both advancing and receding contact angle measurements were performed. Four solvents were used in the contact angle measurements: ethylene glycol, formamide, and deionised water for the acid-base component (γ^{AB}), and diiodo methane for the van der Waals component (γ^{LW}). The organic solvents were acquired commercially (VWR, Radnor, PA, USA). Advancing-receding contact angle measurements[96] were conducted and the surface energies were determined via the geometric mean approximation. **Table 7.1** summarises the surface energy values of the liquid probes used in this work from Della Volpe; γ^{+} is the acid

component of surface energy, γ^- is the alkaline component and γ^{Total} is the total surface energy.[55, 67]

Table 7.1: The surface tensions of the liquids used in the contact angle measurements at 25 ^oC.[67]

Liquid Probes	γ^{LW} (mJ/m^2)	γ^+ (mJ/m^2)	γ^- (mJ/m^2)	γ^{Total} (mJ/m^2)
Diiodomethane	50.8	0	0	50.8
Water	21.8	65.0	10.0	72.8
Formamide	35.6	1.95	65.7	58.2
Ethylene glycol	31.4	1.58	42.5	47.8

The growth of the macroscopic crystals has already been discussed earlier in the work; however, once all of the available facets were experimented on, the crystals had to be regenerated to give a pristine surface. They were left to hang in a supersaturated solution once more for at least 2 weeks, before being washed in a cyclohexane bath to quench further crystallisation.

7.2.4 Polymeric Solutions

Copovidone (Kollidon 64), shown in **Figure 7.3**, was dissolved in deionised water for 12 hours under stirring, at set weight percentages by volume up to and including 20%. The values of the polymer concentration are reported in terms of the volume fraction (φ_p), which is the volume of the polymer as a fraction of the whole volume of the solution. The contact angle of copovidone solutions on crystal facets were measured using the same method as above.

The density of the polymer solutions was measured using a digital density meter PAAR DMA 46 (Stantor Redcroft, London, UK). For each measurement 10 mL of fluid were injected, the system was washed and calibrated with DI water between consecutive measurements.

Surface tension values for the polymer solutions were obtained by pendant drop analysis using the same contact angle goniometer and software given earlier (please refer to Appendix 2 for a short description of the method). Each measurement undertaken had six repeats performed, where the drops ranged from 6 to 12 μL in volume. The measurements were performed in an air-conditioned room at about 24 ± 2 ºC. Prior to the measurement of the polymer solutions, the instrument was calibrated using droplets of deionised water with assumed surface energies of 72.8 mJ/m^2. Similar measurements were conducted in heptane, to determine the van der Waals component of the surface tension of the liquid. Both copovidone and water are practically insoluble in heptane, thus it was assumed that the interfacial mass transport of components, from one phase to the other, was negligible. For the measurement in heptane trial measurements were performed with water, in order to obtain the interfacial tension corresponding to van der Waals component of the surface tension of DI water, 21.8 mJ/m^2.

The water uptake of the polymer upon storage conditions, was determined using a mass balance with a heating element incorporated into it. The polymer was placed on an aluminium pan and left to dry at ~100 ºC until no mass change was observed. This revealed a water uptake of around 5 % by weight. The values for the density and the volume fraction of polymer presented therefore account for it.

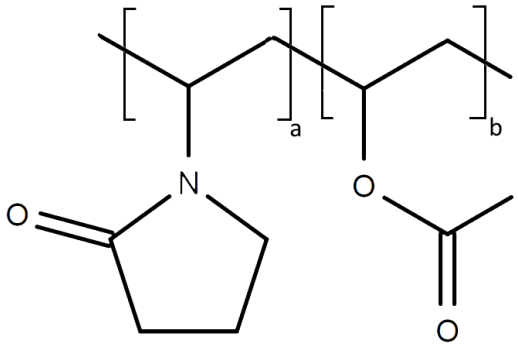


Figure 7.3: The skeletal structure of the copovidone used where the ratio between the vinylpyrrolidone (a) and vinyl acetate (b) in the copolymer is roughly 1:1.2.

7.2.5 DLS

DLS measurements were performed on the aqueous polymer solutions, of varying polymeric volume fractions, at different temperatures; a Malvern Zetasizer μV (Malvern Instruments, Malvern, UK) was employed along with disposable polystyrene cuvettes. The samples were equilibrated for five minutes prior to each measurement at the designated temperature. Each measurement was repeated at least ten times and the averaged data are presented here in the form of correlograms.

7.2.6 Langmuir balance tensiometry

The Langmuir-Blodgett trough, also known as Langmuir balance, was used to measure the surface activity of the polymeric solutions. The instrument used was a Nima 102M (Nima Technology, Warwick, UK) Langmuir-Blodgett trough along with paper based Wilhelmy plates. For the experiments, 20 μL solutions of copovidone dissolved in dichloromethane, were used. The solution, used in each measurement, was spread on the surface of the water and left for 10 minutes for the dichloromethane to evaporate. The speed of the barrier was set at 10 mm per minute. The measurements were performed in a temperature controlled room, at 24 ± 2 ^{o}C.

7.3 Results

7.3.1 XPS analysis

XPS analysis was conducted on the three major facets expressed on the macroscopic single crystals of P-Monoclinc Carbamazepine. Considering the structure of the molecule, five chemical environments were identified for the C1s component as shown in **Figure 7.4**; the C=C-H environment appearing on the aromatic rings, the C=C-C environment on the azepine ring, the C=C-C= connecting the azepine ring with one of the aromatic rings, the N-$CONH_2$ environment of the carboxamide and the C=C-N group connecting the azepine with the carboxamide regions. The first three chemical environments are quite similar chemically due to the absence of any strong electronegative/electropositive atoms compared to the Carbon

atom. Thus, they were all assumed to have a similar binding energy of 284.8 eV, which is corroborated in the literature. The C=C-N group was found from literature to have a binding energy of 285.5 eV, and the N-$CONH_2$ to be at around 289 eV. For the N1s component, two chemical environments were identified, one associated with the primary amine and the other one associated with the tertiary amine. The former has a binding energy of 400.6 eV and the latter a binding energy of 400 eV. The deconvoluted data for the C1s components of the data of each facet are shown in **Figure 7.5** and the elemental composition of each facet is tabulated in **Table 7.2**. An optimization algorithm was employed for the deconvolution, where an FWHM value of about 1.1 eV and 1.3 eV were used for the C1s and N1s, respectively. For every facet examined the polar components, oxygen and nitrogen, showed greater deviation than the carbon relative to the bulk Carbamazepine composition. This trend was previously observed in the XPS of amide compounds.[4, 306]

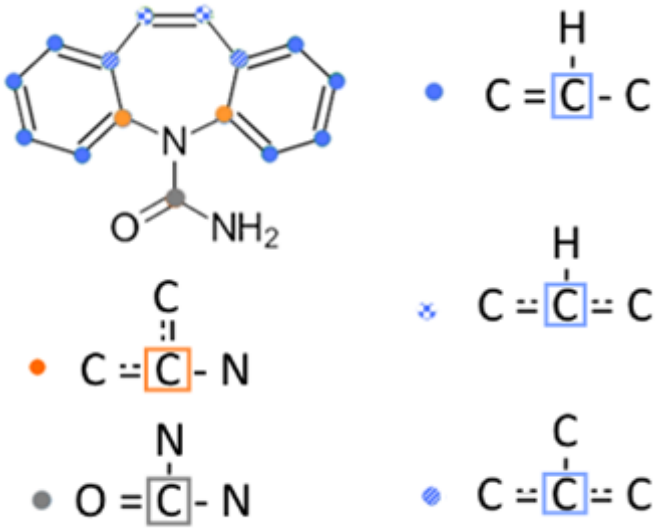
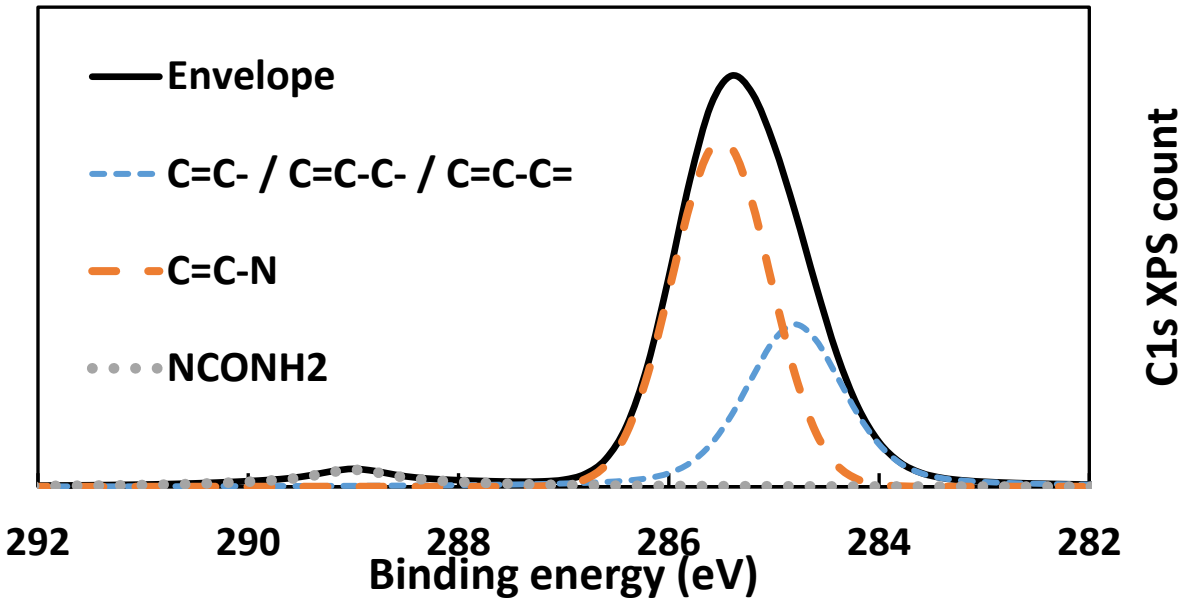
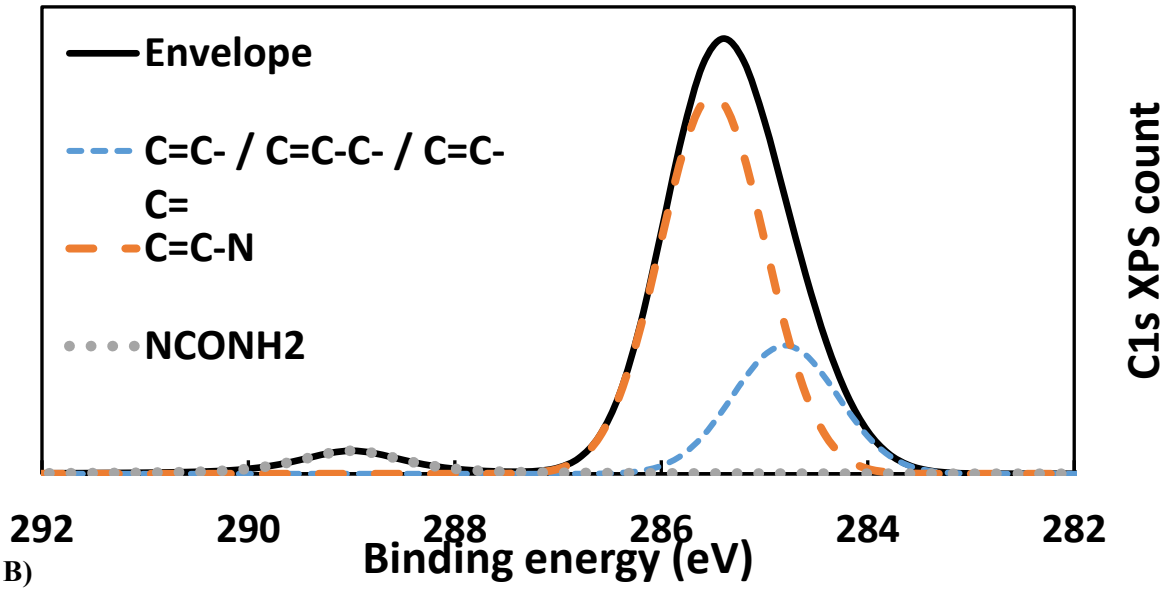


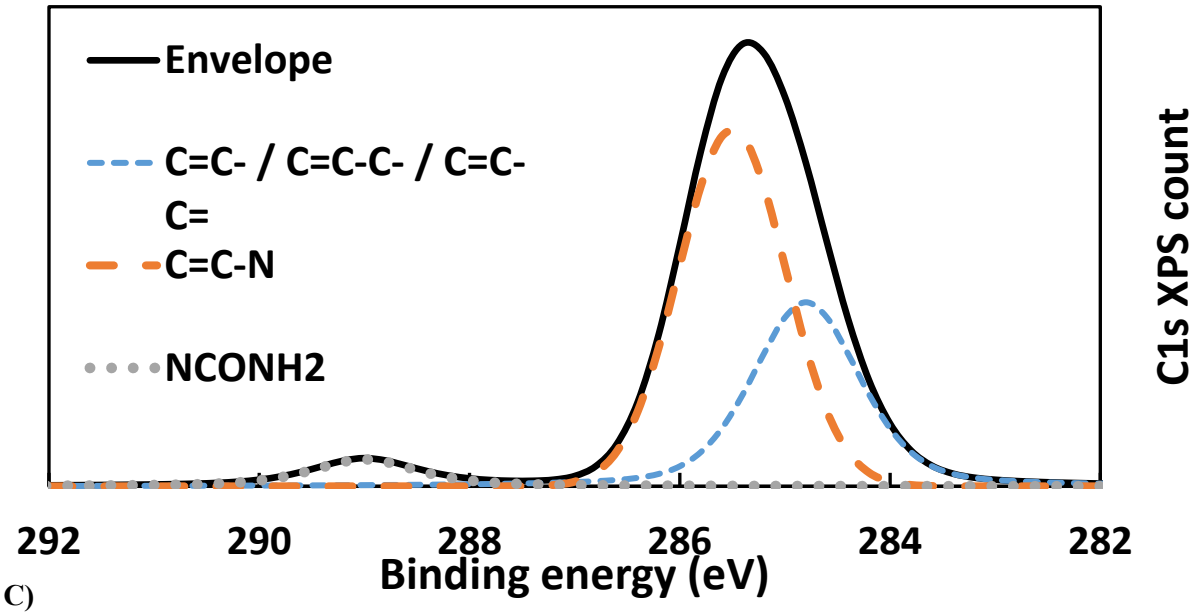
Figure 7.4: The 5 local environments identified for the C1s in Carbamazepine. The three in blue are considered near identical in the deconvolution. The dashed double bonds represent the aromatic bonding of the two phenyl rings.


Envelope
C=C- / C=C-C- / C=C-C=
C=C-N
NCONH2
C1s XPS count
292
290
288
286
284
282
Binding energy (eV)

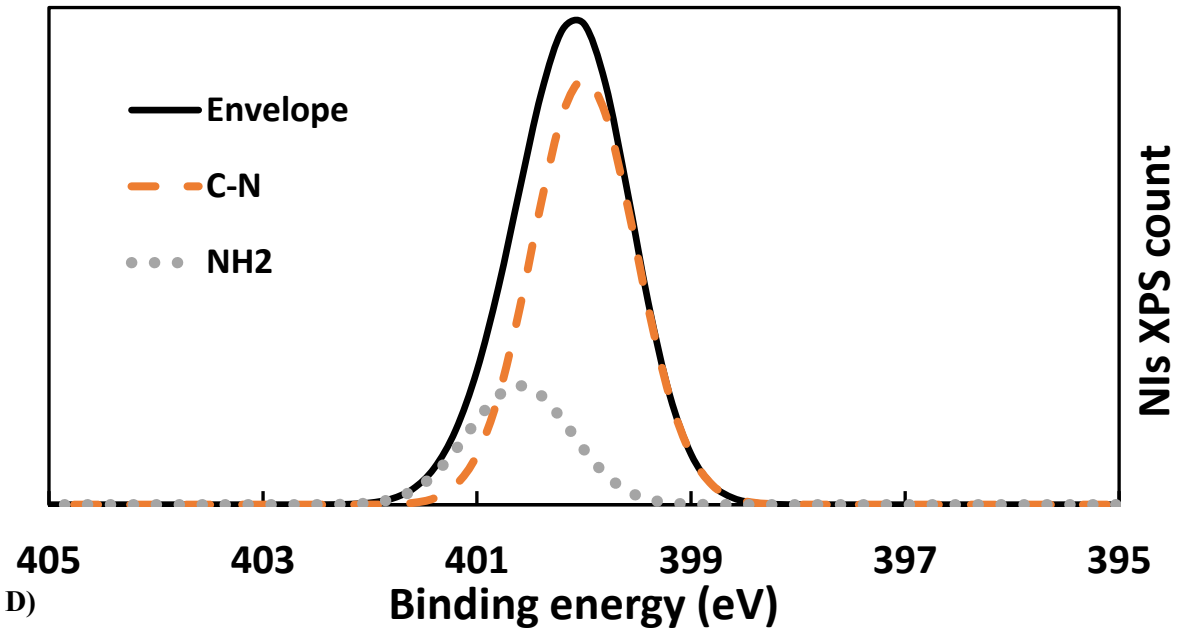
A)


Envelope
C=C- / C=C-C- / C=C-C=
C=C-N
NCONH2
C1s XPS count
292
290
288
286
284
282
Binding energy (eV)

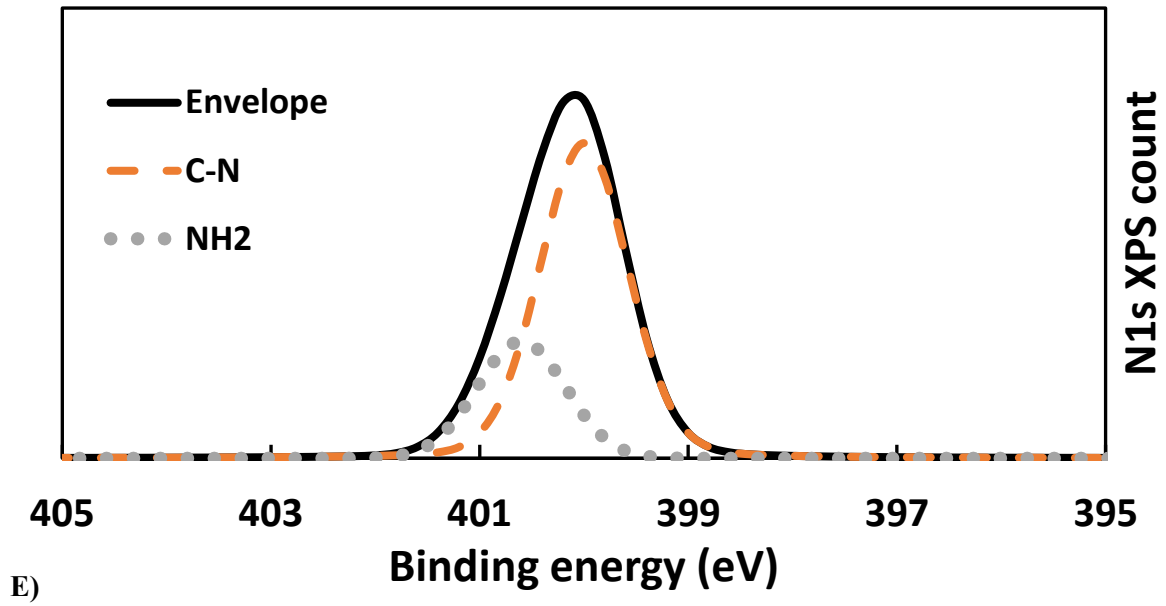
B)


Envelope
C=C- / C=C-C- / C=C-C=
C=C-N
NCONH2
C1s XPS count
292
290
288
286
284
282
Binding energy (eV)

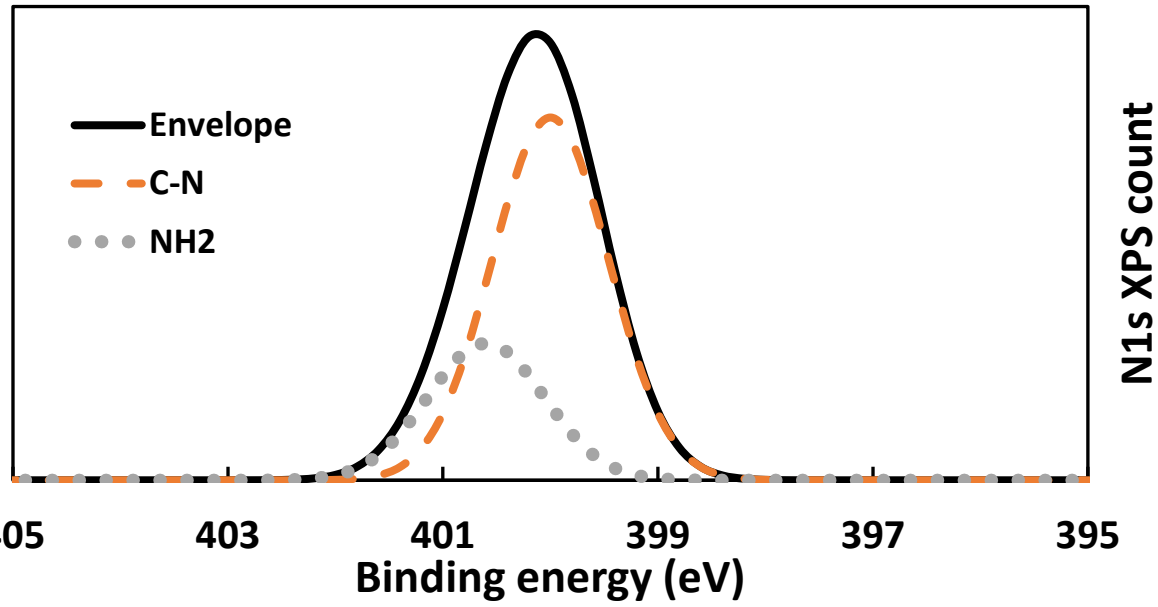
C)


Envelope
C-N
NH2
NIs XPS count
405
403
401
399
397
395
Binding energy (eV)

D)



E)



F)

Figure 7.5: The deconvoluted C1s spectra for A) (101) facet, B) (010) facet and C) (001) facet, as also the N1s spectra for D) (101) facet, E) (010) facet and F) (001) facet.

Table 7.2: The elemental composition of carbamazepine's facets as measured with XPS.

	C atomic %	N atomic %	O atomic %
Facet (101)	82.3	7.7	10
Facet (010)	81.2	12.2	6.6
Facet (001)	81.4	11.8	6.8
Theoretical	83.3	11.1	5.6

7.3.2 Surface Energy Anisotropy

The equilibrium contact angles were calculated using the equations 2.55-2.57, from advancing-receding contact angle measurements with polar liquid probes, presented in **Table 7.3**. The corresponding results for diiodomethane have been presented in Chapter 5. The surface energies were calculated using Young's equation and the geometric mean approximation. Contrary to Chapter 5 only three facets are reported here, as the number of relatively large (112) facets expressed on the crystals, was not sufficient to obtain reasonable amount of measurements. Diiodomethane shows a higher affinity to the three facets compared with water. This indicates that the van der Waals interactions are dominant in carbamazepine crystals, even though the molecule appears to be quite polar. By using the geometric mean approximation, we obtained both the basic and acidic surface energy components for the crystal facets. The surface energy values are given in **Table 7.4** further on. On the same table, a surface energy hydrophilicity factor, H, is defined by the ratio of the acid-base over the van der Waals component of surface energy.

Table 7.3: The equilibrium contact angles for the three polar solvents on the different facets calculated from the subsequent results of advancing and receding measurements.

Facet	Solvent Probes		
	Water (°)	**Ethylene Glycol (°)**	**Formamide (°)**
(101)	71.7	48.1	60.1
(010)	66.6	44.3	56.5
(001)	60.3	45.4	49.6

Table 7.4: The surface energy values calculated from the averaged contact angles.

Facet	γ^{LW} **(mJ/m^2)**	γ^{+} **(mJ/m^2)**	γ^{-} **(mJ/m^2)**	γ^{AB} **(mJ/m^2)**	γ^{Total} **(mJ/m^2)**	**H = γ^{AB}/ γ^{LW}**
(101)	44.2	0.01	4.2	0.40	44.6	0.01
(010)	37.0	0.38	6.5	3.1	40.1	0.08
(001)	36.6	0.57	8.9	4.5	41.1	0.12

Direct comparison of the XPS data with the contact angles measured lead to some interesting observations. Nitrogen appears in two forms in Carbamazepine: as a carboxamide group where it forms a C-NH_2 bond, and on the azepine structure as a tertiary amine. As expected, the (101) site is the most hydrophobic, as expressed by the water contact angle, as it has the smallest polar component; seen by the sum of the nitrogen (N %) and oxygen (O %) content, found in **Table 7.2**. Similarly, it is the most acidic one. The (001) facet shows the greatest hydrophilicity, which is expected given it has the highest basic component and water has a greater acidic component of surface energy, according to Della Volpe.[67]

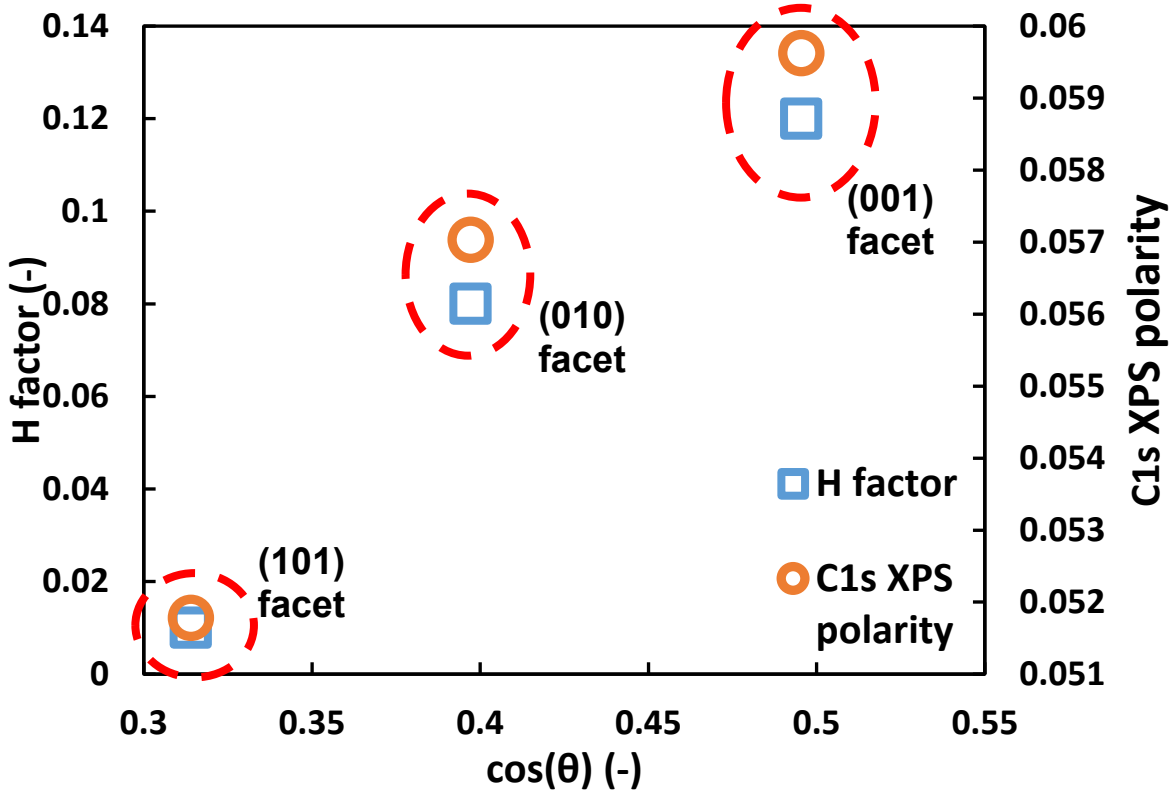


Figure 7.6: Plot showing the correlation of hydrophilicity, measured as the cosine of the advancing contact angle of water on individual crystal facets, with the surface energy hydrophilicity factor, H, and with the C1s XPS polarity. The facets corresponding to every set of points are illustrated on the figure.

In **Figure 7.6**, it can be seen that the surface energy hydrophilicity factor, H, provides a good correlation for the hydrophilicity of individual facets, as measured by the cosine of the advancing contact angle of water. The C1s XPS polarity, given by the ratio between the relative contributions of the N-$CONH_2$ over the contribution of the other two components of the C1s spectrum also seems to correlate well with the hydrophilicity. This is an important finding, verifying that the steric hindrance associated with the tertiary nitrogen, limits the ability of the particular functional group to contribute in the formation of acid-base interactions.

The results obtained from the analysis of the anisotropic behaviour of the material are in good qualitative agreement with similar works obtained on different compounds. The

importance of the distinct components of the surface energy has been reaffirmed. Furthermore, the validity of XPS as a surface probing tool, enabling the determination of the hydrophilicity of individual crystal facets, has also been reaffirmed.

7.3.3 Wettability with polymeric solutions

The addition of polymer in a liquid gives rise to surface activity similar to the one observed when a surfactant is added to a liquid. This phenomenon can be observed with DLS measurements. [303, 304, 306, 307, 313] The surface activity of copovidone molecules at different concentrations was obtained with a Langmuir balance. The values of surface activity against the polymer volume fractions are shown in **Figure 7.7**. On this same figure, the three solution regimes can be identified; the dilute, the semi-dilute and the concentrated.[308-309]

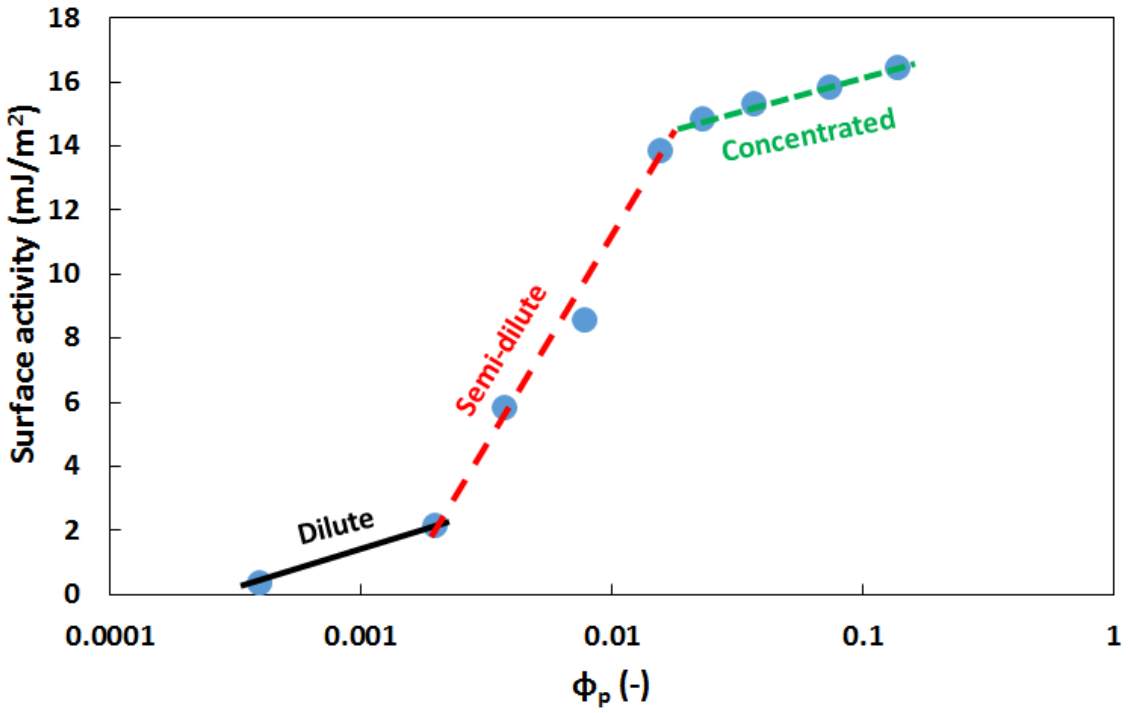
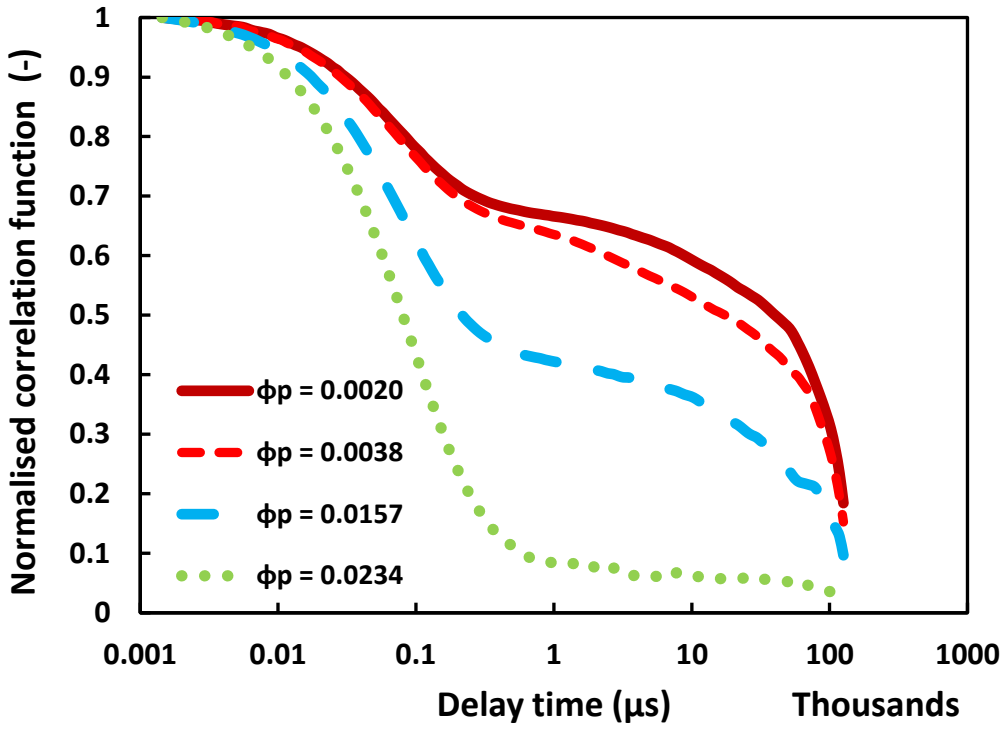


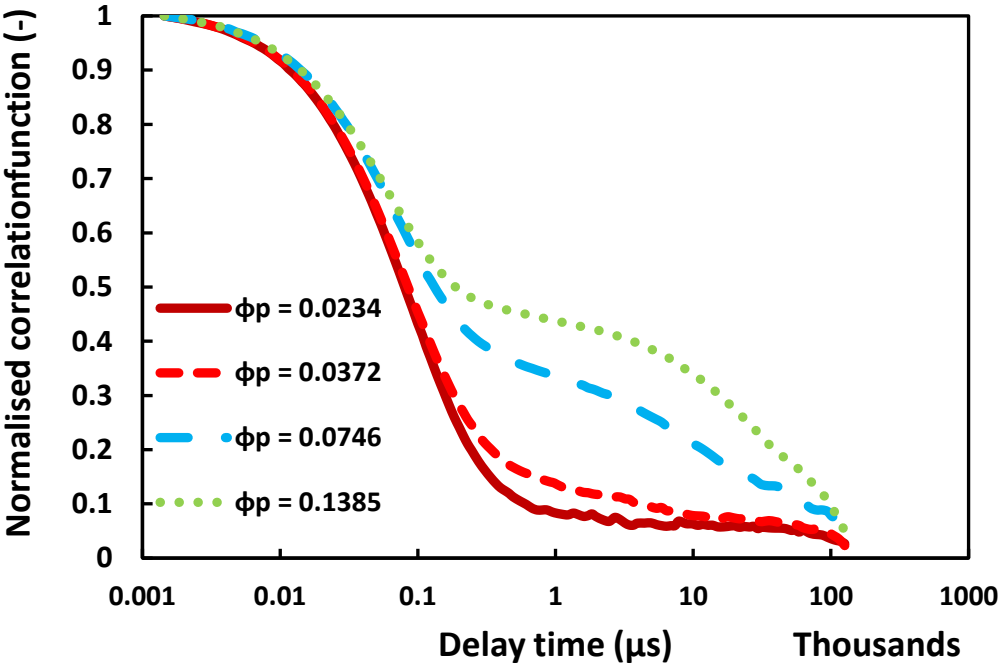
Figure 7.7: The variation of the surface activity of solution at different polymer concentrations.

DLS measurements were employed to visualise the behaviour of the polymer in solution at the three solution regimes. In DI water, the equipment cannot measure anything, since no scattering takes place. However, upon the addition of polymer, scattering occurs leading to

correlograms similar to those shown in **Figure 7.8**. Similar to the behaviour observed in polyvinylpyrrolidone, increasing the amount of polymer, at the semi-dilute region, leads to a decrease of the slow mode of the autocorrelation function, which is depicted as the disappearance of the second shoulder of the correlogram, shown in **Figure 7.8 A**. This shift has been correlated with the effects of going from theta to good solvent conditions. However, in the dilute region, the addition of polymer leads to the reappearance of the slow mode.



A)



B)

Figure 7.8: The correlogram from the DLS measurement for different polymer solutions A) in the semi-dilute region and B) in the concentrated region.

Figure 7.9 depicts the variation of the surface tension of the polymer solution, measured using the pendant drop in air method, as a function of the volume fraction of polymer in solution. According to the literature, the variation of the surface energy is better described in terms of an equation with the form:

$$\gamma_{LV,p} = a + b\varphi_p^c \qquad \text{Eq. 7.1}$$

In this equation $\gamma_{LV,p}$ stands for the surface tension of the solution and φ_p is the volume fraction of the polymer. The rest of the symbols are fitting coefficients. Fitting of the values give the following values for the coefficients of this equation: a = 73.01, b = -36.37 and c = 0.055. The fit line associated with this equation is, also, shown on **Figure 7.9**.

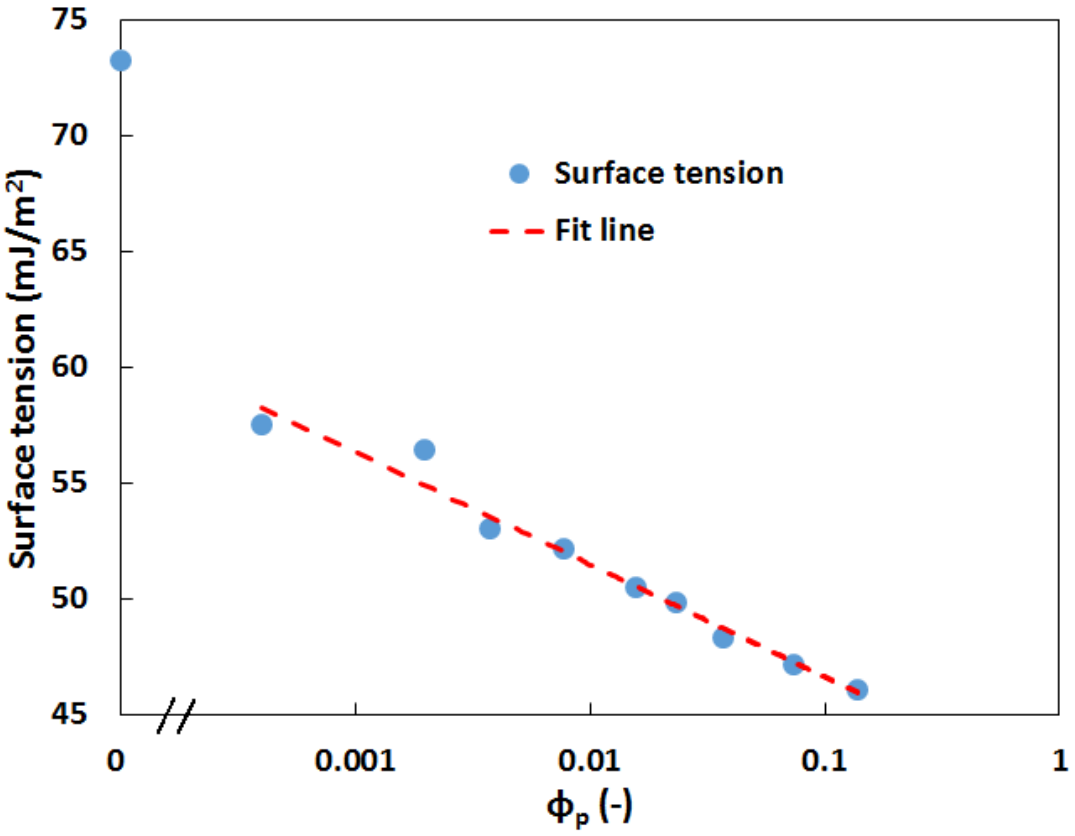


Figure 7.9: The surface energy variation of the polymer solution for different amounts of polymer, the surface tension at no polymer content is shown at around 73 mJ/m^2.

During pendant drop measurements in heptane, the polymer solution droplet interacts with the surrounding fluid only by means of van der Waals interactions, providing a measurement for the liquid-liquid interfacial tension. Considering a surface tension of 21.4 mJ/m^2 for heptane, the van der Waals component of the surface tension for the polymer solution can be calculated. **Figure 7.10** shows the interfacial tension ($\gamma_{Interfacial}$) and the two components of the surface energy of the polymer solutions. Using the values for the interfacial tension between the aqueous solution of copovidone and heptane, the work of adhesion (W_{AB}) between the aqueous solution and heptane could be obtained according to the following equation:

$$W_{AB} = \gamma_{LV,C7} + \gamma_{LV,p} - \gamma_{Interfacial} \qquad \text{Eq. 7.2}$$

In the above equation, $\gamma_{LV,C7}$ is the surface tension of heptane and $\gamma_{LV,p}$ is the surface tension of the polymer solution, obtained by pendant drop measurements in air. Then, to calculate the van der Waals component of the surface tension, one should recall the definition of work of adhesion:

$$W_{AB} = 2\left(\sqrt{\gamma_{LV,C7}^{LW}\,\gamma_{LV,p}^{LW}} + \sqrt{\gamma_{LV,C7}^{+}\,\gamma_{LV,p}^{-}} + \sqrt{\gamma_{LV,C7}^{-}\,\gamma_{LV,p}^{+}}\right) \qquad \text{Eq. 7.3}$$

In the above equation superscript LW describes the van der Waals component of the surface tension, + stands for the basic part of the acid-base component of the surface tension and – for the acid part of the acid-base component of the surface tension. However, as heptane exhibits only van der Waals interactions, the last two terms of the right-hand side of equation 7.3 are equal to zero. Thus, combining equations 7.2 and 7.3 the following equation is obtained:

$$\gamma_{LV,C7} + \gamma_{LV,p} - \gamma_{Interfacial} = 2\sqrt{\gamma_{LV,C7}^{LW}\,\gamma_{LV,p}^{LW}} \qquad \text{Eq. 7.4}$$

The first term on the left-hand side of equation 7.4 is obtained from **Figure 7.9**, the second one is known from literature and the third one was calculated from the pendant drop measurements in heptane. On the right-hand side, the first term is equal as to the second term of the left-hand side. Thus, using equation 7.4, the van der Waals component of the surface tension of the polymer solution could be obtained by simple rearrangement.

Increasing polymer loading leads to a decrease in the total value of the surface tension, as shown in **Figure 7.9.** However, when it comes to the specific components of the surface tension an increase was observed in the value of the van der Waals component and a decrease was observed for the acid-base component. In particular, the van der Waals component of the surface tension of water is 21.8 mJ/m^2, whereas the aqueous solutions of copovidone exhibit van der Waals component of surface tension in the region of 33-38 mJ/m^2. On the other hand, the acid-base component of the surface tension of water is at 51.8 mJ/m^2 and it diminishes to values below 22 mJ/m^2.

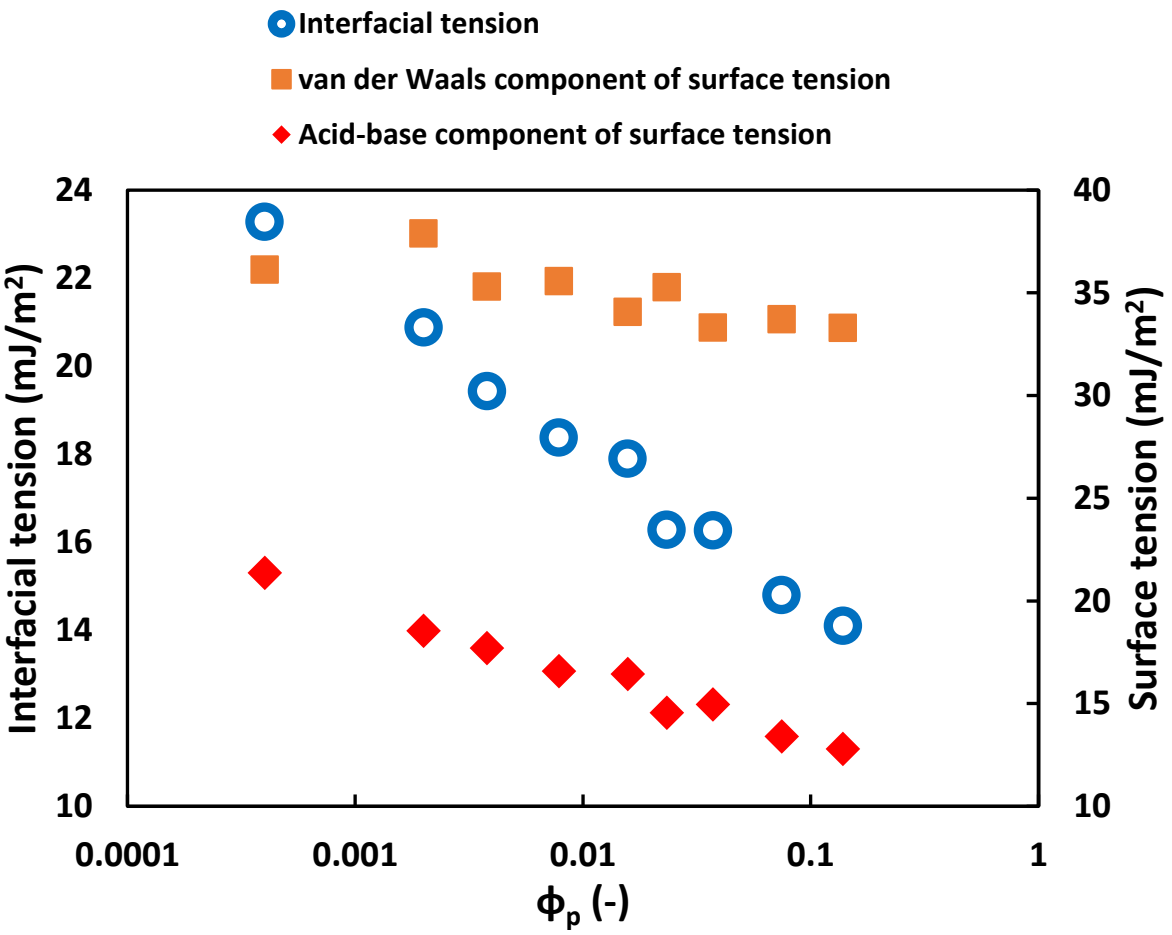
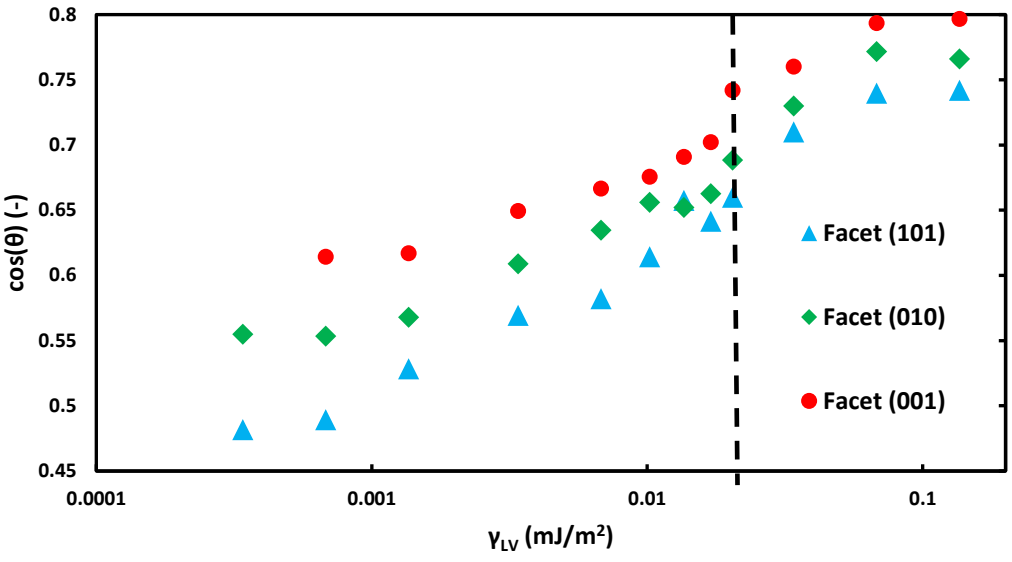


Figure 7.10: The interfacial work and the two components of the surface energy of the polymer solution, at different polymer loadings.

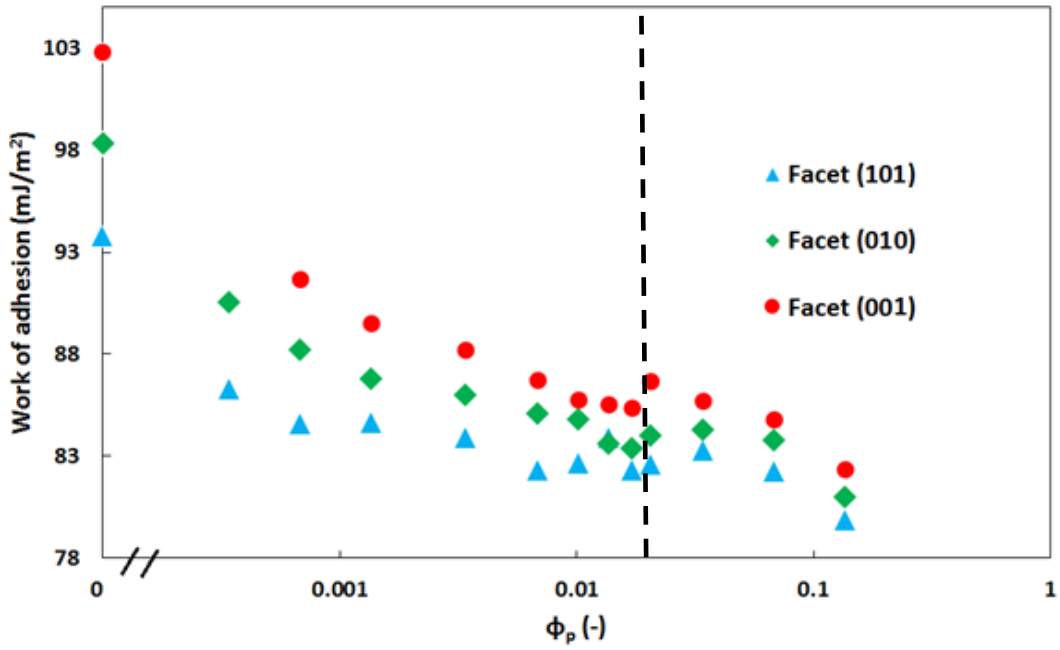
As shown earlier, through the contact angle measurements, the surface energy anisotropy is not very prominent between the three facets of p-monoclinic carbamazepine. Each of the facets have quite similar surface energy values. This is reflected, also, in the contact angles for the copovidone solutions on the particular facets. In **Figure 7.11 B**, the work of adhesion between individual facets and the copovidone solutions is shown. The work of adhesion was calculated using Young's equation:

$$W_{AB} = \gamma_{LV,p}\,(1 + \cos(\theta)) \qquad \text{Eq. 7.5}$$

in this equation W_{AB} stands for the work of adhesion, $\gamma_{LV,p}$ is the surface tension of the polymer solution and θ is the value of contact angle, which can be found in **Figure 7.11 A** and it was obtained, of course, from contact angle wettability measurements.[298]



A)



B)

Figure 7.11: A) The wettability of polymer solutions and B) The work of adhesion of the polymer solutions on the different facets. The dotted line describes the limit between the semi-dilute and the concentrated region.

The most intriguing finding is that the work of adhesion decreases as the total surface energy of the three facets increases. In particular, the (001) facet exhibits the highest work of adhesion with the aqueous solutions of polymer. This is attributed to the high ratio between the van der Waals and the acid-base component of surface energy compared with the other two facets. In other words, as the (001) facet carries a larger acid-base component of the surface energy, it provides a more favourable substrate for the polymer solution, that exhibits a higher polarity ratio (the ratio between the acid-base and the van der Waals component of the surface energy) than DI water. From **Figure 7.11 B**, one could see the improvement in wettability as the polymer content of the aqueous solution increases. It is interesting that despite the small magnitude of surface activity at small polymer loading, the improvement in wettability can be quite substantial, decreasing up to about 10 ^{o}. At the tail of the plot of the work of adhesion, an interesting behaviour is observed. Moving from left to right, on the figure, a constant negative slope is observed (at least for facets (001) and (010)), indicating a monotonic relation between surface tension and work of adhesion. Then at the concentrated region limit, the point after which the contact angle reaches its minimum value (corresponding to maximum value of cos(θ)), a sudden jump is observed, leading to a small maximum and then the trend becomes decreasing again. The same jump could be seen by careful observation of the same region for the values of cos(θ).

7.4 Discussion

7.4.1 Anisotropic properties of p-monoclinic carbamazepine and implications on crystallisation

The concept of anisotropy has been reaffirmed and established for the p-monoclinic carbamazepine system. p-Monoclinic carbamazepine was found not to exhibit as strong surface energy anisotropy as other pharmaceutical materials, studied in the past.[4-6, 310] This observation is not decoupled from the fact that carbamazepine's molecule does not include a large number of highly polar functional groups and from the specific spatial organisation of the molecules in

the unit cell of the particular polymorph. The absence of strong anisotropy was highlighted by the surface energy values calculated. In particular, the values for the dispersive component calculated for the facets (001) and (010) are within the vicinity of experimental error. This concept, of weak anisotropy, was further reaffirmed in the work of adhesion measurements between the polymer solutions and crystal facets.

The XPS analysis verifies the anisotropic nature of the surface chemistry of crystals of p-monoclinic carbamazepine. Furthermore, it verifies literature studies, based on in silico tools, claiming that this anisotropy stems from the type, the number and the orientation of the functional groups exposed in each facet.[282] Contact angle measurements with various organic liquids showed that this anisotropy gives rise to different surface energies at each facet. All the components of the surface energy identified, using the geometric mean approximation, were different between each facet. This surface energy anisotropy can be seen as work of adhesion anisotropy, as shown by the contact angle measurements of the polymer solutions on individual p-monoclinic carbamazepine facets. These measurements showcased the importance of taking into consideration all three components of surface energy: van der Waals, acidic, and basic. Even though the (101) facet has the highest total surface energy, it was found to have the lowest work of adhesion when interacting with the polymer solutions. This was attributed to the specificity of acid and base interactions on each facet, which are determined by the orientation of polar functional groups present at the surface. This topic will be discussed in greater detail further down in the discussion section.

Only the primary amine is a reliable electron donor in carbamazepine thus, it can be speculated that the basic component of the surface energy stems from it. Nonetheless the magnitude of its influence, on different facets, is determined by various factors: the orientation of the amine, the interaction of neighbouring amines to form dimeric structures, and its interactions with other functional groups. Similar arguments could be made for the array of

electron accepting groups contributing to the basic component of the surface energy. XPS measurements further validated the concept of anisotropy, showing that the atomic composition of each facet is different from the theoretical bulk composition of the crystal. From the quantitative analysis of the XPS spectra, it can be seen that the amount of the primary amine, the driving force for the acidic component of surface energy, is much smaller than the combined contribution of both the tertiary amine and, mostly, the carbonyl, which both drive the basic component of the surface energy.

Nevertheless, it seems that there is a correlation between the primary amine content and the hydrophilicity of an individual facet. Among the available functional groups, primary amines are the likeliest to form hydrogen bonds. The (001) facet, the only one where the primary amine component is greater than the tertiary one, is also the most hydrophilic. However, one should also note that it also has the biggest total surface energy acid-base component, casting doubts over whether the earlier assertion can solely be attributed to the primary amine content.

As mentioned in Chapter 3, the Wulff-Chernov formalism constitutes the backbone of numerous computational models, used for the prediction of crystal habit at various conditions. In 1901, the Russian crystallographer and mineralogist, Professor George Wulff[311] proposed, on the ground of the ideas of Professor Josiah W. Gibbs, that the equilibrium shape of a crystal, exhibiting N number of facets, is such that to satisfy the following criterion:

$$\frac{\gamma_1}{h_1} = \frac{\gamma_2}{h_2} = \cdots = \frac{\gamma_N}{h_N} = constant \qquad \text{Eq. 7.6}$$

in the above equation γ_i stands for the surface energy of facet i and h_i is the distance of the facet from the centre of the crystal. Experimental work, has revealed that this criterion was holding true only for really small particles, growing from solution or from micron sized seeds. However, it was shown that for cases, resembling the top seeded solution growth method employed in

this chapter, where millimetre sized seeds are used, the seed particles were not reaching the predicted equilibrium shape. Instead they were reaching the so-called steady state crystal habit. This was attributed to the mass transport limitations imposed by the large size of the particle, posing limitations in the growth. On this ground, Professor Alexander Chernov,[163] proposed the following alternative criterion to describe the process leading to the steady state crystal habit:

$$\frac{R_1}{h_1} = \frac{R_2}{h_2} = \cdots = \frac{R_N}{h_N} = constant \qquad \text{Eq. 7.7}$$

where R_i stands for the rate of growth of facet i. This last equation constitutes the ground of the infamous Wulff-Chernov formalism, widely used in computational models for the prediction of crystal habit.

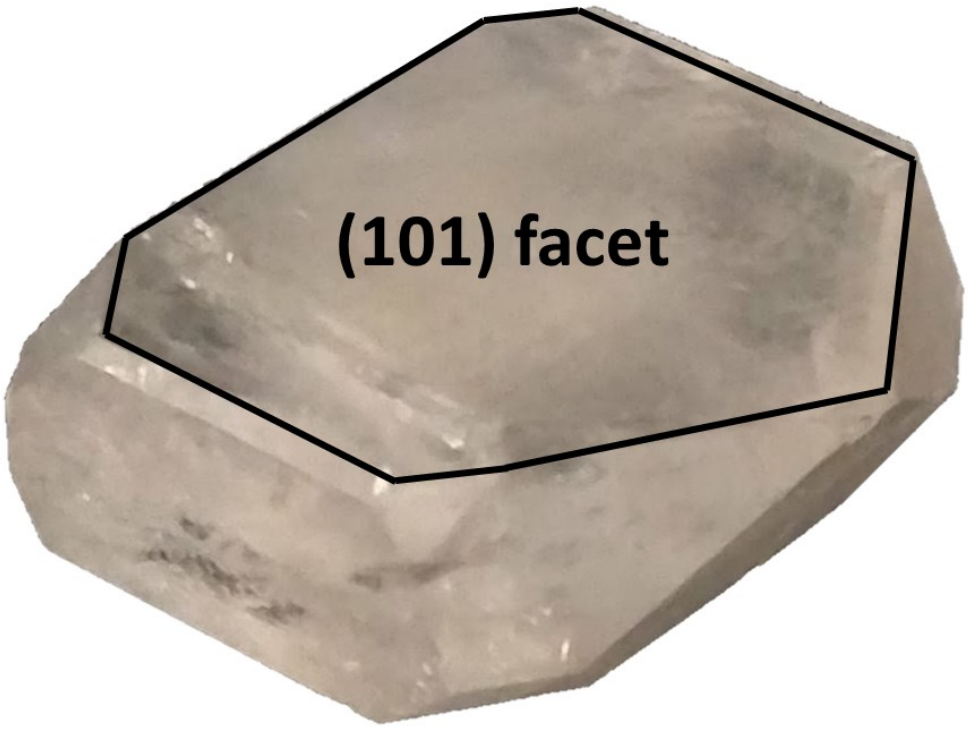


Figure 7.12: Stereoscopic image, of a macroscopic crystal grew via top seeded solution growth, showing the dominant (101) facet.

Taking into account the crystal habit of numerous crystals (one can be seen in **Figure 7.1** and another one in **Figure 7.12**), it is evident that the facet (101) is the dominant one, in the case under consideration. Considering that this facet carries the highest surface energy from those identified, it is evident that the habit of the crystals grew in this study are not in agreement with the Wulff construction.

This finding should be seen in conjunction with the discussion at the beginning of this section, regarding the lack of strong anisotropic behaviour by p-monoclinic carbamazepine. For instance, in the case of p-monoclinic carbamazepine, one could not identify a strongly hydrophobic facet, significantly differentiating from the rest; this does not preclude the possibility of the existence of such a facet that for various reasons is not expressed in the crystals produced. In fact, in one of the pioneering papers in the field of surface energy anisotropy, Heng et al. were forced to use razor blades to slice form I paracetamol crystals in order to reveal the strongly hydrophobic (010) facet that it was otherwise not expressed on the surface of the macroscopic crystals.[4] Nevertheless, the inconsistency between the habit of the crystals of p-monoclinic carbamazepine, obtained via different routes, and the Wulff construction is not something dramatic. In fact, as it has been exhaustively explained in Chapter 3, severe limitations identified in the very early models, developed to predict crystal habit, propelled the development of more accurate models, including the Chernov construction. Furthermore, it is expected that for compounds not exhibiting strong anisotropy, such as p-monoclinic carbamazepine, the affinity to the Wulff construction to be less profound.

7.4.2 Wettability with polymer solutions

The values of the van der Waals component of the surface energy for the polymer solutions were determined via pendant drop measurements in heptane and are presented in **Figure 7.10**. Using Fowkes' approach, the acid base component can be obtained by subtracting the van der Waals component from the total surface energy of the polymer solutions,

determined via pendant drop measurements in air. Owing to the nature of the polymer under consideration, it was not possible to use a polar solvent with well-defined van der Waals and acid-base components, in a similar way to how heptane was used. This is because copovidone is quite soluble in polar solvents. Furthermore, due to the ill-conditioning of the set of equations, it was not possible to obtain reliable values for the acid-base component of the aqueous solutions at different polymer concentrations. Ill conditioning has been reported in literature for systems of non-linear equations used for the determination of the different components of surface energy. It effectively means that even the smallest changes to the value of the measured contact angle, diffuse and amplify downstream, leading to peculiar results.[312-315] Furthermore, one should recall that surface active molecules behave differently upon contact with different surfaces. Thus, correlation of pendant drop and contact angle measurements, for a polymer solution, is not necessarily going to yield sensible results. This argument may cast doubts about comparing pendant drop measurements obtained in air with pendant drop measurements obtained in a liquid, such as heptane.

At this point, a very interesting observation arises. It is a well-established fact, the surface tension of a polymeric solution is equal to the surface tension of the solvent, minus the surface activity associated with the quantity of the polymer.[315, 316, 322, 323, 324, 325] The results of this work, suggest that this is true only for the value of the total surface tension. However, it does not seem to hold at the individual components. Upon pendant drop measurements in heptane, aqueous copovidone solutions were measured to exhibit an increase in the van der Waals component of the surface tension (from 21.8 mJ/m^2 to around 33-38 mJ/m^2). This phenomenon corresponds to a negative value of the van der Waals component of the surface activity induced by the polymer. Positive surface activity comes from the adsorption of the surface active agents at the interface between two interacting phases, at a particular orientation. For instance, surfactants in an aqueous solution in contact with an oil will adsorb on the interface with their hydrophobic

tails pointing towards the oil. In this case it seems that owe to the hydrophobic nature of heptane, the copovidone molecules probably exhibit some sort of desorption from the interface region.

In Chapter 6, the HSP of copovidone was measured accurately and it was found to exhibit a strong van der Waals component. This appears to be manifested in an increase in the van der Waals component of the surface tension of aqueous solutions of copovidone. Besides the changes in the van der Waals component of the surface tension, it should be noted, that the increase in wettability, may be favoured by changes in the split between the acid (γ^+) and the base (γ^-) components of the surface tension, as well. According to Della Volpe split the acid component of the surface tension of water is about 6.5 times bigger than the basic one. This ratio could shift in favour of one or the other. Considering the numbers presented in **Table 7.4**, this shift should be towards an even stronger contribution of the acid component.

This work establishes the correlation between the polymer aggregation in solution and the surface activity of the solution. As revealed from the DLS measurements, the concentration of the polymer can determine whether the system is exhibiting good or theta solvent behaviour.[301, 309, 317] The transition from theta to good solvent behaviour, as shown by the disappearance of the slow mode shoulder from the DLS correlogram observed in **Figure 7.8 A**, indicates that polymer aggregation can be more prominent at low concentrations. It is noteworthy that the polymer solution does not exhibit a linear behaviour in its aggregate formation. The polymer solution in the semi-dilute region shows a decrease in the relative abundance of aggregates up to $\varphi_p = 0.0234$, the point where the system enters the concentrated region, indicating that in the semi-dilute region good solvent conditions exist. Then in the concentrated region, the solutions starts to once more have an increased tendency towards the formation of aggregates. Thus, the slow shoulder, which disappeared at $\varphi_p = 0.0234$, started rising again, as it can be observed in **Figure 7.8 B**. This overall non-linear behaviour is not

uncommon in polymer solutions and possibly corresponds to a critical solution concentration, not unlike a critical micelle concentration.[304] Previous works, investigating phenomena in systems similar to ours and using modified Florry-Huggins models, have explained such phenomena on the grounds of hydrogen bonding.[301, 317-318]

Such cluster formation behaviour, exhibited by an aqueous non-ionic polymer solution, has been found to be related to hydrogen bonding. DLS measurements performed on samples of copovidone at different temperatures show that an increase in temperature favours cluster formation whereas lower temperature leads to a shift toward a good solvent behaviour. According to classical Florry-Huggins theory, elevated temperatures lead to a decrease in the free energy of mixing, promoting homogenisation; however, in this case elevated temperatures promoted the opposite. Higher temperatures interrupt hydrogen bonding (necessary for good solvent behaviour) leading to higher relative cluster formation. This is depicted in **Figure 7.13**, in the context of a polymer solution with $\varphi_p \approx 0.0157$ (assuming negligible variation in the water density).

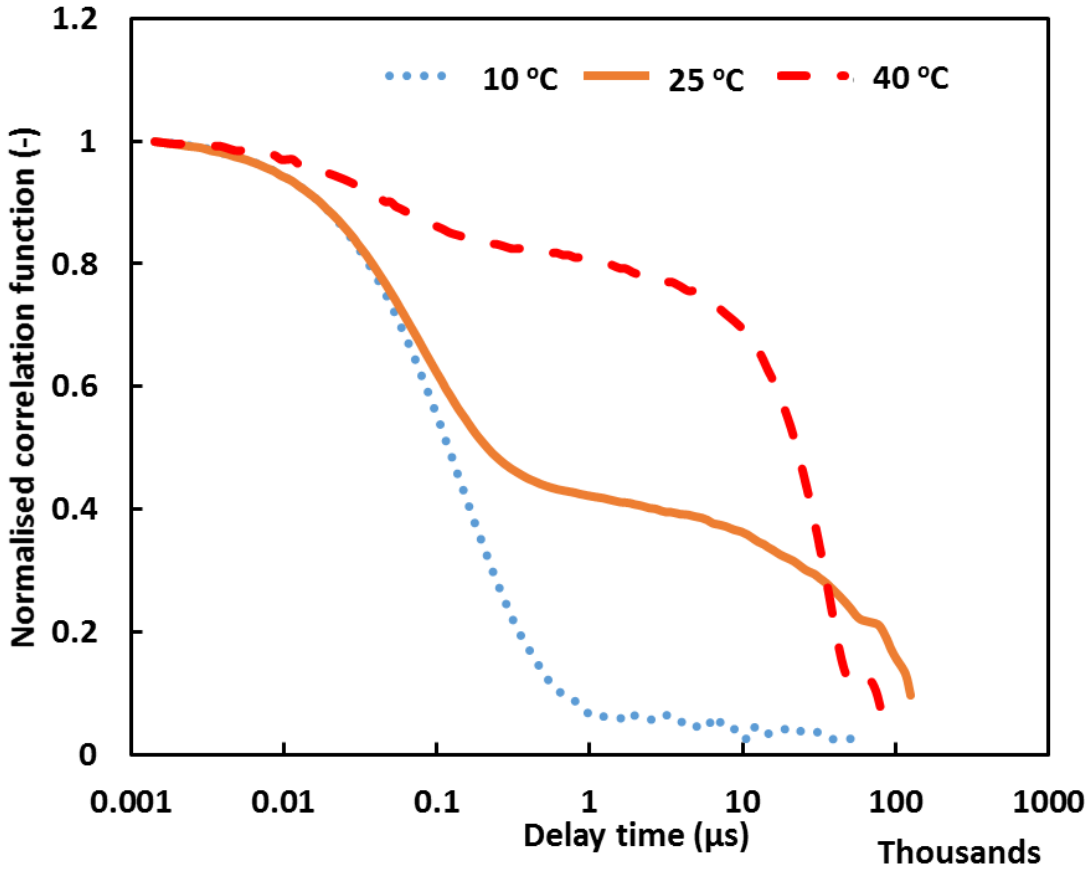


Figure 7.13: The correlograms obtained for a polymer solution with $\varphi_p = 0.0157$ at three different temperatures.

It is interesting that, even at the dilute region, the surface activity seems to be sufficient to cause a substantial improvement in wetting. Interestingly, the surface activity increases faster in the semi-dilute region, i.e. in the region where the relative abundance of polymer aggregates tends to decrease shifting to a more homogenised system. On the other hand, in the dilute and concentrated regions, where there is a large relative abundance of clusters, the surface activity increases slowly. This probably suggests that the aggregates do not tend to move towards the three phase contact line owing to the hydrophobic nature of the surface of carbamazepine, i.e. they can be viewed as micelles with a hydrophilic shell consisting of the polar functional groups of copovidone, and a hydrophobic core consisting of the aliphatic backbones. Thus, they do not contribute significantly to the change of the surface activity amd the improvement of

wettability. This phenomenon is manifested very clearly in **Figure 7.11 A**. As the contact angle measurements are getting in the concentrated region, one could observe that the values of cos(θ) are start forming a plateau, indicating that despite any decrease in the work of cohesion of the wetting fluid, wettability is not going to be improved. In the same context, the slope of the **Figure 7.11 B**, seems to become more negative in the concentrated region. Overall, it can be suggested that the wetting of carbamazepine by aqueous solutions of copovidone improves quite dramatically in the semi-dilute region, thanks to the migration of free polymers to the three phase contact line. However, in the concentrated region, where aggregation dominates this improvement in wettability slows down, owe to the lack of free polymers to migrate towards the three phase contact line.

7.5 Conclusions

This work utilised a number of well-established experimental approaches to investigate, for the first time, the anisotropic wettability of pharmaceutical materials by polymeric excipient solutions. The energetic surface anisotropy of p-monoclinic carbamazepine was studied thoroughly for the first time, as was the surface energy of aqueous copovidone solutions at different polymer loadings. It was shown that despite the fact that the surface energy anisotropy of p-monoclinic carbamazepine is not as profound as for other compounds, owing to the limited number of functional groups, its influence is still clear. Furthermore, this study verified the directionality of acid-base interactions and their sharp distinction from the van der Waals interactions, notably due to hydrogen bonding. Most importantly it provides a correlation between the aggregation in polymer solutions and wettability. It highlights that for the system under investigation the wettability of p-monoclinic carbamazepine by aqueous solutions of copovidone is dictated by the migration of polymers to the three phase contact line.

The findings from this chapter can have a direct impact on pharmaceutical process development; especially in the development of a framework for the mechanistic understanding

of processes, such as wet granulation, where capillarity and capillary forces are important. A more rational framework for the optimisation of the amount of binder required can be designed just with knowledge of the surface properties of the material of interest, significantly reducing the use of trial and error.

8. Interfacial phenomena in the dehydration of pharmaceutical channel hydrates

8.1 Introduction

Desolvation induced concomitant polymorphism, i.e. the appearance of more than one anhydrous polymorphs upon desolvation is not uncommon in molecular crystals.[319-320] Since desolvation is a process dictated by heat and mass transfer phenomena, it can be speculated that changes in the desolvation conditions can influence the ratio of the polymorphs obtained. Over the years, different experimental and computational approaches have been proposed to quantify mixtures of polymorphs. Owe to the nature of the techniques employed, the mass fraction of the different polymorphs could be obtained. However, as discussed on the introductory Chapters 2 and 3, it is not uncommon, in pharmaceutical process development and in drug product development, mass fractions to be of little importance. In systems with a relatively large surface area to volume ratio, interfacial phenomena dominate over bulk phenomena and the quantity of importance is the ratio of the surface areas of the two polymorphs. In this context the aim of this chapter is to provide some insights on the mechanisms underpinning desolvation induced concomitant polymorphism and then to showcase how IGC can be employed to quantify the surface area ratio of two polymorphs, proving the hypothesised mechanism of desolvation induced concomitant polymorphism.[45] This application of IGC for the determination of the mixture components is grounded on the findings of Chapter 4 on the "Importance of Packing on IGC measurements". In this direction, a brief introduction to the concept of polymorphism would be presented at the beginning of the chapter. This will be followed by an introduction to carbamazepine, the model drug used in this study. Then the results of the work will be presented, followed by some conclusions. Considering that polymorphism of the APIs is crucial for the formulation of drug products, the findings of this study directly target major challenges of pharmaceutical industry.

8.2 Polymorphism

The term polymorphism refers to the ability of the constituent components (ranging from ions to molecules) of a crystal to arrange to more than one crystalline phases.[321] Even though the effects of polymorphism have been observed for centuries, the discovery of polymorphism is attributed to Professor Eilhard Mitscherlich. In 1826,[322] Professor Mitscherlich presented evidences for the existence of two forms of sulphur; one monoclinic and one rhombic. On that time, he was not aware of any other crystalline forms of sulphur and thus he called the phenomenon dimorphism (meaning two forms, in Greek).

From a thermodynamic perspective, a compound existing in crystalline form, at fixed values of temperature and pressure, can only exhibit a single stable polymorph. Any other polymorph of this compound observed under these specified conditions is considered metastable. Thus, there would always exist a thermodynamic driving force pushing it to convert to the most stable polymorphic form. This thermodynamic driving force is described by means of the Gibbs free energy of the polymorph and is calculated according to the infamous equation (where the subscript i denotes a polymorph):

$$G_i = H_i - TS_i \qquad \text{Eq. 8.1}$$

where G_i is the Gibbs free energy, H_i and S_i are the enthalpy and the entropy of the system at the given conditions and T is the temperature. In **Figure 8.1** a qualitative plot, summarising the behaviour of the three components with temperature, is shown. One should notice that even though pressure affects the thermodynamics of the system, it importance is omitted for pharmaceutical crystals. This is because, the range of pressures used in pharmaceutical process development, does not influence the thermodynamics of the crystals significantly.

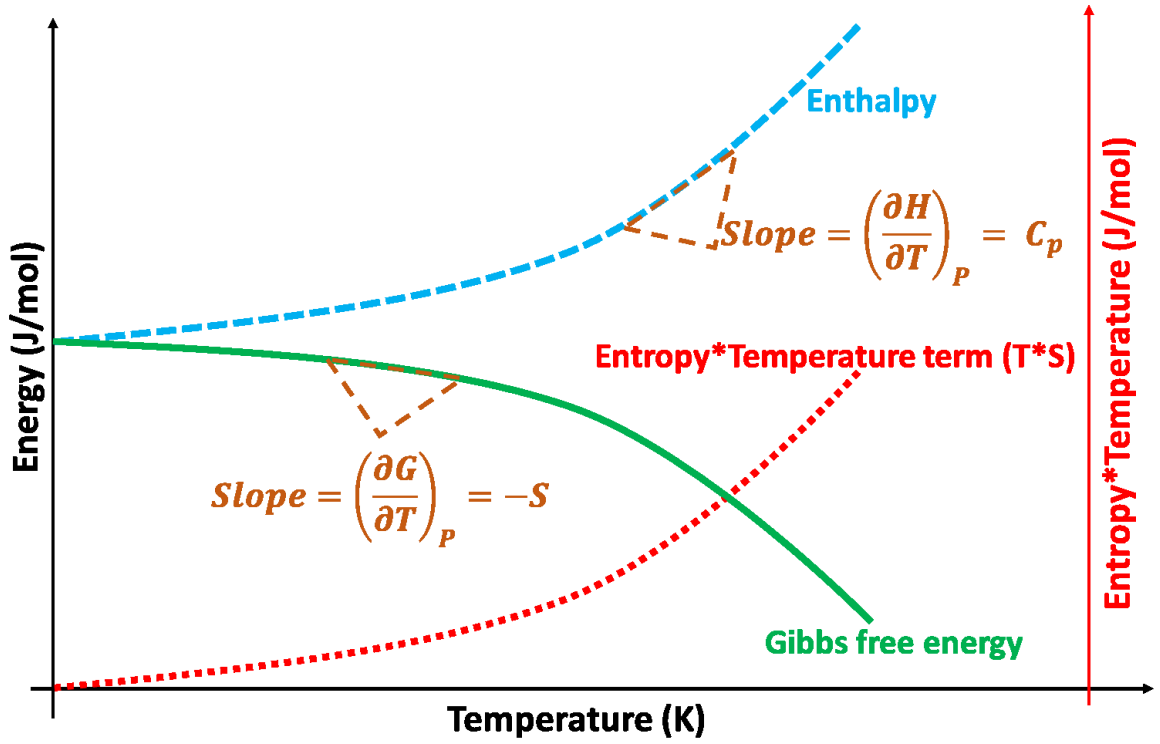


Figure 8.1: Schematic representation of the variation of enthalpy, entropy and Gibbs free energy of a crystalline material, with temperature. The slope of the enthalpy curve provides the magnitude of the heat capacity of the material at the specified temperature. Similarly, the slope in the Gibbs free energy curve can be used to calculate the entropy of the system.[323]

For the case of a compound exhibiting two (or more) polymorphs, as the temperature changes, a shift in the relative magnitude of the value of the Gibbs free energy the two polymorphs can occur, leading to a change in the order of stability. This phenomenon is called enantiotropic transition. On the other hand, some solids exhibit only a single stable polymorph and thus they are called monotropic. In this case all the other polymorphs appear as metastable. These phenomena are illustrated in **Figure 8.2**.

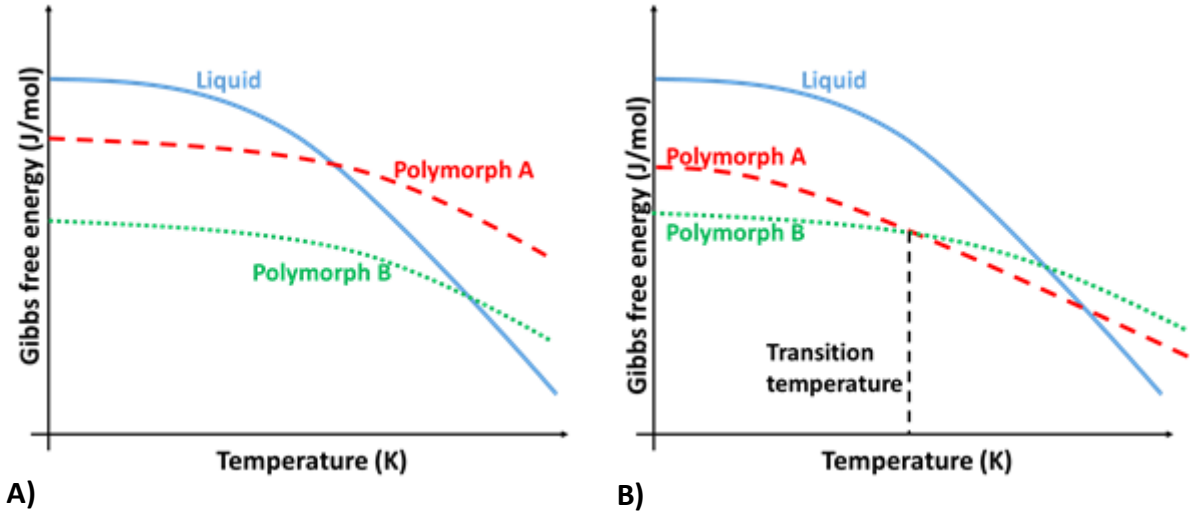


Figure 8.2: Schematics describing, qualitatively the thermodynamics of A) a monotropic and B) an enantiotropic system.[323]

During crystallisation in solution, certain polymorphs can appear at conditions where they are considered metastable, owe to the kinetic nature of the process. This behaviour is attributed to the Ostwald rule of stages, as it has been addressed in Section 3.3.2.

In cases where more than one polymorphs emerge, the quantification of the resulting polymorphs was found to be a quite intriguing problem, subjected to various limitations associated with the techniques used and the nature of the material under examination. As expected, different polymorphs exhibit different surface energy. Thus, IGC measurements have been proposed as a tool enabling the quantification of the polymorphs present in a sample. The findings of Chapter 4, suggest that FD-IGC measurements, combined with *in silico* studies, can quantify mixtures of polymorphs, on the basis of their relative surface area. In other words a framework exists enabling the quantification of the relative surface area occupied by each polymorph. This metric is particularly useful if the mixture of the two polymorphs is going to be processed via process operations involving the formation of interfaces.

8.2.1 The importance of polymorphism in drug product development

The solubility of a compound, in a specific solvent, should always be determined, via dissolution experiments (crystallisation experiments are not reliable as contamination can

inhibit crystal growth in a supersaturated solution), on the basis of the most stable polymorph. It is not uncommon to encounter situations were an investigator is claiming, erroneously, that metastable polymorphs result to higher solubility.[324-329] This statement is not accurate, as metastable polymorphs can result to higher apparent solubility, but as the solution does not have some sort of memory, it cannot result to an increase in actual solubility.

The concept of increase in apparent solubility is very neatly explained in terms of the classical Flory-Huggins theory. During the dissolution of a compound X, exhibiting two polymporphs, in a solvent Y at constant temperature, four types of intermolecular interactions exist. The Y-Y interactions between the solvent molecules, the $X_{(solute)}$-Y interactions between the solvent and solute molecules in solution, the $X_{(solute)}$- $X_{(solute)}$ between molecules of the compound X in solution and the $X_{(solid)}$-Y interactions between the solvent molecules and the molecules of the solid. The intermolecular energy of the first three types of interactions is independent of the polymorphic form, whereas the fourth one is not. In fact, for the fourth case the intermolecular interactions are weaker for a metastable polymorph. Thus, the energetic penalty is smaller for the metastable phase, resulting in higher apparent solubility.

This concept of enhanced apparent solubility is particularly useful in drug product development. However, the tendency of the metastable polymorph to transform to a stable one, creates regulatory issues. As a matter of fact, the well known case of ritonavir recall upon the discovery of a metastable polymorph, highlights the importance of polymorphism selection in drug product development.[330] In this context, one should remember that the rate of transformation of a metastable polymorph to a stable one is subjected to factors such as the storage temperature and humidity.

8.3 The case of carbamazepine dihydrate

Carbamazepine dihydrate, one of carbamazepine's solvates, is employed as the model compound in this work, aiming to investigate the mechanisms of dehydration induced

polymorphism. Carbamazepine is a quite interesting compound exhibiting plethora of anhydrous forms and solvates. Until recently, four anhydrous forms were known, namely the trigonal, the c-monoclinic, the triclinic and the p-monoclinic.[284] An amorphous phase has also been isolated.[331-332] The stability trend of the amorphous forms at ambient conditions is summarised in **Figure 8.3**. Recently, a metastable catemeric polymorph has been isolated using templating. Anhydrous carbamazepine was found to exhibit enantiotropic behaviour at around 90 °C,[327] with the anhydrous triclinic polymorph becoming the most stable form, instead of the p-monoclinic one.

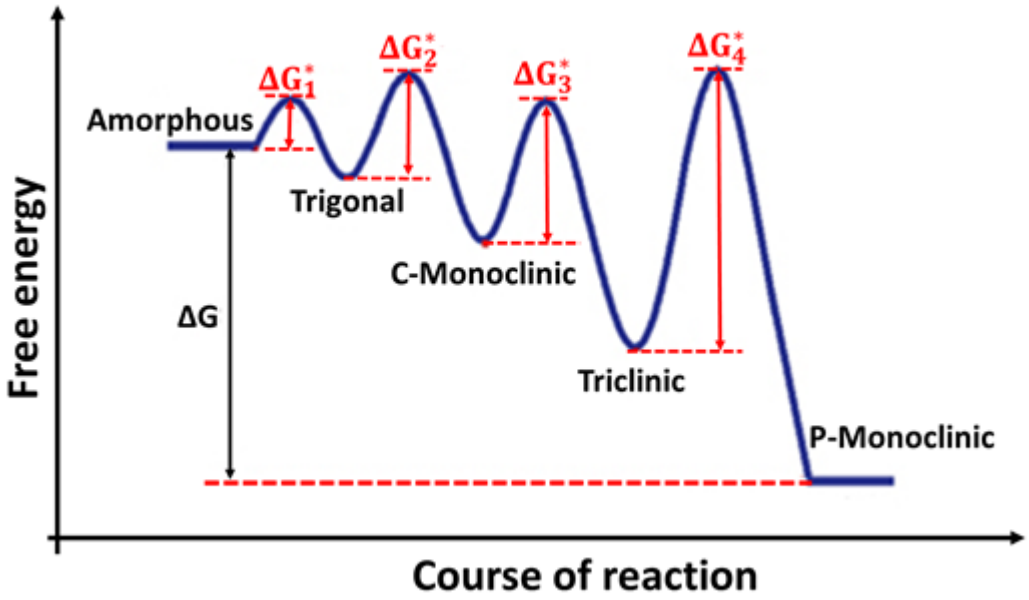


Figure 8.3: Schematic showing the thermodynamic stability of the four main anhydrous polymorphs of carbamazepine at ambient conditions.

Carbamazepine dihydrate, one of carbamazepine's numerous solvates,[36, 333-335] crystallises in the presence of water.[336] It is a channel hydrate and the water channels are aligned parallel to the (h00) and (0k0) crystallographic planes, as shown in **Figure 8.4**. Structural analysis of the crystal packing shows that there is a system of alternating weakly and strongly attached planes, parallel to the (0k0) crystallographic plane. This is a consequence of the

hydrogen bond network associated with the channel hydrates, giving rise to a stronger attraction compared with the attractions associated with the dispersive interactions. Carbamazepine dihydrate usually crystallises to acicular shaped crystals or elongated plates. Depending on the crystallisation conditions, the crystals may create agglomerates.

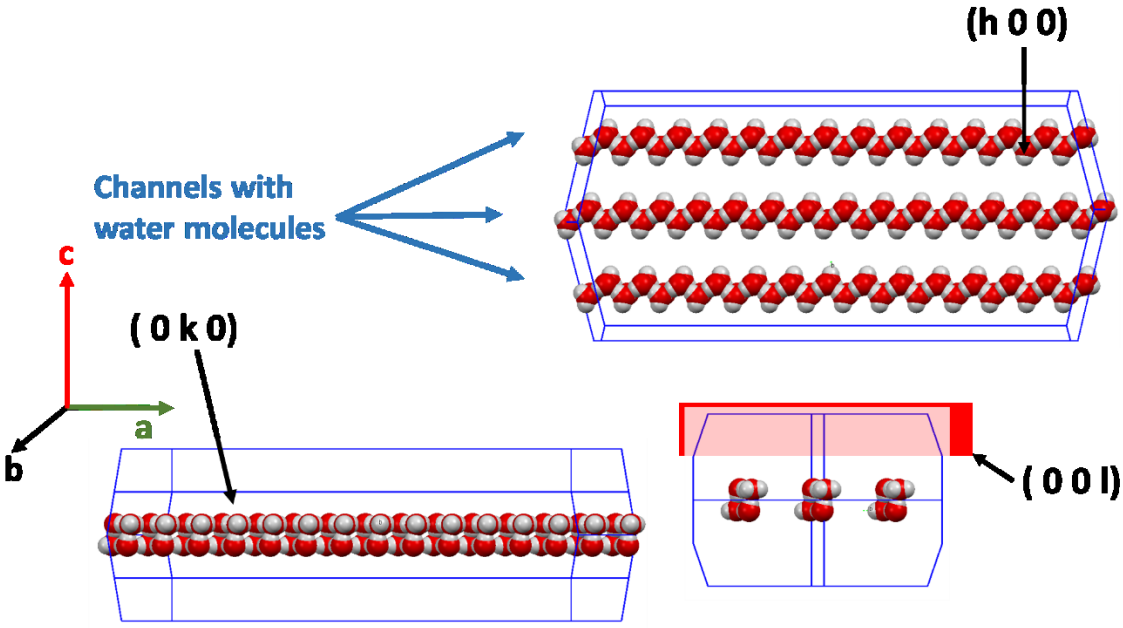


Figure 8.4: BFDH morphology of carbamazepine dihydrate showing the water channels and having the major crystallographic planes.

Desolvation studies on carbamazepine's solvates, showed that the plethora of polymorphic forms is associated with complexities on dehydration thermodynamics.[48, 50, 337] Interesting findings have been reported for the dehydration of carbamazepine dihydrate at mild temperatures in the presence of different types of vapours. The key findings of these studies are summarised in **Figure 8.5**. A very intriguing observation, is that as the molecular mobility provided during dehydration increases, a more stable anhydrous polymorphic form is obtained. This observation suggests that the dehydration induced polymorphism is governed in a great extent by the Ostwald rule of stages. This observation suggests the presence of an amorphous intermediate during dehydration the fate of which, in other words how fast will crystallise and

towards what polymorph, is governed by the molecular mobility. In addition, structural changes, such as whiskers and cracks, have been observed to accompany dehydration. It has been speculated that the cracks act as sites of preferential nucleation for certain metastable polymorphs. Thus, their presence may be associated with dehydration induced polymorphism.

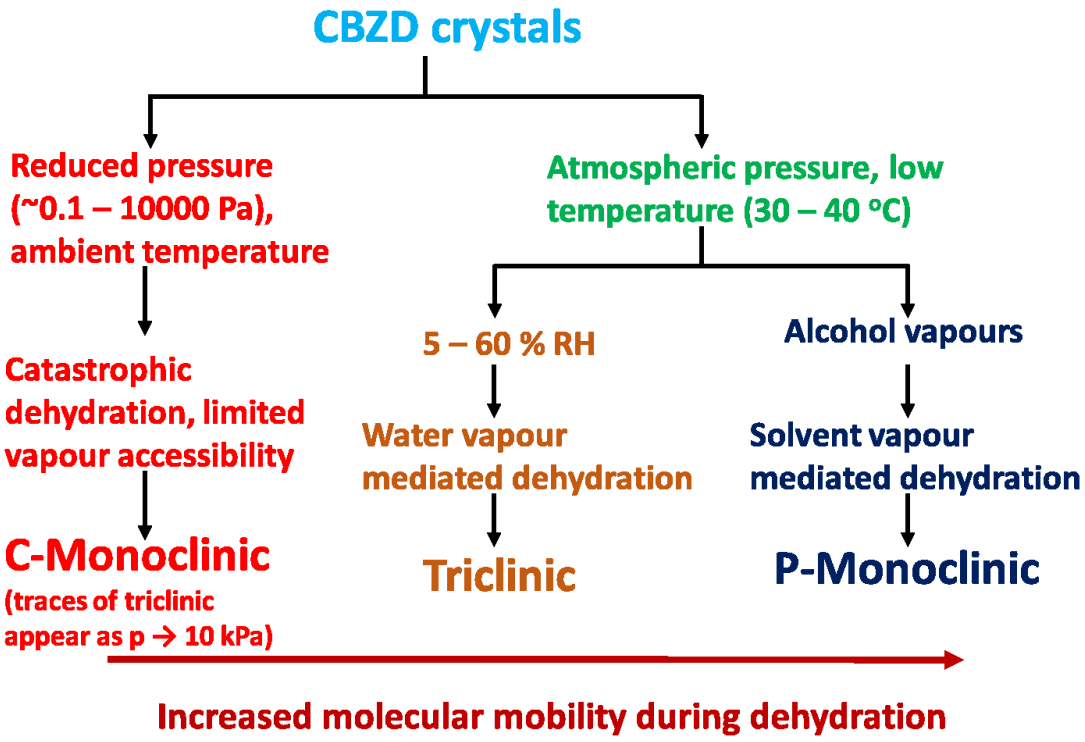


Figure 8.5: Schematic summarising the anhydrous polymorphic outcomes obtained, by other investigators, via experiments at mild temperatures.

However, the crystals investigated in those studies all have similar crystal habits, as they are produced from similar methods (cooling crystallisation). In this work, different crystallisation approaches are exploited to produce, among others, prismatic crystals of carbamazepine dihydrate with size ranging from ~10μm to ~1cm. Needle shaped crystals will be studied as well. The main hypothesis is that the changes achieved with various crystallisation conditions in features, such as crystal size, crystal habit and number of defects, can potentially influence dehydration induced polymorphism.

8.4 Experimental methodology

8.4.1 Materials used

Anhydrous carbamazepine was purchased from Apollo Scientific, Stockport, UK and all the solvents used (both for recrystallisation and IGC measurements) were purchased from VWR, Radnor, PA, USA.

8.4.2 Crystallisation and characterisation of macroscopic crystals of carbamazepine dihydrate via a bioinspired method

As it was shown in Chapters 5 and 7, macroscopic crystals are quite versatile as they enable the study of the intrinsic properties of the crystal, not scaling with size. For the purposes of this work, macroscopic crystals could shade light in the dehydration mechanisms of carbamazepine dihydrate.

For the growth of the macroscopic crystal of p-monoclinic carbamazepine used in Chapters 5 and 7, solvent evaporation was used. Those crystals were containing only one component, carbamazepine. However, carbamazepine dihydrate contains both water and carbamazepine molecules. Aqueous solutions have been used for the crystallisation of α-lactose monohydrate (containing both lactose and water), however it should be mentioned that α-lactose monohydrate is a sugar, readily soluble in water. On the other hand, carbamazepine is sparingly soluble in water. Thus, the option of following the same strategy, for macroscopic single crystal growth, as in the case of α-lactose monohydrate, is not viable.

The use of mixtures of solvents, containing water and a water miscible organic solvent, does not offer an alternative pathway either. In order for the macroscopic crystal of carbamazepine dihydrate to be stable in a mixture of water with ethanol or methanol, two alcohols used industrially for the crystallisation of carbamazepine dihydrate, the mixture should contain at least 30 % and 40 % per volume water respectively. In the presence of such a large amount of water, the solubility of carbamazepine drops significantly, thus the growth of macroscopic crystals will be unpractical.

Carbamazepine dihydrate usually crystallises in needle shaped crystals. This kind of elongated crystals are not suitable neither for use as seeds, for macroscopic single crystal growth, nor for extensive studies. As mentioned in Chapter 3, sodium taurocholate[238] has been used for the crystallisation of carbamazepine dihydrate with a more compact shape. Nevertheless, the crystals obtained where in the sub-millimetre scale, unsuitable for use in macroscopic single crystal growth. Scaling up that process would require the use of vast amounts of surfactant, increasing the possibility of excessive contamination of the crystal.

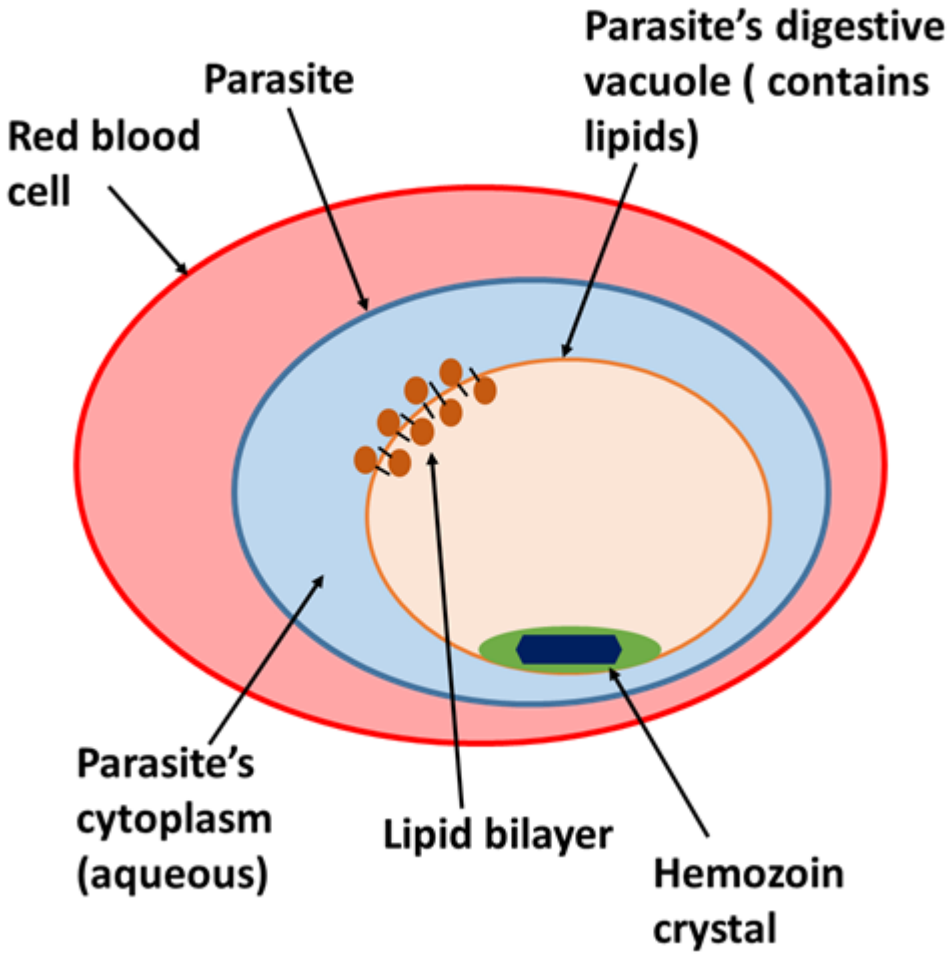


Figure 8.6: Schematic showing the crystallisation of hemozoin crystals, by a malaria parasite, inside a red blood cell.

The work on the crystallisation of hemozoin crystals by malaria parasites offers a pathway for the development of a bioinspired strategy for the growth of prismatic macroscopic

single crystals of carbamazepine dihydrate.[338] Malaria parasites attack and reside in red blood cells. The hematin, existing in red blood cells, is toxic for the parasites. Thus, the parasites tend to crystallise hematin to hemozoin, in their digestive vacuole, a lipid rich organelle, as a mean for detoxification.[199, 203] The schematic in **Figure 8.6** depicts the mechanism employed by a parasite residing in a red blood cell to crystallise hemozoin crystals.[202]

A number of elaborate studies suggest that the hemozoin crystals nucleate on the phospholipid membrane of the digestive vacuole. Hematin and other components required for the crystal growth of hemozoin, are synthesised in the, mainly aqueous, cytoplasm. From there, they are transported to the digestive vacuole, via means of mechanisms that they are not clear yet. Thanks to this continuous flow of material, the supersaturation in the digestive vacuole is sustained, enabling the growth of hemozoin crystals. A two-phase bioinspired solution, comprising of an aqueous and an organic phase, has been employed, enabling the growth of relatively (for a protein) large crystals. However, in that case, contrary to what happens in the digestive vacuole, hemozoin crystals were seeded at the interface between the two faces.

In Chapter 3, a thorough discussion was performed on the influence of additives in the crystallisation of small molecules used in solid oral dosage forms. A brief mention is made on the importance of macromolecular structures in biomineralisation. Nevertheless, the crystallisation of hemozoin in malaria parasites highlights the importance of lipids, which are amphiphilic molecules, in biological crystallisation.

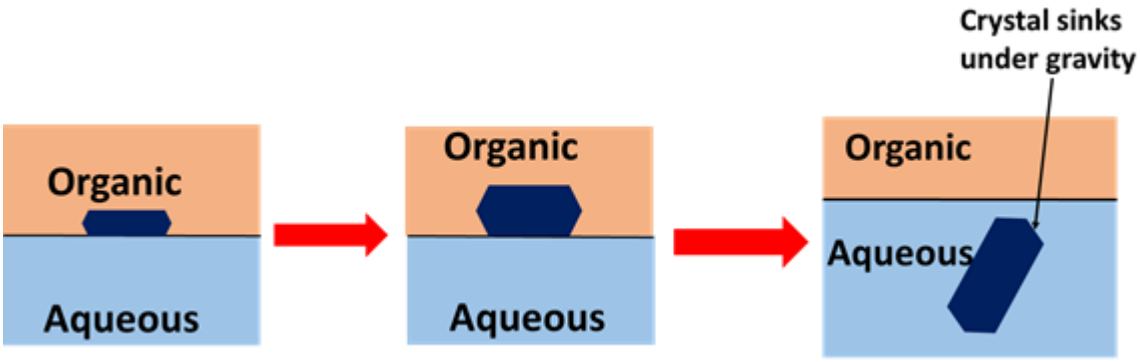


Figure 8.7: Schematic showing the growth of a crystal in the bioinspired crystal growth system developed.

To reproduce this system a two phase liquid-liquid system, comprising of a water rich and an organic solvent rich phase was proposed, as the one shown in **Figure 8.7**. Cooling crystallisation was performed in order to obtain nucleation at the interface between the two liquids. For the experiment to be successful, the organic solvent should be slightly miscible to water and lighter than water. In addition, carbamazepine should have a higher solubility in it rather than in water. Literature findings suggest that light alcohols, such as methanol and ethanol, in the absence of stirring, lead to the crystallisation of needle shaped crystals. In fact, as the system was shifting from methanol to ethanol, the crystals were becoming more needle shaped. This was attributed to the fact that the activity of water in the system was becoming less profound. First principle calculations for the water activity in a three component system comprising of carbamazepine, water and either ethanol or methanol, do not exist in literature. However, the water activity for a water – methanol system, at 25 ^{o}C, comprising of 60 % v/v methanol and 40 % v/v water was found to be, based on single component UNIFAC[339] calculations, 3.419 and the methanol activity was determined to be 0.613. In a similar system, containing ethanol, instead of methanol, the numbers calculated were 1.295 and 1.256 respectively. These numbers appear to provide a simple mechanistic explanation. The water activity is a measure on how strongly the water molecules interact, relative to their standard

state. Thus, one can make an over simplistic argument, which nevertheless it does not necessary deviate from reality, that if in the binary system the activity of the water is very high, this may be reflected, in the ternary system containing carbamazepine. This is not unreasonable, as from simple molecular intuition, one should see, that, probably, the water molecules have stronger affinity to interact with alcohol molecules, rather than with carbamazepine molecules. Thus, the high affinity of water molecules towards methanol molecules, limits their interactions with the crystal. On the other hand, as the water activity in ethanol is lower, it may indicate that more water molecules have the potential to interact with the hydrogen bond network of the carbamazepine dihydrate, facilitating the appearance of long needles. Inarguably, stirring also has an effect. However, for the case of ethanol, even for stirring rates higher than those reported in this study, the author did not observe prismatic shaped crystals.

For the purposes of this study, it was decided to use a heavier alcohol, butanol, so to compare it with lighter alcohols and two ketones, namely butanone and cyclohexanone. The two ketones were chosen as they satisfy the criteria set in the previous paragraph. In addition, it was hypothesised that interesting comparisons could be made between butanone and butanol, as they have the same carbon chain length but different functional group. The solubility of water in these organic solvents was found in literature. The activity of water and organic solvent in saturated, with water, binary solutions of the aforementioned organic solvents was calculated via UNIFAC method as follow: for water saturated butanol solution the activity of water is 0.593 and butanol activity is 0.768, for water saturated butanone solution the activity of water is 0.828 and the activity of butanone is 1.03, finally, for water saturated cyclohexanone solution the activity of water is 4.52 and the activity of cyclohexanone is 0.966.

So, for the experiment, 100 mL of the organic solvent were stirred, under reflux, with 150 mL of deionised water. As the two liquids are partially miscible, an emulsion was formed. Then anhydrous p-monoclinic carbamazepine was added and left overnight to dissolve. In most

of the experiments about 7 g of material were used. The emulsion was left for 24 hours to separate in two liquid phases and then a negative temperature gradient of 1 °C per day was applied on the system. After, a few days the first crystals appear in the interface between the two liquid phases; the upper phase was containing the organic solvent and some water and the bottom phase was mainly aqueous. The crystals were growing, at the interface as the temperature was decreasing; surface tension forces were sufficient to keep them on the interface. Some of the crystals grew quite big and under the effect of gravity they sank in the aqueous phase, overcoming the effects of surface forces. There, the concentration of carbamazepine was low and the growth halted. When the system reached 5 °C, the experiment stopped and the crystals were harvested and washed. Owe to the long duration of the experiments, it was not possible to perform detailed studies on the thermodynamics and kinetics of crystallisation.

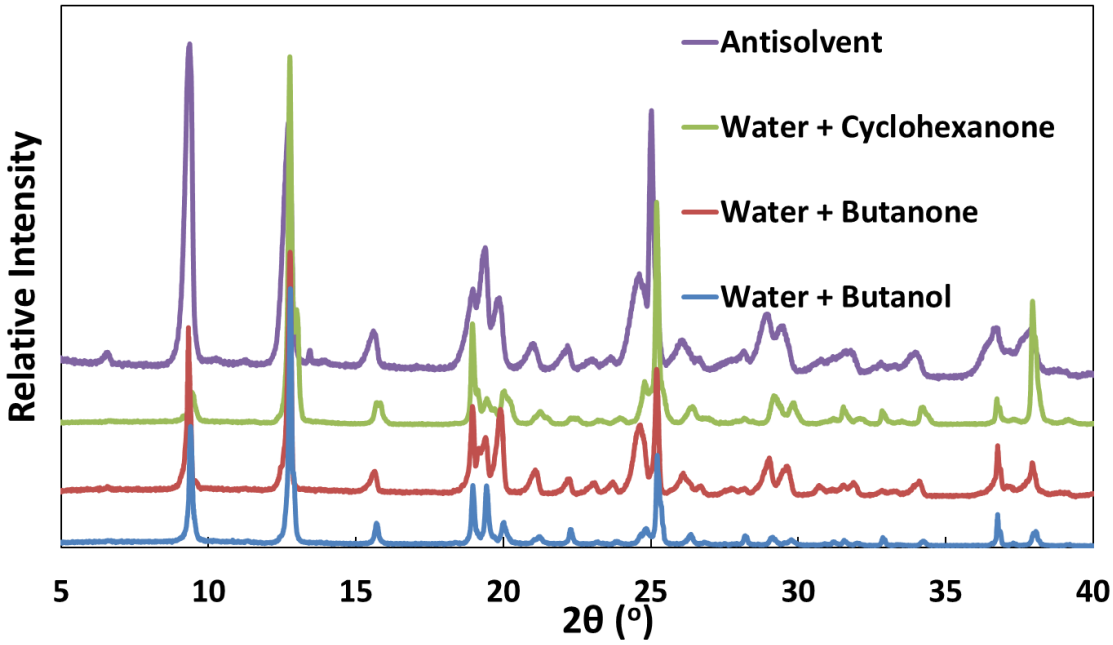


Figure 8.8: XRPD spectra for the crystals obtained from the bioinspired crystallisation system, verifying that the crystals are indeed carbamazepine dihydrate. The spectrum from material obtained via antisolvent crystallisation is used for comparison.

The nucleation and the growth were taking place on the organic side of the interface. The carbamazepine molecules required for crystal growth were provided by the organic phase. The water dissolved in the organic phase was sufficient to keep the carbamazepine dihydrate crystals stable and prevent their transformation to anhydrous, irrespectively of the organic solvent used. This is illustrated in the XRPD plots obtained from the crystals harvested from systems containing different solvents (carbamazepine dihydrate obtained via antisolvent crystallisation is used as the standard for comparison). As water molecules were incorporated in the crystal lattice the amount of water dissolved in the organic phase was decreasing. The aqueous phase was then acting as a sink providing water molecules to replace the crystallised water molecules. The transport of water molecules was taking place by means of simple diffusion. A concentration gradient from the water rich aqueous phase to the water poor organic phase was facilitating diffusion.

8.4.3 Producing carbamazepine dihydrate crystals with different aspect ratios

The following protocols were used to produce crystals with different crystal habits (the protocol described for the crystallisation of macroscopic carbamazepine dihydrate is termed Protocol 1):

Protocol 2: 0.05 g/mL of anhydrous carbamazepine (as received) were dissolved under heating in an ethanol-water (60:40 %v/v) mixture. Then the mixture was left to cool down slowly in quiescent. The solution was filtered out and the crystals were washed and then left to dry.

Protocol 3: 0.1 g/mL of anhydrous carbamazepine (as received) were dissolved under heating in a methanol-water (50:50 %v/v) mixture. Then the mixture was left to cool down for 12 hours without stirring. The solution was filtered out and the crystals were washed and then left to dry.

Protocol 4: 0.1 g/mL of anhydrous carbamazepine (as received) were dissolved under heating in a methanol-water (60:40 %v/v) mixture. Then the mixture was left to cool down for 12 hours

under stirring (500 rpm). The solution was filtered out and the crystals were washed and then left to dry.

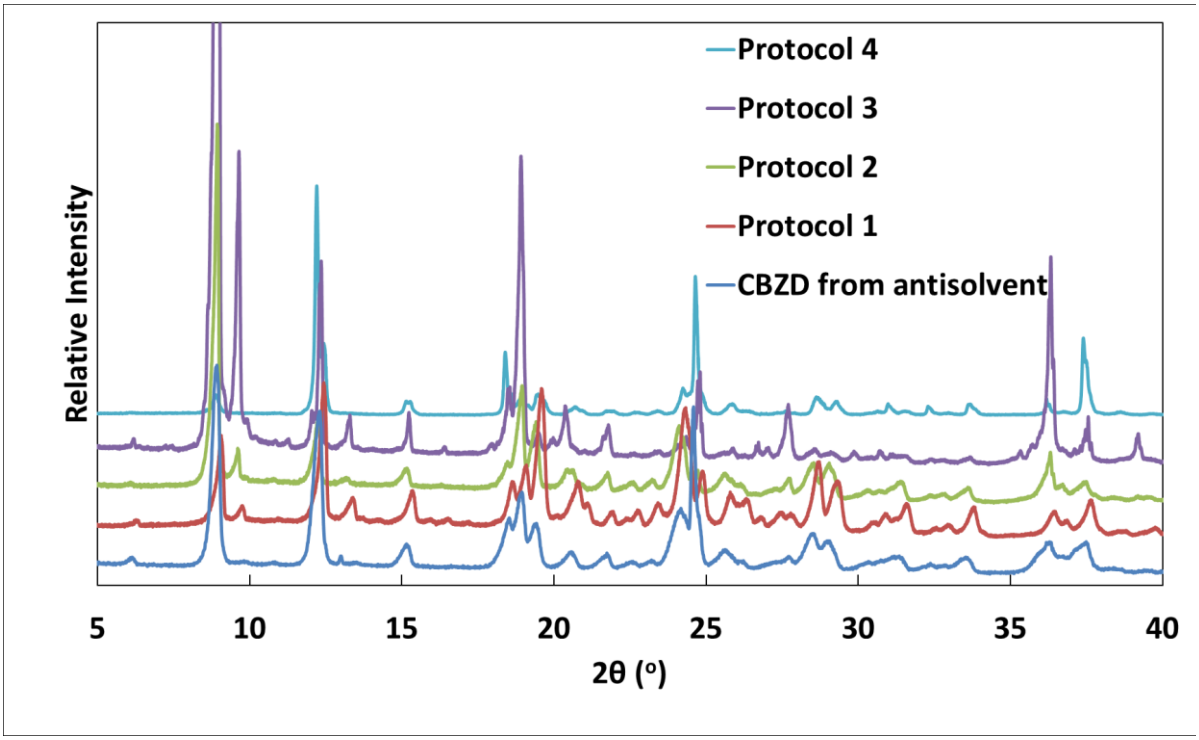


Figure 8.9: XRD spectra of the crystals obtained from the four different protocols compared with carbamazepine dihydrate obtained from antisolvent crystallisation.

XRPD analysis, shown in **Figure 8.9**, verifies that the crystals obtained from these protocols are carbamazepine dihydrate. Dehydration/weight loss experiments were, also, used to verify the water content in the crystals. Crystals from each protocol were placed in different petri dishes and their mass was determined. Then they were put in an oven at 50 ^{o}C and they were left to dehydrate for 24 hours. Five samples were used for each protocol. The mass decrease after they were for crystals from protocols one to three about 13.1 ± 0.2 %. However, for particles from Protocol 4 a smaller change was reported 12.4 ± 0.3 %. This signifies that there is, probably, a trace amount of p-monoclinic carbamazepine crystallising owe to the effects of the Ostwald rule of stages.

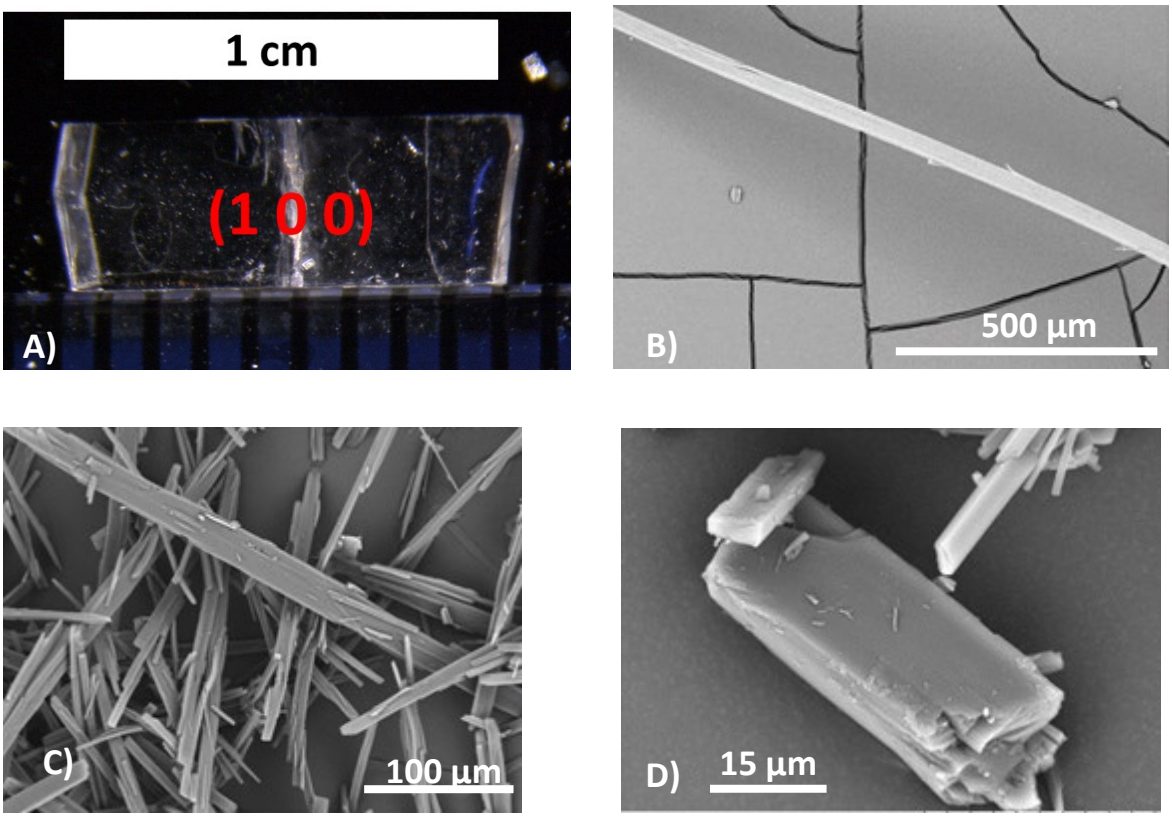


Figure 8.10: Microscopy images showing the examples of the crystals obtained from the four different protocols, A) stereoscopic image of a macroscopic crystal from Protocol 1, B) SEM image of a needle shaped crystal of carbamazepine dihydrate obtained from Protocol 2, C) SEM image of crystals of carbamazepine dihydrate obtained from Protocol 3 and D) SEM image of carbamazepine dihydrate crystals obtained from Protocol 4.

In **Figure 8.10**, images of the crystals obtained from the aforementioned protocols are presented. It can be seen that the characteristic size of the crystals increases from the first to the fourth protocol. The crystals from protocols one to three exhibit (100) as their major facet.

8.4.4 Structural changes associated with dehydration

8.4.4.1 Crack formation

Previous studies have revealed the appearance of various types of cracks on the surface of carbamazepine dihydrate, which have been associated with dehydration.[48, 340] Quite intriguingly, the most distinct cracks were appearing on the (100) facet and they were parallel to the water channels. In this work, macroscopic crystals, obtained from Protocol 1, were employed to investigate the surface cracks formed upon dehydration, using microscopy. The crystals were placed on a heating stage mounted on the optical microscope, enabling the on-line monitoring of crack formation. Results from this investigation are shown in **Figure 8.11**. From the images three major types of cracks can be reported. The first one includes the cracks parallel to the water channels. The other two types of cracks appear to have either a clockwise or an anticlockwise orientation with respect to the first type of already known cracks, but they appear on the same angle with respect to the primary type of cracks. The cracks of the first type have a much bigger gap space compared with the other two types.

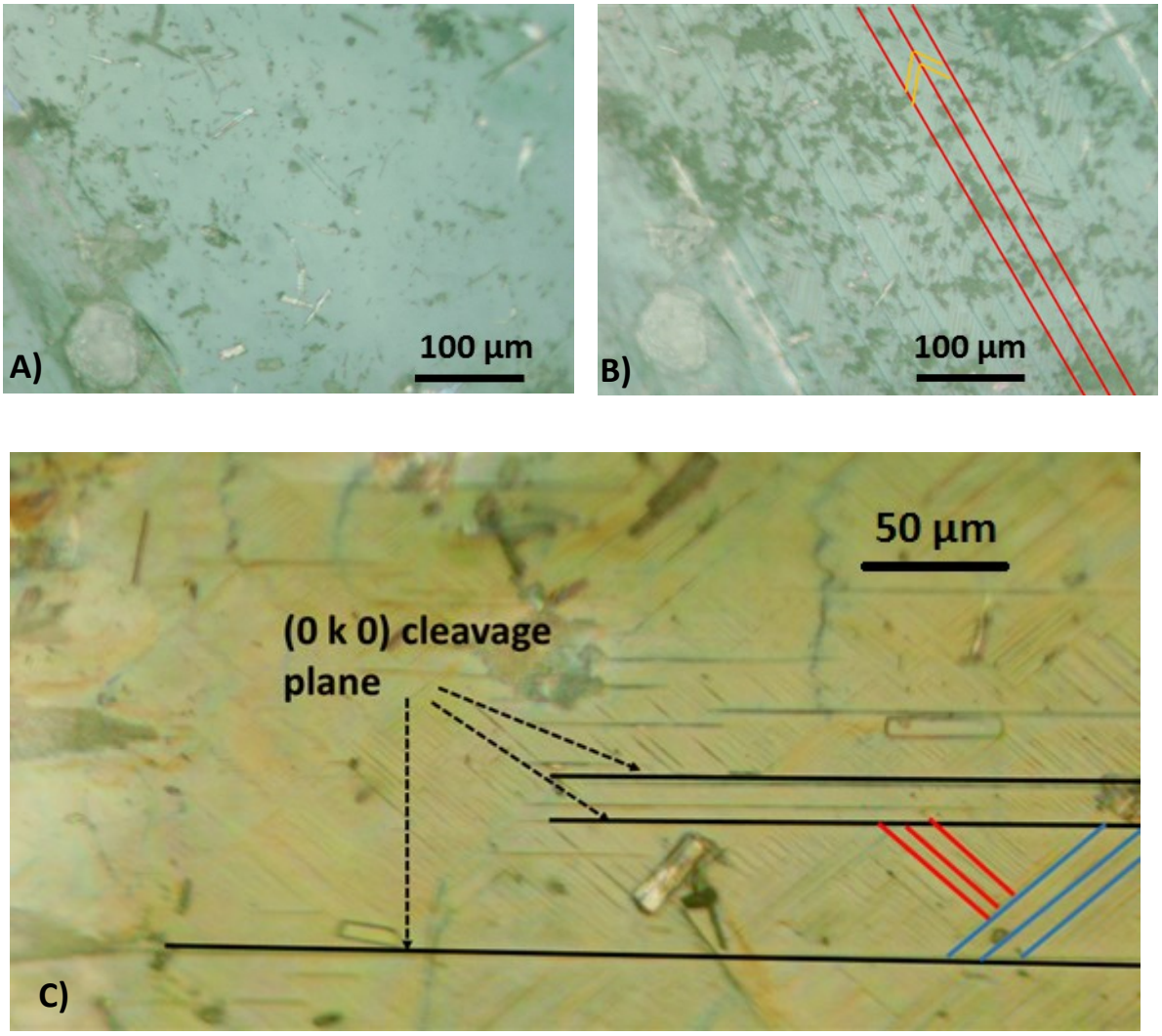


Figure 8.11: A) A sections of the (100) facet before start dehydration. B) The same section, when the three types of cracks have appeared. C) The (100) facet of another crystal exposed in dehydration showing the similar types of cracks.

Careful examination of SEM images reveals that these cracks also appear in crystals obtained from Protocols 2 and 3 as well. On the other hand, crystals from Protocol 4 do not exhibit this kind of well-ordered cracks, but they exhibit a random network of cracks as the one shown in **Figure 8.13**. These structural differences provide evidences for the different molecular mechanisms triggered upon dehydration.

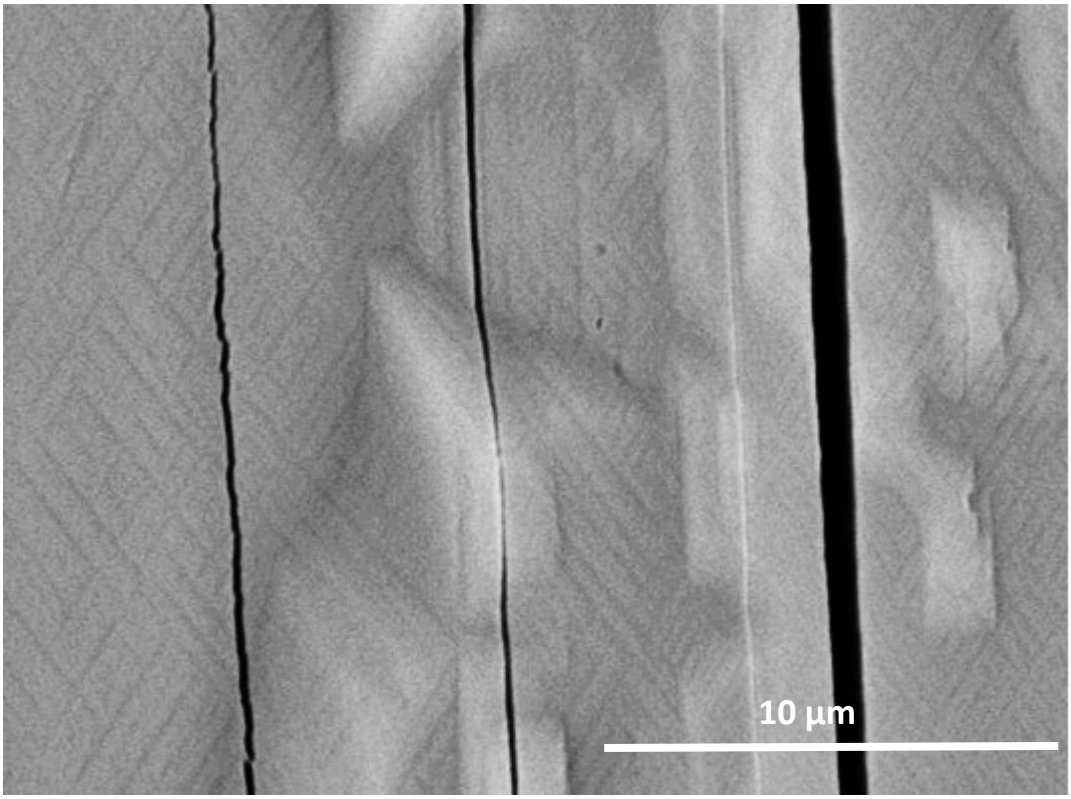


Figure 8.12: SEM image of the (100) facet of a carbamazepine dihydrate crystal, not exposed in dehydration, exhibiting the three types of cracks reported with optical microscope. The cracks are created from the vacuum induced dehydration. The image has been processed, post-capture, to enhance contrast.

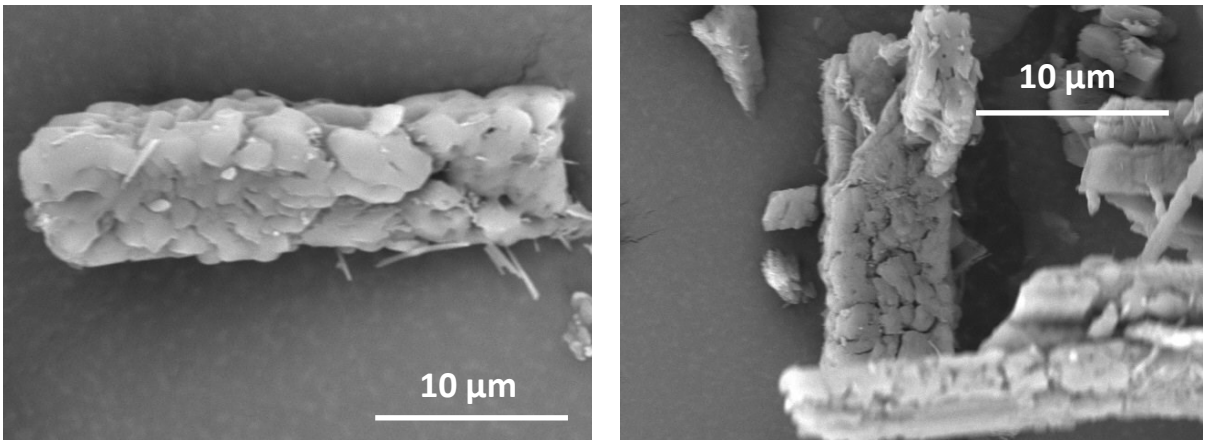


Figure 8.13: SEM images of crystals from Protocol 4 dehydrated at 90 °C.

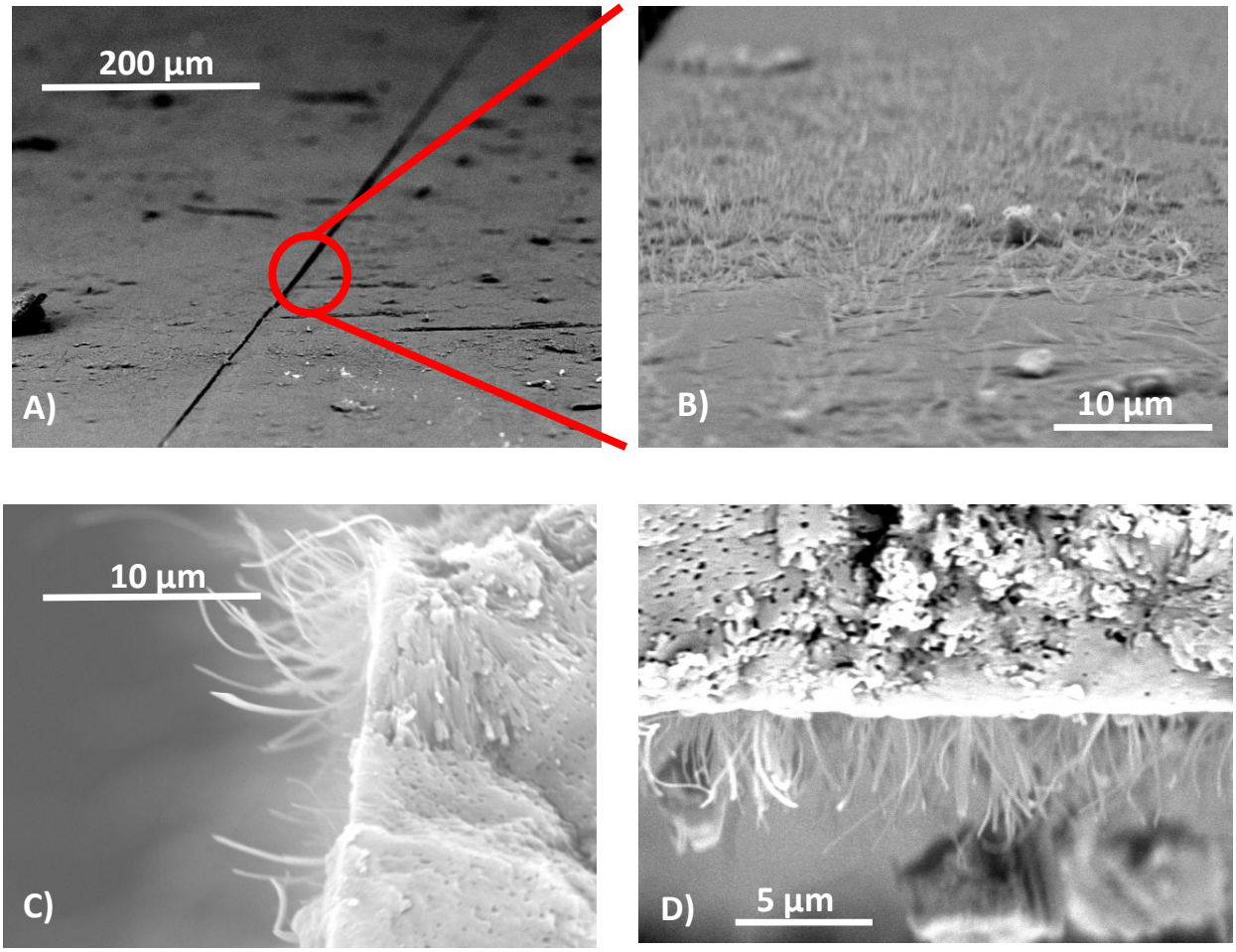


Figure 8.14: A) SEM image from the (100) facet of a crystal dehydrated partially at 50 ºC. B) A magnified image of the area marked with the red circle, showing the whiskers growing on the facet. C, D) Images showing whiskers growing on (020) facet.

Macroscopic cracks parallel to the water channels appear only on the surface of the (100) facet, whereas the rest of the facets do not exhibit such a feature. However, whiskers appear in all the facets, as can be seen in **Figure 8.14**. This is important, as it highlights that the cracks are not niches promoting the growth of whiskers.

Interestingly whiskers do not seem to appear on the surface of the crystals dehydrated partially under vacuum like the one shown in **Figure 8.15**. Similar results were obtained for crystals dehydrated fully under vacuum, as those shown in Figure. Furthermore, it is interesting

that it was possible to obtain fully dehydrated material, not exhibiting whisker growth, by vacuum dehydration.

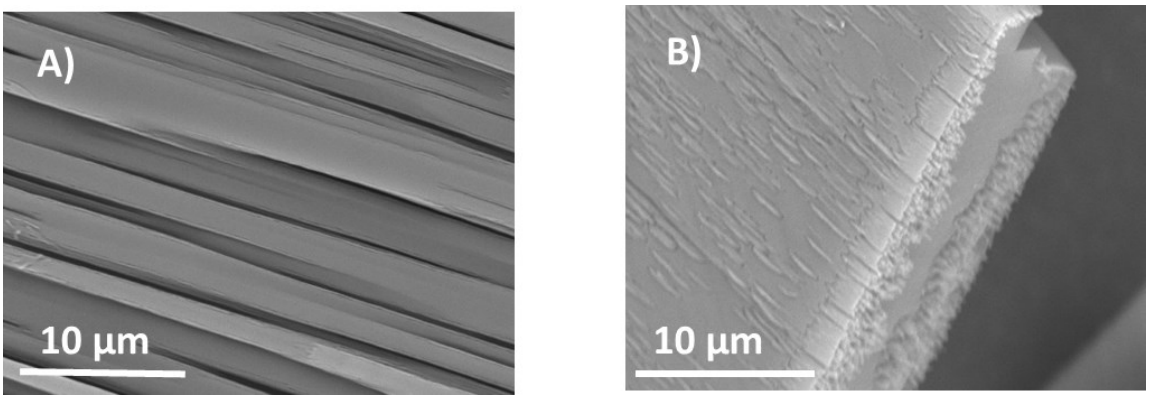


Figure 8.15: SEM images from crystals fully dehydrated under vacuum at ambient pressure, showing the absence of any long whiskers.

8.4.4.2 Cracks are formed inside the crystal

Macroscopic crystals were employed to study the mechanism determining the formation of the macroscopic cracks on the (100) facet, which are parallel to the water channels. The crystals were placed in an oven for a few minutes, to ensure that dehydration will be initiated, but the cracks would not have appeared on the surface. Then the crystals were sliced, with a razor blade. The cut was performed on a 90 ^{o} angle with respect to the channels (i.e. the cut and the channels are forming a right angle). The dissected crystals were then put vertically in the SEM. It is clearly depicted in the images of **Figure 8.16 A-D** that cracks appear in the centre of the crystal, propagating towards the surface. In **Figure 8.16 E-F**, the crystal was left to dehydrate extensively, before dissected and put under the SEM. In this case, the cracks have sufficient time to propagate throughout the volume of the crystal, creating this intriguing structure, of a particle comprising of slabs. The whiskers appear on the surface before the cracks manage to propagate up to the surface. Even though whiskers can grow from inside the cracks, no evidences exist suggesting any preference towards this.

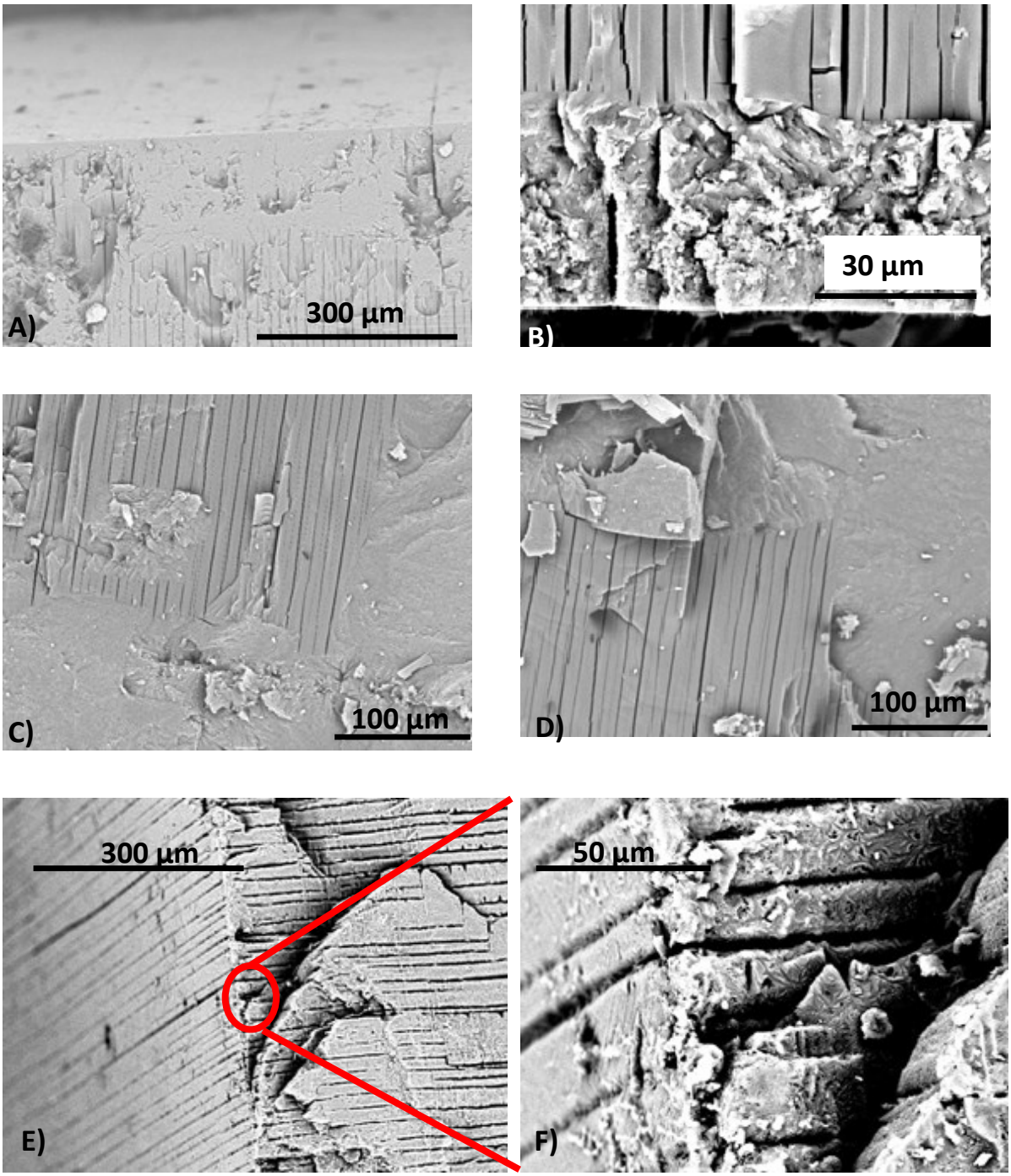


Figure 8.16: A-D) SEM images showing cracks that propagating from the core of the crystal towards the (100) facet. E) SEM image showing cracks propagated to the surface. F) Magnification of image (E).

8.4.4 Dehydration induced concomitant polymorphism

Crystals from all the protocols were exposed in three different dehydration conditions; 50, 70 and 90 ^{o}C under ambient pressure in a lab oven, for two hours. At this point, a few things should be mentioned regarding the selection of the dehydration temperatures. It was decided not to perform experiments at temperatures higher than 90 ^{o}C. Above this point the enantiotropic transition occurs and the material becomes very prone to sublimation as well. This will cause issues especially in cases where the anhydrous p-monoclinic carbamazepine is one of the resulting polymorphs. As the glass transition temperature of amorphous carbamazepine was determined to be around 56 ^{o}C,[341] it was decided to have one data point below this temperature. This is to check whether an abrupt change is observed above this temperature that can be attributed to an amorphous intermediate appearing during dehydration.

XRD and SEM were used to investigate the polymorphism of the dried material. The results for all the cases are summarised in **Figure 8.17** depicting the polymorphic outcome from each dehydration. Two distinct behaviours are observed. Crystals from protocols one, two and three dehydrate towards the metastable anhydrous triclinic polymorph when exposed at dehydration temperatures of 50 ^{o}C and 70 ^{o}C. The same crystals dehydrate towards a mixture of the anhydrous triclinic and p-monoclinic polymorphs when dehydrates at 90 ^{o}C. On the other hand, the crystals from Protocol 4, consistently dehydrate towards the mixture of triclinic and p-monoclinic polymorphs.

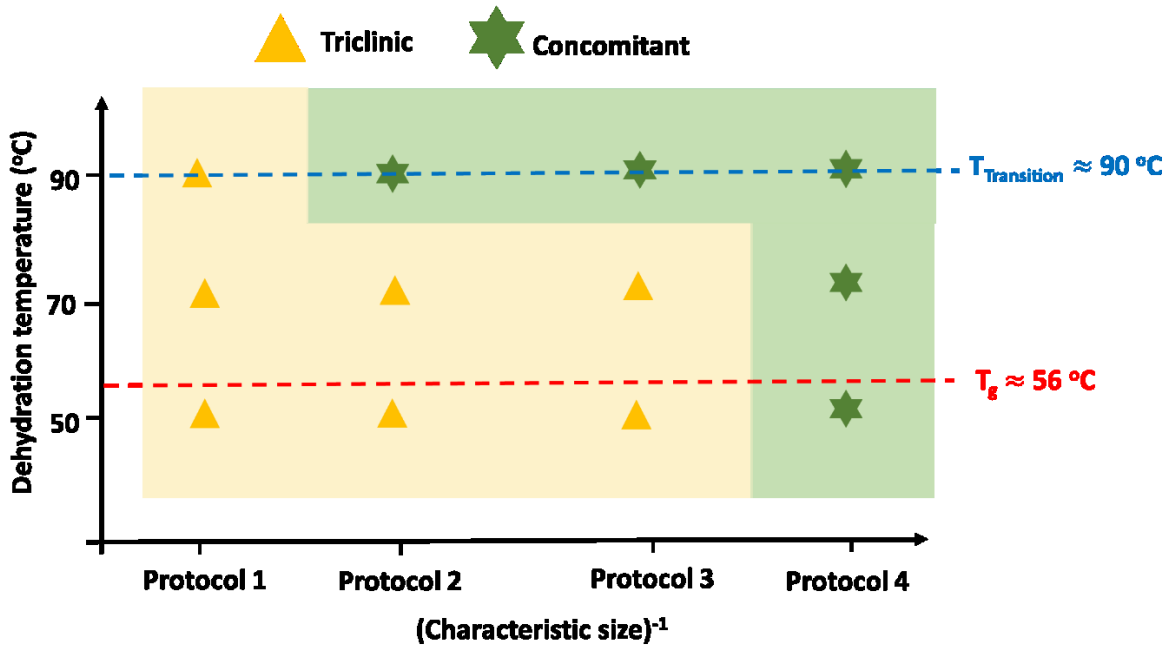


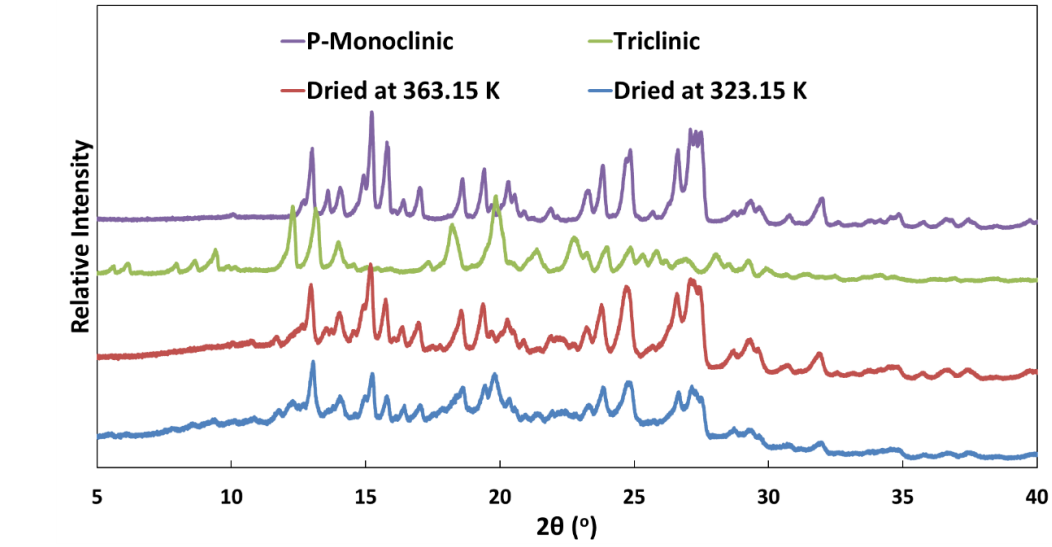
Figure 8.17: Schematic summarizing the polymorph obtained from the dehydration of crystals obtained from different protocols under different dehydration temperatures. The triangle corresponds to the situations where only triclinic polymorph was observed, whereas the star corresponds to the cases were a mixture of p-monoclinic and triclinic polymorphs was observed.

8.4.6 Polymorph quantification by means of IGC

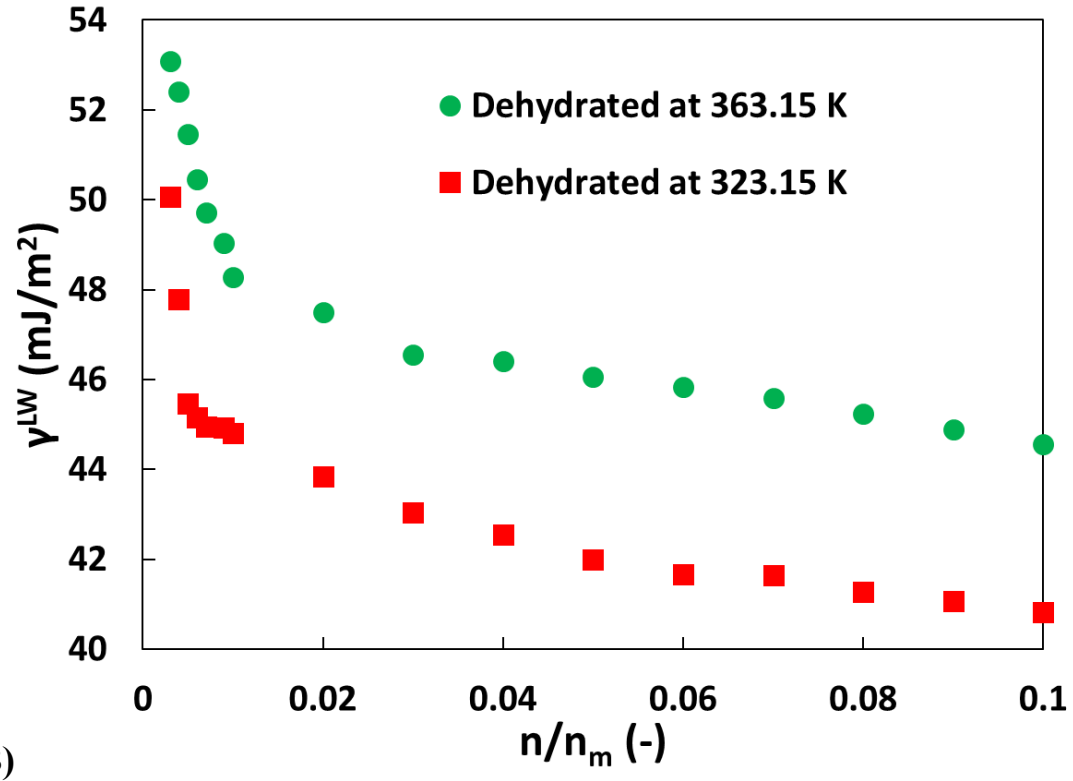
It has been shown that the possibility of dehydration induced concomitant polymorphism exists for certain cases. Quantification of the amount of p-monoclinic and triclinic polymorph occurring upon dehydration, by means of IGC, can provide a better understanding for the mechanisms determining concomitant polymorphism upon dehydration. The *in silico* tools extensively discussed in chapters four and five would be used.

The main surface energy sites exhibited by the anhydrous p-monoclinic carbamazepine are already known from Chapter 5. In this section, the surface energy map of the anhydrous triclinic carbamazepine will be measured, by means of IGC. Using the aforementioned *in silico* tool, the main surface energy sites exhibited by the anhydrous triclinic carbamazepine will be determined. Following that, *in silico* studies will be performed on the surface energy maps of

anhydrous samples obtained by dehydrating carbamazepine dihydrate, prepared by Protocol 4, at 50 ^{o}C and 90 ^{o}C; the samples have been found to exhibit dehydration induced concomitant polymorphism. These *in silico* investigations will enable the determination of the relative surface area each of the two polymorphs occupy.



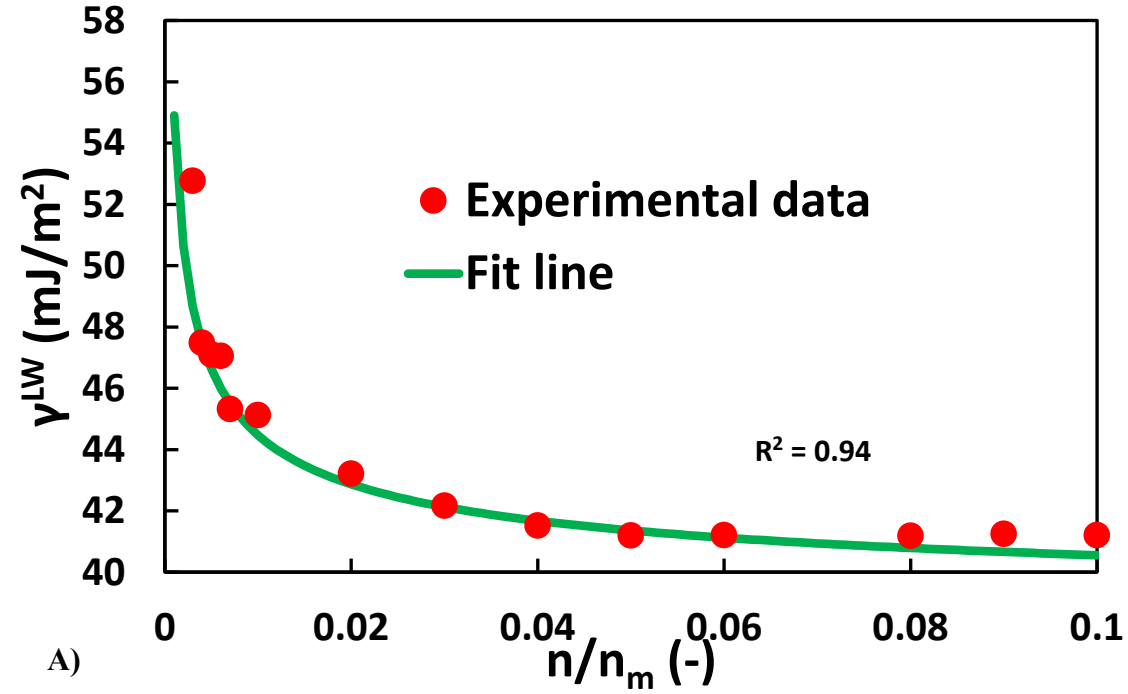
A)



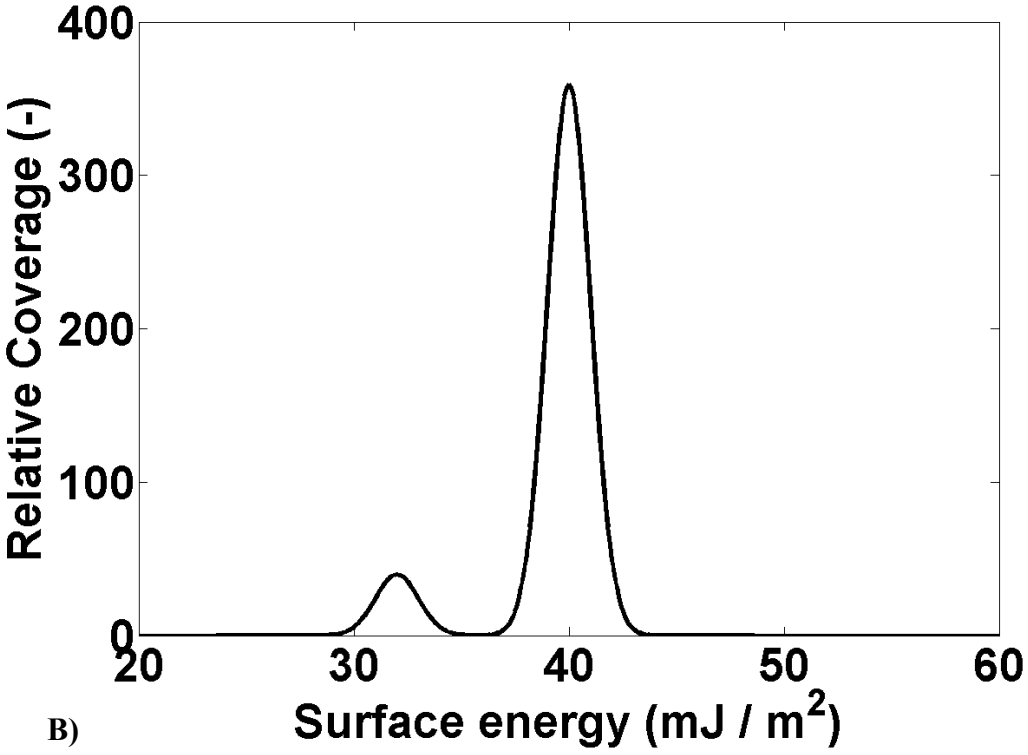
B)

Figure 8.18: A) The XRPD patterns obtained from the dehydration of carbamazepine dihydrate from Protocol 4 at two different temperatures compared with the patterns of two anhydrous carbamazepine polymorphs, the stable p-monoclinic and the metastable triclinic. B) The surface energy maps obtained from the IGC measurements on dehydrated crystals from Protocol 4; the dehydration temperatures are shown in the legend.

The surface energy of the anhydrous triclinic polymorph was measured, by means of IGC, using the same method described in Chapter 5. The results of the measurement are shown in **Figure 8.19 A**. The, the surface energy distribution was determined.[20] The fitting line on **Figure 8.19 A** indicates the calculated surface energy map, corresponding to the surface energy distribution shown in **Figure 8.19 B**. As can be seen very good agreement was achieved corresponding to an $R^2>0.9$. As can be seen from the surface energy distribution the sample exhibits two main surface energy sites, one at $\gamma^{LW}\approx32$ mJ/m^2 and another one at $\gamma^{LW}\approx 40$ mJ/m^2.



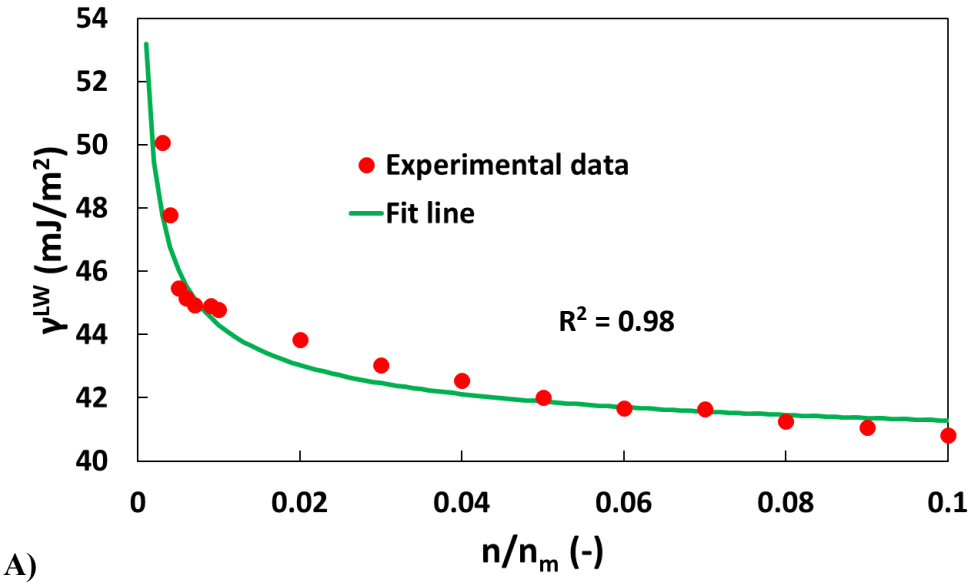
A)



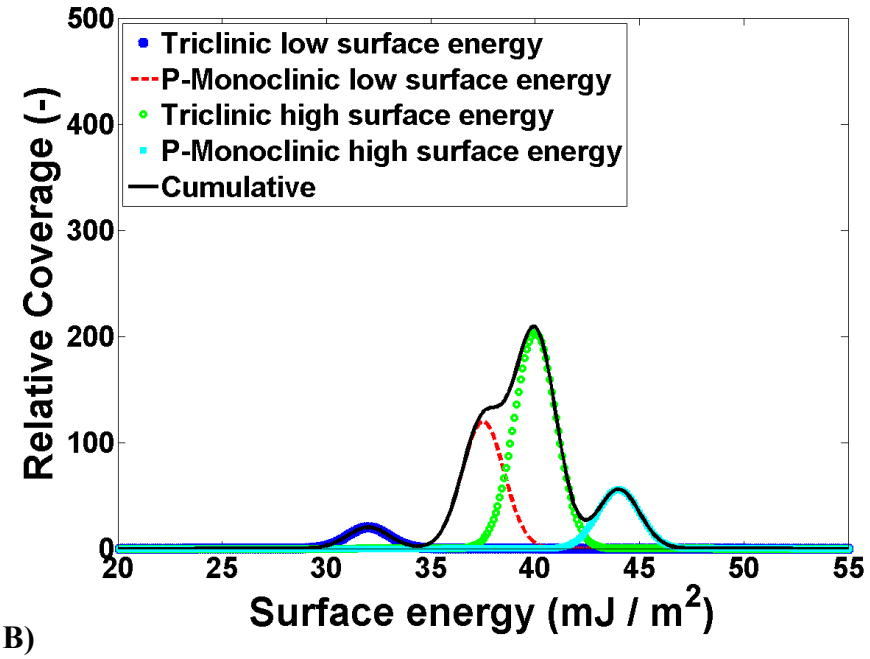
B)

Figure 8.19: A) The surface energy map obtained for anhydrous triclinic carbamazepine. B) The surface energy distribution corresponding to the surface energy map, showing two major peaks.

Using these results, the computational algorithm was tuned appropriately for the determination of the surface energy distributions of the dehydrated samples. It was assumed that the samples can exhibit only four surface energy sites, two attributed to the p-monoclininc anhydrous carbamazepine and two attributed to the anhydrous triclinic carbamazepine. The two distinct surface energy sites of the anhydrous triclinic carbamazepine have been calculated a few lines before and the corresponding values have been reported. The two sites of attributed to the p-monoclinic carbamazepine were assumed to have surface energies of $\gamma^{LW} \approx 37.5$ mJ/m^2 and $\gamma^{LW} \approx 44.2$ mJ/m^2 respectively. The latter corresponds to the surface energy of the (100) facet of the anhydrous p-monoclinic carbamazepine, whereas the former is an average value obtained from the surface energy values of the other sites identified in Chapter 5. It was decided not to use all the reported sites for the anhydrous p-monoclinic carbamazepine in order to reduce the computational burden and because some of them exhibit relatively similar values.

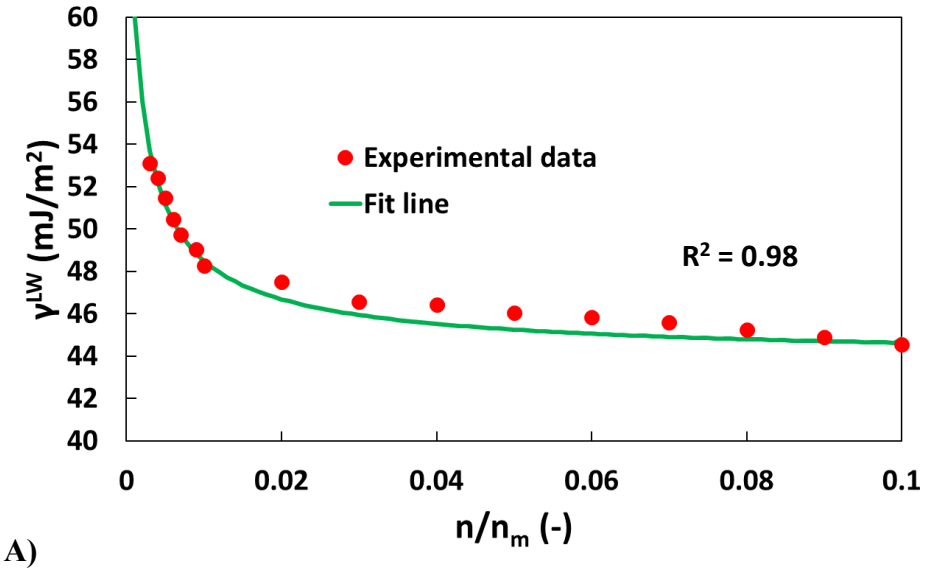


A)

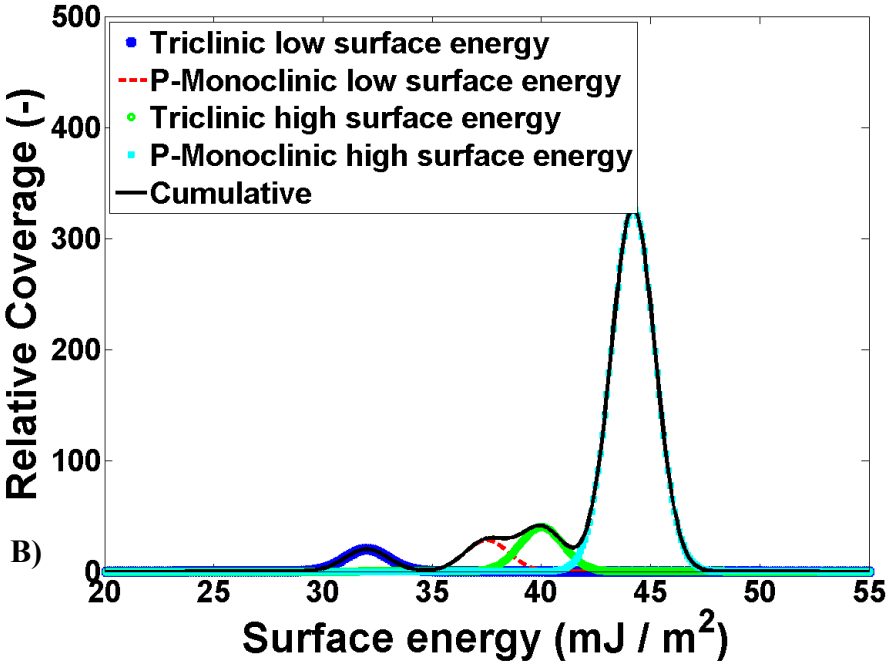


B)

Figure 8.20: A) The surface energy map obtained for material obtained from the dehydration of carbamazepine dihydrate crystals obtained from Protocol 4 at 50 ºC. B) The surface energy distribution corresponding to the surface energy map, showing the peaks corresponding to the anhydrous triclinic and p-monoclinic polymorphs (one low and one high surface energy site was assumed for each of the anhydrous polymorphs, in order to decrease the computational complexities).



A)



B)

Figure 8.21: A) The surface energy map obtained for material obtained from the dehydration of carbamazepine dihydrate crystals obtained from Protocol 4 at 90 °C. B) The surface energy distribution corresponding to the surface energy map, showing the peaks corresponding to the anhydrous triclinic and p-monoclinic polymorphs (one low and one high surface energy site was assumed for each of the anhydrous polymorphs, in order to decrease the computational complexities).

The results from the deconvoloution of the surface energy are shown in **Figures 8.20 B and 8.21 B**. The fit lines, in each figure, represent the lines obtained from the surface energy distributions corresponding to each of the samples. It can be seen that there is quite good agreement between the experimental and the modelled data. From the results it seems that for the material dehydrated 50 ^{o}C the peaks corresponding to the anhydrous metastable triclinic polymorph dominate, whereas the metastable anhydrous p-monoclinic polymorph dominates the sample obtained by dehydration at 90 ^{o}C.

As it has been mentioned, the material produced from Protol, is expected to contain some amount of the anhydrous p-monoclinic carbamazepine. Obviously, the amount of p-monoclinic carbamazepine identified by means of both XRPD and IGC is much higher, indicating that some of the dihydrate, dehydrates towards the anhydrous p-monoclinic polymorph. By carefully looking the XRPD peaks, one could notice that the peaks of the anhydrous triclinic polymorph are more profound for the material dehydrated at 50 ^{o}C, contrary to the material dehydrated at 90 ^{o}C. Here, it should be noticed that SEM imaging was used for polymorph identification and the presence of whiskers in crystals obtained by dehydration at 90 ^{o}C, were considered as indicative of the presence of the anhydrous triclinic polymorph.

8.5 Discussion

8.5.1 Crystallising macroscopic hydrates on an interface

This work establishes a bioinspired methodology for the growth of macroscopic single crystals. This methodology exploits the partial miscibility of water in certain organic solvent. The organic solvent is able to dissolve larger amounts of the anhydrous carbamazepine compared to water. The water activity in the organic phase of the system, for the organic solvents used in this study, seems to be sufficient to sustain the nucleation and growth of carbamazepine dihydrate. In his work on the crystallisation of hemozoin crystals by malaria parasites, Professor Peter Vekilov, proposes that the hemozoin nuclei is surrounded by

phospholipids in some sort of a droplet facilitating its growth.[202] It's not impossible to speculate that an analogous mechanism maybe true for the growth of macroscopic crystals of carbamazepine dihydrate via the methodology proposed here. In other words, a metastable droplet, formed at the interface between the two liquid phases may exist facilitating the nucleation and growth of carbamazepine dihydrate. However, the proposed system is very vibrations sensitive. Even slight vibrations, may distract the equilibrium at the interface between the two liquids, making the crystals to sink, prematurely, in the aqueous phase. Thus, it was not possible to use any optical monitoring systems to study the crystal growth methodology. Observations made from the walls of the glass jacketed vessel, where the growth was taking place, may support the claim for a droplet facilitated crystal growth mechanism. Nevertheless, without more thorough studies, no solid conclusions could be extracted.

The macroscopic crystals obtained do not show any polarity. In other words, the bottom and the top facets, the one looking towards the organic phase and the one looking towards the aqueous phase, are identical. This observation backs the argument made in section 8.4.2, on the "Crystallisation and characterisation of macroscopic crystals of carbamazepine dihydrate via a bioinspired method", that crystal growth takes place on the organic side of the liquid-liquid interface. In case that one of the facets was in contact with a different liquid compared to the other it was expected that it will exhibit different growth. This observation is in-line with the possibility of a droplet facilitated crystal growth mechanism.

Carbamazepine dihydrate crystals were obtained with all three organic solvents used in this study. This, combined with the observations of the previous paragraph, suggests that the activity of the water, dissolved in the organic phase, is sufficient to facilitate the nucleation and sustain the growth of carbamazepine dihydrate crystals. Considering that no seeding is performed, this means that for the given systems, with the given amount of dissolved anhydrous material, carbamazepine dihydrate is the single most stable form of carbamazepine. On the

ground of this argument, one could question why a two-phase system is required. Technically an organic solvent, such as cyclohexanone, saturated with water, could perform the same job. The answer to this is that the two liquids system proposed in this study, allows the crystal to grow on a liquid-liquid interface. On the other hand, for a system comprising of water saturated cyclohexanone, carbamazepine dihydrate crystals were going to grow on the walls of the crystallisation vessel, owe to the low supersaturation used. Crystals growing in such a way will have more defects and removing them from the walls of the vessel, by means of mechanical force, will damage them.

The growth of needle shaped carbamazepine dihydrate crystals is driven by the hydrogen bond network, associated with the water molecules in the channels. In literature, the vast majority of the studies dealing with carbamazepine dihydrate, use aqueous solutions of alcohols to crystallise it. The strong hydrogen bonding associated with these solvents is expected to facilitate the growth towards the direction of the hydrogen bond network. In the case of carbamazepine dihydrate, water molecules are an essential part of the crystal lattice. Thus, strong association with a particular facet, promotes the elongation of that facet, instead of inhibiting. In one sense, they do not compete with carbamazepine molecules, but they work synergistically. One should also notice, that carbamazepine molecule does not have strong hydrogen bonding functional groups. Thus, the growth of the carbamazepine dihydrate in any other direction other than the one facilitated by the hydrogen bond network is extremely unfavourable, as water molecules are key part of the crystal lattice.

For the case of the bioinspired crystal growth methodology, proposed in this chapter, only the carbamazepine dihydrate crystals obtained from cyclohexanone exhibit prismatic crystal habit, deviating from the acicular type of crystals obtained from the other three solvents (and generally from any other solvent combinations found in literature). In particular, the crystal habit becomes more prismatic as the solvent system shifts from butanol to butanone and then

to cyclohexanone. This trend can be explained qualitatively using the notions discussed in the previous paragraph, as well as the literature findings, on the influence of solvents in crystal growth, outlined in Chapter 3. The trend is in line with the trend of the activity of water in the binary solution of water and the organic solvent; water activity increases from butanol to butanone and then to cyclohexanone. As it has been speculated increased water activity suggests that the water molecules are strongly interacting with the organic solvent molecules. Thus, they exhibit less interactions with the growing crystal. This limits the driving force facilitating the elongation of carbamazepine dihydrate crystals via the hydrogen bond network. As mentioned before, the reader should keep in mind that crystallisation is taking place in a ternary system containing water, organic solvent and carbamazepine. Thus, the conclusions derived from the activity of water in binary solutions is just a qualitative speculation and they should not be used for the design of mechanistic models. The ability to manipulate the crystal habit by tuning the organic solvent used in this bioinspired system is a quite intriguing finding showing that crystal growth is taking place on the interface and inside the organic phase, whereas the aqueous phase act, mainly as a sink of water molecules.

Overall, the proposed methodology is a robust alternative for the growth of hydrates of poorly water soluble molecules. Traditionally, macroscopic crystals were grown via top seeded solution growth, as the one described in Chapter 7 and elsewhere in literature. However, this bioinspired method introduces a pathway for nucleating crystals directly on a liquid-liquid interface. Thus, all the issues associated with the accumulation of defects during top seeded solution growth or growth on the walls of a vessel, are removed. In this context, the applicability of this methodology could be expanded for the growth of large protein crystals were the small mechanical forces may jeopardise the crystals.

8.5.2 Dehydration induced concomitant polymorphism and quantification

The results obtained for dehydration induced polymorphism and presented in **Figure 8.17** are quite interesting. Crystals obtained from protocols one, two and three exhibit behaviour in line with the results found in literature. At dehydration temperatures of 50 and 70 ^{o}C, where the molecular mobility provided is low, the metastable anhydrous triclinic polymorph is obtained. Whereas at 90 ^{o}C, the molecular mobility is sufficient to enable some nucleation of the stable anhydrous p-monoclinic polymorph, leading to a mixture of two polymorphs.

On the other hand material from Protocol 4 seems to consistently dehydrate towards a mixture of the two polymorphs. Quantification performed via means of IGC shows that for the material dehydrated at 50 ^{o}C, the amount of the anhydrous triclinic polymorphs is less compared to the material obtained from dehydration at 90 ^{o}C. This observation agrees with the analysis conducted in the previous paragraph, having the concept of molecular mobility in its epicentre.

Nevertheless, the question remains why the material from Protocol 4 exhibits such peculiar behaviour. It has been proposed that this can be an indication of size dependent dehydration induced polymorphism.[342-343] However, for this argument to hold true, the particles obtained from all four protocols exhibit Biot (Bi) dimensionless numbers much smaller than one. Bi is a quantity determining the ration between conductive and convective heat transfer phenomena and it is calculated according to the formula:

$$Bi = \frac{hL^2}{k} \qquad \text{Eq. 8.2}$$

where h and k are the film heat transfer coefficient and thermal conductivity, respectively. The geometric parameter *L* is given by the ratio of the volume over the surface area of the particle. When the magnitude of $Bi \ll 1$ then the temperature gradients inside the body are negligible. For pharmaceutical crystals the magnitude of k takes values from 0.2 to 0.5 $W*m^{-1}*K^{-1}$. Similarly the magnitude of *h* was assumed to be around 10-50 $W*m^{-2}*K^{-1}$. The magnitude of

L varies significantly and estimates were performed using images obtained from optical microscopy and SEM.

Considering that the trace amount of p-monoclinic carbamazepine, in the batch produced by Protocol 4, it can be speculated that this anhydrous material, acts as template, driving the dehydration induced polymorphism towards the anhydrous p-monoclinic polymorph. The traces of p-monoclinic carbamazepine are engulfed in the crystals of carbamazepine dihydrate. As dehydration commences the temperature throughout the crystals is uniform, thanks to the very small Bi number. The carbamazepine dihydrate around the p-monoclinic carbamazepine core moves from dihydrate to amorphous and then to p-monoclinic very quickly. On the same time the material on the surface dehydrates moving to the amorphous intermediate phase. Owe to the lack of templating recrystallisation is not that fast. Depending on the molecular mobility provided the p-monoclinic carbamazepine phase grows from inside. The theoretical basis for this kind of glass to crystalline transitions has been described extensively in literature.[218, 344] The same templating phenomenon was not observed when samples of pure carbamazepine dihydrate obtained from protocols two and three were seeded with p-monoclinic carbamazepine obtained separately.

8.5.3 Structural changes during dehydration

Using macroscopic crystals, it was possible to prove that macroscopic ordered cracks, appearing on the (100) facet of carbamazepine dihydrate crystals upon exposure in dehydration conditions, are formed inside the crystal, propagating towards the surface. This feature is not commonly encountered in literature. In fact, in the majority of the studies, cracks nucleate on the surface of a material, propagating inside the material. However, in a paper published in 2013, discussing the dehydration kinetics of 5-nitrouracil hydrate, the possibility of cracks nucleating from inside the crystal has been proposed.[345] Nonetheless, in that case, the compound used was not a channel hydrate as carbamazepine dihydrate (although older studies

have erroneously proposed that 5-nitrouracil hydrate was indeed a channel hydrate). The aforementioned macroscopic cracks are accompanied by smaller cracks, as shown in **Figures 8.11 and 8.12**.

During the dehydration of a stoichiometric hydrate, water is removed in the form of vapours. So, as long as the hydrated material is exposed to conditions favouring dehydration, the water molecules would start to evaporate leaving their equilibrium positions inside the crystal lattice. Molecules close to the surface will eventually escape. However, water molecules deep inside the crystal will not. Even if they are removed from the channel, they will be trapped. The trapped water molecules will lead to the build-up of vapour pressure inside the crystal. On the same, the points from where water molecules have departed from are essentially points of preferential crack nucleation. The presence of points of crack nucleation, combined with the build-up of pressure, provides the necessary and sufficient conditions for the crack propagation. Owe to the presence of channels the (0k0) cleavage plane is much more prone to breakage. Thus, the cracks, stemming from inside the crystal, propagate towards the surface, via the route provided by the (0k0) cleavage plane. In previous studies, in the absence of channels providing a distinctively favourable cleavage plane, random cracks were appearing on the surface, as the water was trapped in unlinked voids inside the crystal lattice. It should be noticed that occasionally cracks perpendicular to the

The appearance of smaller cracks with a clockwise and counter clockwise orientation with respect to the macroscopic cracks (corresponding to other cleavage planes) can be viewed as an artefact of the removal of water molecules via less favourable routes and/or as a product of stress accumulation associated with the transition from the less dense dihydrate phase to the denser anhydrous forms. The clockwise or counterclockwise orientation of these cracks seems to be random. The respective angles formed, were measured, from SEM images like the one shown in **Figure 8.13**, and found to be relatively constant 111 ± 2^{o}, indicating secondary

preferential cleavage planes. The fact that the crystals dehydrating towards the anhydrous p-monoclinic polymorph exhibit a random network of cracks instead of well-defined cracks, indicates differences in the dehydration mechanisms, associated with the dehydration induced polymorphism scheme proposed a couple of paragraphs before.

8.5.4 Growth of whiskers

The growth of needle shaped structures (whiskers) on surfaces, as an artefact of a chemical reaction or some sort of thermal treatment, is a topic of active research, influencing numerous industries. In thin films industry, the appearance of whiskers on the surface of thin films has been a subject of interest, as it was found to be associated with reliability problems, arising, over time, in microelectronics. Different models have been proposed to explain this phenomenon, describing the appearance of whiskers as an artefact of a stress relief process. In a paper published in 1994, Tu, proposed a mechanism describing the formation of whiskers on the surface of bimetallic films.[346] The whiskers were growing owe to the chemical reaction at the interface between the two metals. The chemical potential of the reaction was used as a measure to calculate the rate of whisker growth. Surface defects were proposed to act as nucleation sites for the whisker growth, becoming a key point of the whole theory.

A number of studies, have been conducted to investigate the growth of hollow crystals on the surface of materials undergoing sublimation. The studies have been expanded to both metals[347] and organic materials.[348] In one of the most recent studies, dealing with the appearance of hollow crystals in organic crystals exposed in a temperature gradient, Martins suggested that the observed hollow crystals are the relics of dissipative structures, dissipating heat by the enhancement of convective mass transport.[349] The hollow structures grow following the temperature gradient, towards lower temperatures. The high aspect ratio structures provide sufficiently high surface area to volume ratio to facilitate heat dissipation. Sublimed material for the growth of these structures is provided by means of convection. There is a striking

difference, between the mechanisms determining the formation of whiskers in metals, and the mechanisms determining the formation of hollow crystals. The former refers to a close system, the behaviour of which could be explained in terms of relatively simple thermodynamic concepts. On the other hand sublimation, similarly to desolvation/dehydration, is an inherently non-equilibrium process. Thus, the appearance of the dissipative structures is a topic that should be discussed in the context set by the pioneer work of Professor Ilya Prigogine for which he received the Nobel Laureate in 1977.[350]

It is evident that for dehydration were the anhydrous p-monoclinic carbamazepine prevails, over the anhydrous triclinic polymorph, the presence of whiskers is small. Contrary for cases were the only triclinic polymorph is obtained, the whiskers are denser. Thus, it is not unreasonable, for the systems under consideration, to correlate whiskers with the anhydrous triclinic polymorph. As it was shown, whiskers do not appear in dehydration at ambient temperature under vacuum. This observation suggests that, indeed, whiskers in this case may be relics of heat dissipation mechanism.

However, in the cases reported in literature, the mass required for the growth of whiskers is provided by means of convection through sublimed material. However, the sublimation temperature of carbamazepine's polymorphs is higher than 90 ^{o}C, the highest dehydration temperature used in this study. Thus, it can be suggested that the material needed for the growth of the whiskers, is convectively transferred along with the water vapours. One should appreciate that during the dehydration, towards the anhydrous triclinic form, an amorphous phase is strongly present. The amorphous material has higher apparent solubility when compared with its crystalline counterparts. Thus, it can be more easily transported by means of convection.

8.6 Conclusions

This work exploits fundamental concepts of crystal engineering to explore aspects of dehydration. By employing different crystallisation approaches, it was possible to obtain carbamazepine dihydrate crystals with different sizes; ranging from a few microns to a few centimetres. The development of a bioinspired method enabling the growth of macroscopic hydrates of purely water-soluble molecules is a key milestone of this work. It is possible to tune crystal habit by manipulating the organic solvents used. Simple UNIFAC calculations seem to provide a useful toolbox for some qualitative predictions.

Macroscopic crystals were found to provide a versatile platform for the study of aspects of dehydration. In particular, they enable the investigation of crack formation associated with the dehydration of channel hydrates. For the first time it was shown that during the dehydration of channel hydrates, crack formation is happening inside the crystals and the cracks propagate to the surface. A mechanism describing the growth of whiskers was proposed as well. It is key to appreciate

This study shades light on the mechanisms of dehydration induced polymorphism. It highlights the importance of molecular mobility, provided during dehydration, on the determination of the polymorphic form of the anhydrous material obtained. This concept can be of crucial importance in the design of drying processes, enabling the isolation of stable polymorphs. The results presented reinforce the opinion that, upon the dehydration of carbamazepine dihydrate, an amorphous intermediate phase is formed, that quickly recrystallises.

IGC measurements, were used to verify some of the findings on dehydration induced concomitant polymorphism, showing the versatility of the tool, when it is combined with *in silico* tools. Nevertheless, the interpretation of the IGC data should be performed with great care. One should recall that the numbers obtained from the combination of IGC experiments

and *in silico* studies, correspond to the relative surface area of each of the polymorphs. An amount of the anhydrous triclinic polymorph is expected to be in the form of whiskers. Thus, the mass fraction of the anhydrous triclinic polymorph is expected to be smaller, owe to the large surface area to volume ratio of the whiskers.

9. Conclusions

9.1 General conclusions

The work conducted in this thesis can be roughly divided in four main parts. The first part comprises of Chapters 2 and 3. In these chapters, the reader is introduced to the fundamentals of interfacial phenomena and to their implications to pharmaceutical process development and drug product performance. The author does not claim that this is the first work dealing with this subject. Nevertheless, it is one of the few works, providing a holistic and critical overview of the most recent findings in the field. In this context, it contributes to the enhancement of the efforts towards the creation of a mechanistic framework, linking interactions at the molecular level to the macroscopic behaviour observed at the three main interfaces of pharmaceutical importance; namely the solid-solid, the solid-liquid, the solid-vapour and the liquid-liquid. Especially at the interfaces involving a solid surface, it is evident that all the efforts towards the development of robust predictive tools is limited owe to the lack of a framework explaining the facet specific properties of crystalline solids or the concept of particle anisotropy in general. In this context, the first two chapters of this work elucidate the sources of the anisotropy and the main bottlenecks faced by the community.

As the development of novel drug products requires a shift towards systems were the importance of interfacial phenomena becomes increasingly important, it is argued that there is a need for the development of techniques for the accurate probing of surface properties. IGC has emerged as a potentially ground-breaking technique for this scope. Nonetheless, despite its use by many industrial and academic organisations, it has not managed to be established as an accredited technique for regulatory purposes. In other words, filing of new drug products does not involve any parameters that can be measured with IGC. It is argued that this can be associated with the lack of consistency observed between measurements on the same material by different groups. This cannot, necessarily, be attributed to the instrument per se; it can be

associated with factors such as different material history and contamination. However, the results of this work highlight that, unfortunately, severe deficiencies exist, explaining, in part, the lack of confidence by regulatory bodies towards IGC. In this context, the second part of this thesis, covering the Chapters 4 to 6 aims to deliver solutions to some of the issues associated with good experimental practice in different types of measurements with IGC.

In Chapter 4, the influence of silanised glass wool and packing structure is discussed. The results suggest that the silanised glass wool can potentially have an impact on the quality of the measurements. Using a combination of IGC data and in silico experiments, it was possible to create a map describing the effect of silanised glass wool on the measurement of the surface energy different materials. The proposed map can be used as a rule of thumb for the selection of the optimum amount of silanised glass wool. For materials with $\gamma^{LW} < 35$ mJ/m^2, the effects of silanised glass wool can be significant even if its relative amount is small. Owe to the highly non-linear nature of heterogeneous adsorption, it was not possible to create a map fitting all the possible scenaria. The authors encourage researchers to engage in the use of in silico studies with the aid of the tools developed in previous study and expanded in this one. In the second part of Chapter 3, a combination of experimental and in silico studies were used again to show that for the case of powder mixtures, the IGC measurements are not influenced. Different types of packing were examined verifying that in the range of surface energies examined, the IGC measurements are not affected by the packing structure. In this a significant step forward is performed; Monte Carlo simulations were performed to study heterogeneous adsorption in the context of IGC. These simulations are quite computationally expensive, compared with the IGC models used in previous studies. However, they provide unprecedented accuracy. Thus, they can be used, along with wettability studies and IGC measurements in proof of concept studies, to validate the accuracy of IGC measurements. Overall this chapter makes a significant contribution towards the development of effective protocols for accurate surface energy

measurements. It gives to the investigators the tools to carefully select the amount of silanised glass wool required for their measurements. On the same time, it provides the seeds for more advanced studies, towards the consolidation of IGC as an important technique.

One of the main advantages of IGC, is that it enables measurements in ambient temperatures. From a fundamental physicochemical perspective, it is obvious that even small variations in the temperature of the measurements can lead issues to the measurements. As the temperature increases, the surface energy decreases. This can lead to changes in the spreading pressure associated with adsorption. Since IGC is an adsorption based technique, this has a direct impact on the accuracy of the measurements. Chapter 4 commences with the presentation of a couple of peculiar cases, where the IGC measurements on two different polymorphs of carbamazepine, suggest an increase in the surface energy. By using theoretical arguments, grounded on the adsorption fundamentals, as they have been introduced by the pioneers of the field, it was revealed that these peculiarities are artefacts of the effects of spreading pressure. In this context, a thorough road map was proposed, in order to take into account the effects of spreading pressure and correct the IGC measurements. A combination of IGC measurements, wettability measurements, SEM images and in silico experiments were used to verify the validity of this road map. The results of this chapter have, again, the potential to become game changers in the development of standard operating procedures for IGC measurements. The investigators were encouraged to look some of their previous works in the light of the new road map. The results enhance the notion, put forward by the author and others in the field, that the IGC measurements should be complimented by complimentary techniques. Especially wettability measurements were found to be particularly useful. The results from Chapters 3 and 4 reinforce the use of surface energy deconvolution schemes, enabling the determination of surface energy anisotropy from IGC measurements, quantifying the relative abundance of the different facets.

As a number of the materials used in pharmaceutical industry are amorphous in nature, Hansen Solubility Parameters (HSP) are also a useful type of thermodynamic quantities of interest. The fifth chapter deals with the improvement of the accuracy of IGC measurements for the determination of HSP. However, the most profound finding of this chapter is not the extrapolation process for the accurate determination of the χ interaction parameter and HSP. The most prolific finding is the discovery of the interfacial χ interaction parameter; a quantity with smaller magnitude than the bulk χ interaction parameter predicted by the classical Flory-Huggins equation. This finding could be of particular importance for the design of industrial processes dominated by the formation of an interface between an amorphous material and a liquid.

Overall, Chapters 4 to 6 provide a useful guideline for the development of accurate standard operating procedures for the accurate execution of IGC measurements. They show that even though deficiencies exist, they do not infringe the unprecedented capabilities of the technique. The results presented on the wettability and energetic surface anisotropy of p-monoclinic carbamazepine and HSP of copovidone will be used in Chapter 6, dealing with some concepts of dissolution.

Dissolution is a multi-step and quite intriguing process, of particular importance for pharmaceutical process development and for the study of the performance of drug products. Considering that oral dosage forms constitute the backbone of pharmaceutical industry, it is evident that their further development requires the intense study of dissolution. The development of new drug substances creates numerous challenges, owe to their poor bioavailability. It was found, in previous studies, that formulating the poorly soluble drug substances with hydrophilic polymers improves their bioavailability. Because of the multi-step nature of dissolution, an articulated investigation requires to isolate the different steps and study the influence of individual components of the drug product in each one of them. Chapter 7

focuses on the anisotropic wettability of p-monoclinic carbamazepine with aqueous copovidone solutions. A thorough study of the anisotropic surface properties of p-monoclinic carbamazepine was performed following the notions of similar works on other drug substances. Aqueous polymer solutions were prepared, at different concentrations, and their surface properties were studied; pendant drop measurements in air and heptane were used to calculate the surface tension of the solutions and Langmuir balance measurements were used to quantify the surface activity of the solution. The results suggest that the addition of a surface active agent lowers the surface tension of a liquid, nevertheless, the decrease is not necessarily affecting both components of the surface tension on the same way. In fact, it was shown that for the case of copovidone, one of them, the van der Waals one, appears to increase, whereas the acid-base one was decreasing. It was not possible to derive an empirical correlation between the magnitude of the components of the surface activity of polymer solution at different concentrations and the HSP of the polymer, owe to this peculiar behaviour. Nevertheless, it was shown, that surface activity has two different components and definitely the correlation between their magnitude of the polymer is something keep investigating.

Chapter 7 provides a qualitative correlation between the aggregation behaviour of the polymer and the surface activity. Most importantly, this study verifies that even a small amount of polymer can substantially decrease the spreading coefficient between the crystal facets and the aqueous solution of polymer. This indicates that the presence of the polymer can significantly speed up the wettability step of dissolution. The results can be further used for the development of mechanistic understanding of processes such as wet granulation, where there is an immense need for understanding of the influence of anisotropic particle properties on the formation of liquid bridges.

Chapter 8 deals with another process of great interest in pharmaceutical industry, drying. Crystal engineering approaches have been used to tune the particle size and habit of

carbamazepine dihydrate. A novel bioinspired method has been deployed for the growth of macroscopic crystals of the dihydrate. This new method enables the growth of hydrates comprising of strongly hydrophobic molecules. Using tailored experiments, it was possible to elucidate the mechanisms of dehydration induced polymorphism and reveal some of the aspects of dehydration induced crack formation. For the first time, it has been shown that the cracks in channel hydrates are nucleated inside the crystal owe to the departure of water molecules for the channels. In Chapter 3 it has been shown that in silico studies can be used to quantify the relative amount of two different polymorphs in a mixture, in terms of relative surface area. Using this tool, it was possible to test and validate a hypothesis on the dehydration induced polymorphism mechanisms, based on the polymorphic stability of anhydrous carbamazepine, its glass transition temperature and the presence of trace amounts of p-monoclinic carbamazepine. Further studies are required with other compounds to investigate whether these findings can be generalised for a wide range of compounds. Especially the mechanism via which the trace amounts of anhydrous p-monoclinic carbamazepine act as templates, determining dehydration induced polymorphism, should be investigated further. This is because, it can provide a robust framework for the control of dehydration induced polymorphism, analogous to the use of seeding for the control of crystallisation processes. It is the author's opinion that in this investigation the interfacial interactions between the crystalline and the amorphous phase, could be of crucial importance.

9.2 Criticism on aspects of this work

In Chapters 4, 5 and 6 the van der Waals component of the surface energy and HSP was used, extensively, in the investigation of the physicochemical phenomena influencing the quality of IGC measurements. As it has been mentioned in the aforementioned chapters this decision was taken, as the van der Waals interactions are better understood, enabling more confidence in the observed data and minimising the use of not well established theoretical

concepts. Thanks to the exhaustive theoretical, computational and experimental studies conducted by numerous pioneers in the field of interfacial phenomena, it was possible to create a framework enabling the robust and thorough understanding of interactions including van der Waals forces. This is not the case for acid-base interactions. Thanks to the robustness of the geometric mean approximation for van der Waals interactions, it was possible to perform very elaborate combinations of experimental data and in silico experiments.

In Chapters 4 and 6 two amorphous materials were in the epicentre of the investigations, silanised glass wool and copovidone respectively. As it has been discussed at the end of Chapter 6, it is not expected the silanised glass wool to undergo any effects of plasticisation owe to moisture sorption. For copovidone, the T_g was determined, using IGC, and found to be quite close to the one reported in literature for dry material. Thus, the effects of moisture uptake were negligible as well. However, because of the nature of the investigations conducted, it will have been a good practice if the materials were stored under different controlled conditions, in order to assess the importance of storage on the surface energy of the silanised glass wool and the HSP of copovidone.

Nevertheless, this approach was not followed in Chapter 7, where the geometric mean approximation, a notion with just a small glimpse of theoretical support, was used for the calculation of the anisotropic surface properties. This casts doubts about some of the conclusions, even though the key findings on the decrease of wettability with small addition of polymer, thanks to the surface activity of the polymer, are undoubtful. Even though, from a mathematical perspective, the geometric mean approximation is the simplest method for the calculation of surface energies, the inherent non-linearities, associated with this approximation, prevented the calculation of the acid and the base component of the surface tension of the polymer solutions, as it was giving rise to an ill posed system. It is the author's opinion that the use of well characterised polymer surfaces for the deconvolution of the acid and the base

component of the surface tension, would not necessarily solve the problem, eliminating all the doubts regarding the calculated magnitude of the acid and the base component of the surface tension. This is because wettability studies on polymers are affected by the liquid penetration in the soft material and by the re-orientation of functional groups upon contact of the liquid with the polymer. These phenomena are liquid dependent, making the selection of probe solvents very difficult. Similarly, the use of silanised surfaces, would not be a great idea, as it would require very good control over the silanisation procedure and extensive characterisation of the silanised surfaces. This was going to create additional problems.

The results presented in Chapter 8 verify the applicability of surface energy heterogeneity as a metric for polymorph quantification; enabling the use of IGC measurements in the study of the mechanisms determining dehydration induced concomitant polymorphism. However, under agitated bed drying (or any other form of drying involving the use of mechanical force), defects are created on the surface of the crystals. Furthermore, new facets appear owe to breakage. Thus, the applicability of IGC in this context is limited. Furthermore, the fact that it was not possible to isolate macroscopic crystals of the anhydrous triclinic polymorph can create doubts about the robustness of the conclusions presented.

Some of the most intrinsic findings of the work presented in Chapter 8, come from the SEM images of macroscopic crystals of carbamazepine dihydrate. Some of the crystals were cut using razor blade to examine the evolution of cracks and to study the differences between the bulk and the surface. This process may have caused damage to the samples that may have had consequences on the results observed. Immersing the crystals in epoxy prior to cutting them, may have minimised the doubts created. The epoxy would have allowed a more precise cutting, ensuring that the crystals, susceptible to mechanical force, would not be damaged. Nevertheless, this process of epoxy coating prior to cutting is more common in studies involving metals and alloys; not organic crystals. This process may have caused damage to the

whiskers. Furthermore, the penetration of epoxy in the cracks may have resulted to damage as well. Therefore, an interesting investigation would be one elucidating the effects of epoxy coating on the surfaces features of organic single crystals, such as cracks and whiskers.

The findings of this chapter suggest that traces anhydrous p-monoclinic carbamazepine, crystallising owe to the Ostwald rule of stages, provide a template driving dehydration induced polymorphism. The same templating phenomenon was not observed when samples of pure carbamazepine dihydrate were seeded with p-monoclinic carbamazepine. It was not possible to study the exact mechanism of this phenomenon, even though solid-solid interactions between the crystals of the two compounds are expected to be important. Despite the fact that carbamazepine exhibits an intriguing polymorphic behaviour, while exhibiting numerous solvates, may not be a suitable candidate for the investigation of the mechanisms dictating dehydration induced concomitant polymorphism. A material, which has much slower dehydration kinetics could have been chosen.

9.3 Directions for future work

From very early on, it was evident that a focus on van der Waals interactions would have enabled more flexibility in terms of physicochemical aspects of interfacial phenomena. This was found to be true. The expansion of a lot of the concepts developed in this work, requires a more fundamental understanding of the exact nature of the action of specific acid-base interactions. Intuitively it should be understood that this is a multidisciplinary task. It is the opinion of the author that the direction, of the investigators in this field, is not right. Using endless number of solvents and statistical regression models was never the way to advance in physical chemistry and it is not expected to be the way forward in the future. A more fundamental understanding should be achieved, at first, enabling the understanding of the competition between long and short range interactions at different levels and different interfaces. Kinetic studies on the formation of interfaces would shade light in a lot of the

questions dominating the field. The formation of an interface is an inherently complex phenomenon and is very poorly understood in the most important, from an industrial perspective interface, the solid-solid one.

Then it will be easier to develop mechanistic simplifications, similar to the geometric mean approximation, to implement the findings of fundamental studies in experimental measurements, performed at a daily basis. It will also to be easier to assess the magnitude of the difference in the influence between the different types of forces at the different interfaces.

A unifying theory, bringing together spreading pressure and diffusion phenomena is also required for the development of a universally acceptable type of IGC measurements. This can become true decoupled from the studies proposed in the previous paragraph. It will enable the easier integration of IGC measurements in industry and regulatory bodies.

From a more practical perspective, of course, the notions of this work can found applicability in numerous industrial processes, not limited in pharmaceutical processes. Some work, worth sharing here, has been done in the field of dry coating. The coating of cohesive pharmaceutical powders (host particles) with nanopowders (guest particles) is gaining ground as a tool for the improvement of the performance of drug products. Considering that the silica nanopowders are not marketed in the form of primary particles, but in the form of aggregates, an efficient dry coating process should enable both the deaggregation of silica nanoparticles and the adhesion of primary silica nanoparticles on the surface of the host particles. **Figure 9.1** provides a visualisation of this process.

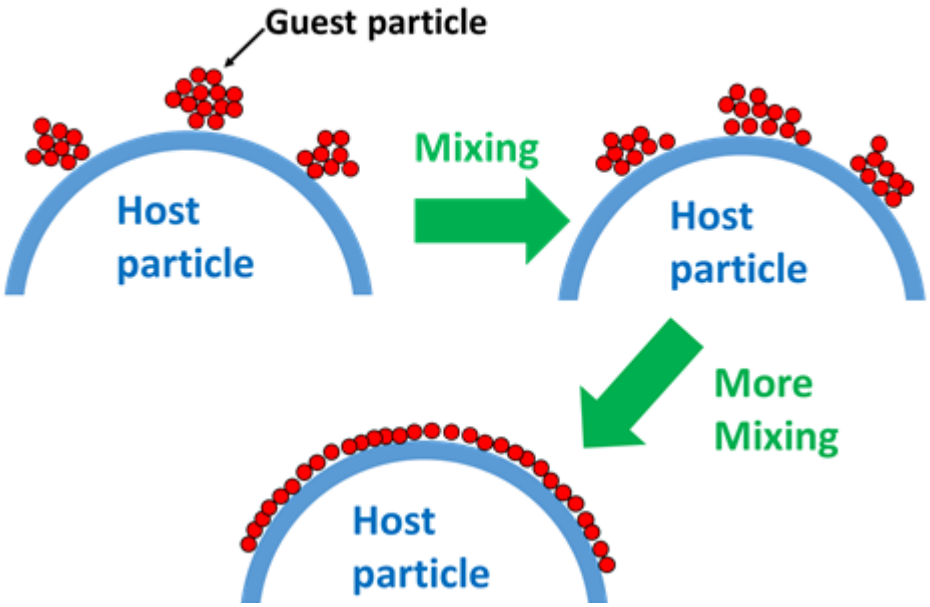


Figure 9.1: Schematic representation of the dry coating process, commencing with the deaggregation of silica nanoparticles and proceeding with the coverage of the surface of the host particle by primary silica nanoparticles.

For the phenomenological understanding of dry coating, two mechanisms have been proposed, a thermodynamic/spreading coefficient one and a kinetic one. The former states that if the spreading coefficient between the host and guest particles is positive, then dry coating is thermodynamically feasible and it will eventually happen as long as sufficient mixing intensity is provided. On the other hand if the spreading coefficient is negative, then no dry coating will ever happen irrespectively of the mixing intensity provided. The latter mechanism suggests that dry coating is purely driven by kinetics and that for any combination of host and guest particles dry coating will happen as long as some reasonable mixing intensity is provided. The relative coverage at different times can be calculated from the amount of the mixing intensity, using empirical correlations. These mechanisms have already been tested in the context of liquid marbles. The kinetic based mechanism was the winner in that battle. Of course, it should be considered that the investigators, in these studies, have relied on the classical geometric mean approximation to describe acid-base interactions. However, it is the opinion of the author, of

this work, that the use of geometric mean approximation, in this case, is not a robust reason to reject the whole work. It may cast doubts on the accuracy of some of the numbers, but not on the general outcomes. Otherwise, the majority of the work in the field of interfacial phenomena should be rejected.

For the purposes of this work, hydrophilic silica was used to coat two drug substances (p-monoclinic carbamazepine and monoclinic paracetamol) and two excipients (α-lactose monohydrate and mannitol). The drug substances were recrystallized in methanol. The excipients were used as received. The surface energies of the host particles were measured, at 35 ^{o}C and 32 % RH, using IGC. The temperature of the measurement was chosen to account for the increase in temperature during processing. The RH was set at 32 %, as dry coating is not, generally, performed in a sealed environment. The effects of the spreading pressure of water were omitted, the results were corrected only for the spreading pressure of the solvents used in the measurement.

The surface energy of the guest particles was measured at 35 ^{o}C and at different values of RH, as shown in **Figure 9.2**. This was done to see the variation of the behaviour of the material with RH. Finite dilution measurements were performed and the values reported in **Figure 9.2** are the values of the total surface energy at a surface coverage of 0.1. As can be seen even though the surface energy seems to decrease with increasing RH, the hydrophilicity of the material increases, as the composition of the surface energy changes, with the importance of the acid-base component becoming increasingly important.

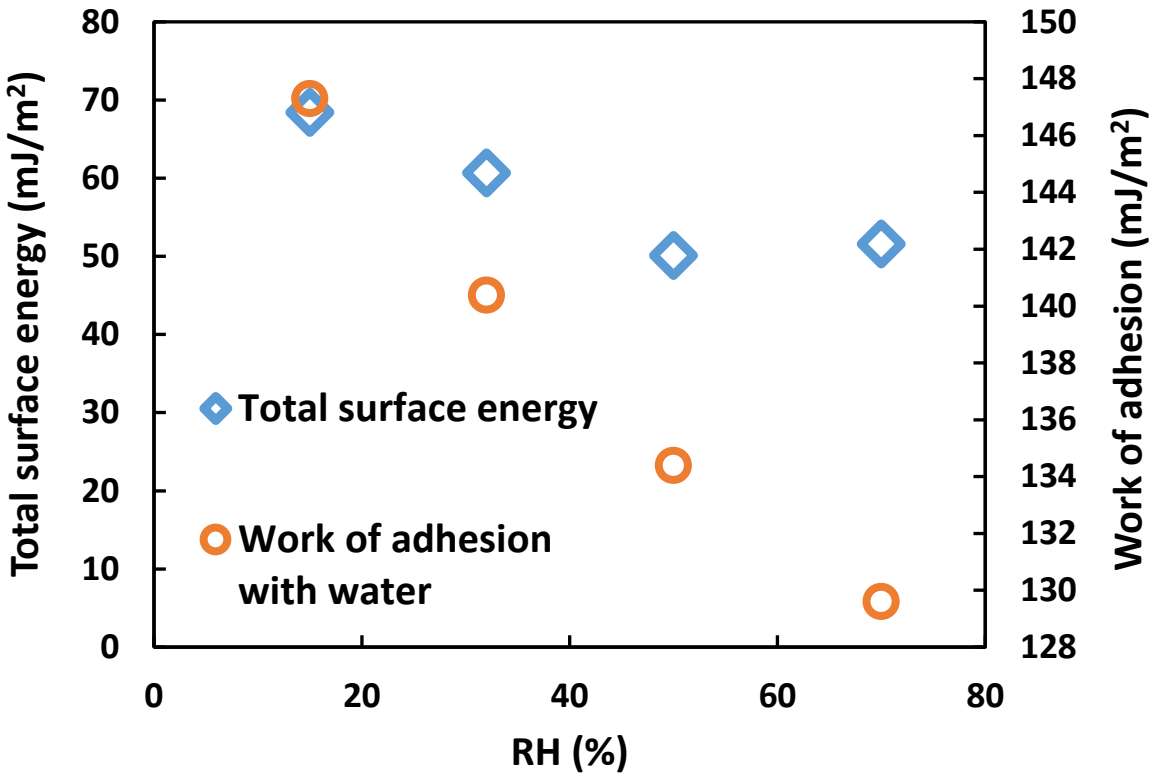


Figure 9.2: Plot showing the variation of the total surface energy of hydrophilic silica nanoparticles, with RH, and the corresponding values of work of adhesion with water.

The spreading coefficient was calculated according to the infamous equation:

$$S = W_{AB} - W_C = 2\left(\sqrt{\gamma_A^{LW}\gamma_B^{LW}} + \sqrt{\gamma_A^{+}\gamma_B^{-}} + \sqrt{\gamma_A^{-}\gamma_B^{+}}\right) - 2\gamma_B^{Total} \qquad \text{Eq. 9.1}$$

In the above equation, S stands for the spreading coefficient, W_{AB} is the work of adhesion between a combination of host and guest particles and W_C is the work of cohesion between the guest particles (B). The geometric mean approximation was used, as a convenient equation to calculate the work of adhesion. The work of cohesion is measured by just multiplying the total surface energy of the guest particles by a factor of two. The values obtained are plotted in **Figure 9.3**.

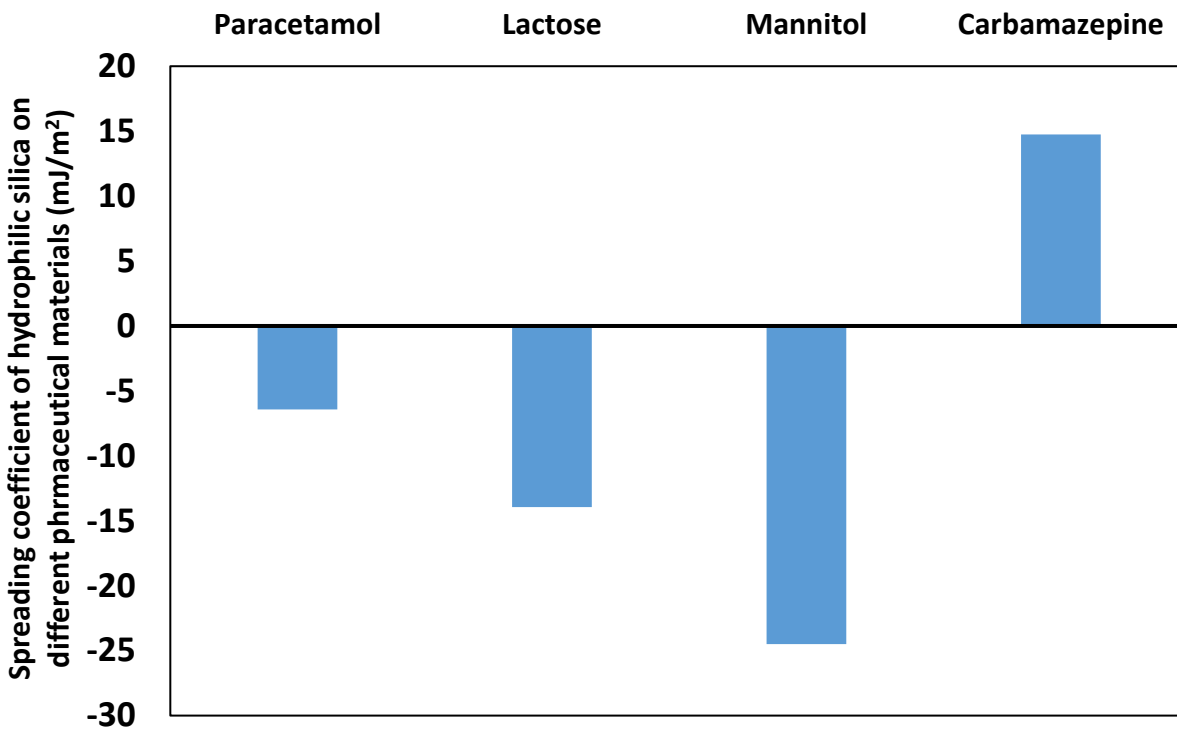


Figure 9.3: The spreading coefficient calculated for the materials used in this study.

Dry coating was performed using 1 % by mass guest particles loading in a 25 mL beaker, on a sieve shaker for 14 hours. If the spreading coefficient based theory is correct, dry coating was only going to be observed for carbamazepine. As can be seen from the images shown in **Figure 9.4**, this is not the case. In fact, dry coating was observed on each material. Thus, it seems that the spreading coefficient base hypothesis is not valid.

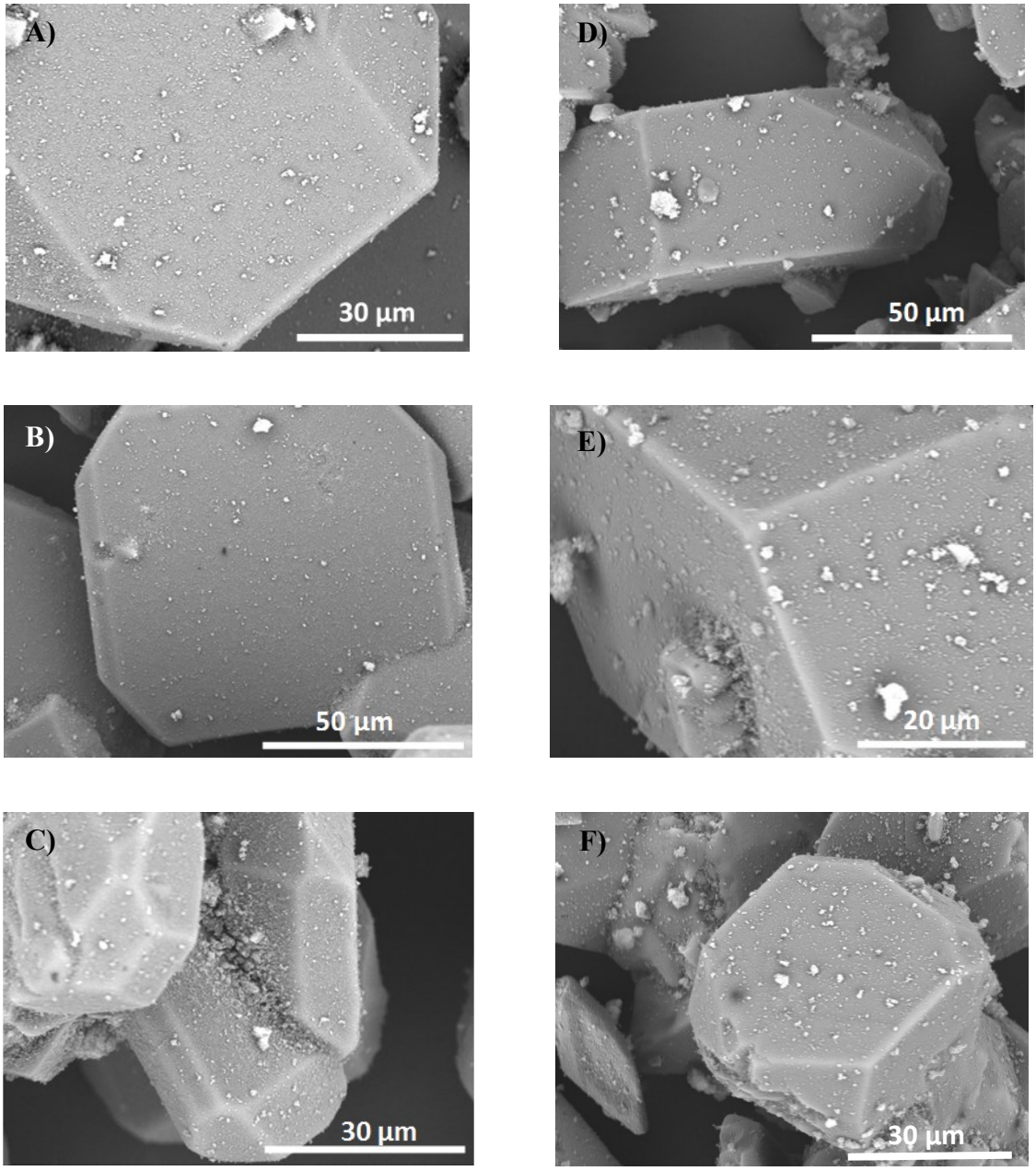
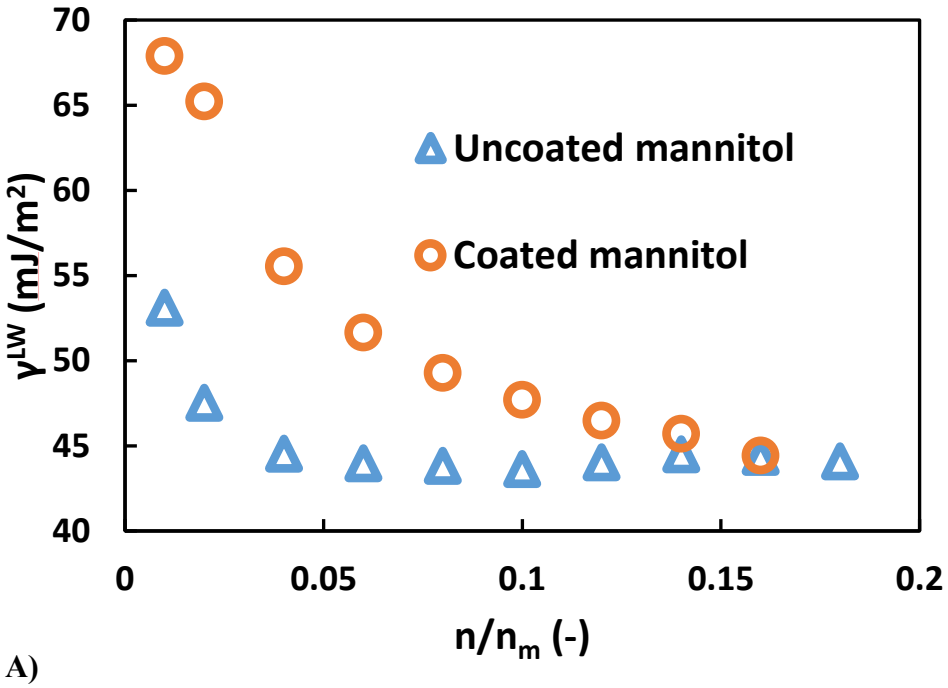


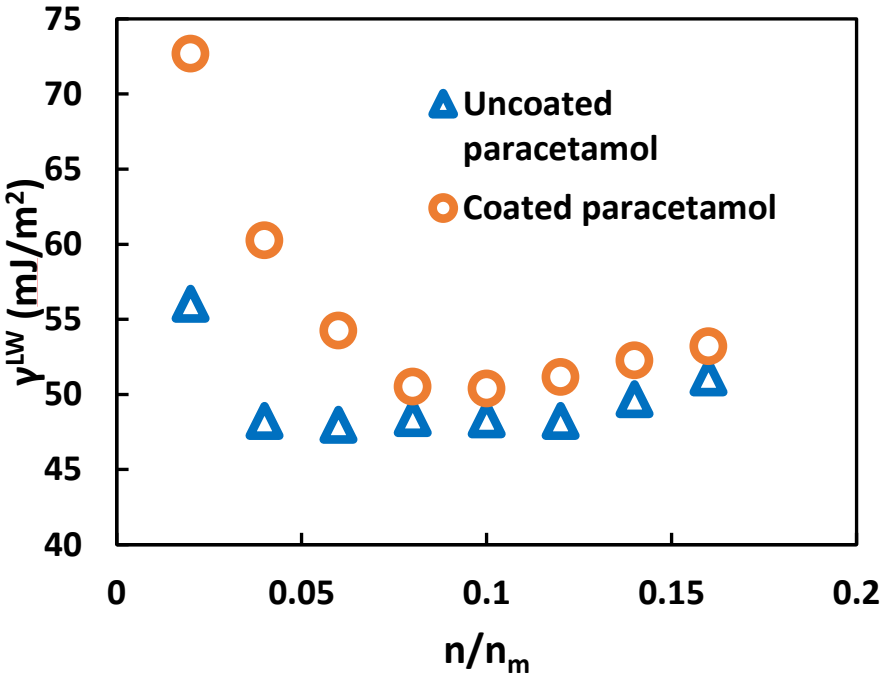
Figure 9.4: SEM images of dry coated A-C) paracetamol and D-F) p-monoclinic carbamazepine.

The dry coating was found to decrease the cohesion[8-9] of both carbamazepine and paracetamol by about 30 %. Surface energy measurements were conducted on coated material. It was shown that the surface energy increased with coating. This may seem counterintuitive, as higher surface energy was expected to favour cohesion. However, it is not. It is in line with previous studies, conducted with AFM, suggesting that the decrease in cohesiveness is mainly thanks to the effects of increased roughness.[241] The careful investigator should appreciated that

owe to the small size of the primary particles of silica aggregates, capillary phenomena are very important in the measurement of the surface energy of pure silica.



A)



B)

Figure 9.5: The surface energy maps of coated and uncoated A) mannitol and B)paracetamol

References

1. Gibbs, J. W., On the equilibrium of heterogeneous substances. *Transactions of the Connecticut Academy of Science* **1876,** *3*, 108-248.
2. Benet, L. Z., The Role of BCS (Biopharmaceutics Classification System) and BDDCS (Biopharmaceutics Drug Disposition Classification System) in Drug Development. *Journal of Pharmaceutical Sciences* **2013**, 102 (1), 34-42
3. Hadjittofis, E.; Zhang, G. Z. G.; Heng, J. Y. Y., Interfacial phenomena. In *Developing Solid Oral Dosage Forms*, 2nd ed.; Qiu, Y.; Chen, Y.; Zhang, G. Z. G.; Yu, L.; Mantri, R. V., Eds. Academic Press: New York, 2017.
4. Heng, J. Y. Y.; Bismarck, A.; Lee, A. F.; Wilson, K.; Williams, D. R., Anisotropic Surface Energetics and Wettability of Macroscopic Form I Paracetamol Crystals. *Langmuir* **2006,** *22*, 2760-2769.
5. Heng, J. Y. Y.; Bismarck, A.; Lee, A. F.; Wilson, K.; Williams, D. R., Anisotropic surface chemistry of aspirin crystals. *Journal of Pharmaceutical Sciences* **2007,** *96* (8), 2134-2144.
6. Ho, R.; Heng, J. Y. Y.; Dilworth, S. E.; Williams, D. R., Wetting Behavior of Ibuprofen Racemate Surfaces. *The Journal of Adhesion* **2008,** *84* (6), 483-501.
7. Shah, U. V.; Olusanmi, D.; Narang, A. S.; Hussain, M. A.; Gamble, J. F.; Tobyn, M. J.; Heng, J. Y. Y., Effect of crystal habits on the surface energy and cohesion of crystalline powders. International Journal of Pharmaceutics **2014,** 472 91-2), 140-147.
8. Shah, U. V.; Olusanmi, D.; Narang, A. S.; Hussain, M. A.; Hinder, S. J.; Heng, J. Y. Y., Decoupling the Contribution of Surface Energy and Surface Area on the Cohesion of Pharmaceutical Powders. *Pharmaceutical Research* **2014,** *32*, 248-259.
9. Shah, U. V.; Olusanmi, D.; Narang, A. S.; Hussain, M. A.; Tobyn, M. J.; Heng, J. Y. Y., Decoupling the contribution of dispersive and acid-base components of surface energy on the cohesion of pharmaceutical powders. *International Journal of Pharmaceutics* **2014,** *475* (1–2), 592-596.
10. Modi, S. R.; Dantuluri, A. K. R.; Puri, V.; Pawar, Y. B.; Nandekar, P.; Sangamwar, A. T.; Perumalla, S. R.; Sun, C. C.; Bansal, A. K., Impact of Crystal Habit on Biopharmaceutical Performance of Celecoxib. *Crystal Growth & Design* **2013,** *13* (7), 2824-2832.
11. Williams, H. D.; Trevaskis, N. L.; Charman, S. A.; Shanker, R. M.; Charman, W. N.; Pouton, C. W.; Porter, C. J. H., Strategies to Address Low Drug Solubility in Discovery and Development. *Pharmacological Reviews* **2013,** *65* (1), 315.
12. Theodorakis, P. E.; Muller, A. E.; Craster, V. R.; Matar, K. O., Superspreading: Mechanisms and Molecular Design. *Lagmuir* **2015,** *31* (8), 2304-2309.
13. Fowkes, F. M., Dispersion Force Contributions to Surface and Interfacial Tensions, Contact Angles, and Heats of Immersion. In *Contact Angle, Wettability, and Adhesion*, American Chemical Society: 1964; Vol. 43, pp. 99-111.
14. Fowkes, F. M., Attractive forces at interfaces. *Industrial & Engineering Chemistry* **1964,** *56* (12), 40-52.
15. Kwok, D. Y.; Li, D.; Neumann, A. W., Fowkes' surface tension component approach revisited. *Colloids and Surfaces A: Physicochemical and Engineering Aspects* **1994,** *89* (2), 181-191.
16. Fowkes, M. F.; Mostafa, A. M., Acid-Base Interactions in Polymer Adsorption. *Industrial & Engineering Chemistry Research* **1978,** *17* (1), 3-7.
17. Mittal, K. L.; Etzler, F. M., Is the World Basic? Lessons from Surface Science. *Contact Angle, Wettability and Adhesion* **2008,** *6* (1), 1-16.
18. Ho, R.; Heng, J. Y. Y., A Review of Inverse Gas Chromatography and its Development as a Tool to Characterize Anisotropic Surface Properties of Pharmaceutical Solids. *KONA Powder and Particle* **2013,** *30*, 164-180.
19. Jefferson, A. E.; Williams, D. R.; Heng, J. Y. Y., Computing the Surface Energy Distributions of Heterogeneous Crystalline Powders. *Journal of Adhesion Science and Technology* **2011,** *25* (4-5), 339-355.

20. Smith, R. R.; Williams, D. R.; Burnett, D. J.; Heng, J. Y. Y., A New Method To Determine Dispersive Surface Energy Site Distributions by Inverse Gas Chromatography. *Langmuir* **2014,** *30* (27), 8029-8035.
21. DiPaola-Baranyi, G.; Guillet, J. E., Estimation of Polymer Solubility Parameters by Gas Chromatography. *Macromolecules* **1978,** *11*, 228-235.
22. Ito, K.; Guillet, J. E., Estimation of Solubility Parameters for Some Olefin Polymers and Copolymers by Inverse Gas Chromatography. *Macromolecules* **1979,** *12*, 1163-1167.
23. Adamska, K.; Bellinghausen, R.; Voelkel, A., New procedure for the determination of Hansen solubility parameters by means of inverse gas chromatography. *Journal of Chromatography A* **2008,** *1195* (1–2), 146-149.
24. Hansen, C. M. The Three Dimensional Solubility Parameter and Solvent Diffusion Coefficient and Their Importance in Surface Coating Formulation. The Technical University of Denmark, 1967.
25. Trasatti, S.; Parsons, R., Interphases in systems of conducting phases: Recommendations 1985 Supersedes provisional version published 1983. *Journal of Electroanalytical Chemistry and Interfacial Electrochemistry* **1986,** *205* (1–2), 359-376.
26. Mei, R.; Shang, H.; Klausner, J. F.; Kallman, E., A Contact Model for the Effect of Particle Coating on Improving the Flowability of Cohesive Powders. *KONA Powder and Particle* **1997,** *15*, 132-141.
27. Tomas, J., Fundamentals of cohesive powder consolidation and flow. *Granular Matter* **2004,** *6*, 75-86.
28. Tomas, J.; Kleinschmidt, S., Improvement of Flowability of Fine Cohesive Powders by Flow Additives. *Chemical Engineering and Technology* **2009,** *32* (10), 1470-1483.
29. Tobyn, M.; Staniforth, J. N.; Morton, D.; Harmer, Q.; Newton, M. E., Active and intelligent inhaler device development. *International Journal of Pharmaceutics* **2004,** *277*, 31-37.
30. Ho, R.; Naderi, M.; Heng, J. Y. Y.; Williams, D. R.; Thielmann, F.; Bouza, P.; Keith, R. A.; Thiele, G.; Burnett, D. J., Effect of Milling on Particle Shape and Surface Energy Heterogeneity of Needle-Shaped Crystals. *Pharmaceutical Research* **2012,** *29*, 2806-2816.
31. Han, X.; Ghoroi, C.; To, D.; Chen, Y.; Davé, R., Simultaneous micronization and surface modification for improvement of flow and dissolution of drug particles. *International Journal of Pharmaceutics* **2011,** *415* (1–2), 185-195.
32. Giry, K.; Péan, J. M.; Giraud, L.; Marsas, S.; Rolland, H.; Wüthrich, P., Drug/lactose co-micronization by jet milling to improve aerosolization properties of a powder for inhalation. *International Journal of Pharmaceutics* **2006,** *321* (1–2), 162-166.
33. Prime, D.; Atkins, P. J.; Slater, A.; Sumby, B., Review of dry powder inhalers. *Dry Powder Formulations for Inhalation* **1997,** *26* (1), 51-58.
34. Ho, R.; Dilworth, S. E.; Williams, D. R.; Heng, J. Y. Y., Role of Surface Chemistry and Energetics in High Shear Wet Granulation. *Industrial & Engineering Chemistry Research* **2011,** *50*, 9642-9649.
35. Lin, S.-Y.; Li, M.-J.; Lin, K.-H., Hydrophilic excipients modulate the time lag of time-controlled disintegrating press-coated tablets. *AAPS PharmSciTech* **2004,** *5* (4), 25-29.
36. Meyer, M. C.; Straughn, A. B.; Jarvi, E. J.; Wood, G. C.; Pelsor, F. R.; Shah, V. P., The Bioinequivalence of Carbamazepine Tablets with a History of Clinical Failures. *Pharmaceutical Research* **1992,** *9* (12), 1612-1616.
37. Sun, C. C., Decoding Powder Tabletability: Roles of Particle Adhesion and Plasticity. *Journal of Adhesion Science and Technology* **2001,** *25* (4-5), 483-499.
38. Modi, S. R.; Dantuluri, A. K. R.; Perumalla, S. R.; Sun, C. C.; Bansal, A. K., Effect of Crystal Habit on Intrinsic Dissolution Behavior of Celecoxib Due to Differential Wettability. *Crystal Growth & Design* **2014,** *14* (10), 5283-5292.
39. Jain, T.; Sheokand, S.; Modi, S. R.; Ugale, B.; Yadav, R. N.; Kumar, N.; Nagaraja, C. M.; Bansal, A. K., Effect of differential surface anisotropy on performance of two plate shaped crystals of aspirin form I. *European Journal of Pharmaceutical Sciences* **2017,** *99*, 318-327.
40. Thiel, P. A.; Madey, T. E., The interaction of water with solid surfaces: Fundamental aspects. *Surface Science Reports* **1987,** *7* (6), 211-385.

41. Infantes, L.; Motherwell, S., Water clusters in organic molecular crystals. *CrystEngComm* **2002,** *4* (75), 454-461.
42. Authelin, J.-R., Thermodynamics of non-stoichiometric pharmaceutical hydrates. *International Journal of Pharmaceutics* **2005,** *303* (1–2), 37-53.
43. Thielmann, F., Introduction into the characterisation of porous materials by inverse gas chromatography. *Journal of Chromatography A* **2004,** *1037* (1–2), 115-123.
44. Thielmann, F.; Burnett, D. J.; Heng, J. Y. Y., Determination of the Surface Energy Distributions of Different Processed Lactose. *Drug Delivery and Industrial Pharmacy* **2007,** *33* (11), 1240-1253.
45. Smith, R. R.; Shah, U. V.; Parambil, J. V.; Burnett, D. J.; Thielmann, F.; Heng, J. Y. Y., The Effect of Polymorphism on Surface Energetics of D-Mannitol Polymorphs. *The AAPS Journal* **2017,** *19* (1), 103-109.
46. Burnett, D. J.; Thielmann, F.; Booth, J., Determining the critical relative humidity for moisture-induced phase transitions. *International Journal of Pharmaceutics* **2004,** *287* (1–2), 123-133.
47. Burnett, D. J.; Thielmann, F.; Sokoloski, T.; Brum, J., Investigating the moisture-induced crystallization kinetics of spray-dried lactose. *International Journal of Pharmaceutics* **2006,** *313* (1–2), 23-28.
48. Khoo, J. Y. Thermodynamic stability and kinetic analysis of pharmaceutical channel hydrate during dehydration process. Imperial College, 2010.
49. Khoo, J. Y.; Heng, J. Y. Y.; Williams, D. R., Agglomeration Effects on the Drying and Dehydration Stability of Pharmaceutical Acicular Hydrate: Carbamazepine Dihydrate. *Industrial & Engineering Chemistry Research* **2010,** *49*, 422-427.
50. Khoo, J. Y.; Shah, U. V.; Schaepertoens, M.; Williams, D. R.; Heng, J. Y. Y., Process-induced phase transformation of carbamazepine dihydrate to its polymorphic anhydrates. *Powder Technology* **2013,** *236*, 114-121.
51. van der Waals, J. D., The Equation of State for Gases and Liquids. In *Nobel Lectures, Physics*, Elsevier Publishing Company: Amsterdam, 1967.
52. Keesom, W. H., The second viral coefficient for rigid spherical molecules, whose mutual attraction is equivalent to that of a quadruplet placed at their centre. *Proceedings of the Royal Netherlands Academy of Arts and Sciences* **1915,** *18*, 636-646.
53. Debye, P.; Huckel, E., The theory of electrolytes. I. Lowering of freezing point and related phenomena. *Physikalische Zeitschrift* **1923,** *24* (9), 185-206.
54. London, F., The general theory of molecular forces. *Transactions of the Faraday Society* **1937,** *33*, 8b-26.
55. Van Oss, C. J.; Chaudhury, M. K.; Good, R. J., Interfacial Lifshitz-van der Waals and polar interactions in macroscopic systems. *Chemical Reviews* **1988,** *88* (6), 927-941.
56. Arunan, E.; Desiraju Gautam, R.; Klein Roger, A.; Sadlej, J.; Scheiner, S.; Alkorta, I.; Clary David, C.; Crabtree Robert, H.; Dannenberg Joseph, J.; Hobza, P.; Kjaergaard Henrik, G.; Legon Anthony, C.; Mennucci, B.; Nesbitt David, J., Definition of the hydrogen bond (IUPAC Recommendations 2011). *Pure and Applied Chemistry* **2011,** 83 (8), 1637-1641.
57. Hamaker, H. C., The London—van der Waals attraction between spherical particles. *Physica* **1937,** *4* (10), 1058-1072.
58. Lifshitz, E. M., The theory of Molecular Attractive Forces between Solids. *Soviet Physics Uspekhi* **1956,** *2* (1), 73-83.
59. Derjaguin, B. V.; Landau, L., Theory of the stability of strongly charged lyophobic sols and of the adhesion of strongly charged particles in solutions of electrolytes. *Progress in Surface Science* **1941,** *43* (1), 30-59.
60. Pethica, B. A., Are electrostatic potentials between regions of different chemical composition measurable? The Gibbs–Guggenheim principle reconsidered, extended and its consequences revisited. *Physical Chemistry Chemical Physics* **2007,** *9* (47), 6253-6262.

61. Brown, R., A brief account of microscopical observations made in the months of June, July and August, 1827, on the particles contained in the pollen of plants; and on the general existence of active molecules in organic and inorganic bodies. *Philisophical Magazine* **1827,** *4*, 161-173.
62. Stetefeld, J. M., S.A.; Patel, T.R., Dynamic light scattering: a practical guide and applications in biomedical sciences. *Biophys Rev* **2016,** *8* (4), 409-427.
63. Siegret, A. J. F. *On the fluctuations in signals returned by many independently moving scatterers.*; MIT, Cambridge: 1949.
64. Owens, D. K.; Wendt, R. C., Estimation of the surface free energy of polymers. *Journal of Applied Polymer Science* **1969,** *13* (8), 1741-1747.
65. Girifalco, F. A.; Good, R. J., A Theory for the Estimation of Surface and Interfacial Energies. I. Derivation and Application to Interfacial Tension. *Journal of Physical Chemistry* **1957,** *61* (7), 904-909.
66. Wu, S., Calculation of Interfacial Tension in Polymer Systems. *Journal of Polymer Science* **1971,** *34* (1), 1741-1747.
67. Volpe, C. D.; Siboni, S., Some Reflections on Acid–Base Solid Surface Free Energy Theories. *Journal of colloid and interface science* **1997,** *195* (1), 121-136.
68. Derjaguin, B. V.; Muller, V. M.; Toporov, Y. P., Effect of contact deformations on the adhesion of particles. *Journal of Colloid and Interface Science* **1975,** *53* (2), 314-326.
69. Chen, Y. L.; Helm, C. A.; Israelachvili, J. N., Molecular mechanisms associated with adhesion and contact angle hysteresis of monolayer surfaces. *The Journal of Physical Chemistry* **1991,** *95* (26), 10736-10747.
70. Yoshizawa, H.; Israelachvili, J., Fundamental mechanisms of interfacial friction. 2. Stick-slip friction of spherical and chain molecules. *The Journal of Physical Chemistry* **1993,** *97* (43), 11300-11313.
71. Nosonovsky, M., Model for solid-liquid and solid-solid friction of rough surfaces with adhesion hysteresis. *The Journal of Chemical Physics* **2007,** *126* (22), 224701.
72. Fowkes, F. M.; Mostafa, M. A., Acid-Base Interactions in Polymer Adsorption. *Industrial & Engineering Chemistry Product Research and Development* **1978,** *17* (1), 3-7.
73. Drago, R. S.; Vogel, C. G.; Needham, E. T., A Four-Parameter Equation for Predicting Enthalpies of Adduct Formation. *Journal of American Chemical Society* **1971,** *93* (23), 6014-6026.
74. Mulliken, R. S., Lewis acids and basesa nd molecular complexe. *The Journal of Chemical Physics* **1971,** *93*, 6014-6026.
75. Gutmann, V., Coordination chemistry of certain transition-metal ions. The role of the solvent. *Coordination Chemistry Reviews* **1967,** *2* (2), 239-256.
76. Young, T., An Essay on the Cohesion of Fluids. *Philosophical Transactions of the Royal Society of London* **1805,** *95*, 65-87.
77. Bangham, D. H., The Gibbs adsorption equation and adsorption on solids. *Transactions of the Faraday Society* **1937,** *33*, 805-811.
78. Bangham, D. H.; Razouk, R. I., Adsorption and the wettability of solid surfaces. *Transactions of the Faraday Society* **1937,** *33*, 1459-1463.
79. Bangham, D. H.; Razouk, R. I., The wetting of charcoal and the nature of the adsorbed phase formed from saturated vapours. *Transactions of the Faraday Society* **1937,** *33*, 1463-1472.
80. Fox, H. W.; Zisman, W. A., The spreading of liquids on low energy surfaces. I. polytetrafluoroethylene. *Journal of Colloid Science* **1950,** *5* (6), 514-531.
81. Neumann, A. W.; Good, R. J.; Hope, C. J.; Sejpal, M., An equation-of-state approach to determine surface tensions of low-energy solids from contact angles. *Journal of Colloid and Interface Science* **1974,** *49* (2), 291-304.
82. Good, R. J., Spreading pressure and contact angle. *Journal of Colloid and Interface Science* **1975,** *52* (2), 308-313.
83. Busscher, H. J.; Van Pelt, A. W. J.; De Jong, H. P.; Arends, J., Effect of spreading pressure on surface free energy determinations by means of contact angle measurements. *Journal of Colloid and Interface Science* **1983,** *95* (1), 23-27.

84. Good, R. J., Contact angle, wetting, and adhesion: a critical review. *Journal of Adhesion Science and Technology* **1992,** *6* (12), 1269-1302.
85. Bormashenko, E.; Bormashenko, Y.; Whyman, G.; Pogreb, R.; Musin, A.; Jager, R.; Barkay, Z., Contact Angle Hysteresis on Polymer Substrates Established with Various Experimental Techniques, Its Interpretation, and Quantitative Characterization. *Langmuir* **2008,** *24* (8), 4020-4025.
86. Whyman, G.; Bormashenko, E.; Stein, T., The rigorous derivation of Young, Cassie–Baxter and Wenzel equations and the analysis of the contact angle hysteresis phenomenon. *Chemical Physics Letters* **2008,** *450* (4), 355-359.
87. Eral, H. B.; 't Mannetje, D. J. C. M.; Oh, J. M., Contact angle hysteresis: a review of fundamentals and applications. *Colloid and Polymer Science* **2013,** *291* (2), 247-260.
88. Israelachvili, J. N.; Gee, M. L., Contact angles on chemically heterogeneous surfaces. *Langmuir* **1989,** *5* (1), 288-289.
89. Brandon, S.; Marmur, A., Simulation of Contact Angle Hysteresis on Chemically Heterogeneous Surfaces. *Journal of Colloid and Interface Science* **1996,** *183* (2), 351-355.
90. Extrand, C. W., Water Contact Angles and Hysteresis of Polyamide Surfaces. *Journal of Colloid and Interface Science* **2002,** *248* (1), 136-142.
91. Extrand, C. W., Contact Angles and Hysteresis on Surfaces with Chemically Heterogeneous Islands. *Langmuir* **2003,** *19* (9), 3793-3796.
92. Nosonovsky, M., Multiscale Roughness and Stability of Superhydrophobic Biomimetic Interfaces. *Langmuir* **2007,** *23* (6), 3157-3161.
93. Nosonovsky, M.; Bhushan, B., Multiscale effects and capillary interactions in functional biomimetic surfaces for energy conversion and green engineering. *Philosophical Transactions of the Royal Society A: Mathematical, Physical and Engineering Sciences* **2009,** *367 (1893)*, 1511-1539.
94. Bormashenko, E., Wetting transitions on biomimetic surfaces. *Philosophical Transactions of the Royal Society A: Mathematical, Physical and Engineering Sciences* **2010,** *368*, 4695.
95. Bhushan, B.; Jung, Y. C., Natural and biomimetic artificial surfaces for superhydrophobicity, self-cleaning, low adhesion, and drag reduction. *Progress in Materials Science* **2011,** *56* (1), 1-108.
96. Tadmor, R., Line Energy and the Relation between Advancing, Receding, and Young Contact Angles. *Langmuir* **2004,** *20* (18), 7659-7664.
97. Cassie, A. B. D., Wettability of porous surfaces. *Transactions of the Faraday Society* **1944,** *40*, 546-550.
98. Cassie, A. B. D.; Baxter, S., Wettability of porous surfaces. *Transactions of the Faraday Society* **1944,** *40*, 546-551.
99. Cassie, A. B. D., Contact angles. *Discussions of Faraday Society* **1948,** *3*, 11-16.
100. Wenzel, R. N., Resistance of solid surfaces to wetting by water. *Industrial and Engineering Chemistry* **1936,** *28*, 988-994.
101. Theodorakis, P. E.; Müller, E. A.; Craster, R. V.; Matar, O. K., Insights into surfactant-assisted superspreading. *Current Opinion in Colloid & Interface Science* **2014,** *19* (4), 283-289.
102. Theodorakis, P. E.; Muller, E. A.; Craster, R. V.; Matar, O. K., Modelling the superspreading of surfactant-laden droplets with computer simulation. *Soft Matter* **2015,** *11* (48), 9254-9261.
103. Langmuir, I., The constitution and fundamental propertis of solids and liquids. Part I. Solids. *Journal of the American Chemical Society* **1916,** *38* (11), 2221-2295.
104. Langmuir, I., he constitution and fundamental propertis of solids and liquids. Part II. Liquids. *Journal of the American Chemical Society* **1917,** *39* (9), 1848-1906.
105. Adam, N. K., The properties and molecular structure of thin films of palmitic acid on water. Part I. *Proceedings of the Royal Society of London. Series A* **1921,** *99* (699), 336.
106. Adam, N. K., The properties and molecular structure of thin films. Part II.—Condensed films. *Proceedings of the Royal Society of London. Series A* **1922,** *101* (712), 452.
107. Blodgett, K. B., Films Built by Depositing Successive Monomolecular Layers on a Solid Surface. *Journal of the American Chemical Society* **1935,** *57* (6), 1007-1022.

108. Gibbs, J. W., On the equilibrium of heterogeneous substances. *Transactions of the Connecticut Academy of Science* **1878,** *16*, 343-524.
109. Rudzinski, W.; Everett, D. H., *Adsorption of Gases on Heterogeneous Surfaces*. Academic Press: San Diego, 1992; p 578.
110. Smith, R. R. Surface Energy Heterogeneity Mapping of Pharmaceutical Solids by Inverse Gas Chromatography. Imperial College London, London, 2015.
111. Einstein, A., On the movement of small particles suspended in a stationary liquid demanded by the molecular-kinetic theory of heat. *Annalen Der Physik* **1905,** *322* (8), 549-560.
112. Smit, B., Grand canonical Monte Carlo simulations of chain molecules: adsorption isotherms of alkanes in zeolites. *Molecular Physics* **1995,** *85* (1), 153-172.
113. Roma, F.; Ramirez-Pastor, A. J.; Riccardo, J. L., Configurational entropy for adsorbed linear species „k-mers…. *Journal of Chemical Physics* **2001,** *114* (24), 10932-10937-10932-10937.
114. Tswett, M. S., Physical chemical studies on chlorophyll adsorptions. *Berichte der Deutschen botanischen Gesellschaft* **1906,** *24*, 316-323.
115. Hamieh, T.; Schultz, J., New approach to characterise physicochemical properties of solid substrates by inverse gas chromatography at infinite dilution: II. Study of the transition temperatures of poly(methyl methacrylate) at various tacticities and of poly(methyl methacrylate) adsorbed on alumina and silica. *First International Conference on Inverse Gas Chromatography* **2002,** *969* (1–2), 27-36.
116. Dorris, G. M.; Gray, D. G., Adsorption, spreading pressure, and london force interactions of hydrocarbons on cellulose and wood fiber surfaces. *Journal of Colloid and Interface Science* **1979,** *71* (1), 93-106.
117. Dorris, G. M.; Gray, D. G., Adsorption of n-alkanes at zero surface coverage on cellulose paper and wood fibers. *Journal of Colloid and Interface Science* **1980,** *77* (2), 353-362.
118. Das, C. S.; Larson, I.; Morton, A. V. D.; Stewart, P. J., Determination of the Polar and Total Surface Energy Distributions of Particulates by Inverse Gas Chromatography. *Langmuir* **2011,** *27* (2), 521-523.
119. Coelho, M. C.; Harnby, N., Moisture bonding in powders. *Powder Technology* **1978,** *20* (2), 201-205.
120. Zeng, X. M.; Martin, G. P.; Marriott, C.; Pritchard, J., The Effects of Carrier Size and Morphology on the Dispersion of Salbutamol Sulphate after Aerosolization at Different Flow Rates. *Journal of Pharmacology and Pharmacotherapeutics* **2000,** *52*, 1211-1221.
121. Chew, N. Y. K.; Tang, P.; Chan, H.-K.; Raper, J. A., How Much Particle Surface Corrugation Is Sufficient to Improve Aerosol Performance of Powders? *Pharmaceutical Research* **2005,** *22* (1), 148-152.
122. Young, P. M.; Sung, A.; Traini, D.; Kwok, P.; Chiou, H.; Chan, H.-K., Influence of Humidity on the Electrostatic Charge and Aerosol Performance of Dry Powder Inhaler Carrier based Systems. *Pharmaceutical Research* **2007,** *24* (5), 963-970.
123. Wong, J.; Kwok, P. C. L.; Noakes, T.; Fathi, A.; Dehghani, F.; Chan, H.-K., Effect of Crystallinity on Electrostatic Charging in Dry Powder Inhaler Formulations. *Pharmaceutical Research* **2014,** *31* (7), 1656-1664.
124. Zimon, A. D., Adhesion in a Gas Medium. Sources of Adhesion. In *Adhesion of dust powder*, Consultants Bureau: New York, 1982; Vol. 2nd, pp 93-144-93-144.
125. Padmadisastra, Y.; Kennedy, R. A.; Stewart, P. J., Influence of carrier moisture adsorption capacity on the degree of adhesion of interactive mixtures. *International Journal of Pharmaceutics* **1994,** *104* (1), R1-R4.
126. Tardos, G. I.; Gupta, R., Forces generated in solidifying liquid bridges between two small particles. *Powder Technology* **1996,** *87* (2), 175-180.
127. Bika, D.; Tardos, G. I.; Panmai, S.; Farber, L.; Michaels, J., Strength and morphology of solid bridges in dry granules of pharmaceutical powders. *Scale-Up in Particle Processing* **2005,** *150* (2), 104-116.

128. Stewart, P., Particle interaction in pharmaceutical systems. *Pharmacy International* **1986,** *7*, 146-149.
129. Padmadisastra, Y.; Kennedy, R. A.; Stewart, P. J., Solid bridge formation in sulphonamide-Emdex interactive systems. *International Journal of Pharmaceutics* **1994,** *112* (1), 55-63.
130. Danilatos, G. D., Foundations of environmental scanning electron microscopy. *Advances in Electronics and Electron Physics* **1988,** *18*, 662-666.
131. Bragg, W. L.; Williams, E. J., The effect of thermal agitation on atomic arrangement in alloys. *Proceedings of the Royal Society of London. Series A* **1934,** *145* (855), 699.
132. Williams, E. J., The effect of thermal agitation on atomic arrangement in alloys-III. *Proceedings of the Royal Society of London. Series A - Mathematical and Physical Sciences* **1935,** *152* (875), 231.
133. Bragg, W. L.; Williams, E. J., The effect of thermal agitaion on atomic arrangement in alloys—II. *Proceedings of the Royal Society of London. Series A - Mathematical and Physical Sciences* **1935,** *151* (874), 540.
134. Huggins, L. M., Solutions of Long Chain Compounds. *Journal of Chemical Physics* **1941,** *9* (5), 440.
135. Flory, P. J., Thermodynamics of High Polymer Solutions. *Journal of Chemical Physics* **1941,** *9* (8), 660-661.
136. Scatchard, G., Equilibria in Non-electrolyte Solutions in Relation to the Vapor Pressures and Densities of the Components. *Chemical Reviews* **1931,** *8* (2), 321-333.
137. Hildebrand, J. H., A Critique of the Theory of Solubility of Non-Electrolytes. *Chemical Reviews* **1949,** *44* (1), 37-45.
138. Hildebrand, J. H.; Scott, R. L., The Entropy of Solution of Nonelectrolytes. *The Journal of Chemical Physics* **1952,** *20* (10), 1520-1521.
139. Saeki, S.; Namiki, T.; Tsubokawa, M.; Yamaguchi, T., Theoretical prediction of the upper and lower critical solution temperatures in aqueous polymer solutions based on the corresponding states theory. *Polymer* **1987,** *28* (1), 93-96.
140. Cheluget, E. L.; Weber, M. E.; Vera, J. H., Modifications of the Flory—Huggins—Goldstein Model for Accurate Description of Closed-Loop Phase Diagrams. *Chemical Engineering Science* **1993,** 48 (8), 1415-1426.
141. Matsuyama, A.; Tanaka, F., Theory of solvation-induced reentrant coil–globule transition of an isolated polymer chain. *The Journal of Chemical Physics* **1991,** *94* (1), 781-786.
142. Sato, T.; Matsuda, Y., Macromolecular Assemblies in Solution: Characterization by Light Scattering. *Polymer Journal* **2009,** *41*, 241.
143. Patterson, D.; Tewari, Y. B.; Schreiber, H. P.; Guillet, J. E., Application of Gas-Liquid Chromatography to the Thermodynamics of Polymer Solutions. *Macromolecules* **1971,** *4* (3), 356-359.
144. Kalikmanov, V. I., Classical Nucleation Theory. In *Nucleation Theory*, Kalikmanov, V. I., Ed. Springer Netherlands: Dordrecht, 2013; pp 17-41.
145. Pan, W.; Kolomeisky A. B.; Vekilov, P. G., Nucleation of ordered solid phases of proteins via a disordered high-density state: phenomenological approach. T*he Journal of Chemical Physics* **2005,** 122 (17), 174905.
146. Gebauer, D.; Kellermeier, M.; Gale, J. D.; Bergstrom, L.; Colfen, H., Pre-nucleation clusters as solute precursors in crystallisation. *Chemical Society Reviews* **2014,** *43* (7), 2348-2371.
147. Sleutel, M.; Lutsko, J.; Van Driessche, A. E.; Duran-Olivencia, M. A.; Maes, D., Observing classical nucleation theory at work by monitoring phase transitions with molecular precision. *Nature Communications* **2014,** 5, 5598.
148. De Yoreo, J. J.; Gilbert, P. U. P. A.; Sommerdijk, N. A. J. M.; Penn, R. L.; Whitelam, S.; Joester, D.; Zhang, H.; Rimer, J. D.; Navrotsky, A.; Banfield, J. F.; Wallace, A. F.; Michel, F. M.; Meldrum, F. C.; Cölfen, H.; Dove, P. M., Crystallization by particle attachment in synthetic, biogenic, and geologic environments. *Science* **2015,** *349* (6247), aaa-6760.
149. Evans, J. S., Aragonite-associated biomineralization proteins are disordered and contain interactive motifs. *Bioinformatics* **2012,** *28* (24), 3182-3185.

150. Evans, J. S., "Liquid-like" biomineralization protein assemblies: a key to the regulation of non-classical nucleation. *Crystal Engineering Communications* **2013,** *15* (42), 8388-8394.
151. Singha, S. K.; Das, P. K.; Maiti, B., Inclusion of line tension effect in classical nucleation theory for heterogeneous nucleation: A rigorous thermodynamic formulation and some unique conclusions. *The Journal of Chemical Physics* **2015,** *142* (10), 104706.
152. McGraw, R. L.; Winkler, P. M.; Wagner, P. E., Temperature Dependence in Heterogeneous Nucleation with Application to the Direct Determination of Cluster Energy on Nearly Molecular Scale. *Scientific Reports* **2017,** *7* (1), 16896.
153. Delmas, T.; Shah, U. V.; Roberts, M. M.; Williams, D. R.; Heng, J. Y. Y., Crystallisation of the orthorhombic form of acetaminophen: Combined effect of surface topography and chemistry. *Powder Technology* **2013,** *236*, 24-29.
154. Shah, U. V.; Amberg, C.; Diao, Y.; Yang, Z.; Heng, J. Y. Y., Heterogeneous nucleants for crystallogenesis and bioseparation. *Current Opinion in Chemical Engineering* **2015,** *8*, 69-75.
155. Shah, U. V.; Parambil, J. V.; Williams, D. R.; Hinder, S. J.; Heng, J. Y. Y., Preparation and characterisation of 3D nanotemplates for protein crystallisation. *Powder Technology* **2015,** *282*, 10-18.
156. Lapidot, T.; Heng, J. Y. Y., Functionalized Mesoporous Silica for the Control of Crystallization Fouling. *Industrial & Engineering Chemistry Research* **2016,** *55* (44), 11475-11479.
157. Erdemir, D.; Lee, A. Y.; Myerson, A. S., Nucleation of Crystals from Solution: Classical and Two-Step Models. *Accounts of Chemical Research* **2009,** *42* (5), 621-629.
158. Sun, C. C.; Sun, W.; Price, S.; Hughes, C.; Ter Horst, J.; Veesler, S.; Lewtas, K.; Myerson, A.; Pan, H.; Coquerel, G.; van den Ende, J.; Meekes, H.; Mazzotti, M.; Rosbottom, I.; Taulelle, F.; Black, S.; Mackenzie, A.; Janbon, S.; Vekilov, P.; Threlfall, T.; Turner, T.; Back, K.; Cuppen, H.; Toroz, D.; Sefcik, J.; Lovelock, J.; Hammond, R.; Candoni, N.; Simone, E.; Ward, M.; Bertran, C. A.; Vetter, T.; Sear, R.; De Yoreo, J.; Davey, R.; Anwar, J.; Santiso, E.; Wu, D. T.; Roberts, K.; Peters, B.; Schroeder, S.; Jones, F.; Rasmuson, A.; Cölfen, H.; Zeglinski, J.; Salvalaglio, M., Solvent and additive interactions as determinants in the nucleation pathway: general discussion. *Faraday Discussions* **2015,** *179* (0), 383-420.
159. Salvalaglio, M.; Mazzotti, M.; Parrinello, M., Urea homogeneous nucleation mechanism is solvent dependent. *Faraday Discussions* **2015,** *179* (0), 291-307.
160. Yamazaki, T.; Kimura, Y.; Vekilov, P. G.; Furukawa, E.; Shirai, M.; Matsumoto, H.; Van Driessche, A. E. S.; Tsukamoto, K., Two types of amorphous protein particles facilitate crystal nucleation. *Proceedings of the National Academy of Sciences* **2017,** *114* (9), 2154.
161. Burton, W. K.; Cabrera, N.; Frank, F. C., The Growth of Crystals and the Equilibrium Structure of their Surfaces. *Philosophical Transactions of the Royal Society of London. Series A, Mathematical and Physical Sciences* **1951,** *243* (866), 299-358.
162. Frank, F. C., Crystal growth and dislocations. *Advances in Physics* **1952,** *1* (1), 91-109.
163. Chernov, A. A., Reviews of Topical Problems: the Spiral Growth of Crystals. *Soviet Physics Uspekhi* **1961,** *4* (1).
164. Chernov, A. A., *Modern Crystallography III: Crystal Growth*. 1984; Vol. 36.
165. Reviakine, I.; Georgiou, D. K.; Vekilov, P. G., Capillarity Effects on Crystallization Kinetics: Insulin. *Journal of the American Chemical Society* **2003,** *125* (38), 11684-11693.
166. Vekilov, P. G.; Chernov, A. A., The Physics of Protein Crystallization. *Solid State Physics* **2003,** *57*, 1-147.
167. Rimer, J. D.; An, Z.; Zhu, Z.; Lee, M. H.; Goldfarb, D. S.; Wesson, J. A.; Ward, M. D., Crystal Growth Inhibitors for the Prevention of l-Cystine Kidney Stones Through Molecular Design. *Science* **2010,** *330* (6002), 337.
168. Boek, E. S.; Briels, W. J.; van Eerden, J.; Feil, D., Molecular-dynamics simulations of interfaces between water and crystalline urea. *The Journal of Chemical Physics* **1992,** *96* (9), 7010-7018.
169. Boek, E. S.; Briels, W. J.; Feil, D., Interfaces between a Saturated Aqueous Urea Solution and Crystalline Urea: A Molecular Dynamics Study. *The Journal of Physical Chemistry* **1994,** *98* (6), 1674-1681.

170. Liu, X. Y.; Boek, E. S.; Briels, W. J.; Bennema, P., Analysis of morphology of crystals based on identification of interfacial structure. *The Journal of Chemical Physics* **1995,** *103* (9), 3747-3754.
171. Gilmer, G. H.; Bennema, P., Simulation of Crystal Growth with Surface Diffusion. *Journal of Applied Physics* **1972,** *43* (4), 1347-1360.
172. Furukawa, Y., Snow and ice crystals. *Physics Today* **2007,** *60* (12), 70-71.
173. Berliner, J. F. T., Crystal Urea: Industrial Development and Properties. *Industrial & Engineering Chemistry* **1936,** *28* (5), 517-522.
174. Bisker-Leib, V.; Doherty, M. F., Modeling the Crystal Shape of Polar Organic Materials: Prediction of Urea Crystals Grown from Polar and Nonpolar Solvents. *Crystal Growth & Design* **2001,** *1* (6), 455-461.
175. Bisker-Leib, V.; Doherty, M. F., Modeling Crystal Shape of Polar Organic Materials: Applications to Amino Acids. *Crystal Growth & Design* **2003,** *3* (2), 221-237.
176. Salvalaglio, M.; Vetter, T.; Mazzotti, M.; Parrinello, M., Controlling and Predicting Crystal Shapes: The Case of Urea. *Angewandte Chemie International Edition* **2013,** *52* (50), 13369-13372.
177. Li, J.; Tilbury, C. J.; Joswiak, M. N.; Peters, B.; Doherty, M. F., Rate Expressions for Kink Attachment and Detachment During Crystal Growth. *Crystal Growth & Design* **2016,** *16* (6), 3313-3322.
178. Tilbury, C. J.; Green, D. A.; Marshall, W. J.; Doherty, M. F., Predicting the Effect of Solvent on the Crystal Habit of Small Organic Molecules. *Crystal Growth & Design* **2016,** *16* (5), 2590-2604.
179. Li, J.; Tilbury, C. J.; Kim, S. H.; Doherty, M. F., A design aid for crystal growth engineering. *Progress in Materials Science* **2016,** *82*, 1-38.
180. Nosonovsky, M.; Ramachandran, R., Geometric Interpretation of Surface Tension Equilibrium in Superhydrophobic Systems. *Entropy* **2015,** *17* (7).
181. Shah, U. V.; Olusanmi, D.; Narang, A. S.; Hussain, M. A.; Gamble, J. F.; Tobyn, M. J.; Heng, J. Y. Y., Effect of crystal habits on the surface energy and cohesion of crystalline powders. *International Journal of Pharmaceutics* **2014,** *472* (1–2), 140-147.
182. Sudha, C.; Srinivasan, K., Understanding the effect of solvent polarity on the habit modification of monoclinic paracetamol in terms of molecular recognition at the solvent crystal/interface. *Crystal Research and Technology* **2014,** *49* (11), 865-872.
183. Toroz, D.; Hammond, R. B.; Roberts, K. J.; Harris, S.; Ridley, T., Molecular dynamics simulations of organic crystal dissolution: The lifetime and stability of the polymorphic forms of para-amino benzoic acid in aqueous environment. *Proceedings of 17th International Conference on Crystal Growth and Epitaxy (ICCGE-17)* **2014,** *401*, 38-43.
184. Toroz, D.; Rosbottom, I.; Turner, T. D.; Corzo, D. M. C.; Hammond, R. B.; Lai, X.; Roberts, K. J., Towards an understanding of the nucleation of alpha-para amino benzoic acid from ethanolic solutions: a multi-scale approach. *Faraday Discussions* **2015,** *179,* 79-114.
185. Cruz-Cabeza, A. J.; Davey, R. J.; Sachithananthan, S. S.; Smith, R.; Tang, S. K.; Vetter, T.; Xiao, Y., Aromatic stacking – a key step in nucleation. *Chemical Communications* **2017,** *53* (56), 7905-7908.
186. Black, J. F. B.; Cardew, P. T.; Cruz-Cabeza, A. J.; Davey, R. J.; Gilks, S. E.; Sullivan, R. A., Crystal nucleation and growth in a polymorphic system: Ostwald's rule, p-aminobenzoic acid and nucleation transition states. *CrystEngComm* **2018,** *20* (6), 768-776.
187. Martinez, C. R.; Iverson, B. L., Rethinking the term "pi-stacking". *Chemical Science* **2012,** *3* (7), 2191-2201.
188. Cabrera, N.; Levine, M. M.; Plaskett, J. S., Hollow Dislocations and Etch Pits. *Physical Review* **1954,** *96* (4), 1153-1153.
189. Vermilyea, D. A., On the formation of etch pits at dislocations. *Acta Metall Matter.* **1958,** *6* (5), 381-382.
190. Kuvadia, Z. B.; Doherty, M. F., Effect of Structurally Similar Additives on Crystal Habit of Organic Molecular Crystals at Low Supersaturation. *Crystal Growth & Design* **2013,** *13* (4), 1412-1428.
191. Sizemore, J. P.; Doherty, M. F., A New Model for the Effect of Molecular Imposters on the Shape of Faceted Molecular Crystals. *Crystal Growth and Design* **2009,** *9* (6), 2637-2645.

192. Hammond, R. B.; Ramachandran, V.; Roberts, K. J., Molecular modelling of the incorporation of habit modifying additives: α-glycine in the presence of l-alanine. *CrystEngComm* **2011,** *13* (15), 4935-4944.
193. Chow, A. H. L.; Chow, P. K. K.; Zhongshan, W.; Grant, D. J. W., Modification of acetaminophen crystals: influence of growth in aqueous solutions containing p-acetoxyacetanilide on crystal properties. International Journal of Pharmaceutics **1985,** 24, 239-258.
194. Poloni, L. N.; Ward, M. D., The Materials Science of Pathological Crystals. *Chemistry of Materials* **2014,** *26* (1), 477-495.
195. Rimer, J. D.; Kolbach-Mandel, A. M.; Ward, M. D.; Wesson, J. A., The role of macromolecules in the formation of kidney stones. *Urolithiasis* **2017,** *45* (1), 57-74.
196. Poloni, L. N.; Ford, A. P.; Ward, M. D., Site Discrimination and Anisotropic Growth Inhibition by Molecular Imposters on Highly Dissymmetric Crystal Surfaces. *Crystal Growth & Design* **2016,** *16* (9), 5525-5541.
197. Poloni, L. N.; Zhong, X.; Ward, M. D.; Mandal, T., Best Practices for Real-Time in Situ Atomic Force and Chemical Force Microscopy of Crystals. *Chemistry of Materials* **2017,** *29* (1), 331-345.
198. Yang, X.; Qian, G.; Duan, X.; Zhou, X., Impurity Effect of l-Valine on l-Alanine Crystal Growth. *Crystal Growth & Design* **2013,** *13* (3), 1295-1300.
199. Weissbuch, I.; Leiserowitz, L., Interplay Between Malaria, Crystalline Hemozoin Formation, and Antimalarial Drug Action and Design. *Chemical Reviews* **2008,** *108* (11), 4899-4914.
200. Fong, K. Y.; Wright, D. W., Hemozoin and antimalarial drug discovery. *Future medicinal chemistry* **2013,** *5* (12), 1437-1450.
201. Olafson, K. N.; Ketchum, M. A.; Rimer, J. D.; Vekilov, P. G., Molecular Mechanisms of Hematin Crystallization from Organic Solvent. *Crystal Growth & Design* **2015,** *15* (11), 5535-5542.
202. Vekilov, P. G.; Rimer, J. D.; Olafson, K. N.; Ketchum, M. A., Lipid or aqueous medium for hematin crystallization? *CrystEngComm* **2015,** *17* (41), 7790-7800.
203. Ketchum, M. A.; Lee, A. M.; Vekilov, P. G.; Rimer, J. D., Biomimetic Assay for Hematin Crystallization Inhibitors: A New Platform To Screen Antimalarial Drugs. *Crystal Growth & Design* **2017,** *17* (1), 197-206.
204. Colfen, H., Double-hydrophilic block copolymers: synthesis and application as novel surfactants and crystal growth modifiers. *Macromolecule Rapid Communications* **2001,** *22* (4), 219-252.
205. Kuldipkumar, A.; Tan, Y. T. F.; Goldstein, M.; Nagasaki, Y.; Zhang, G. G. Z.; Kwon, G. S., Amphiphilic Block Copolymer as a Crystal Habit Modifier. *Crystal Growth & Design* **2005,** *5* (5), 1781-1785.
206. Öner, M.; Norwig, J.; Meyer, W. H.; Wegner, G., Control of ZnO Crystallization by a PEO-b-PMAA Diblock Copolymer. *Chemistry of Materials* **1998,** *10* (2), 460-463.
207. Aamir, E.; Nagy, Z. K.; Rielly, C. D., Optimal seed recipe design for crystal size distribution control for batch cooling crystallisation processes. 2010; Vol. 65, pp 3602-3614.
208. Nagy, Z. K.; Braatz, R. D., Advances and New Directions in Crystallization Control. *Annual Review of Chemical and Biomolecular Engineering* **2012,** *3* (1), 55-75.
209. Chung, S. H.; Ma, D. L.; Braatz, R. D., Optimal seeding in batch crystallization. *The Canadian Journal of Chemical Engineering* **1999,** *77* (3), 590-596.
210. Gadewar, S. B.; Hofmann, H. M.; Doherty, M. F., Evolution of Crystal Shape. *Crystal Growth & Design* **2004,** *4* (1), 109-112.
211. Anwar, J.; Zahn, D., Uncovering Molecular Processes in Crystal Nucleation and Growth by Using Molecular Simulation. *Angewandte Chemie International Edition* **2011,** *50* (9), 1996-2013.
212. Köster, U., Surface crystallization of metallic glasses. *Materials Science and Engineering* **1988,** *97*, 233-239.
213. Diaz-Mora, N.; Zanotto, E. D.; Hergt, R.; Müller, R., Surface crystallization and texture in cordierite glasses. *Journal of Non-Crystalline Solids* **2000,** *273* (1), 81-93.

214. Yoshioka, M.; Hancock, B. C.; Zografi, G., Crystallization of Indomethacin from the Amorphous State below and above Its Glass Transition Temperature. *Journal of Pharmaceutical Sciences* **1994,** *83* (12), 1700-1705.
215. Wu, T.; Yu, L., Surface Crystallization of Indomethacin Below T_g. *Pharmaceutical Research* **2006,** *23* (10), 2350-2355.
216. Zhu, L.; Wong, L.; Yu, L., Surface-Enhanced Crystallization of Amorphous Nifedipine. *Molecular Pharmaceutics* **2008,** *5* (6), 921-926.
217. Wu, T.; Yu, L., Origin of Enhanced Crystal Growth Kinetics near T_g Probed with Indomethacin Polymorphs. *The Journal of Physical Chemistry B* **2006,** *110* (32), 15694-15699.
218. Musumeci, D.; Powell, C. T.; Ediger, M. D.; Yu, L., Termination of Solid-State Crystal Growth in Molecular Glasses by Fluidity. *Physical Chemistry Letters* **2014,** *5*, 1705-1710.
219. Chandler, D., Interfaces and the driving force of hydrophobic assembly. *Nature* **2005,** *437*, 640-647.
220. Prasad, K. V. R.; Ristic, R. I.; Sheen, D. B.; Sherwood, J. N., Dissolution kinetics of paracetamol single crystals. *International Journal of Pharmaceutics* **2002,** 238, 29-41.
221. Stillinger, H. F., Structure in aqueous solutions of nonpolar solutes from the standpoint of scaled-particle theory. *Journal of Solution Chemistry* **1973,** *2* (2/3), 141-158.
222. Lippold, B. C.; Ohm, A., Correlation between wettability and dissolution rate of pharmaceutical powders. *International Journal of Pharmaceutics* **1986,** 28, 67-74.
223. Modi, S. R.; Dantuluri, A. K. R.; Puri, V.; Pawar, Y. B.; Nandekar, P.; Sangamwar, A. T.; Perumalla, S. R.; Sun, C. C.; Bansal, A. K., Impact of Crystal Habit on Biopharmaceutical Performance of Celecoxib. *Crystal Growth and Design* **2013,** *13*, 2824-2832.
224. Olusanmi, D.; Roberts, K. J.; Ghadiri, M.; Ding, Y., The breakage behaviour of Aspirin under quasi-static indentation and single particle impact loading: Effect of crystallographic anisotropy. *International Journal of Pharmaceutics* **2011,** *411* (1), 49-63.
225. Varughese, S.; Kiran, M. S. R. N.; Solanko, K. A.; Bond, A. D.; Ramamurty, U.; Desiraju, G. R., Interaction anisotropy and shear instability of aspirin polymorphs established by nanoindentation. *Chemical Science* **2011,** *2* (11), 2236-2242.
226. Varughese, S.; Kiran, M. S. R. N.; Ramamurty, U.; Desiraju, G. R., Nanoindentation as a Probe for Mechanically-Induced Molecular Migration in Layered Organic Donor–Acceptor Complexes. *Chemistry – An Asian Journal* **2012,** *7* (9), 2118-2125.
227. Chikhalia, V.; Forbes, R. T.; Storey, R. A.; Ticehurst, M., The effect of crystal morphology and mill type on milling induced crystal disorder. 2006; Vol. 27, pp 19-26.
228. Chamarthy, S. P.; Pinal, R., The nature of crystal disorder in milled pharmaceutical materials. *Frontiers in Formulation Science (Formula V - 2007)* **2008,** 331, 68-75.
229. Shah, U. V.; Wang, Z.; Olusanmi, D.; Narang, A. S.; Hussain, M. A.; Tobyn, M. J.; Heng, J. Y. Y., Effect of milling temperatures on surface area, surface energy and cohesion of pharmaceutical powders. *International Journal of Pharmaceutics* **2015,** *495* (1), 234-240.
230. Adhiyaman, R.; Basu, S. K., Crystal modification of dipyridamole using different solvents and crystallization conditions. *International Journal of Pharmaceutics* **2006,** *321* (1), 27-34.
231. Chow, A. H. L.; Hsia, C. K.; Gordon, J. D.; Young, J. W. M.; Vargha-Butler, E. I., Assessment of wettability and its relationship to the intrinsic dissolution rate of doped phenytoin crystals. *International Journal of Pharmaceutics* **1995,** *126* (1), 21-28.
232. Fukumori, Y.; Fukuda, T.; Hanyu, Y.; Takeuchi, Y.; Osako, Y., Coating of Pharmaceutical Powders by Fluidized Bed Process. I. Aqueous Enteric Coating with Methacrylic Acid-Ethylacrylate Copolymer and the Dissolution Behavior of Products. *Chemical&Pharmaceutical Bulletin* **1987,** *35* (7), 2949-2957.
233. Tay, T.; Das, S.; Stewart, P., Magnesium stearate increases salbutamol sulphate dispersion: What is the mechanism? *International journal of pharmaceutics* **2010,** *383* (1–2), 62-69.
234. Tay, T.; Morton, D. A. V.; Gengenbach, T. R.; Stewart, P. J., Dissolution of a poorly water-soluble drug dry coated with magnesium and sodium stearate. *European Journal of Pharmaceutics and Biopharmaceutics* **2012,** *80* (2), 443-452.

235. Karde, V.; Ghoroi, C., Influence of surface modification on wettability and surface energy characteristics of pharmaceutical excipient powders. *International Journal of Pharmaceutics* **2014,** *475* (1–2), 351-363.
236. Karde, V.; Panda, S.; Ghoroi, C., Surface modification to improve powder bulk behavior under humid conditions. *Powder Technology* **2015,** *278*, 181-188.
237. Theodorakis, P. E.; Müller, E. A.; Craster, R. V.; Matar, O. K., Superspreading: Mechanisms and Molecular Design. *Langmuir* **2015,** *31* (8), 2304-2309.
238. Rodriguez-Hornedo, N.; Murphy, D., Surfactant-facilitated crystallization of dihydrate carbamazepine during dissolution of anhydrous polymorph. *Journal of Pharmaceutical Sciences* **2004,** *93* (2), 449-460.
239. Kao, C.-C.; Chen, S.-C.; Sheu, M.-T., Lag time method to delay drug release to various sites in the gastrointestinal tract. *Journal of Controlled Release* **1997,** *44* (2–3), 263-270.
240. Zema, L.; Maroni, A.; Foppoli, A.; Palugan, L.; Sangalli, M. E.; Gazzaniga, A., Different HPMC Viscosity Grades as Coating Agents for an Oral Time and/or Site-Controlled Delivery System: An Investigation into the Mechanisms Governing Drug Release. *Journal of Pharmaceutical Sciences* **2007,** *96* (6), 1527-1536.
241. Jallo, L. J.; Chen, Y.; Bowen, J.; Etzler, F.; Dave, R., Prediction of Inter-particle Adhesion Force from Surface Energy and Surface Roughness. *Journal of Adhesion Science and Technology* **2011,** *25* (4-5), 367-384.
242. von Helmholtz, R., Untersuchungen über Dämpfe und Nebel, besonders über solche von Lösungen. *Annalen der Physik.* **1886,** *263* (4), 508-543.
243. Langmuir, I., The adsorption of gases on plane surfaces of glass, mica and platinum. *Journal of the American Chemical Society* **1918,** *40* (9), 1361-1403.
244. Vrentas, J. S.; Vrentas, C. M., Sorption in glassy polymers. *Macromolecules* **1991,** *24* (9), 2404-2412.
245. Berens, A. R.; Hopfenberg, H. B., Diffusion and relaxation in glassy polymer powders: 2. Separation of diffusion and relaxation parameters. *Polymer* **1978,** *19* (5), 489-496.
246. Garner, W. E., *Chemistry of the Solid State*. Butterworths Scientific Publications: London, 1956.
247. Ostwald, W., Studdien über die Bildung und Umwandlung fester Körper. *Zeitschrift für Physikalische Chemie* **1897,** *22*, 289-330.
248. Newell, H. E.; Buckton, G.; Butler, D. A.; Thielmann, F.; Williams, D. R., The use of inverse phase gas chromatography to study the change of surface energy of amorphous lactose as a function of relative humidity and the processes of collapse and crystallisation. *International Journal of Pharmaceutics* **2001,** *217* (1), 45-56.
249. Newell, H. E.; Buckton, G., Inverse gas chromatography: investigating whether the technique preferentially probes high energy sites for mixtures of crystalline and amorphous lactose. *Pharmaceutical Research* **2004,** *21*, 1440-1444.
250. Yang, J.; Sliva, A.; Banerjee, A.; Dave, R. N.; Pfeffer, R., Dry particle coating for improving the flowability of cohesive powders. *Powder Technology* **2005,** *158* (1–3), 21-33.
251. Chen, Y.; Jallo, L.; Quintanilla, M. A. S.; Dave, R., Characterization of particle and bulk level cohesion reduction of surface modified fine aluminum powders. *Colloids and Surfaces A: Physicochemical and Engineering Aspects* **2010,** *361* (1), 66-80.
252. Hersey, J. A., Ordered mixing: A new concept in powder mixing practice. *Powder Technology* **1975,** *11* (1), 41-44.
253. Salter, G. F.; Farnish, R. J.; Bradley, M. S. A.; Burnett, A. J., Segregation of binary mixtures of particles during the filling of a two-dimensional representation of a hopper. *Journal of Process and Mechanical Engineering* **2000,** *214* (3), 197-208.
254. Deng, T.; Paul, K. A.; Bradley, M. S. A.; Immins, L.; Preston, C.; Scott, J. F.; Welfare, E. H., Investigations on air induced segregation of pharmaceutical powders and effect of material flow functions. *Powder Technology* **2010,** *203* (2), 354-358.

255. Ho, R.; Muresan, A. S.; Hebbink, G. A.; Heng, J. Y. Y., Influence of fines on the surface energy heterogeneity of lactose for pulmonary drug delivery. *International Journal of Pharmaceutics* **2010,** *388* (1–2), 88-94.
256. Jones, M. D.; Price, R., The Influence of Fine Excipient Particles on the Performance of Carrier-Based Dry Powder Inhalation Formulations. *Pharmaceutical Research* **2006,** *23* (8), 1665-1674.
257. Pfeffer, R.; Dave, R. N.; Wei, D.; Ramlakhan, M., Synthesis of engineered particulates with tailored properties using dry particle coating. *Granulation and Coating of Fine Powders* **2001,** *117* (1–2), 40-67.
258. Zhou, Q. T.; Qu, L.; Larson, I.; Stewart, P. J.; Morton, D. A. V., Improving aerosolization of drug powders by reducing powder intrinsic cohesion via a mechanical dry coating approach. *International Journal of Pharmaceutics* **2010,** *394* (1–2), 50-59.
259. Das, S. C.; Zhou, Q.; Morton, D. A. V.; Larson, I.; Stewart, P. J., Use of surface energy distributions by inverse gas chromatography to understand mechanofusion processing and functionality of lactose coated with magnesium stearate. *European Journal of Pharmaceutical Sciences* **2011,** *43* (4), 325-333.
260. Zhou, Q. T.; Armstrong, B.; Larson, I.; Stewart, P. J.; Morton, D. A. V., Understanding the influence of powder flowability, fluidization and de-agglomeration characteristics on the aerosolization of pharmaceutical model powders. *European Journal of Pharmaceutical Sciences* **2010,** *40* (5), 412-421.
261. Polizzi, M.; Langdon, B. A.; Beach, L. E.; Mullarney, M. P., Applying dry powder coatings. *Pharmaceutical Technology* **2011,** *35* (10), 94-102.
262. Kwan, C. C.; Ghadiri, M.; Papadopoulos, D. G.; Bentham, A. C., The Effects of Operating Conditions on the Milling of Microcrystalline Cellulose. *Chemical Engineering and Processing: Process Intensification* **2003,** *26* (2), 185-190.
263. Kwan, C. C.; Chen, Y. Q.; Ding, Y. L.; Papadopoulos, D. G.; Bentham, A. C.; Ghadiri, M., Development of a novel approach towards predicting the milling behaviour of pharmaceutical powders. *European Journal of Pharmaceutical Sciences* **2004,** *23* (4–5), 327-336.
264. Heng, J. Y. Y.; Thielmann, F.; Williams, D. R., The Effects of Milling on the Surface Properties of Form I Paracetamol Crystals. *Pharmaceutical Research* **2006,** *23* (8), 1918-1927.
265. York, P.; Ticehurst, M. D.; Osborn, J.; Roberts, R.; Rowe, R., Characterization of surface energetics of milled DL propranolol hydrochloride using inverse gas chromatography and molecular modeling. *International Journal of Pharmaceutics* **1998,** *174* (1793-1804).
266. Otte, A.; Carvajal, M. T., Assessment of Milling-Induced Disorder of Two Pharmaceutical Compounds. *Journal of Pharmaceutical Sciences* **2010,** *100* (5), 1793-1804.
267. Feeley, J. C.; York, P.; Sumby, B. S.; Dicks, H., Determination of surface properties and flow characteristics of salbutamol sulphate, before and after micronisation. *International Journal of Pharmaceutics* **1998,** *172* (1–2), 89-96.
268. Grimsey, I.; Feeley, P.; York, P., Analysis of the surface energyof pharmaceutical powders by inverse gas chromatography. *Journal of Pharmaceutical Sciences* **2002,** *91*, 571-583.
269. Gamble, J. F.; Leane, M.; Olusanmi, D.; Tobyn, M.; Šupuk, E.; Khoo, J.; Naderi, M., Surface energy analysis as a tool to probe the surface energy characteristics of micronized materials—A comparison with inverse gas chromatography. *International Journal of Pharmaceutics* **2012,** *422* (1–2), 238-244.
270. Braun, J. M.; Guillet, J. E., Determination of crystallinity of olefin copolymers and polyolefin powders by inverse gas chromatography. *Polymer Chemistry* **1975,** *13* (5), 1119-1131.
271. Yla-Maihaniemi, P. P.; Heng, J. Y. Y.; Thielmann, F.; Williams, D. R., Inverse Gas Chromatographic Method for Measuring the Dispersive Surface Energy Distribution for Particulates. *Langmuir* **2008,** *24*, 9551-9557.
272. Tan, G.; Qu, L.; Morton, D. A. V.; Larson, I., A strategy to evaluate the surface energy of high packing efficiency fine powders via inverse gas chromatography. *Powder Technology* **2017,** *320*, 470-473.

273. Hardy, W. B., The spreading of fluids on glass. *Philosophical Magazine* **1919,** *38* (223), 49-55.
274. Hardy, W. B., The Tension of Composite Fluid Surfaces and the Mechanical Stability of Films of Fluid. *Proceedings of the Royal Society of London. Series A, Mathematical and Physical Sciences* **1912,** *86* (591), 610-635.
275. Hardy, W. B., The Tension of Composite Fluid Surfaces. No. II. *Proceedings of the Royal Society of London. Series A, Mathematical and Physical Sciences* **1913,** *88* (603), 313-333.
276. Hardy, W. B., The Influence of Chemical Constitution upon Interfacial Tension. *Proceedings of the Royal Society of London. Series A, Mathematical and Physical Sciences* **1913,** *88* (603), 303-313.
277. Hirasaki, G. J., Structural interactions in the wetting and spreading of van der Waals fluids. *Journal of Adhesion Science and Technology* **1993,** *7* (3), 285-322.
278. Israelachvili, J. N., *Intermolecular and Surface Forces*. 3rd ed.; Academic Press: Oxford, 2011.
279. Domingo-García, M.; López-Garzón, F. J.; López-Garzón, R.; Moreno-Castilla, C., Gas chromatographic determination of adsorption isotherms, spreading pressures, london force interactions and equations of state for n-alkanes on graphite and carbon blacks. *Journal of Chromatography A* **1985,** *324*, 19-28.
280. Vukov, A. J.; Gray, D. G., Properties of Carbon Fiber Surfaces. In *Inverse Gas Chromatography*, 1st ed.; American Chemical Society: Washington D.C., 1989; Vol. 391, pp 168-184.
281. Lee, H. L.; Luner, P., Adsorption characteristics of alkylketene dimer sized papers determined by inverse gas chromatography at finite concentration. 1991; Vol. 146, pp 195-205.
282. Parambil, J. V.; Poornachary, S. K.; Hinder, S. J.; Tan, R. B. H.; Heng, J. Y. Y., Establishing template-induced polymorphic domains for API crystallisation: the case of carbamazepine. *CrystEngComm* **2015,** *17* (33), 6384-6392.
283. Hammond, C., *Intoduction to Crystallography*. Oxford University Press: Oxford, 1992.
284. Grzesiak, A. L.; Lang, M.; Kibum, K.; Matzger, A. J., Comparison of the Four Anhydrous Polymorphs of Carbamazepine and the Crystal Structure of Form I. *Journal of Pharmaceutical Sciences* **2003,** *92* (11), 2260-2271.
285. Choi, P.; Kavassalis, T. A.; Rudin, A., Estimation of Hansen Solubility Parameters for (Hydroxyethyl) and (Hydroxypropyl) cellulose through Molecular Simulation. *Industrial & Engineering Chemistry Research* **1994,** *33* (12), 3154-3159.
286. Hansen, C. M.; Just, L., Prediction of Environmental Stress Cracking in Plastics with Hansen Solubility Parameters. *Industrial & Engineering Chemistry Research* **2001,** *40* (1), 21-25.
287. Lindvig, T.; Michelsen, M. L.; Kontogeorgis, G. M., A Flory–Huggins model based on the Hansen solubility parameters. *Fluid Phase Equilibria* **2002,** *203* (1), 247-260.
288. Belmares, M.; Blanco, M.; Goddard, W. A.; Ross, R. B.; Caldwell, G.; Chou, S. H.; Pham, J.; Olofson, P. M.; Thomas, C., Hildebrand and Hansen solubility parameters from Molecular Dynamics with applications to electronic nose polymer sensors. *Journal of Computational Chemistry* **2004,** *25* (15), 1814-1826.
289. Gupta, J.; Nunes, C.; Vyas, S.; Jonnalagadda, S., Prediction of Solubility Parameters and Miscibility of Pharmaceutical Compounds by Molecular Dynamics Simulations. *The Journal of Physical Chemistry B* **2011,** *115* (9), 2014-2023.
290. Hancock, B. C.; York, P.; Rowe, R. C., The use of solubility parameters in pharmaceutical dosage form design. *International Journal of Pharmaceutics* **1997,** *148* (1), 1-21.
291. Mohammad, M. A.; Alhalaweh, A.; Velaga, S. P., Hansen solubility parameter as a tool to predict cocrystal formation. *International Journal of Pharmaceutics* **2011,** *407* (1), 63-71.
292. Chomcharn, N.; Xanthos, M., Properties of aspirin modified enteric polymer prepared by hot-melt mixing. *International Journal of Pharmaceutics* **2013,** *450* (1), 259-267.
293. Thipparaboina, R.; Kumar, D.; Chavan, R. B.; Shastri, N. R., Multidrug co-crystals: towards the development of effective therapeutic hybrids. *Drug Discovery Today* **2016,** *21* (3), 481-490.
294. Puig, C. C.; Meijer, H. E. H.; Michels, M. A. J.; Segeren, L. H. G. J.; Vancso, G. J., Characterization of Glass Transition Temperature and Surface Energy of Bituminous Binders by Inverse Gas Chromatography. *Energy & Fuels* **2004,** *18* (1), 63-67.

295. Jadhav, N. R.; Gaikwad, V. L.; Nair, K.; Kadam, H., Glass transition temperature: Basics and application in pharmaceutical sector. *Asian Journal of Pharmaceutics* **2009,** *3*, 82-89.
296. Saito, H.; Tsutsumi, D.; Inoue, T., Temperature Dependence of the Flory Interaction Parameter in a Single-Phase Mixture of Poly(hydroxy ether of bisphenol-A) and Poly(ether sulfone). *Polymer Journal* **1990,** *22*, 128.
297. Galilei, G., *Discorsi e dimostrazioni matematiche intorno a due nuove scienze attinenti la meccanica e i movimenti locali* Simeoni Arti Grafiche: Verona, 2011.
298. Mittal, K. L., Contact angle, wettability and adhesion. Scrivener Publishing: 2003; pp 87-97.
299. Nosonovsky, M.; Bhushan, B., W Why re-entrant surface topography is needed for robust oleophobicity. *Philosophical Transactions of the Royal Society A: Mathematical, Physical and Engineering Sciences* **2016,** *374* (2073).
300. Bonn, D.; Bertrand, E.; Shahidzahed, N.; Ragil, K.; Dobbs, H. T.; Posazhennikova, A. I.; Broseta, D.; Meunier, J.; Indekeu, J. O., Complex wetting phenomena in liquid mixtures: frustrated-complete wetting and competing intermolecular forces. *Journal of Physics: Condensed Matter* **2001,** *13*, 4903-4914.
301. Sun, T.; King, H. E., Aggregation Behavior in the Semidilute Poly(N-vinyl-2-pyrrolidone)/Water System. *Macromolecules* **1996,** *29* (9), 3175-3181.
302. Kjøniksen, A.-L.; Iversen, C.; Nyström, B.; Nakken, T.; Palmgren, O., Light Scattering Study of Semidilute Aqueous Systems of Chitosan and Hydrophobically Modified Chitosans. *Macromolecules* **1998,** *31* (23), 8142-8148.
303. Lee, H. J.; Won, J.; Lee, H.; Kang, Y. S., Solution properties of poly(amic acid)–NMP containing LiCl and their effects on membrane morphologies. *Journal of Membrane Science* **2002,** *196* (2), 267-277.
304. Sutherland, E.; Mercer, S. M.; Everist, M.; Leaist, D. G., Diffusion in solutions of micelles. What does dynamic light scattering measure? *Journal of Chemical & Engineering Data* **2008,** *54* (2), 272-278.
305. Mortazavi, M.; Nosonovsky, M., Adhesion, Wetting, and Superhydrophobicity of Polymeric Surfaces. In *Polymer Adhesion, Friction, and Lubrication*, John Wiley & Sons, Inc., Hoboken, NJ, USA: 2013; pp. 177–226.
306. Spinato, C.; Giust, D.; Vacchi, I. A.; Ménard-Moyon, C.; Kostarelos, K.; Bianco, A., Different chemical strategies to aminate oxidised multi-walled carbon nanotubes for siRNA complexation and delivery. *Journal of Materials Chemistry B* **2016,** *4* (3), 431-441.
307. Topel, Ö.; Çakır, B. A.; Budama, L.; Hoda, N., Determination of critical micelle concentration of polybutadiene-block-poly (ethyleneoxide) diblock copolymer by fluorescence spectroscopy and dynamic light scattering. *Journal of Molecular Liquids* **2013,** *177*, 40-43.
308. Yaminsky, V. V.; Ninham, B. W.; Stewart, A. M., Surface Activity and Ion Exchange. A Study via Surface Tension, Wetting Tension, and Surface Force Techniques. *Langmuir* **1996,** *12* (3), 836-850.
309. Maestro, A.; Hilles, H. M.; Ortega, F.; Rubio, R. G.; Langevin, D.; Monroy, F., Reptation in langmuir polymer monolayers. *Soft Matter* **2010,** *6* (18), 4407-4412.
310. Ho, R.; Hinder, S. J.; Watts, J. F.; Dilworth, S. E.; Williams, D. R.; Heng, J. Y. Y., Determination of surface heterogeneity of d-mannitol by sessile drop contact angle and finite concentration inverse gas chromatography. *International Journal of Pharmaceutics* **2010,** *387* (1–2), 79-86.
311. Wulff, G., Zur Frage der Geschwindigkeit des Wachstums und der Auflösung der Krystallflächen. *Zeitschrift für Krystallographie und Mineralogie* **1901,** *4*, 449-530.
312. Good, R. J.; Hawa, A. K., Acid/Base Components in the Molecular Theory of Adhesion. *The Journal of Adhesion* **1997,** *63* (1-3), 5-13.
313. Azioune, A.; Chehimi, M. M.; Miksa, B.; Basinska, T.; Slomkowski, S., Hydrophobic Protein−Polypyrrole Interactions: The Role of van der Waals and Lewis Acid−Base Forces As Determined by Contact Angle Measurements. *Langmuir* **2002,** *18* (4), 1150-1156.
314. Della Volpe, C.; Maniglio, D.; Brugnara, M.; Siboni, S.; Morra, M., The solid surface free energy calculation: I. In defense of the multicomponent approach. *Journal of Colloid and Interface Science* **2004,** *271* (2), 434-453.

315. Lee, J.; Zhou, Z.-L.; Behrens, S. H., Characterizing the Acid/Base Behavior of Oil-Soluble Surfactants at the Interface of Nonpolar Solvents with a Polar Phase. *The Journal of Physical Chemistry B* **2015,** *119* (22), 6628-6637.
316. Kabalnov, A., Monolayer Frustration Contributions to Surface and Interfacial Tensions: Explanation of Surfactant Superspreading. *Langmuir* **2000,** *16* (6), 2595-2603.
317. Sun, T.; King, H. E., Pressure-induced reentrant phase behavior in the poly(N-vinyl-2-pyrrolidone)--water system. *Physical Review E* **1996,** *54* (3), 2696-2703.
318. Matsusaka, S.; Maruyama, H.; Matsuyama, T.; Ghadiri, M., Triboelectric charging of powders: A review. *Chemical Engineering Science* **2010,** *65* (22), 5781-5807.
319. Bernstein, J.; Davey, R. J.; Henck, J.-O., Concomitant Polymorphs. *Angewandte Chemie International Edition* **1999,** *38* (23), 3440-3461.
320. Bhattacharya, S.; Saha, B. K., Polymorphism through Desolvation of the Solvates of a van der Waals Host. *Crystal Growth & Design* **2013,** *13* (2), 606-613.
321. Bernstein, J., *Polymorphism in Molecular Crystals*. Clarendon Press: Oxford, 2002.
322. Obituary Notices of Fellows Deceased *Proceedings of the Royal Society of London* **1863,** *13*.
323. Hadjittofis, E.; Isbell, M. A.; Karde, V.; Varghese, S.; Ghoroi, C.; Heng, J. Y. Y., Influences of Crystal Anisotropy in Pharmaceutical Process Development. *Pharmaceutical Research* **2018,** *35* (5), 100.
324. Beckmann, W.; Boistelle, R.; Sato, K., Solubility of the A, B, and C polymorphs of stearic acid in decane, methanol, and butanone. *Journal of Chemical & Engineering Data* **1984,** *29* (2), 211-214.
325. Romero, S.; Escalera, B.; Bustamante, P., Solubility behavior of polymorphs I and II of mefenamic acid in solvent mixtures. *International Journal of Pharmaceutics* **1999,** *178* (2), 193-202.
326. Tong, H. H. Y.; Yu Shekunov, B.; York, P.; Chow, A. H. L., Characterization of Two Polymorphs of Salmeterol Xinafoate Crystallized From Supercritical Fluids. *Pharmaceutical Research* **2001,** *18* (6), 852-858.
327. Park, K.; Evans, J. M. B.; Myerson, A. S., Determination of Solubility of Polymorphs Using Differential Scanning Calorimetry. *Crystal Growth & Design* **2003,** *3* (6), 991-995.
328. Pudipeddi, M.; Serajuddin, A. T. M., Trends in Solubility of Polymorphs. *Journal of Pharmaceutical Sciences* **2005,** *94* (5), 929-939.
329. Lee, E. H., A practical guide to pharmaceutical polymorph screening & selection. *Asian Journal of Pharmaceutical Sciences* **2014,** *9* (4), 163-175.
330. Bauer, J.; Spanton, S.; Henry, R.; Quick, J.; Dziki, W.; Porter, W.; Morris, J., Ritonavir: An Extraordinary Example of Conformational Polymorphism. *Pharmaceutical Research* **2001,** *18* (6), 859-866.
331. Arlin, J.-B.; Price, L. S.; Price, S. L.; Florence, A. J., A strategy for producing predicted polymorphs: catemeric carbamazepine form V. *Chemical Communications* **2011,** *47* (25), 7074-7076.
332. Christian, P.; Röthel, C.; Tazreiter, M.; Zimmer, A.; Salzmann, I.; Resel, R.; Werzer, O., Crystallization of Carbamazepine in Proximity to Its Precursor Iminostilbene and a Silica Surface. *Crystal Growth & Design* **2016,** *16* (5), 2771-2778.
333. Fleischman, S. G.; Kuduva, S. S.; McMahon, J. A.; Moulton, B.; Bailey Walsh, R. D.; Rodríguez-Hornedo, N.; Zaworotko, M. J., Crystal Engineering of the Composition of Pharmaceutical Phases: Multiple-Component Crystalline Solids Involving Carbamazepine. *Crystal Growth & Design* **2003,** *3* (6), 909-919.
334. Johnston, A.; Johnston, B. F.; Kennedy, A. R.; Florence, A. J., Targeted crystallisation of novel carbamazepine solvates based on a retrospective Random Forest classification. *CrystEngComm* **2008,** *10* (1), 23-25.
335. Cruz-Cabeza, A. J.; Day, G. M.; Jones, W., Structure prediction, disorder and dynamics in a DMSO solvate of carbamazepine. *Physical Chemistry Chemical Physics* **2011,** *13* (28), 12808-12816.
336. Harris, R. K.; Ghi, P. Y.; Puschmann, H.; Apperley, D. C.; Griesser, U. J.; Hammond, R. B.; Ma, C.; Roberts, K. J.; Pearce, G. J.; Yates, J. R.; Pickard, C. J., Structural Studies of the Polymorphs of

Carbamazepine, Its Dihydrate, and Two Solvates. *Organic Process Research & Development* **2005,** *9* (6), 902-910.
337. Khoo, J. Y.; Williams, D. R.; Heng, J. Y. Y., Dehydration Kinetics of Pharmaceutical Hydrate: Effects of Environmental Conditions and Crystal Forms. *Drying Technology: An International Journal* **2010,** *28*, 1164-1169.
338. Olafson, K. N.; Rimer, J. D.; Vekilov, P. G., Growth of Large Hematin Crystals in Biomimetic Solutions. *Crystal Growth & Design* **2014,** *14* (5), 2123-2127.
339. Fredenslund, A.; Jones, R. L.; Prausnitz, J. M., Group-contribution estimation of activity coefficients in nonideal liquid mixtures. *AIChE Journal* **1975,** *21* (6), 1086-1099.
340. Kachrimanis, K.; Griesser, U. J., Dehydration Kinetics and Crystal Water Dynamics of Carbamazepine Dihydrate. *Pharmaceutical Research* **2012,** *29*, 1143-1157.
341. Li, Y.; Han, J.; Zhang, G. Z. G.; Grant, J. W.; Suryanarayanan, R., In Situ Dehydration of Carbamazepine Dihydrate: A Novel Technique to Prepare Amorphous Anhydrous Carbamazepine. *Pharmaceutical Development and Technology* **2000,** *5* (2), 257-266.
342. Minkov, V. S.; Beloborodova, A. A.; Drebushchak, V. A.; Boldyreva, E. V., Furosemide Solvates: Can They Serve As Precursors to Different Polymorphs of Furosemide? *Crystal Growth & Design* **2014,** *14* (2), 513-522.
343. Beloborodova, A. A.; Minkov, V. S.; Rychkov, D. A.; Rybalova, T. V.; Boldyreva, E. V., First Evidence of Polymorphism in Furosemide Solvates. *Crystal Growth & Design* **2017,** *17* (5), 2333-2341.
344. Sun, Y.; Zhu, L.; Kearns, K. L.; Ediger, M. D.; Yu, L., Glasses crystallize rapidly at free surfaces by growing crystals upward. *Proceedings of the National Academy of Sciences of the United States of America* **2011,** *108* (15), 5990-5995.
345. Okoth, M. O.; Vrcelj, R. M.; Sheen, D. B.; Sherwood, J. N., Dehydration mechanism of a small molecular solid: 5-nitrouracil hydrate. *Crystal Engineering Communications* **2013,** *15*, 8202-8213.
346. Tu, K. N., Irreversible processes of spontaneous whisker growth in bimetallic Cu-Sn thin-film reactions. *Physical Review B* **1994,** *49* (3), 2030-2034.
347. Hou, H.; Xie, Y.; Li, Q., Structure-directing self-organized, one-dimensional ZnO single-crystal whiskers. *Solid State Sciences* **2005,** *7* (1), 45-51.
348. Mallet, F.; Petit, S.; Lafont, S.; Billot, P.; Lemarchand, D.; Coquerel, G., Crystal Growth Mechanism in a Solution of Hollow Whiskers of Molecular Compounds. *Crystal Growth & Design* **2004,** *4* (5), 965-969.
349. Martins, D.; Stelzer, T.; Ulrich, J.; Coquerel, G., Formation of Crystalline Hollow Whiskers as Relics of Organic Dissipative Structures. *Crystal Growth & Design* **2011,** *11* (7), 3020-3026.
350. Prigogine, I., Time, Structure, and Fluctuations. *Science* **1978,** *201* (4358), 777.
351. Berry, J. D.; Neeson, M. J.; Dagastine, R. R.; Chan, D. Y. C.; Taborf, R. F., Measurement of surface and interfacial tension using pendant drop tensiometry. *Journal of Colloid Interface Science* **2015**, 454, 226-237.

Appendix 1: Supplementary information on the calculation of spreading pressure

This section provides some calculations and analysis, in order to offer more clarity in the work featured in the article.

A.1.1 The concept of spreading pressure

Spreading pressure is a quantity influenced by the adsorbent, the adsorbate and the conditions of the experiment (temperature, presence of humidity etc.). It is calculated according to the following equation:

$$\pi_e = RT \int_0^{P_0} \Gamma \, d(\ln(P)) \qquad \text{Eq. A.1.1}$$

In the above equation, π_e stands for the spreading pressure, γ_S and γ_{SV} are the surface energy of the solid and of the solid vapour interface respectively, Γ is the surface excess, R, T and P have the same meaning as in the ideal gas law.

The integration is performed over the whole isotherm i.e. from $P/P_0=0$ to $P/P_0=1$ (P_0 is the saturation pressure). From an experimental perspective two main limitations exist. IGC operators, usually, pack material with a total surface area of about 1 m^2 or more. This is done in order to improve the accuracy of the experiment. This means, that the injection system of the chromatographic instrument should be able to inject sufficient amount of solvent to cover the whole surface area of the material. If this is not the case, then the experimental points are collected for lower values of surface coverage and then extrapolation is performed. However, there is a further experimental limitation associated with the quality of the chromatograms. At injections aiming for high values of surface coverage is not uncommon to record flat top peak chromatograms. Their occurrence is problematic, since it is not possible to calculate their

retention time. This type of chromatograms further limits our ability to perform injections at high values of surface coverage with fine powder materials.

As mentioned above, extrapolation is used in order to predict the behaviour of the surface excess adsorption isotherms at high values of P/P_0. A number of isotherms have been developed over the years in order to study adsorption phenomena on different types of materials. A thorough discussion of the features of individual isotherms is beyond the scope of this work. In this work a BET type of isotherm was employed as the base on which extrapolations were performed. The general formula for the BET isotherm is given as follow:

$$\theta = \frac{C\left(\frac{P}{P_0}\right)}{\left(1-\left(\frac{P}{P_0}\right)\right) * \left(1 + C\left(\frac{P}{P_0}\right) - \left(\frac{P}{P_0}\right)\right)} \qquad \text{Eq. A.1.2}$$

In equation A.1.2, θ is the fractional coverage, C is an adsorption exponential constant, P_0 is the saturation pressure and P is the pressure. A plot of this equation can be seen in figure 1. As can be seen in the same plot, a two-term exponential model can fit this equation particularly well, with an R^2 of 0.996.

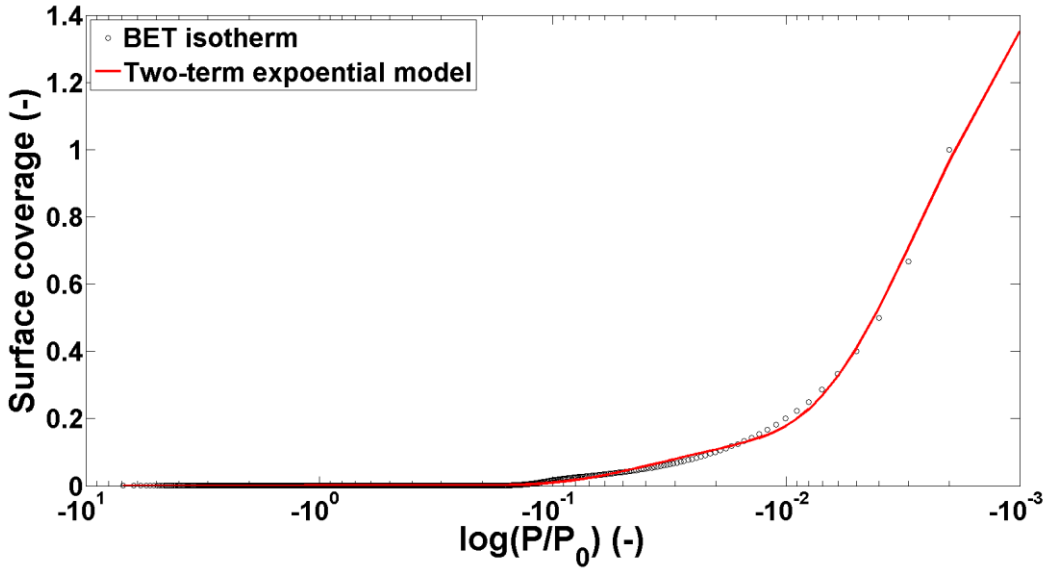


Figure A.1.1: Plot of a theoretical BET adsorption isotherm along with a two-term exponential fit.

Figure A.1.2 illustrates a number of surface excess adsorption isotherms obtained from octane experiments on P-Monoclinic Carbamazepine at two temperatures (30 and 40 ºC). The agreement between the experimental data and the two-term exponential fit is quite good, highlighting its applicability for the purposes of this work.

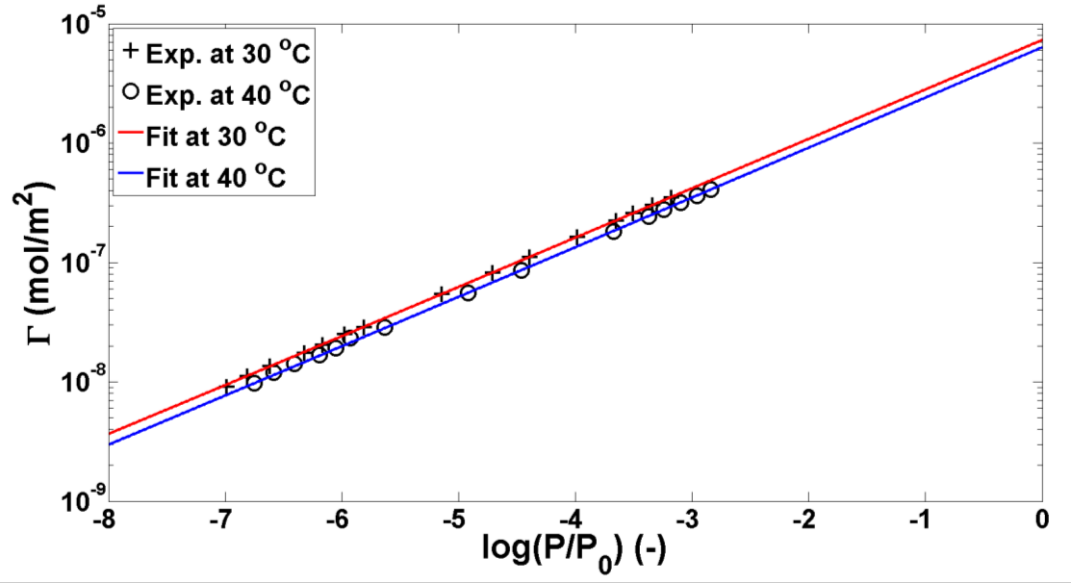


Figure A.1.2: The surface excess adsorption isotherms obtained for octane at two temperatures (30 and 40 °C) along with the fit lines obtained from two-term exponential fitting. The logarithmic plot in both axes enables better visualisation of the good agreement. The area below the curves shown in the figure above is used to calculate the magnitude of spreading pressure for octane at the two temperatures.

A.1.2 The roadmap for the correction of IGC data

FD-IGC is an established technique for the determination of surface energy heterogeneity of crystalline materials. Thus, there was no reason to present its fundamentals in the main body of the article. However, in this section of the supplementary information, a more thorough explanation will be performed, including the notions introduced by this work. Figure 3 is going to be used as a guide for the discussion that follows.

At point one of **Figure A.1.3**, the retention volumes measured for three different alkanes, at a specific temperature and at different values of the relative pressure are shown. From these data, since the number of moles injected is known, BET plots can be constructed, as shown in point two, to enable the calculation of the relative coverage associated with each value of relative pressure. Moving in point three, one can see two plots. The one on the left is similar to the plot

at point one. It shows the retention volume at different values of surface coverage. One can now pick values from all three alkanes, at the same value of surface coverage and using the Schultz's plot shown on the right part of point three, to calculate, from the slope of the plot, the surface energy for that particular value of surface coverage. By repeating the same process for different values of surface coverage she can plot a graph of surface energy against coverage. This graph is depicted at point five.

Each individual value plotted on the graph at point five corresponds to $\gamma_S = \gamma_{SV} + \gamma_\pi$, where γ_π is the influence of spreading pressure. This influence is calculated at point four. The isotherms are plotted for each alkane and numerical integration is performed. Then the spreading pressure is calculated and introduced on the Schultz's plot. From the slope of the Schultz's plot, the value of γ_π can be calculated. This value is then subtracted from each individual point of the plot obtained at point five, in order to find the corrected value of surface energy, γ_{SV}, for the different values of surface coverage.

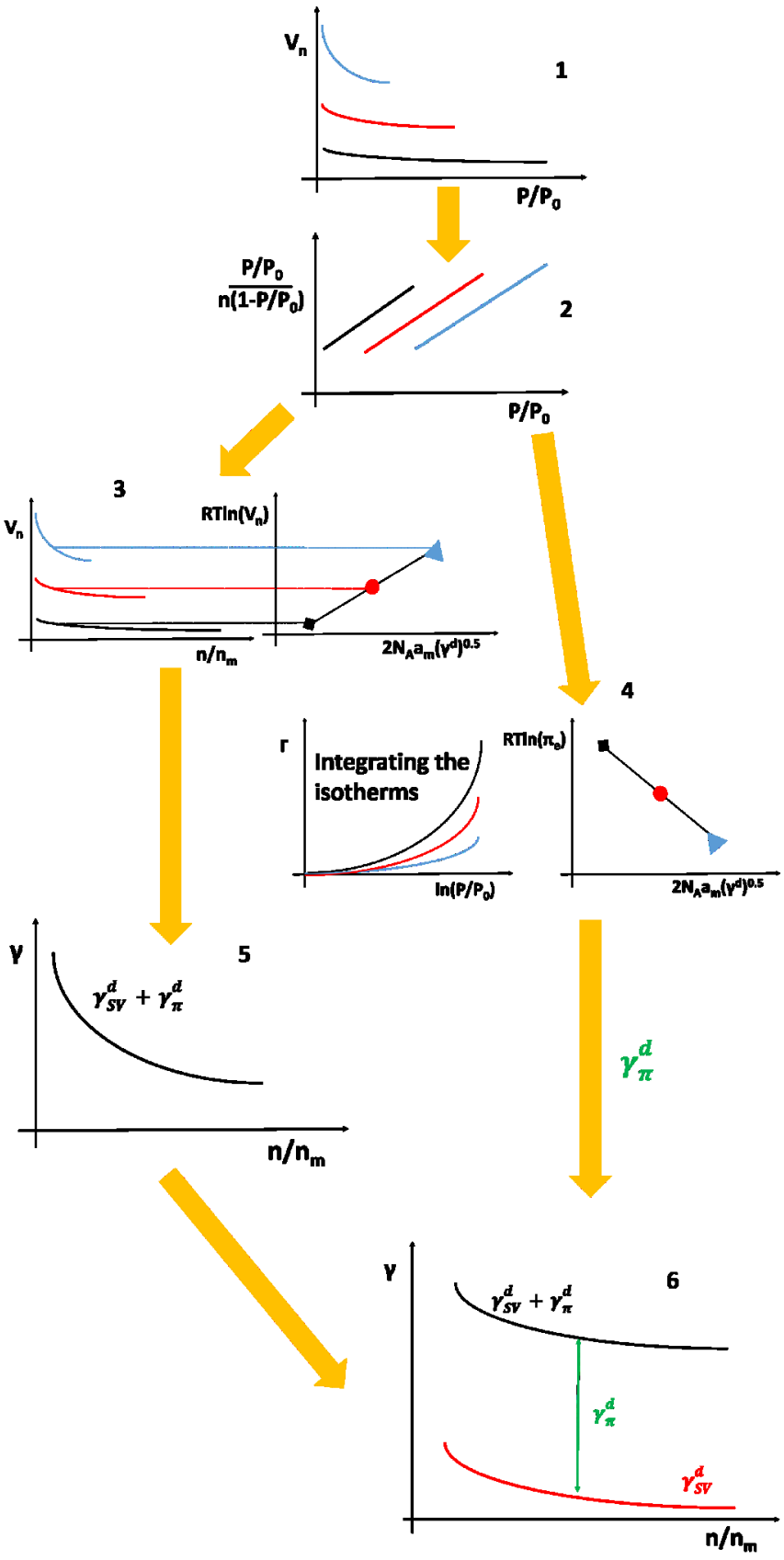


Figure A.1.3: Schematic showing the workflow for the determination of the corrected value of surface energy, using IGC data.

Appendix 2: Pendant drop measurements

Pendant drop measurements enable the calculation of the surface tensions of fluids. Let's consider a droplet of a liquid hanging from a needle, similar to the one used for contact angle measurements, in another fluid (which can be a liquid or a gas). The dimensions of this droplet are given in Figure A.2.1 (the figure is in cylindrical coordinates, meaning that it is described by two direction vectors, z and r and an angle, φ). If someone draws a tangent at any point on the perimeter (s) of the droplet, then a contact angle φ is formed.

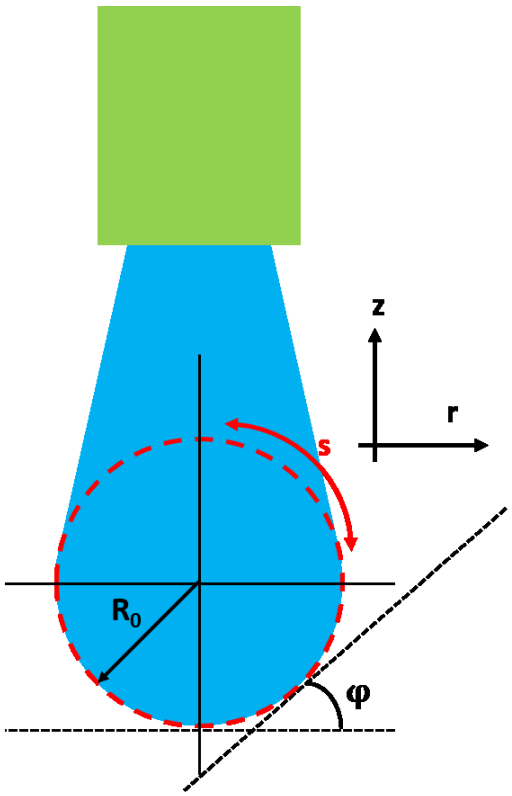


Figure A.2.1: Schematic depiction of a droplet hanging in a fluid. The schematic used cylindrical coordinates.

The change in the radius (R_0) of this droplet, interacting with the surrounding medium via an interfacial surface tension γ, is governed by the Young-Laplace equation, describing the pressure change (ΔP) required to change the radius from R_1 to R_2:

$$\Delta P = P_0 - gz\left(\rho_{droplet} - \rho_{bulk}\right) = \gamma\left(\frac{1}{R_1} - \frac{1}{R_2}\right) \qquad \text{Eq. A.2.1}$$

In the above equation P_0 is the reference pressure at the point where the value of z is taken to be zero (usually is at the bottom of the droplet), g is the acceleration of gravity and z is the vertical direction from the point of reference. Furthermore, $\rho_{droplet}$ is the density of the droplet and ρ_{bulk} is the density of the surrounding liquid.

In cylindrical coordinates, the dynamic behaviour of the system can be described in terms of a set of three first order ordinary differential equations:

$$R_0\frac{d\varphi}{ds} = 2 - \frac{g\left(\rho_{droplet} - \rho_{bulk}\right)R_0^2}{\gamma}\left(\frac{z}{R_0}\right) - \frac{\sin(\varphi)\,R_0}{r}$$

$$= 2 - Bo\left(\frac{z}{R_0}\right) - \frac{\sin(\varphi)\,R_0}{r}$$

$$\frac{dr}{ds} = \cos(\varphi) \qquad \text{Eq. A.2.2-2.4}$$

$$\frac{dz}{ds} = \sin(\varphi)$$

In equation A.2.2, the term Bo stands for the dimensionless Bond parameter describing the ratio between gravitational and surface tension forces acting on the droplet.

Using a camera set-up, similar to the one used in contact angle measurements, one could measure the dimensions of a droplet and try to fit the measured data, for the relationship between the radius and the parameters z, φ and s, in the above set of equations. By doing that and using appropriate optimization, the values for the interfacial tension between the droplet and the surrounding fluid can be obtained. Numerous images can be used to produce a statistically significant sample. If the measurements are performed in air, the resulting value is the total surface tension of the liquid of the droplet. A very detailed explanation of the algorithm used for the calculation of the interfacial tension can be found in literature, along with the corresponding theory.[351]